LOW-VALENT AND LOW-COORDINATE TITANIUM AND MOLYBDENUM COMPLEXES SUPPORTED WITH BULKY AMIDO LIGANDS

by

ADAM REID JOHNSON

B. A., Oberlin College

(1993)

Submitted to the Department of Chemistry
in Partial Fulfillment of the Requirements
for the Degree of

DOCTOR OF PHILOSOPHY

at the

MASSACHUSETTS INSTITUTE OF TECHNOLOGY

September, 1997

Signature of Author_____
Department of Chemistry
July 2· 1997

Certified by_____
Christopher C. Cummins
Thesis Supervisor

Accepted by_____
Dietmar Seyferth
Chairman, Departmental Committee on Graduate Students

This doctoral thesis has been examined by a Committee of the Department of Chemistry as follows:

Professor Richard R. Schrock_____
Chairman

Professor Christopher C. Cummins_____
Thesis Supervisor

Professor Alan Davison_____

To Wendy

I love you,
Not only for what you are,
But for what I am
When I am with you.

I love you,
Not only for what
You have made of yourself,
But for what
You are making of me.

Roy Croft

According to convention there is a sweet and a bitter, a hot and a cold, and according to convention there is order. In truth there are atoms and a void.

Democritus (400 B.C.)

LOW-VALENT AND LOW-COORDINATE TITANIUM AND MOLYBDENUM COMPLEXES SUPPORTED WITH BULKY AMIDO LIGANDS

by

ADAM REID JOHNSON

Submitted to the Department of Chemistry, September 1997,

in Partial Fulfillment of the Requirements for the Degree of

Doctor of Philosophy in Chemistry

Abstract

Chapter I: Heteroleptic Titanium(III) and -(IV) Complexes with Bulky Ancillary Ligands

Partially deuterated bulky *N-tert*-alkylanilide ligands for the study of low-valent and low-coordinate paramagnetic transition metal complexes were prepared. Using dimethylamide protecting groups, removable with methyl iodide, a wide variety of titanium(IV) complexes of the general formulation $Ti(N[R]Ar)_a(OAr')_b(X)_c$ (Ar' = 2,6-disubstituted aryl, X = dimethylamide, alkyl or halide, a + b + c = 4) were prepared. Various substitutions on the N[R]Ar ligand set allowed for steric and electronic tuning of the titanium center. The heteroleptic Ti(III) alkyl complex $Ti(N[R]Ar)_2(CH[SiMe_3]_2)$ was prepared from $Ti(N[R]Ar)_2(\mu\text{-}Cl)_2\cdot Li(TMEDA)$ and was characterized by X-ray crystallography. Initial reactivity of this alkyl complex was explored.

Chapter II: Molybdenum(V) and -(VI) Chalcogenide Complexes

The terminal Mo(V) chalcogenido complexes $EMo(N[R]Ar)_3$ (E = O, S, Se and Te) were prepared from the reaction of $Mo(N[R]Ar)_3$ with pyridine *N*-oxide, S_8, Se and Te/PEt_3. The complexes were studied by EPR, SQUID magnetometry, cyclic voltammetry and single crystal X-ray diffraction. The Mo-O and Mo-S bond dissociation enthalpies were experimentally determined to be 155.61 ± 1.6 and 104.35 ± 1.2 kcal/mol respectively. Thermolysis of the Mo(V) complexes resulted in *tert*-butyl radical elimination and formation of the terminal Mo(VI) chalcogenido complexes $EMo(NAr)(N[R]Ar)_2$. The

selenido and tellurido derivatives were studied by selenium and tellurium NMR spectroscopy. A first-order decay was measured for the thermolysis reaction for both the oxo and sulfido complexes. The reactivity of $Mo(N[R]Ar)_3$ with a wide variety of chalcogen atom donor reagents was examined.

Chapter III: Activation of a Molybdenum Nitride Derived from Molecular Nitrogen

Treating $NMo(N[R]Ar)_3$ with methyl iodide formed the cationic imido complex $[Mo(NMe)(N[R]Ar)_3][I]$; reduction with coboltocene generated $Mo(NMe)(N[R]Ar)_3$. $Mo(N[R]Ar)_3$ reacted with iodine to give $IMo(N[R]Ar)_3$, with 2-methylaziridine or 7-amino-7-aza-benzonorbornadiene to generate $NMo(N[R]Ar)_3$, HN[R]Ar and propylene or anthracene, and ammonia to generate principally HN[R]Ar. $Mo(N[R]Ar)_3$ did not readily react with *N*-methylaziridine, azetidine, *tert*-butylamine, triethylamine or diethylamine.

Chapter IV: Group 6 Complexes with a Bulky Amide Ligand Containing β-Hydrogens-Synthesis with Mechanistic Implications

The bulky aniline HN[2-Ad]Ar was prepared. $Cr(N[2\text{-}Ad]Ar)_3$ was prepared from $CrCl_3$ and the deprotonated aniline LiN[2-Ad]Ar. Treating the chromium complex with nitric oxide formed $(ON)Cr(N[2\text{-}Ad]Ar)_3$. $Mo(N[2\text{-}Ad]Ar)_3$ was prepared from $MoCl_3(THF)_3$ and LiN[2-Ad]Ar. Treating the molybdenum complex with phosphorous forms $PMo(N[2\text{-}Ad]Ar)_3$. Both molybdenum complexes are examined by single crystal X-ray diffraction. $Mo(N[2\text{-}Ad]Ar)_3$ reacted rapidly with nitric oxide or mesityl azide to generate the diamagnetic nitrosyl or nitride complexes, and slowly with nitrous oxide to generate both products in a 1:1 molar ratio. $Mo(N[2\text{-}Ad]Ar)_3$ competed with $Mo(N[R]Ar)_3$ for nitric oxide to the extent of 20%, but did not compete for nitrous oxide, suggesting that the nitrous oxide N-N bond cleavage is bimolecular as previously observed for the dinitrogen N-N bond cleavage.

Thesis Supervisor: Professor Christopher C. Cummins

Title: Professor of Chemistry

Biographical Note

Adam Reid Johnson was born in New Haven, Connecticut, lived in Medford, Massachusetts for a short time, and was raised in Upper Arlington, Ohio. He graduated from Upper Arlington High School in 1989. He earned a B. A. from Oberlin College and graduated phi beta kappa with High Honors in Chemistry in 1993. He was awarded the Jewett Prize (1991), the Dow Scholarship (1992-3), the Holmes Prize (1993) and received an Honorable Mention in the National Science Foundation Fellowship Competition (1993). He was a National Science Foundation Summer Intern at the University of California, Irvine (1991). He has taught courses in group theory and advanced inorganic chemistry, and supervised laboratory instruction in general and organic chemistry. He has presented papers at local, regional and national American Chemical Society meetings. Subsequent to receiving his Ph. D., Adam will begin postdoctoral research in the laboratory of Ken Raymond at the University of California, Berkeley. His career goal is to teach inorganic and general chemistry at an undergraduate institution with a strong research focus. His hobbies include zymurgy, running, backpacking, cooking and reading. In 1996, he married Wendy Lynne Waggener.

Publications:

1. C_{60} and C_{70} made simply. Craig, N. C.; Gee, G. C.; and Johnson, A. R. *J. Chem. Ed.* **1992**, *69(8)*, 664-6.
2. Site-directed Mutagenesis of Glutathione *S*-Transferase YaYa. Wang, R. W.; Newton, D. J.; Johnson, A. R.; Pickett, C. B.; and Lu, A. Y. H. *J. Biol. Chem.* **1993**, *32(15)*, 23981-5.
3. Cleavage of Titanium Dimethylamides with Methyl Iodide. Johnson, A. R.; Wanandi, P. W.; Cummins, C. C.; and Davis, W. M. *Organometallics*. **1994**, *13*, 2907-9.
4. Nitrogen Atom Transfer Coupled with Dinitrogen Cleavage and Mo-Mo Triple Bond Formation Laplaza, C. E.; Johnson, A. R.; and Cummins, C. C. *J. Am. Chem. Soc.* **1996**, *118*, 709-710
5. Titanium Complexes Stabilized by *N*-(*tert*-Hydrocarbyl)anilide Ligation: A Synthetic Investigation. Johnson, A. R.; Davis, W. M.; and Cummins, C. C. *Organometallics*. **1996**, *15*, 3825-3835.
6. Assembly of Molybdenum/Titanium μ-Oxo Complexes via Radical Alkoxide C-O Cleavage. Peters, J. C.; Johnson, A. R.; Odom, A. L.; Wanandi, P. W.; Davis, W. M.; and Cummins, C. C. *J. Am. Chem. Soc.* **1996**, *118*, 10175-10188.
7. Four-Coordinate Molybdenum(V) and -(VI) Monochalcogenide Complexes: A Synthetic, Mechanistic, Structural, Thermochemical, and Theoretical Study. Johnson, A. R.; Davis, W. M.; Cummins, C. C.; Serron, S.; Nolan, S. P.; Musaev, D. G. and Morokuma, K. *J. Am. Chem. Soc.* **1997**, *Submitted.*
8. *N-Tert*-Alkyl Anilides as Bulky Ancillary Ligands. Johnson, A. R. and Cummins, C. C. *Inorg. Synth.* **1997**, *In Press.*

Table of Contents

List of Figures

List of Schemes

List of Tables

List of Abbreviations Used in Text

A	EPR Coupling Constant
Å	Angstrom (10^{-10} m)
1-Ad	1-Adamantyl
2-Ad	2-Adamantyl
Anal.	Analysis (Elemental)
Ar	Aryl or Argon or 3,5-$C_6H_3Me_2$
Ar_F	2,5-C_6H_3FMe
atm	Atmosphere
br	Broad
Bz	Benzyl, $CH_2C_6H_5$
c_{ij}	Coefficient of Atomic Orbital j in Molecular Orbital i
CACAO	Computer Aided Composition of Atomic Orbitals
calcd.	Calculated
CCD	Charge Coupled Device
cm^{-1}	Wavenumber
Cp	Cyclopentadiene Anion, $C_5H_5^-$
Cp*	Pentamethylcyclopentadiene Anion, $C_5Me_5^-$
cy	Cyclohexyl
d	Doublet or Days
deg (°)	Degrees
DME	1,2-Dimethoxyethane
dmpe	1,2-Bis(dimethylphosphino)ethane
d^n	Number of d-Electrons
E	Element (Usually a Group 16 Element) or Energy
EHC	Extended Hückel Calculation
EI	Electron Impact
EPR	Electron Paramagnetic Resonance
eq.	Number of Equivalents or Equation
Fc/Fc^+	Ferrocene/Ferrocinium
G	Gauss
g	Grams or g-Value (EPR)
GC-MS	Gas Chromatography-Mass Spectrometry
h	Planck's constant
h	Hours

H	Hamiltonian
$H_{ii} = \int \phi_i H \phi_i \, d\tau$	Energy of Atomic Orbital ϕ_i (Ionization Energy or Coloumb Integral)
$H_{ij} = \int \phi_i H \phi_j \, d\tau$	Interaction Energy Between atomic orbitals ϕ_i and ϕ_j (Resonance Integral)
^1H	Proton
^2H	Deuteron
HOMO	Highest Occupied Molecular Orbital
HRMS	High Resolution Mass Spectrometry
Hz	Hertz (sec^{-1})
i-Pr	*iso*-Propyl
IR	Infra-Red
$^nJ_{xy}$	n-Bond Coupling Constant Between Atom x and y
k	Boltzmann's constant
K	Degrees Kelvin
k_r	Rate Constant
L	Neutral Two Electron Donor Ligand
LUMO	Lowest Unoccupied Molecular Orbital
M^+	Parent Ion
m	Multiplet or *Meta*
Me	Methyl
MO	Molecular Orbital
MOAN	Molecular Orbital ANalysis
MS	Mass Spectrometry
NMR	Nuclear Magnetic Resonance
Np	Neopentyl
nph	Neophyl, CH_2CMe_2Ph
o	*Ortho*
ORTEP	Oak Ridge Thermal Elipsoid Plot
OTf	Triflate, $CF_3SO_3^-$
p	*Para*
Ph	Phenyl
ppm	Parts Per Million
py	Pyridine
q	Quartet
R	Generic Alkyl Group
[R]	$C(CD_3)_2CH_3$

$[R_{ph}]$	$C(CD_3)_2C_6H_5$
s	Singlet or Spin Quantum Number
sept	Septet
$S_{ij} = \int \phi_i \phi_j \, d\tau$	Overlap Integral Between ϕ_i and ϕ_j
silox	$OSi(tert\text{-}Bu)_3$
SOMO	Singly Occupied Molecular Orbital
SQUID	Superconducting QUantum Interference Device
T	Absolute Temperature
t	Triplet
t-Bu	*tert*-Butyl
THF	Tetrahydrofuran
TIP	Temperature Independent Paramagnetism
TLA	Three Letter Acronym
TMEDA	Tetramethylethylenediamine
TMS	Tetramethylsilane
UV-vis	Ultra Violet-Visible
VT	Variable Temperature (as in VT-NMR)
X	Anionic One Electron Donor Ligand
χ	Magnetic Susceptibility
δ	Chemical Shift in ppm Downfield From Zero
$\Delta H^{\ddagger}$	Enthalpy of Activation
$\Delta\nu_{1/2}$	Peak Width at Half Height
$\Delta S^{\ddagger}$	Entropy of Activation
ε	Extinction Coefficient
η^x	x-Hapto
λ_{max}	Wavelength with Highest Absorbance
μ	Magnetic Moment, or Bridging Ligand
μ_B	Bohr Magneton
μ_{eff}	Effective Magnetic Moment
μL	Microliter
ν_{xy} or $\nu(X)$	Vibrational Band for an XY Bond or X-Group
θ	Weiss Constant (K)
ψ_k	k'th Molecular Orbital
ϕ_i	i'th Atomic Orbital
ζ_x	Effective Nuclear Charge for Atom X (Exponential Term in Normalized Radial Atomic Orbital Function)

Chapter I: Heteroleptic Titanium(III) and -(IV) Complexes with Bulky ancillary Ligands*

* Reprinted in part with permission from *Organometallics* **1994**, *13*, 1907 (© 1994 American Chemical Society) and *Organometallics* **1996**, *15*, 3825 (© 1996 American Chemical Society).

References begin on page 81

Section 1.1: Introduction.

Cyclopentadienyl complexes of titanium and the other group four elements are being intensely studied due to the wide variety of chemical transformations they mediate.[1,2] One of the most important of these is the Ziegler-Natta polymerization of ethylene and propylene, and there is much synthetic effort towards the development of more effective catalysts for this reaction.[3,4] There are many other uses for titanium reagents including hydrogenation[5] and reductive coupling[6-8] of organic substrates. A major focus of current research in this area is the development of new ligands capable of enhancing the inherent reactivity of the metal center. Noteworthy are the C_2-symmetric *ansa*-metallocenes originally developed by Brintzinger,[9,10] and Cp ligands with pendant amide groups which alter the electronic environment at the metal center relative to titanocene-based reagents.[11,12] One mode of reactivity for these reagents is through the Lewis acidic metal center generated by the formation of an open coordination site.[1,13,14]

In order to develop reagents and catalysts with significantly improved or different properties, transition metal complexes with N- or O-donor ancillary ligands are currently under investigation. One feature common to these ligands is their steric bulk, which stabilizes reactive, low-valent complexes by preventing dimerization or oligimerization. The reactivity of the metal center should be enhanced relative to metallocene complexes due to the enforced low coordination number and decreased electron count at the metal center. The ligand silox (t-Bu_3SiO^-) stabilizes a wide variety of early transition metal complexes,[15-23] while bulky 2,6-*di*-alkyl substituted aryloxide ligands[24-26] and benzamidinate[27,28] ligands are also employed with a good deal of success. However, amides are the most common ligand used, due in large part to the increased steric protection offered by the additional alkyl group on nitrogen relative to oxygen. Bulky amide ligands such as $^-N(SiMe_3)_2$,[29-34] $^-N(Ph)_2$,[35-38] $^-N(Cy)_2$[35,36,39] and $^-N(i\text{-}Pr)_2$[40] have all been used successfully to generate low coordinate transition metal complexes. These low coordinate

References begin on page 81

complexes are generally quite reactive, mediate such reactions as carbon-carbon bond formation,[26] reductive coupling,[22,41] carbonyl insertion[17] and hydrogenation,[17] and stabilize reactive organic fragments.[18]

A significant problem with the ligands which have been used so far is a direct consequence of the low-coordinate environment they stabilize. Low-valent and low-coordinate complexes are often paramagnetic, and are therefore difficult to study spectroscopically due to the line broadening effect of paramagnetic materials on proton NMR signals. Deuterium NMR of paramagnetic materials can theoretically give peaks which are 42 times sharper than the corresponding proton signals;[42,43] therefore, ligands with deuterium incorporation are desirable. Unfortunately, it is neither easy nor cheap to substitute deuterium into standard amide ligands. A novel bulky amide ligand type, the *N-tert*-alkyl anilide,[44] addresses this problem. This ligand readily stabilizes molecules with low coordination numbers and oxidation states,[45-54] mimics the $^{-}N(SiMe_3)_2$ ligand both electronically (the pK_a of aniline and bis(trimethylsilyl)amine are both ~25) and sterically, and allows for simple incorporation of a relatively inexpensive deuterium label. These ligands are readily prepared in multi-gram quantities in only a few steps, and, like $^{-}N(SiMe_3)_2$, are not susceptible to low-energy decomposition pathways such as β-hydrogen elimination or cyclometallation. However, the biggest advantage to using this ligand type is the inherent electronic tunability due to the commercial availability of a wide variety of inexpensive anilines.

The homoleptic titanium(III) tris-anilide complex is monomeric in the solid state.[55] It is a powerful one electron reductant, capable of abstracting halogen atoms from transition metal complexes[56] and organic substrates.[57] It also adds to terminal oxo groups in transition metal complexes, forming the novel "titanoxy" ligand.[53,55] A heteroleptic titanium(III) alkyl complex should exhibit one electron reactivity similar to the tris-anilide, but the metal-carbon bond in the alkyl complex might also be reactive. Although rare, there are examples of heteroleptic complexes in the field of low-coordinate chemistry, including

References begin on page 81

$W(silox)_2(N\text{-}t\text{-}Bu)$.[21] Two-electron chemistry of metal-carbon bonds is also well precedented,[2] but *three*-electron chemistry, two from the metal-carbon bond plus one from the unpaired electron on the metal center, is not. Titanium(III) alkyl complexes would be expected to exhibit one, two and three electron chemistry, given the proper substrates.

This chapter describes the synthesis and characterization of a Ti(III) alkyl complex stabilized with two *N-tert*-alkyl anilide ligands, steric and electronic constraints for the stability of Ti(III) alkyl species in general, and initial reactivity studies demonstrating the potential for one, two and three electron processes involving the single electron in tandem with the reactive metal-carbon bond. In addition, alternate synthetic pathways are presented which, although they do not lead to stable Ti(III) complexes, demonstrate the inherent electronic tunability of the *N-tert*-alkyl anilide ligand. The syntheses in this chapter make extensive use of a recently developed dimethylamide protecting group strategy.[58] The dimethylamide "place holder" is replaced with an iodide by treatment with methyl iodide. This strategy prevents oversubstitution and/or reduction of titanium halide starting materials, and seems general in scope for the synthesis of otherwise inaccessible metal iodide complexes.[59] Much of the work described in this chapter has appeared in print.[58,60,61]

Section 1.2: Synthesis of *N-tert*-alkyl Anilides

(i) HN[R]Ar

Several synthetic methods have been developed and optimized for the *N-tert*-alkyl anilide ligand.[44,61] Hunter[62] prepared *N-tert*-butyl aniline in low yield by methylating phenylacetone imine.[63] This procedure is outlined in Scheme 1.1 for the synthesis of the N[R]Ar ligand ($R = C(CD_3)_2CH_3$; $Ar = 3,5\text{-}C_6H_3Me_2$). Distilled 3,5-dimethylaniline is added to acetone-d_6 in the presence of 4 Å sieves. To prevent significant proton incorporation from adventitious water, the reaction is carried out under a partial vacuum.

References begin on page 81

The crude reaction mixture is monitored directly by ^1H NMR, and the reaction takes from one to four days to go to completion. Removal of the sieves and the excess acetone yields a pale yellow oil ($ArN{=}C(CD_3)_2$, **1.1**) in essentially quantitative yield.

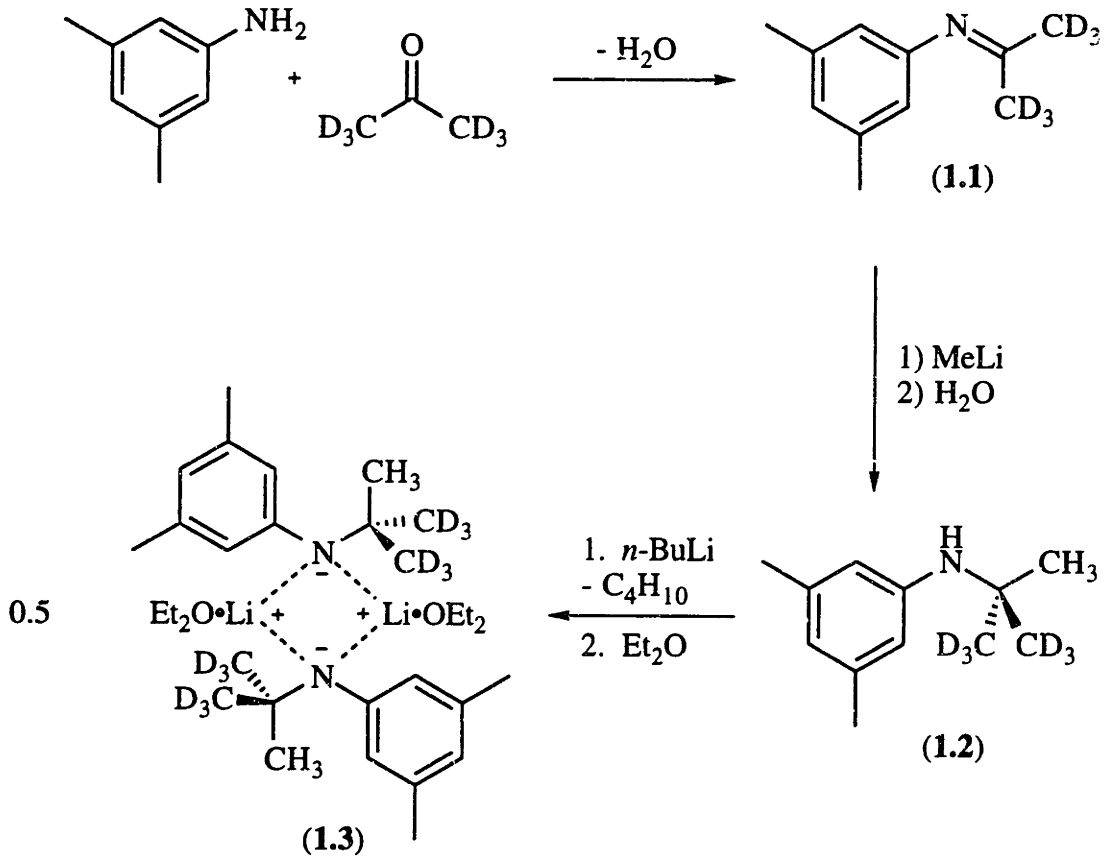

Scheme 1.1: Synthesis of the N[R]Ar Framework

The final conditions used for the methylation of **1.1** to give HN[R]Ar (**1.2**) are a result of extensive optimization. The synthesis is best accomplished by slowly adding a solution of the imine to three equivalents of a just thawed solution of methyllithium. After 18 hours of stirring, the reaction solution is poured over ice to quench the excess methyllithium. The separated organic fraction is a 1:1 mixture of **1.2** and $ArN{=}C(CD_3)(CD_2H)$. Methyllithium deprotonates **1.1** to the extent of about 50% under these conditions; the aqueous quench regenerates the imine. The deuterium isotope effect

References begin on page 81

significantly slows this competing side reaction relative to the unlabeled material, where the yield of the desired addition product is only 9%. The undesired imine is chemically converted back to 3,5-dimethylaniline by the addition of strong aqueous acid, and the two amines are then separated on an alumina column. Complex **1.2** is recovered from the aqueous phase by extraction, and isolated in yields of 40 to 60%.

Deprotonation of **1.2** is straightforward. Addition of *n*-butyllithium to a cold solution of the amine results in a viscous yellow oil after solvent evaporation, but the addition of ether precipitates a fine white microcrystalline powder. An X-ray crystal structure of Et_2O·LiN[R]Ar (**1.3**) confirms the dimeric nature of the product shown in Scheme 1.1.[64]

(ii) HN[R]Ar$_F$[54]

The related ligand, originally prepared by Stokes, having a 2-fluoro-5-methyl substituted aryl group, is prepared similarly to **1.1**, but starting instead with 2-fluoro-5-methylaniline.[54] $Ar_FN{=}C(CD_3)_2$ (**1.4**) is isolated in 73% yield. The methylation step to generate HN[R]Ar$_F$ (**1.5**) proceeds smoothly, in 87% yield, without the formation of any deprotonated enamine. As deuterium is not required for good yields of the methylated product (the synthesis of the fully protiated derivative, HN[*t*-Bu]Ph, is also straightforward and high yielding) this is most likely a result of the reduced electron density at nitrogen due to the ortho fluorine.[45,65] Deprotonation of **1.5** with *n*-butyllithium followed by the addition of ether forms Et_2O·LiN[R]Ar$_F$ (**1.6**) in 73% yield.

(iii) HN[R$_{ph}$]Ar

A third ligand, with significantly increased steric bulk, is prepared by addition of phenyllithium to imine **1.1**. There are no appreciable side products observed in this reaction, and the desired aniline, HN[R$_{ph}$]Ar (**1.7**), is isolated in 74% yield after an

References begin on page 81

aqueous quench. Deprotonation of the aniline with *n*-butyllithium followed by the addition of ether affords $Et_2O{\cdot}LiN[R_{ph}]Ar$ (**1.8**) in 42% yield.

These three anilide ligands are used in metathesis reactions on the $Ti(NMe_2)_xCl_{4-x}$ nucleus to generate most of the complexes discussed in this chapter. Their use offers the ability for rational steric and electronic tuning of the titanium center due to the different steric and electronic profiles of the ligands. Two bulky alkoxide ligands are also used: 2,6-di-*iso*-propylphenoxide (OAr') and 2,6-di-*tert*-butylphenoxide (OAr''). For quick reference, the five ligands and their abbreviations are shown in Figure 1.1.

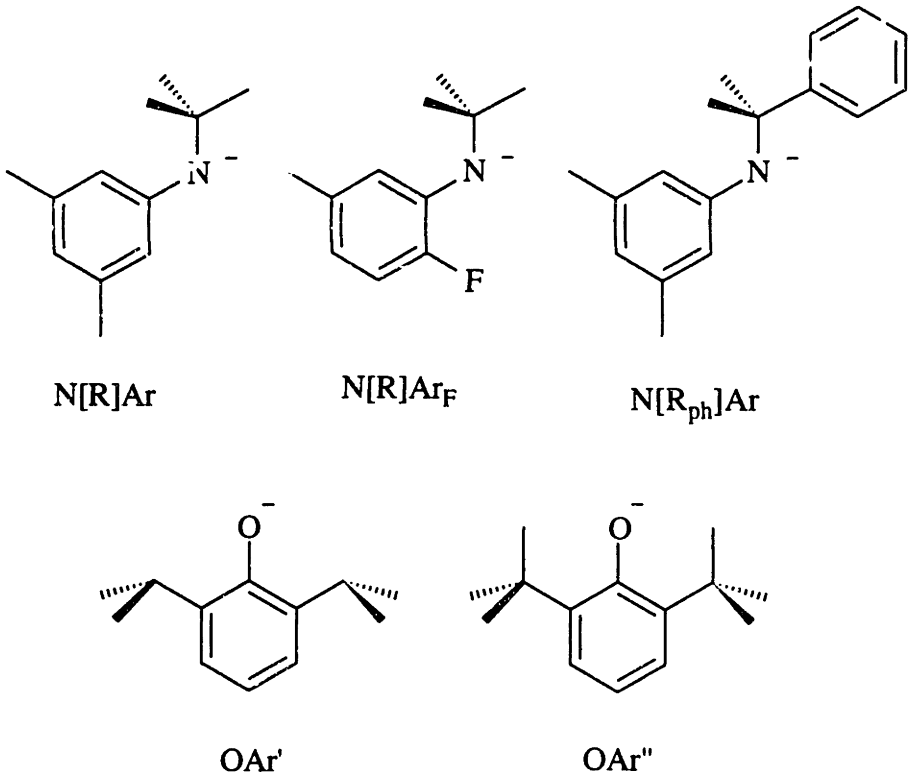

Figure 1.1: The Ligands used for Stabilization of Titanium Complexes

References begin on page 81

Section 1.3: Ti(IV) Complexes with N[R]Ar

(i) Attempted Synthesis of $TiCl_2(N[R]Ar)_2$

$ClTi(N[R]Ar)_3$ is prepared from $TiCl_4(THF)_2$[66] and three equivalents of lithium amide **1.3**.[58] Reduction of the chloride in benzene forms the homoleptic Ti(III) species $Ti(N[R]Ar)_3$ in good yield.[55] In order to allow for alkyl group incorporation on titanium prior to reduction, the dihalide complex $TiCl_2(N[R]Ar)_2$ is a reasonable initial synthetic goal. Treating $TiCl_4(THF)_2$ with two equivalents of **1.3** forms a blood red solution, but analysis of the reaction mixture by ^1H NMR spectroscopy shows both significant side product formation and decomposition. There is evidence for the oversubstituted product $ClTi(N[R]Ar)_3$, which may also arise through a ligand-swapping reaction similar to the conproportionation chemistry that is known for other titanium amides.[67] The dichloride only crystallizes from the crude reaction mixture in very low yield and it has not been possible to separate it from the side products. The dichloride (**1.31**) is prepared by a substantially different route as discussed in Section 1.8. The presence of extra, potentially reducible or substitutable halides in the starting tetrachloride complex does not allow for selective addition of only two anilide groups, but instead suggests the use of a protecting group strategy.

(ii) Synthesis of $TiI_2(N[R]Ar)_2$ (1.10)

It is quite easy to prepare the dichloride complex $TiCl_2(NMe_2)_2$ by conproportionation of $TiCl_4$ and $Ti(NMe_2)_4$ in hexane at elevated temperature.[67] Treating this complex with two equivalents of **1.3** in ether forms the mixed tetraamide species $Ti(NMe_2)_2(N[R]Ar)_2$ (**1.9**) as shown in Scheme 1.2. Using dimethylamide groups as place holders prevents oversubstitution by the N[R]Ar ligand. This oily complex is not isolated or purified, but excess methyl iodide reacts with the dimethylamide groups over a 40 hour period, quaternizing them to $[NMe_4]I$. Methyl iodide does not react with the

References begin on page 81

remaining N[R]Ar ligands under these conditions, and the dark brown crystalline complex $TiI_2(N[R]Ar)_2$ (**1.10**) is isolated in 60% yield. The *ortho* and *para* resonances in the ^1H NMR spectrum, which appear at 7.07 and 6.86 ppm, are good spectroscopic handles for monitoring reactions involving the N[R]Ar ligand. Me_3SiI has been used similarly to remove dimethylamido groups from molybdenum and tungsten.[68] With a dihalide complex prepared, the next goal is the selective monoalkylation of the species, leaving one iodide which can be removed by reduction.

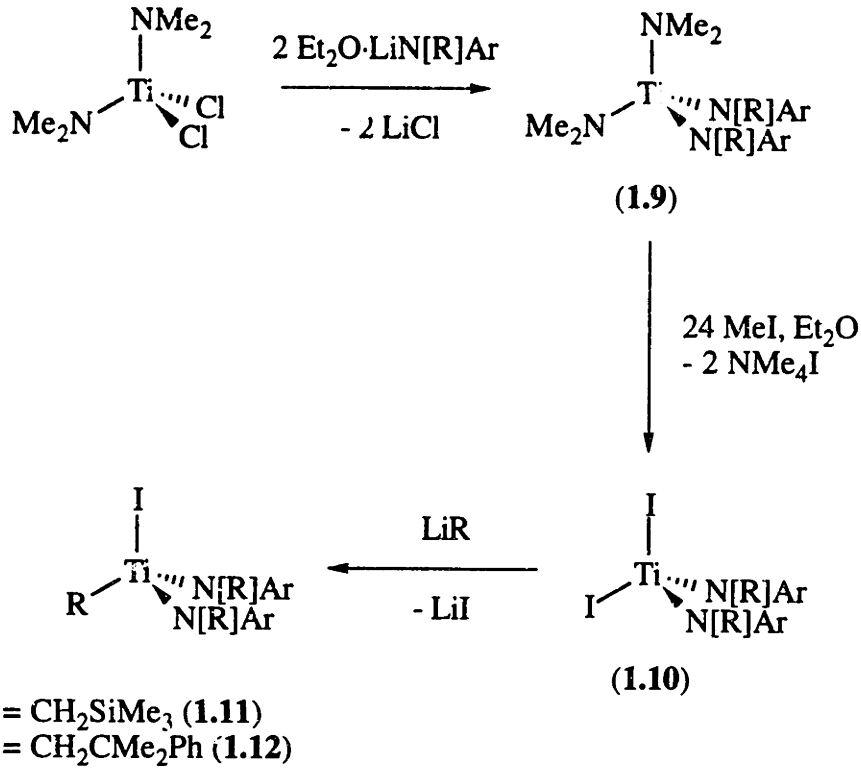

R = CH_2SiMe_3 (**1.11**)
R = CH_2CMe_2Ph (**1.12**)

Scheme 1.2: Synthesis and Reactivity of $TiI_2(N[R]Ar)_2$

(iii) Alkylation of 1.10

A strong alkylating reagent is required to derivatize diiodide **1.10**, as it does not react cleanly or at all with Grignard or dialkylmagnesium reagents. Attempted alkylation with neopentyllithium causes the rapid appearance of a short lived green color, followed by

References begin on page 81

decomposition as monitored by ^{1}H NMR spectroscopy. The green color is reminiscent of $Ti(N[R]Ar)_3$, suggesting reduction. However, the resulting complex "$Ti(N[R]Ar)_2I$" could readily disproportionate or dimerize, and is not expected to be stable. Reduction of the diiodide **1.10** with sodium amalgam in benzene forms sodium iodide, but no green color is observed. Analysis of the crude reaction mixture by ^{1}H NMR spectroscopy shows at least three unknown, diamagnetic products.

Trimethylsilylmethyllithium reacts cleanly with **1.10** in a cold ether solution, forming the alkyl complex $Ti(N[R]Ar)_2(I)(CH_2SiMe_3)$ (**1.11**). However, the complex is oily, preventing isolation or purification of the dark red material. ^{1}H NMR spectroscopy shows the material to be fairly pure, contaminated with a small amount of free aniline **1.2**. The *para* and *ortho* proton NMR resonances appear at 7.00 and 6.83 ppm respectively, and there is a 1:2 ratio of alkyl to anilide, suggesting that monoalkylation occurs selectively. Reduction of the crude material with sodium amalgam in benzene, as in the preparation of $Ti(N[R]Ar)_3$, causes the formation of sodium iodide, but no green color is observed. A ^{2}H NMR spectrum does not show any resonances around 4 ppm, the region expected for a Ti(III) complex. Reducing the complex with sodium amalgam in THF causes a vivid olive green color to appear, but this color fades rapidly to brown. Proton NMR spectroscopy of the crude material shows at least five products.

Complex **1.10** also reacts with $LiCH_2CMe_2Ph$ (neophyl lithium) in a cold ether solution generating the alkyl complex $Ti(N[R]Ar)_2(I)(CH_2CMe_2Ph)$ (**1.12**). The *ortho* and *para* proton resonances appear at 7.15 and 7.11 ppm respectively, and again the monoalkylation product is generated selectively. However, this complex is also a dark red oil like **1.11**, preventing purification. Similar disappointing results are obtained when **1.12** is treated with sodium amalgam in benzene: no paramagnetic products are observed although sodium iodide is formed. These results suggest that, although reduction of a Ti(IV) alkyl halide complex is thermodynamically feasible, either steric or electronic tuning is required in order to make an isolable Ti(III) alkyl complex.

References begin on page 81

Section 1.4: Ti(IV) Complexes with N[R]Ar$_F$

The instability of Ti(III) alkyl complexes generated with the N[R]Ar ligand could be due to the strong electron donating properties of the anilide ligand on the reduced metal center. The 2-fluoro-5-methyl anilide derivative (N[R]Ar$_F$) should be more electron withdrawing due to the ortho fluorine. Additionally, complexes with this ligand are typically more crystalline and therefore easier to isolate and purify.[65] Both the enhanced crystallinity and the altered electronic environment are apparent when attempting to duplicate the synthesis of diiodide **1.10** with the N[R]Ar$_F$ ligand.

(i) Synthesis of Ti(N[R]Ar$_F$)$_2$(I)(NMe$_2$) (1.14)

Dichloride $TiCl_2(NMe_2)_2$ reacts with two equivalents of $Et_2O{\cdot}LiN[R]Ar_F$ (**1.6**) in a chilled ether solution, forming $Ti(N[R]Ar_F)_2(NMe_2)_2$ (**1.13**) as a dark yellow crystalline solid (Scheme 1.3). This complex is significantly more crystalline than the N[R]Ar derivative **1.9**. Although there is no longer a clear spectroscopic handle as with the *ortho* and *para* protons in the N[R]Ar ligand, the reactions depicted in Scheme 1.3 are readily monitored by ^{1}H NMR spectroscopy by observing the dimethylamide resonance, which appears at 3.075 ppm in **1.13**.

The mixed tetraamide **1.13** reacts with methyl iodide in a manner analogous to that observed for **1.9**. Addition of 10 equivalents of methyl iodide to **1.13** causes a slow color change to bright red over a period of 18 hours. The $[NMe_4]I$ is removed by filtration, and the product is purified by crystallization from ether. Proton NMR spectroscopy shows a dimethylamide group with a resonance at 3.057 ppm in a one to two ratio with the N[R]Ar$_F$ ligands, showing that the product $Ti(N[R]Ar_F)_2(I)(NMe_2)$ (**1.14**) is only monosubstituted. Suitable conditions for synthesis of the diiodide complex have not been found. This result makes sense from an electronic standpoint. The ortho fluorine substituent, through an inductive electron withdrawing effect, makes the titanium center more electrophilic, thereby increasing Ti-N π interactions. With a decreased lone pair

References begin on page 81

density on the dimethylamide nitrogen, it is less nucleophilic, and less likely to react with methyl iodide. When the first dimethylamide is replaced with an iodide, the remaining dimethylamide has an even stronger Ti-N π interaction, rendering the lone pair unavailable for subsequent reaction. This suggests that the N[R]Ar_F ligand behaves as desired; the electron withdrawing ligand should help stabilize the Ti(III) oxidation state.

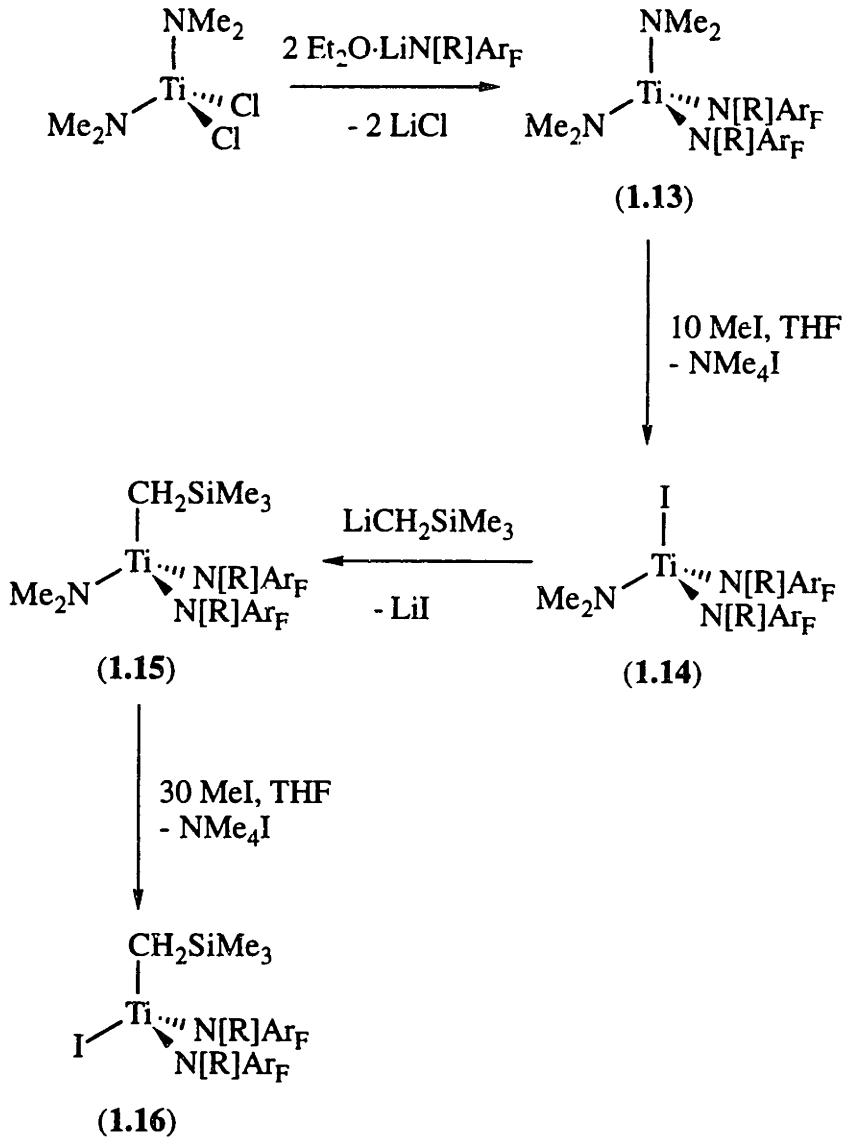

Scheme 1.3: Ti(IV) Complexes with the N[R]Ar_F Ligand

References begin on page 81

(ii) Alkylation of 1.14

Complex **1.14** reacts cleanly with one equivalent of $LiCH_2SiMe_3$ in a chilled pentane solution. After removing lithium iodide by filtration, the mustard yellow alkyl complex $Ti(N[R]Ar_F)_2(CH_2SiMe_3)(NMe_2)$ (**1.15**) crystallizes in 70% yield from pentane. The dimethylamide resonance appears at 3.08 ppm in the ^1H NMR spectrum of **1.15**.

It is possible to remove the remaining dimethylamide group from **1.15** using the methyl iodide reaction, but the choice of solvent is important. Although the reaction does proceed slightly in ether, it is much faster and goes to completion in THF. A large excess of methyl iodide is also required. The substitution of the iodide in **1.14** for the alkyl in **1.15** increases the electron density on titanium, decreases the Ti-N π interaction, and allows for cleavage of the dimethylamide. The iodide complex, $Ti(N[R]Ar_F)_2(I)(CH_2SiMe_3)$ (**1.16**), is isolated as a thick orange-red oil which resists crystallization. The corresponding alkylation of **1.14** with neophyllithium proceeds to give an impure oily compound, and the reaction of this mixture with methyl iodide does not lead to isolable products.

Reduction of the impure alkyl complex **1.16** with sodium amalgam in toluene darkens the solution to deep brown. Analysis of the crude reaction mixture by ^2H NMR spectroscopy shows only small amounts of paramagnetic material. Reduction of the complex in DME gives similar results. The dimethylamide iodide complex **1.14** also does not react cleanly with sodium amalgam in benzene. Proton NMR analysis of the crude reaction mixture shows significant decomposition. No diagnostic green color is ever observed when complexes with the $N[R]Ar_F$ ligand are reduced, suggesting that the ortho fluorine is incompatible with the reactive metal center. There is additional evidence to support this conclusion. Although $ClTi(N[R]Ar_F)_3$ can be made, reduction of the complex with sodium amalgam leads to marked decomposition.[57] Attempts to synthesize $Mo(N[R]Ar_F)_3$ (which is never observed) from $MoCl_3(THF)_3$ and two equivalents of lithium amide **1.6**, by analogy to the preparation of $Mo(N[R]Ar)_3$, result in the formation

References begin on page 81

of the orthometallated Mo(IV) complex shown in Figure 1.2.[69] The incompatibility of an ortho fluorine with Ti(III) is not surprising in retrospect, as $Ti(N[R]Ar)_3$ is known to be a powerful halogen atom abstractor.[56,57] $Ti(N[R]Ar)_3$ abstracts chlorine from chlorobenzene or chloroform, bromine from bromobenzene and iodine from iodobenzene or methyl iodide, but does not abstract fluorine from fluorobenzene. However, the $N[R]Ar_F$ ligand is known to coordinate in a bidentate fashion, with N and F donation,[54] and the proximity of the strongly electrophilic titanium center may allow the aryl fluorine to be activated in an intramolecular reaction.

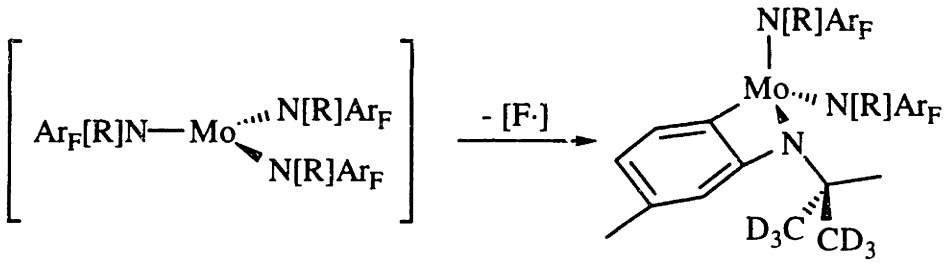

Figure 1.2: Orthometallation of the $N[R]Ar_F$ ligand in a Mo(III) complex

Section 1.5: Ti(IV) Complexes with N[R]Ar and OAr'

A way to decrease electron density at the titanium center without using a fluorinated ligand is by using aryloxide ligands. This is due both to the increased electronegativity of oxygen relative to nitrogen, and to the lower number of electron donating alkyl groups on the ligating atom. There are many examples of early transition metal complexes with *O*-donor ligands, including the three-coordinate Ti(III) complex $Ti(OAr'')_3$.[70] Clearly, 2,6-dialkyl-substituted phenoxides are capable of providing a good deal of steric protection to a metal center. However, to generate a Ti(III) complex with both an aryloxide and a less bulky alkyl substituent, substantial steric protection would be required at the remaining coordination site. Using the N[R]Ar ligand in conjunction with 2,6-di-*iso*-propylphenoxide (OAr') should provide enough steric protection to support titanium alkyl

References begin on page 81

complexes. In related work, Rothwell has synthesized titanium complexes with bulky aryloxide ligands and dimethylamide ligands.[24]

(i) Synthesis of Ti(N[R]Ar)(OAr')$(I)_2$ (1.19)

$TiCl(NMe_2)_3$ is prepared similarly to $TiCl_2(NMe_2)_2$ by conproportionation of $TiCl_4$ and $Ti(NMe_2)_4$ in the appropriate ratio.[67] Treating the monochloride with one equivalent of lithium amide **1.3** in ether leads to rapid substitution and a color change to green-brown. The mixed tetraamide complex Ti(N[R]Ar)$(NMe_2)_3$ (**1.17**) is a mobile brown oil, but the synthetic transformation is clean according to ^1H NMR spectroscopy (Scheme 1.4). The *para* and *ortho* hydrogen resonances appear at 6.65 and 6.58 ppm respectively, while the dimethylamido resonance appears at 2.91 ppm. A single dimethylamide group is selectively cleaved by adding one equivalent of 2,6-di-*iso*-propylphenol to **1.17** in ether; the dimethylamine side product simply evaporates away. There is no obvious color change, and Ti(N[R]Ar)(OAr')$(NMe_2)_2$ (**1.18**) is obtained as a thick dark brown oil after removing the solvent. Again, ^1H NMR spectroscopy shows that the transformation is clean and essentially quantitative. The ligand *para* and *ortho* resonances appear at 6.68 and 6.59 ppm, while the resonance corresponding to the two remaining dimethylamide groups has shifted downfield to 3.04 ppm, suggesting a reduced electron density on titanium. The two remaining dimethylamide groups are removed using the standard deprotection protocol by dissolving **1.18** in THF, adding 10 equivalents of methyl iodide and stirring at room temperature for nine hours. The deep red diiodide Ti(N[R]Ar)(OAr')$(I)_2$ (**1.19**) crystallizes from ether in 65% overall yield from the starting tris-dimethylamide complex.

(ii) Alkylation of 1.19

Complex **1.19** is alkylated with $LiCH_2SiMe_3$ in chilled hexane, causing a rapid color change to light orange and the formation of a white precipitate. Although the reaction appears quantitative and clean by ^1H NMR spectroscopy, it has not been possible to

References begin on page 81

crystallize the material due to its extreme solubility in hydrocarbon solvents. The ^{1}H NMR spectrum is consistent with the proposed chiral-at-metal Ti(IV) complex Ti(N[R]Ar)(OAr')(CH_2SiMe_3)(I) (**1.20**); the diastereotopic methylene group appears as a doublet of doublets at 2.24 and 1.22 ppm, and the diastereotopic *iso*-propyl methyl groups appear as a doublet of doublets at 1.38 and 1.22 ppm.

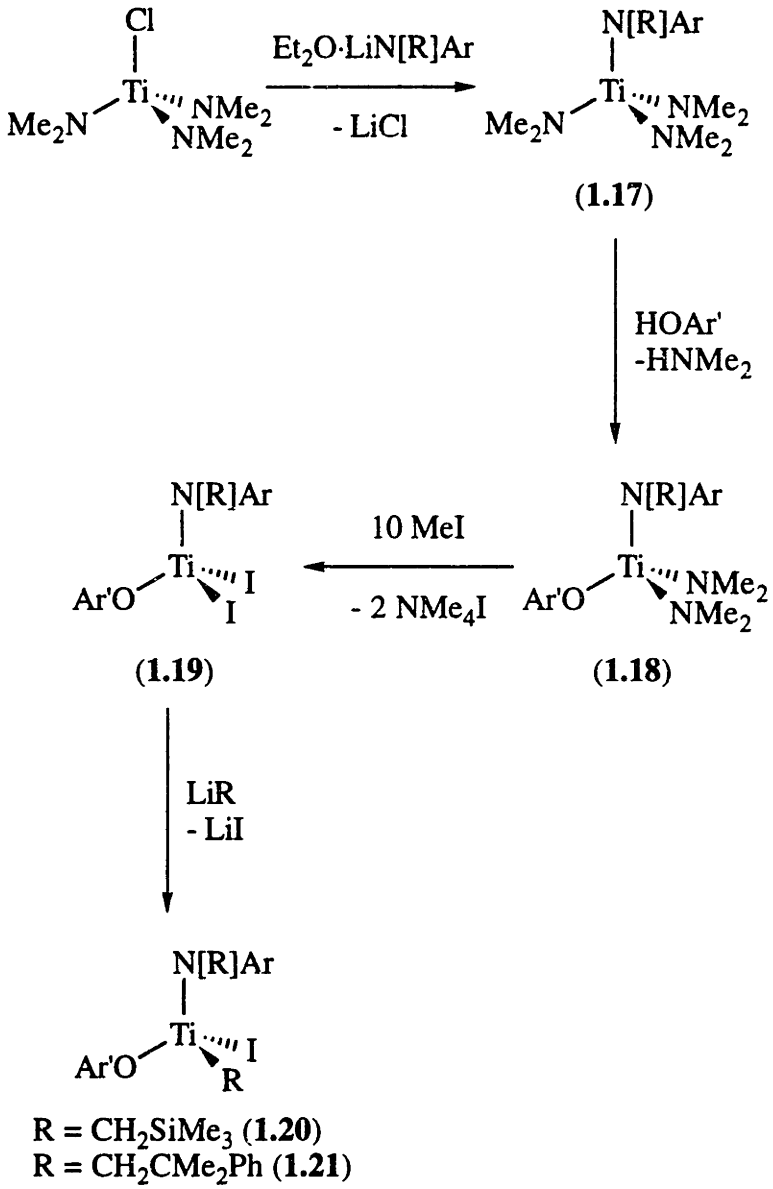

Scheme 1.4: Synthesis of Chiral-at-Metal Ti(IV) Complexes

References begin on page 81

The corresponding neophyl complex, Ti(N[R]Ar)(OAr')(CH_2CMe_2Ph)(I) (**1.21**) is prepared by adding $LiCH_2CMe_2Ph$ to a chilled solution of **1.19** in hexane. Proton NMR spectroscopy again shows the reaction to be clean and essentially quantitative, but the alkyl complex is isolated in only 49% yield by crystallization from pentane due to the extreme hydrocarbon solubility of the complex. Complex **1.21** also exhibits diastereotopic resonances in the ^1H NMR spectrum: the methylene protons appear as two doublets at 2.35 and 2.07 ppm, the *iso*-propyl methyls appear as two doublets at 1.36 and 1.21 ppm, and the neophyl methyls appear as two singlets at 1.32 and 1.24 ppm.

The results obtained with complexes **1.11** and **1.12** suggest carrying out reductions in a polar, coordinating solvent in order to increase the rate. Other researchers have observed that reductions in non-coordinating solvents lead to decomposition or disproportionation reactions.[28,71] Both alkyl complexes **1.20** and **1.21** are reduced with sodium amalgam in either THF or DME, causing a color change to olive green over a 10 minute period. Deuterium NMR analysis of the reaction mixture shows a resonance at 4.6 ppm which rapidly decreases in area; after one hour at room temperature the reaction solution is brown and ^2H NMR spectroscopy shows only resonances in the diamagnetic region. The reduced species have a longer lifetime than those observed in complexes without aryloxide ligation, but they are still too unstable to be isolated. It is possible to store solutions of the green material for several hours at -35 °C, but they gradually become murky brown and ^1H NMR spectra indicate significant decomposition.

$Ti(N[R]Ar)_3$ reacts with $NMo(O\text{-}t\text{-}Bu)_3$ at room temperature, forming the "titanoxy" species $NMo(O\text{-}t\text{-}Bu)_2\{OTi(N[R]Ar)_3\}$ with expulsion of a *tert*-butyl radical.[53] A Ti(III) alkyl complex should react similarly, suggesting a means of characterizing the reduced species by trapping it with the molybdenum complex. Reducing complex **1.20** with sodium amalgam in DME forms a green solution, but after $NMo(O\text{-}t\text{-}Bu)_3$ is added, analysis of the crude material by ^1H NMR spectroscopy is disappointing. There are no resonances due to the $SiMe_3$ fragment, suggesting that the alkyl group has been lost,

References begin on page 81

presumably as TMS. The spectrum is messy, suggesting that decomposition rather than addition to the Mo-O linkage is the primary reaction pathway. The neophyl derivative **1.21** behaves similarly under these conditions.

Section 1.6: Ti(IV) Complexes with N[R_{ph}]Ar and OAr"

The paramagnetic green Ti(III) materials are slightly longer lived with aryloxide ligation, but still decompose rapidly, precluding their isolation or characterization. Although the mode of decomposition of the reduced species is unknown, larger ligands would help prevent intermolecular pathways. The chemistry described in this section uses the bulkier amide N[R_{ph}]Ar and the bulkier aryloxide 2,6-di-*tert*-butylphenoxide (OAr").

(i) Synthesis of Ti(N[R_{ph}]Ar)(OAr")(I)(NMe_2) (1.24)

Treating $TiCl(NMe_2)_3$ with $Et_2O{\cdot}LiN[R_{ph}]Ar$ (**1.8**) in THF forms a greenish brown solution. After rigorous solvent removal by repeated lyophylization from benzene, $Ti(N[R_{ph}]Ar)(NMe_2)_3$ (**1.22**) is isolated as a greenish-brown powder in 83% yield (Scheme 1.5). The dimethylamide resonance in the proton NMR spectrum appears at 2.77 ppm, while the resonance of the aryl methyls of the N[R_{ph}]Ar ligand appears at 1.88 ppm. The phenyl substituent on the N[R_{ph}]Ar ligand gives better crystallinity properties to the mixed tetraamide complex as compared to the N[R]Ar derivative **1.17**.

Complex **1.22** reacts with 2,6-di-*tert*-butylphenol in a manner analogous to that in the preparation of **1.18**, causing a color change to reddish orange after about three hours. The reaction is slow as determined by ^1H NMR spectroscopic monitoring, and requires approximately 20 hours for complete substitution. $Ti(N[R_{ph}]Ar)(OAr")(NMe_2)_2$ (**1.23**) is obtained in 83% yield as an orange powder. The dimethylamide resonance at 3.02 ppm in the ^1H NMR spectrum is shifted downfield relative to that in **1.22**, while the aryl methyl resonance appears at 1.91 ppm. The NMR data are consistent with monosubstitution on titanium with the aryloxide ligand.

References begin on page 81

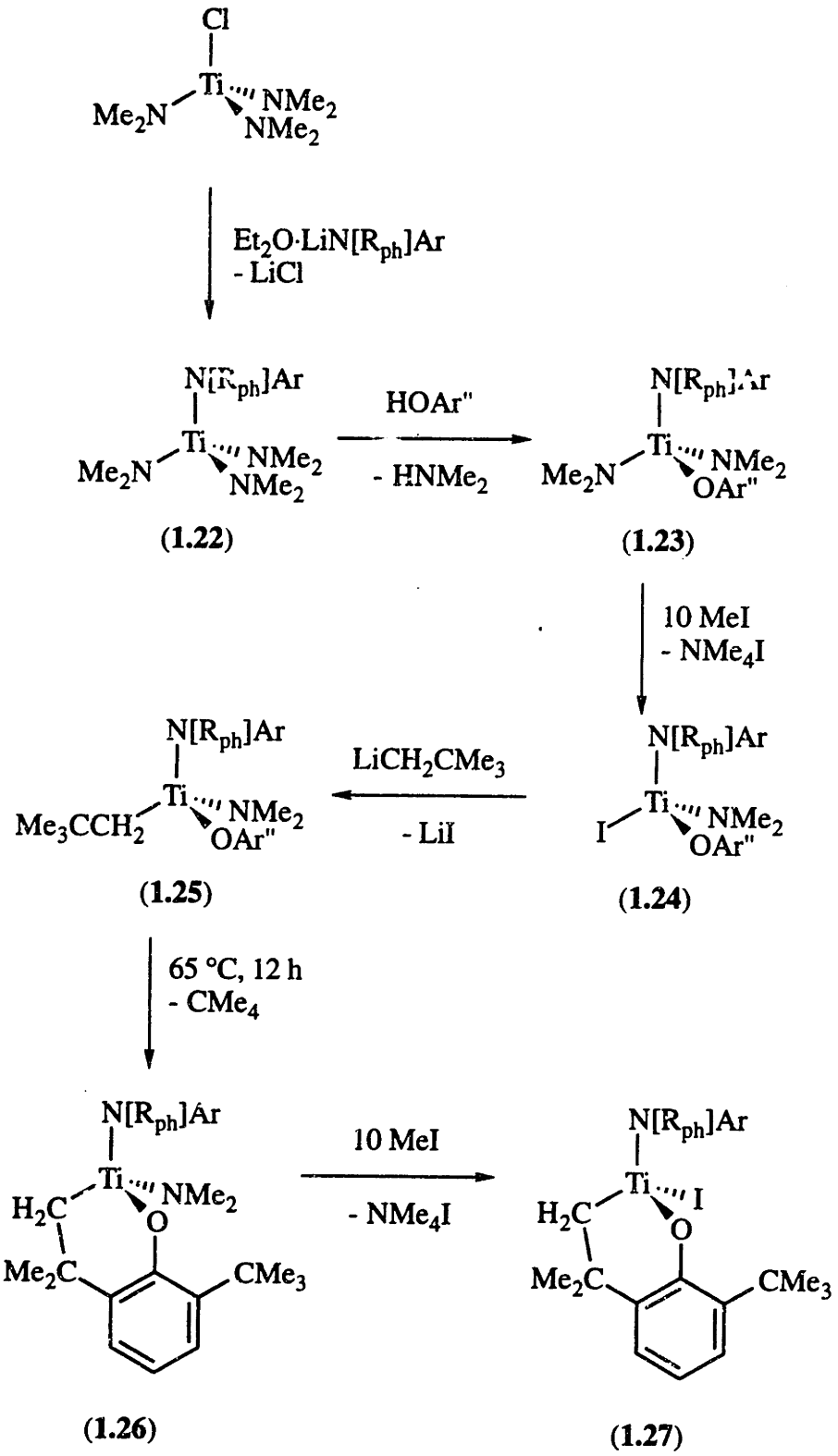

Scheme 1.5: Cyclometallation of a 2,6-di-*tert*-Butylphenoxide Ligand

References begin on page 81

Cleaving a dimethylamide from complex **1.23** with methyl iodide at room temperature is straightforward but sluggish. 10 equivalents over an 18 hour period results in essentially no conversion, but with a large excess of methyl iodide the reaction goes to completion in about 48 hours, generating Ti(N[R_{ph}]Ar)(OAr")(I)(NMe_2) (**1.24**) in 95% isolated yield. The complex is obtained as an orange microcrystalline powder from a chilled pentane solution. The dimethylamide resonance appears at 2.86 ppm in the ^{1}H NMR spectrum, while the aryl methyl resonance is found at 2.18 ppm. It is not possible to remove the dimethylamide group from **1.24** using methyl iodide at room temperature, and attempts to do so by extended thermolysis result in significant decomposition. Apparently the substitution of phenyl for methyl in the N[R_{ph}]Ar ligand leads to enhanced electrophilicity at titanium, strengthening the Ti-N π interaction to the dimethylamide. Complex **1.24** is reduced with sodium amalgam, but no green color is observed and a ^{2}H NMR spectrum shows only diamagnetic materials.

(ii) Cyclometallation of OAr"

Complex **1.24** is readily alkylated with neopentyllithium in a chilled pentane/ether solution. The color of the complex changes from red to yellow after five minutes, and monitoring by proton NMR spectroscopy indicates a clean conversion. However, it has not been possible to isolate this material as a crystalline solid. As the complex, presumed to be Ti(N[R_{ph}]Ar)(OAr")(CH_2CMe_3)(NMe_2) (**1.25**), retains a dimethylamide functionality, the methyl iodide deprotection protocol should effect an amide for iodide replacement, which would be expected to yield a more crystalline complex. However, when this is attempted, no reaction is observed by ^{1}H NMR spectroscopy at room temperature in either ether or THF after several days. Heating the reaction mixture in a sealed reaction bomb results in significant decomposition. The major product crystallizes from the crude reaction mixture in low yield, and its ^{1}H NMR spectrum is indicative of

References begin on page 81

C-H bond activation of one of the *tert*-butyl groups on the phenoxide ligand with loss of the alkyl group. Cyclometallation of the OAr" ligand has been reported by Rothwell.[72-74]

The cyclometallation of **1.25** is much cleaner when methyl iodide is omitted from the thermolysis reaction. Simply heating the complex at 65 °C in THF for several hours causes the loss of the neopentyl group, presumably as neopentane, and C-H bond activation of one aryloxide *tert*-butyl group, cleanly forming the cyclometallated complex $Ti(N[R_{ph}]Ar)(O\text{-}2,6\text{-}C_6H_3[CMe_3][CH_2CMe_2\text{-}])(NMe_2)$ (**1.26**). The oily complex has not been purified for full characterization. Removing the dimethylamide group from **1.26** is accomplished by adding 10 equivalents of methyl iodide and heating at 70 °C for 21 hours. Although there is no color change, $[NMe_4]I$ is observed and no dimethylamide resonance is observed in the ^1H NMR spectrum of the product. Yellow-orange crystals of $Ti(N[R_{ph}]Ar)(O\text{-}2,6\text{-}C_6H_3[CMe_3][CMe_2CH_2\text{-}])(I)$ (**1.27**) are obtained from a chilled pentane solution in 62% overall yield from **1.24** by this two-step one-pot procedure. The aryl methyl resonance appears at 2.20 ppm in the ^1H NMR spectrum. Spectroscopic confirmation of the chiral-at-metal complex is found in the diastereotopic titanium bound methylene, which displays two doublets at 1.47 and 0.83 ppm.

Complex **1.27** is a somewhat bulkier derivative of complexes **1.20** and **1.21**, although the cyclometallation of the aryloxide ligand significantly reduces the steric protection of the titanium center relative to the original design. Reducing **1.27** with sodium amalgam in ether gives rise to a persistent green color; the product exhibits a ^2H NMR signal at approximately 4 ppm. The green material has not been isolated in pure form as it is oily, and decomposes slowly even at -35 °C, preventing further characterization. This complex, which contains amide, aryloxide and alkyl ligation of Ti(III), is quite long lived though, and remains a promising candidate for further study.

Other synthetic pathways into mixed amide-aryloxide ligation of titanium alkyl complexes have not yet been successful. Titanium (IV) complexes with either N[R]Ar and

References begin on page 81

OAr" or N[R_{ph}]Ar and OAr' ligands are not well characterized as they tend to be produced as impure oils, and no further work in this area has been attempted.

Section 1.7: A Ti(III) Complex with N[R_{ph}]Ar

Electronic stabilization of short-lived Ti(III) complexes with electron withdrawing aryloxide ligands leads to significantly longer lifetimes relative to amide complexes and allows for their observation by ^{2}H NMR spectroscopy. The complexes may require more steric protection of the metal center than the single *O*-bound substituent can offer, however. Complexes analogous to **1.11** or **1.12** with the N[R_{ph}]Ar ligand would have that increased steric protection when reduced to Ti(III). Additionally, the lesser degree of substitution observed in the reaction of methyl iodide with **1.23** compared to the reaction with **1.18** suggests an electron withdrawing effect of the N[R_{ph}]Ar ligand relative to the N[R]Ar ligand. However, the reduction of transition metal complexes with alkali metals sometimes leads to decomposition of the desired reduced species through salt mediated disproportionation or other pathways.[28,71] This may be one reason why the titanium (III) complexes with the other ligand sets are not stable. A related example is seen in tungsten chemistry.[56] Reduction of $WCl_4(THF)_2$ with sodium amalgam leads to $W_2Cl_7^-$ or W_2Cl_6, depending on the conditions.[56] Repeating the reduction using the halogen abstracting reagent Ti(N[R]Ar)$_3$ allows for isolation of $WCl_3(THF)_3$. However, there would be a low thermodynamic driving force for using Ti(N[R]Ar)$_3$ to reduce a Ti(IV) alkyl complex. Therefore, it seems reasonable to start at Ti(III), removing the reduction step from the synthesis of the desired Ti(III) alkyl complex.

$TiCl_3(THF)_3$[66] reacts with two equivalents of lithium amide **1.8** in the presence of a large excess of TMEDA as shown in Scheme 1.6. The addition causes a rapid color change from bright blue to olive green. After removing the solvent, only one equivalent of lithium chloride is filtered away from the green solution. Pale green needles are obtained from a cold ether solution, and this material exhibits a broad ^{2}H NMR resonance at 4.84

References begin on page 81

ppm. Complex **1.28** is believed to have the formulation $Ti(N[R_{ph}]Ar)_2(\mu\text{-}Cl)_2Li(TMEDA)$, analogous to the structurally characterized $Ti(N[Cy]_2)_2(\mu\text{-}Cl)_2Li(TMEDA)$ which is prepared by a similar route.[39] However, if a small amount of crystallized **1.28** is treated with excess $CDCl_3$ and examined by ^1H NMR spectroscopy, three equivalents of TMEDA are observed. Rigorous evaporation of solid **1.28** causes a color change to dark brown, and significant decomposition occurs. Dark blood-red $Ti(N[R_{ph}]Ar)_2(Cl)_2$ (**1.29**) is prepared in excellent yield by dissolving **1.28** in $CHCl_3$ and filtering away one equivalent of LiCl. The complex is purified by vapor diffusion of pentane into toluene followed by crystallization at -35 °C. This complex, analogous to **1.11**, has not been investigated further.

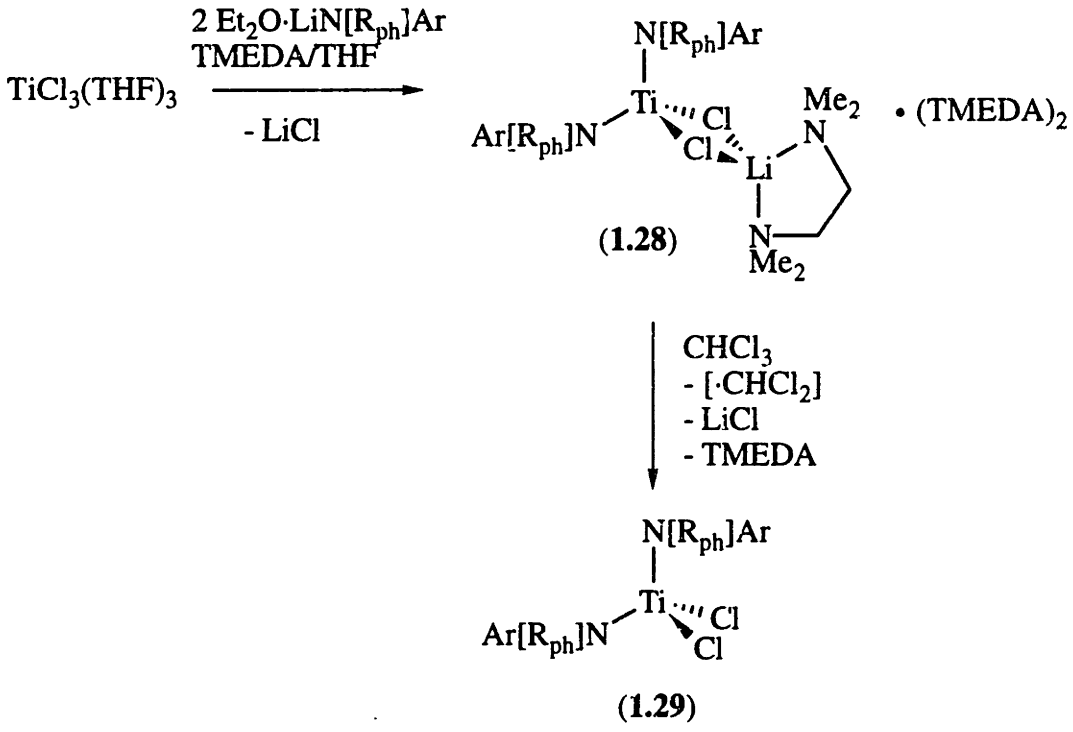

Scheme 1.6: Synthesis of $Ti(N[R_{ph}]Ar)_2Cl_2$ from the "Ate" Complex $Ti(N[R_{ph}]Ar)_2(\mu\text{-}Cl)_2Li(TMEDA)_3$

References begin on page 81

Section 1.8: A Ti(III) Alkyl Complex with N[R]Ar

(i) Synthesis of $Ti(N[R]Ar)_2(\mu\text{-}Cl)_2\cdot Li(TMEDA)$ (1.30)

The electron withdrawing ability of the $N[R_{ph}]Ar$ ligand is not required for stabilization of Ti(III) complexes using this method; the synthesis of the N[R]Ar derivative of "ate" complex **1.28** is directly analogous. Two equivalents of lithium amide **1.3** are added to a THF/TMEDA solution of $TiCl_3(THF)_3$, and bright green needles of $Ti(N[R]Ar)_2(\mu\text{-}Cl)_2\cdot Li(TMEDA)$ (**1.30**) are recovered in 57% yield by crystallization from pentane (Scheme 1.7). Complex **1.30** is well behaved in that it does not retain excess TMEDA, but is extraordinarily air and water sensitive. It, like complex **1.28**, is unstable under vacuum, turning brown, decomposing and becoming diamagnetic. It exhibits a fairly sharp ^2H NMR resonance at 3.81 ppm. A measurement of the magnetic susceptibility by the Evans method[75] gives a value of 2.22 μ_B; this value is typical for d^1 complexes obtained by this technique. SQUID magnetic susceptibility data have not been obtained due to the extreme air and moisture sensitivity of the complex. An EPR spectrum of **1.30** in toluene at room temperature shows a single feature at g = 1.95. The spectrum taken at 103 K is shown in Figure 1.3. The spectrum is approximately axial with broad linewidths (~25 G) which merge g_1 and g_2 into a single feature. The g values of 1.980, 1.964 and 1.930 are obtained by simulation of the spectrum.[76] The elemental analysis results deviate slightly from the calculated values, most likely due to the partial incorporation of THF for TMEDA in the solvation sphere around lithium. The stoichiometry of the complex is verified by treating a small sample of **1.30** with $CDCl_3$. Only a single equivalent of TMEDA is observed in the ^1H NMR spectrum.

References begin on page 81

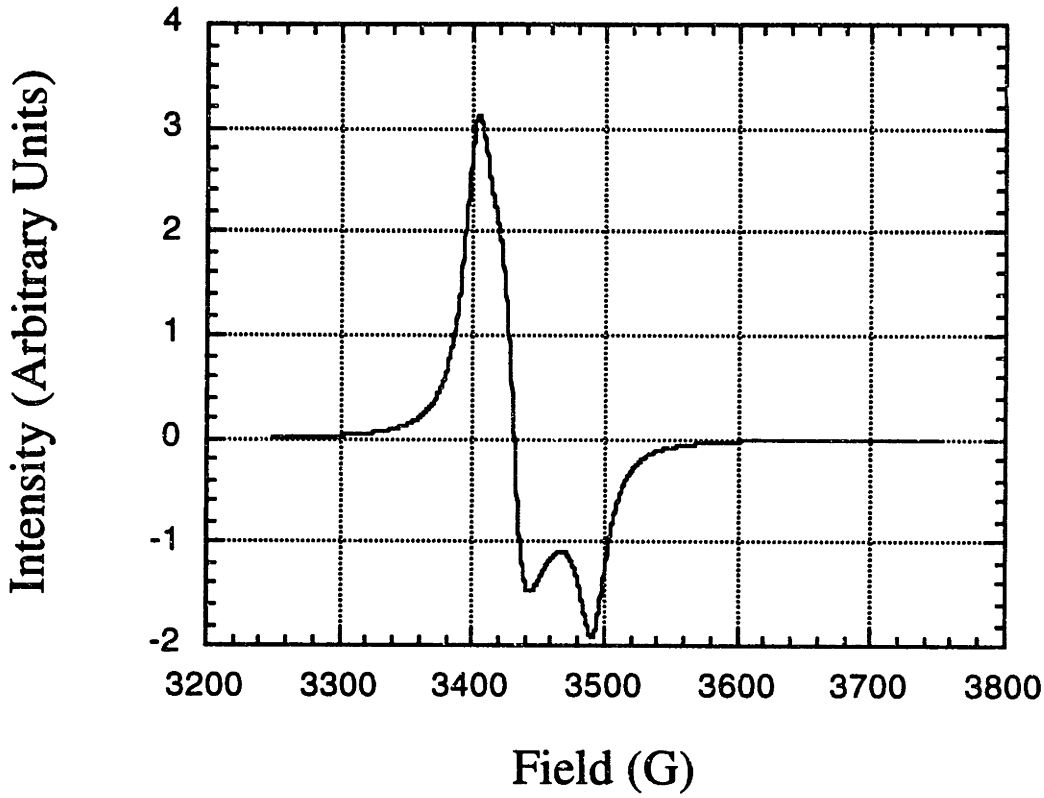

Figure 1.3: EPR spectrum (103 K, toluene) of $Ti(N[R]Ar)_2(\mu\text{-}Cl)_2Li(TMEDA)$ (**1.30**) with g_1 = 1.980, g_2 = 1.964, g_3 = 1.930.

References begin on page 81

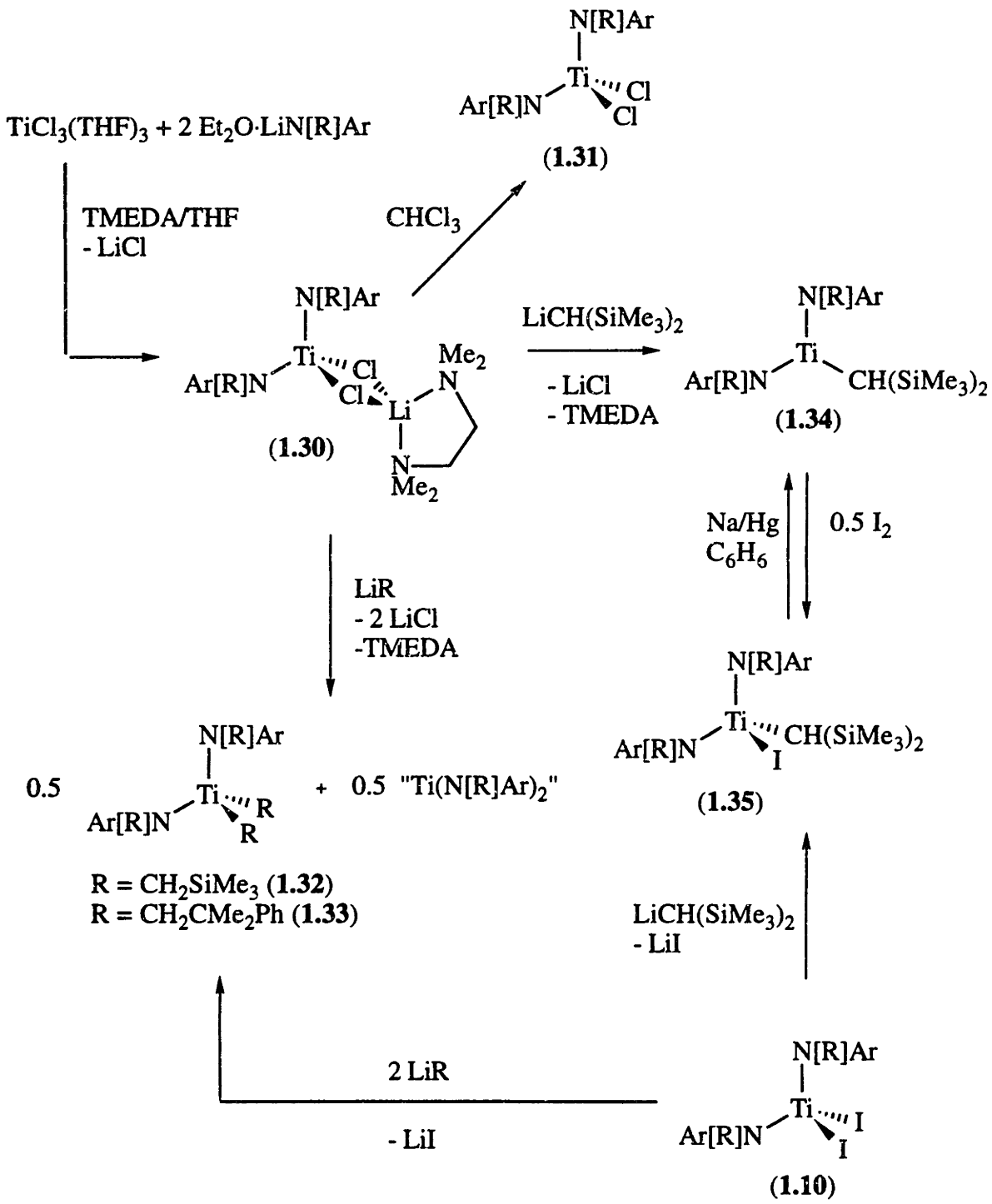

Scheme 1.7: Synthesis of the Stable Ti(III) Alkyl Complex $Ti(N[R]Ar)_2(CH[SiMe_3]_2)$

References begin on page 81

Complex **1.30** reacts with an excess of chloroform, liberating one equivalent of LiCl and generating the dichloride complex $Ti(N[R]Ar)_2(Cl)_2$ (**1.31**), directly analogous to complexes **1.29** and **1.10**. The original preparation of **1.31** from $TiCl_4(THF)_2$, which is not synthetically viable, is described in detail in Section 1.3.

(ii) Alkylation of 1.30

The alkylation of **1.30** with standard alkylating agents is not straightforward. Addition of one equivalent of $LiCH_2SiMe_3$ to a chilled pentane solution of the "ate" complex results in clean conversion to a single diamagnetic product which shows a one to one ratio of ligand to alkyl resonances in the ^1H NMR spectrum. Two equivalents of lithium chloride are recovered from the reaction mixture. If diiodide **1.10** is treated with two equivalents of $LiCH_2SiMe_3$, a lightening of the solution to yellow is observed over the course of one hour, and lithium iodide is formed. An orange-yellow oily solid that is isolated from the reaction mixture in high yield has ^1H NMR resonances which correspond to the product of **1.30** with one equivalent of the alkyllithium reagent. The complex is therefore formulated as $Ti(N[R]Ar)_2(CH_2SiMe_3)_2$ (**1.32**). A similar oily product, the dark brown $Ti(N[R]Ar)_2(CH_2CMe_2Ph)_2$ (**1.34**), is obtained upon alkylation of either **1.10** with two equivalents of $LiCH_2CMe_2Ph$ or **1.30** with one equivalent; the NMR spectra are identical for both sets of conditions. These findings are in line with related work which uses the $N(Cy)_2$ ligand; alkylation of $Ti(N[Cy]_2)(\mu\text{-}Cl)_2Li(TMEDA)$ with $LiCH_2SiMe_3$ results in disproportionation to the Ti(IV) dialkyl and an unknown Ti(II) species.[77] As with these results, the fate of the $Ti(N[R]Ar)_2$ fragment which forms during the alkylation of **1.30** is not known.

(iii) Synthesis of $Ti(N[R]Ar)_2(CH[SiMe_3]_2)$ (1.34)

Clearly, extremely bulky ligands would be required to shut down this supposed disproportionation pathway for standard alkyl groups. However, the bulky alkyl group

References begin on page 81

$CH(SiMe_3)_2$, which has a similar steric profile to the amide $N(SiMe_3)_2$, also offers a good deal of steric protection to the metal center; $Ti(CH[SiMe_3]_2)_3$ is quite stable.[78,79] Treating **1.30** with $LiCH(SiMe_3)_2$ causes a color change to deep green, and two equivalents of LiCl are recovered. The resulting complex, $Ti(N[R]Ar)_2(CH[SiMe_3]_2)$ (**1.34**), is isolated in good yield as a dark green crystalline solid. This complex is extremely halogen, moisture and air sensitive, has a fairly sharp ^2H NMR resonance at 3.97 ppm, and the Evans method[75] magnetic susceptibility measurement gives a value of 2.21 μ_B for the magnetic moment. The SQUID magnetic susceptibility data for **1.34** from 5 to 300 K and a fit to the Curie-Weiss law (μ = 1.66 μ_B; θ = -0.19 K) are shown in Figure 1.4. The data indicate simple paramagnetic behavior over the entire temperature range. An EPR spectrum of **1.34** in toluene at room temperature has an isotropic g value of 1.95; the spectrum taken at 95 K (Figure 1.5) is axial, with the g values of 1.997, 1.962 and 1.918 obtained through simulation of the spectrum.[76]

An X-ray diffraction study performed on a suitable crystal confirms the three-coordinate nature of the alkyl complex. Tables 1.1 and 1.2 give selected bond lengths and angles and Table 1.3 lists the positional parameters and B(eq). An ORTEP diagram of the structure is shown in Figure 1.6. One anilide ligand is engaged in an η^3 interaction of N2, C21 and C26 with the titanium center, reminiscent of that type of interaction in some benzyl complexes. The Ti-N2 bond length is increased by 0.045 Å relative to the Ti-N1 distance. The bond alternation that is observed in the aromatic ring in the anilide containing N2 is typical for complexes with semi-localized π electrons. The structure is similar to that observed for $Ti(N[R]Ar)_3$, where two of the three anilide ligands are coordinated in an η^3 manner.[55]

References begin on page 81

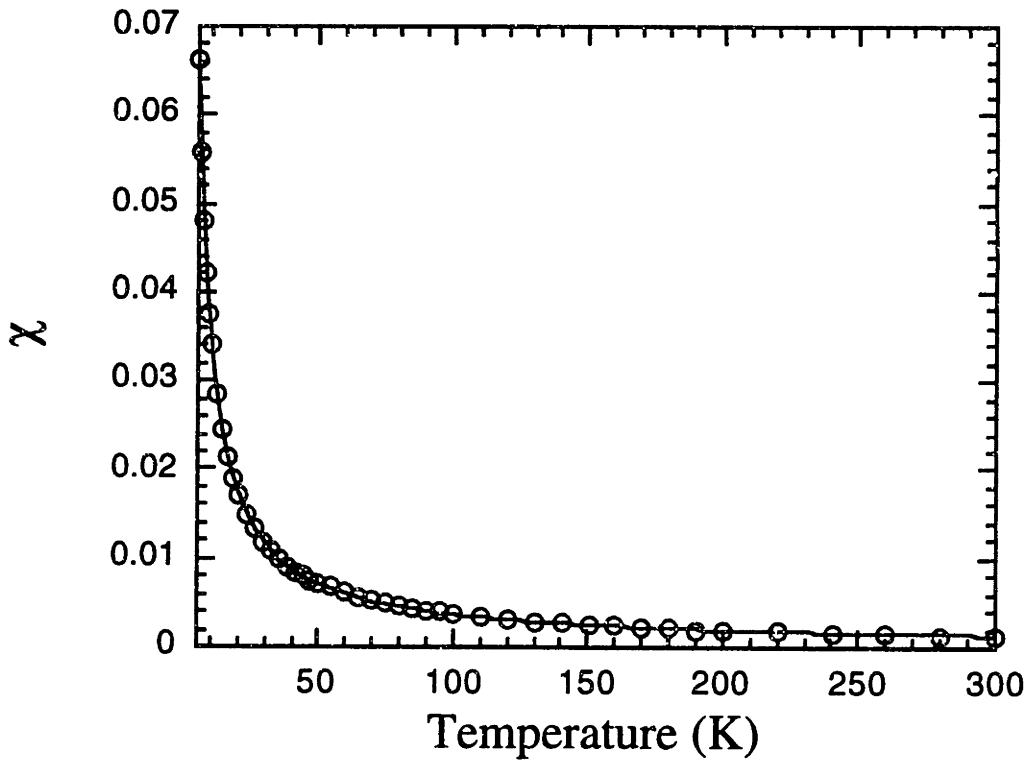

Figure 1.4: SQUID magnetic susceptibility data for solid $Ti(N[R]Ar)_2(CH[SiMe_3]_2)$ (**1.34**) from 5 to 300 K fit to the Curie-Weiss law (μ = 1.66 μ_B, θ = - 0.19 K)

References begin on page 81

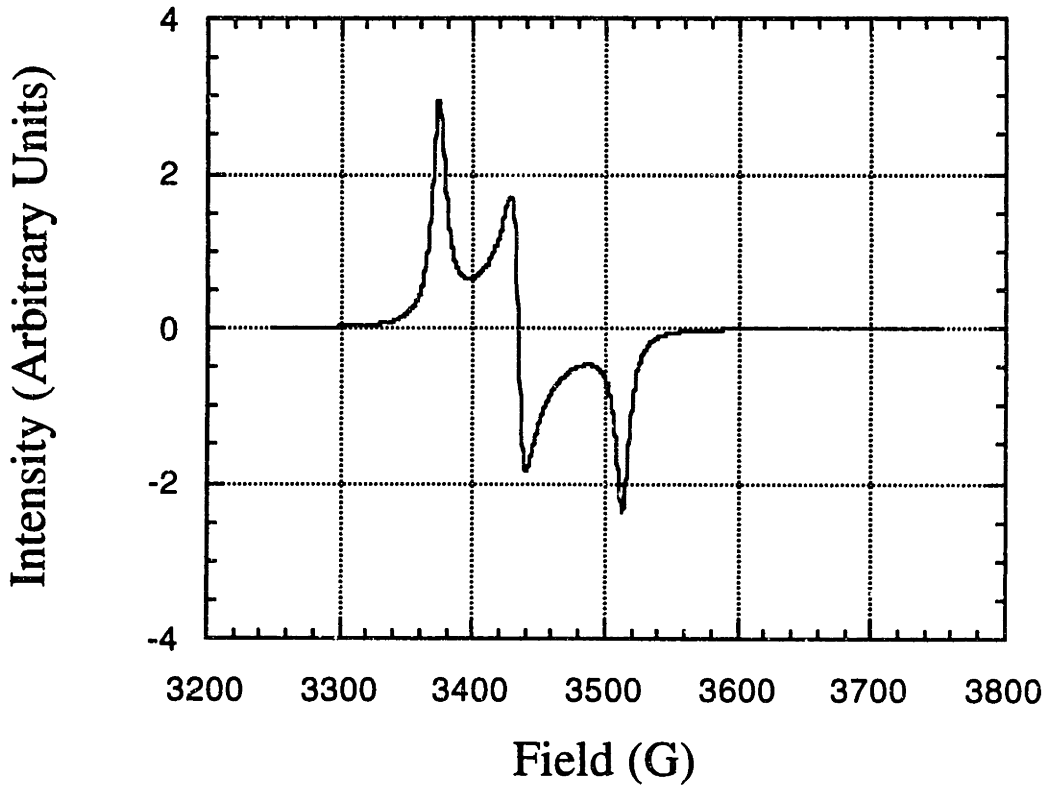

Figure 1.5: EPR spectrum (97 K, toluene) of $Ti(N[R]Ar)_2(CH[SiMe_3]_2)$ (**1.34**) with $g_1 = 1.997$, $g_2 = 1.962$, $g_3 = 1.918$.

References begin on page 81

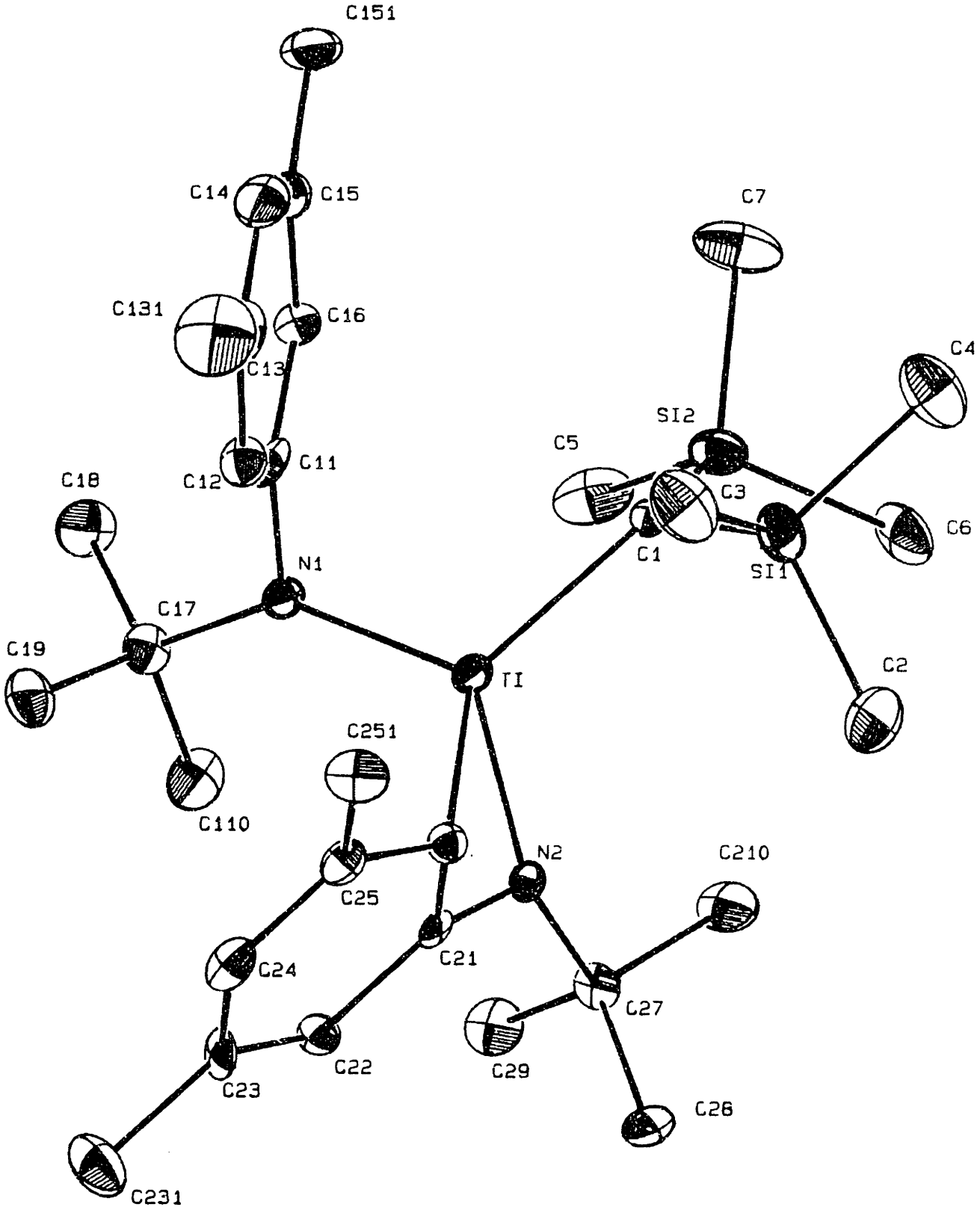

Figure 1.6: ORTEP diagram of $Ti(N[R]Ar)_2(CH[SiMe_3]_2)$ (**1.34**) with thermal ellipsoids drawn at the 30% probability level

References begin on page 81

Table 1.1: Selected Bond Lengths (Å) for $Ti(N[R]Ar)_2[CH(SiMe_3)_2]$ **(1.34)**.

Ti-N1	1.917(5)	Ti-N2	1.962(5)
Ti-C1	2.137(7)	Ti-C26	2.440(8)
Ti-C21	2.407(7)	N1-C17	1.498(8)
N1-C11	1.446(8)	N2-C27	1.506(8)
N2-C21	1.363(9)	C1-Si1	1.862(8)
C1-Si2	1.813(8)		

Table 1.2: Selected Bond Angles (°) for $Ti(N[R]Ar)_2[CH(SiMe_3)_2]$ **(1.34)**.

N1-Ti-C1	116.3(2)	N1-Ti-N2	121.7(2)
N1-Ti-C21	107.3(2)	N1-Ti-C26	63.6(2)
C1-Ti-N2	117.0(3)	C1-Ti-C21	135.5(2)
C1-Ti-C26	115.4(3)	N2-Ti-C21	34.5(2)
N2-Ti-C26	63.6(2)	C21-Ti-C26	34.5(2)
Ti-N1-C17	138.9(4)	Ti-N1-C11	103.4(4)
Ti-C1-Si1	118.8(4)	Ti-C1-Si2	114.7(4)
C11-N1-C17	116.7(5)	C21-N2-C27	143.8(5)
Si1-C1-Si2	117.9(4)	Ti-N2-C27	143.8(5)
Ti-N2-C21	90.9(4)	Ti-C21-N2	54.6(3)
Ti-C21-C22	136.4(5)	Ti-C21-C26	74.0(4)
Ti-C26-C21	71.5(4)	Ti-C26-C25	134.4(5)
N2-C21-C22	129.0(7)	N2-C21-C26	114.4(6)
C21-C26-C25	120.1(7)	C22-C21-C26	116.0(7)

References begin on page 81

Table 1.3: Positional Parameters and B(eq.) for the Non-Hydrogen Atoms of $Ti(N[R]Ar)_2[CH(SiMe_3)_2]$ (**1.34**).

Atom	x	y	z	B(eq.)
Ti	0.2578(1)	0.5145(1)	0.25817(8)	1.50(5)
Si1	-0.0008(2)	0.2413(2)	0.3053(1)	2.66(9)
Si2	-0.0786(2)	0.3866(2)	0.1739(1)	2.52(9)
N1	0.3534(6)	0.5398(5)	0.1672(3)	1.8(2)
N2	0.3014(6)	0.6666(5)	0.3554(3)	1.5(2)
C1	0.0530(7)	0.3513(7)	0.2305(4)	2.0(3)
C2	0.014(1)	0.3485(9)	0.4111(5)	4.6(4)
C3	0.109(1)	0.1445(8)	0.3157(6)	4.4(4)
C4	-0.185(1)	0.1044(8)	0.2744(6)	4.4(4)
C5	-0.004(1)	0.5374(8)	0.1271(5)	4.2(4)
C6	-0.1976(8)	0.4254(8)	0.2396(5)	3.6(3)
C7	-0.190(1)	0.2357(8)	0.0854(5)	4.9(4)
C11	0.3219(8)	0.4002(7)	0.1232(5)	2.0(3)
C12	0.3813(8)	0.3247(7)	0.1522(5)	2.3(3)
C13	0.347(1)	0.1875(8)	0.1137(6)	3.6(4)
C14	0.248(1)	0.1302(8)	0.0405(6)	3.7(4)
C15	0.184(1)	0.2027(8)	0.0072(5)	3.2(3)
C16	0.2163(8)	0.3389(7)	0.0473(4)	2.2(3)
C17	0.4595(8)	0.6538(7)	0.1399(5)	2.2(3)
C18	0.423(1)	0.6397(8)	0.0471(5)	3.6(3)
C19	0.6010(9)	0.6539(7)	0.1635(5)	2.9(3)
C21	0.4231(8)	0.6597(7)	0.3827(4)	1.4(3)
C22	0.5613(8)	0.7662(7)	0.4026(4)	2.0(3)
C23	0.6752(8)	0.7419(8)	0.4163(4)	2.0(3)
C24	0.6598(8)	0.6053(8)	0.4091(4)	2.3(3)
C25	0.5295(8)	0.4977(7)	0.3920(4)	2.0(3)
C26	0.4107(8)	0.5218(7)	0.3798(4)	1.6(1)
C27	0.2657(8)	0.7839(7)	0.3910(5)	2.0(3)
C28	0.3127(8)	0.8223(7)	0.4855(5)	3.1(3)
C29	0.3306(8)	0.9092(8)	0.3552(5)	3.0(3)
C110	0.457(1)	0.7873(7)	0.1863(5)	3.3(3)
C131	0.409(1)	0.1055(9)	0.1482(7)	5.8(5)
C151	0.077(1)	0.1378(8)	-0.0722(5)	4.3(4)
C210	0.1106(9)	0.7311(8)	0.3690(5)	3.4(3)
C231	0.8184(8)	0.8575(8)	0.4360(5)	3.7(4)
C251	0.5174(8)	0.3543(7)	0.3913(5)	2.9(3)

The complex is best regarded as an 11 e^- complex; N1 donates 3 e^- (1 σ + 1 π interaction), N2 and C1 donate 1 e^- each in a σ sense, and the C21-C26 π interaction adds an additional 2 e^-. The titanium carbon bond length of 2.137(7) Å is short relative to those in $(\eta^7\text{-}C_7H_7)$(DMPE)TiEt[80] and $Cp^*_2TiCH_2C(CH_3)_3$[81] (2.211 and 2.231 Å respectively), both relatively electronically saturated relative to **1.34**, and slightly longer than that in $[PhC(NSiMe_3)_2]_2TiMe$ (2.120(5) Å),[28] but not significantly so. The Ti-C bond lengths in

References begin on page 81

the related Ti(III) amide complexes $[Ti(N[\text{-}i\text{-}Pr]_2)_2(Ph)_2][Li(TMEDA)_2]$ (2.173(5) and 2.210(5) Å) and $[Ti(N[SiMe_3]_2)(CH_2Ph)_2][Li(TMEDA)_2]$ (2.18(1) Å) are also similar.

(iv) Interconversion of 1.34 and 1.10

Complex **1.34** is readily oxidized by one electron as demonstrated by its reaction with iodine in benzene solution. The reaction mixture rapidly changes from deep dark green to dark orange-red, and iodide $Ti(N[R]Ar)_2(CH[SiMe_3]_2)(I)$ (**1.35**) is isolated in 68% yield. The methyne proton on the alkyl group exhibits a proton NMR resonance at 3.47 ppm while the aryl methyl resonance appears at 2.18 ppm. Complex **1.34** also reacts rapidly with chlorinated organic solvents, presumably making the chloride homologue of **1.35**. Complex **1.35** is also prepared by direct alkylation of **1.10** with $LiCH(SiMe_3)_2$, although the reaction is exceedingly slow and occurs with some decomposition. Reduction of iodide **1.35** with sodium amalgam in benzene regenerates the titanium (III) complex **1.34** as determined by ^2H NMR spectroscopy.

Section 1.9: Reaction Chemistry of 1.34

The potential for one-electron chemistry with alkyl **1.34** is large, as demonstrated in the previous section, and there is substantial related one-electron chemistry of low valent titanium.[18,22,39,77] The sterically shielded metal-carbon bond is also expected to be reactive, especially since the titanium(III) complexes with the more typical bulky alkyl groups CH_2SiMe_3 and CH_2CMe_2Ph are not isolable. Complex **1.35** should therefore react with a wide variety of unsaturated substrates, demonstrating one, two and even three electron chemistry.

(i) Benzonitrile

When **1.34** is treated with one equivalent of benzonitrile, the solution becomes dark blue. The complex thus formed is believed to be a nitrile adduct,

References begin on page 81

$Ti(N[R]Ar)_2(CH[SiMe_3]_2)(NCPh)$ (**1.36**), and has a ^2H NMR resonance at 4.67 ppm. This resonance gradually disappears over an 18 hour period while an orange precipitate forms. The solid is collected in 82% yield (Scheme 1.8). The orange powder is essentially insoluble in pentane or ether, and si purified by recrystallization from hot THF.

The resonance of the methyne proton on the alkyl group appears at 1.44 ppm in the ^1H NMR, and the aryl methyl resonance is at 2.16 ppm. The ^1H NMR spectrum of the product has a one to one ratio of alkyl to nitrile resonances, and the solubility properties suggest a dimeric formulation: $[Ti(N[R]Ar)_2(CH[SiMe_3]_2)(NCPh)]_2$ (**1.37**). Low-valent titanium complexes are known to mediate both nitrile and ketone coupling reactions.[18,22,41]

(ii) Trimethylsilylazide

Organoazides react with suitable substrates to make imido ligands, delivering the R-N fragment to the metal with subsequent loss of N_2.[45,82-84] These reagents sometimes donate nitrogen atoms to especially reactive metal complexes.[47] Delivery of a nitrogen atom to **1.35** should result in alkyl group migration to form the Ti(IV) imide complex $Ti(N[R]Ar)_2(NCH[SiMe_3]_2)$ by formal insertion of the nitrogen atom into the metal carbon bond. However, the reaction of Me_3SiN_3 with the alkyl complex results in significant decomposition with the formation of multiple intractable products, even when starting the reaction at temperatures below -100 °C.

References begin on page 81

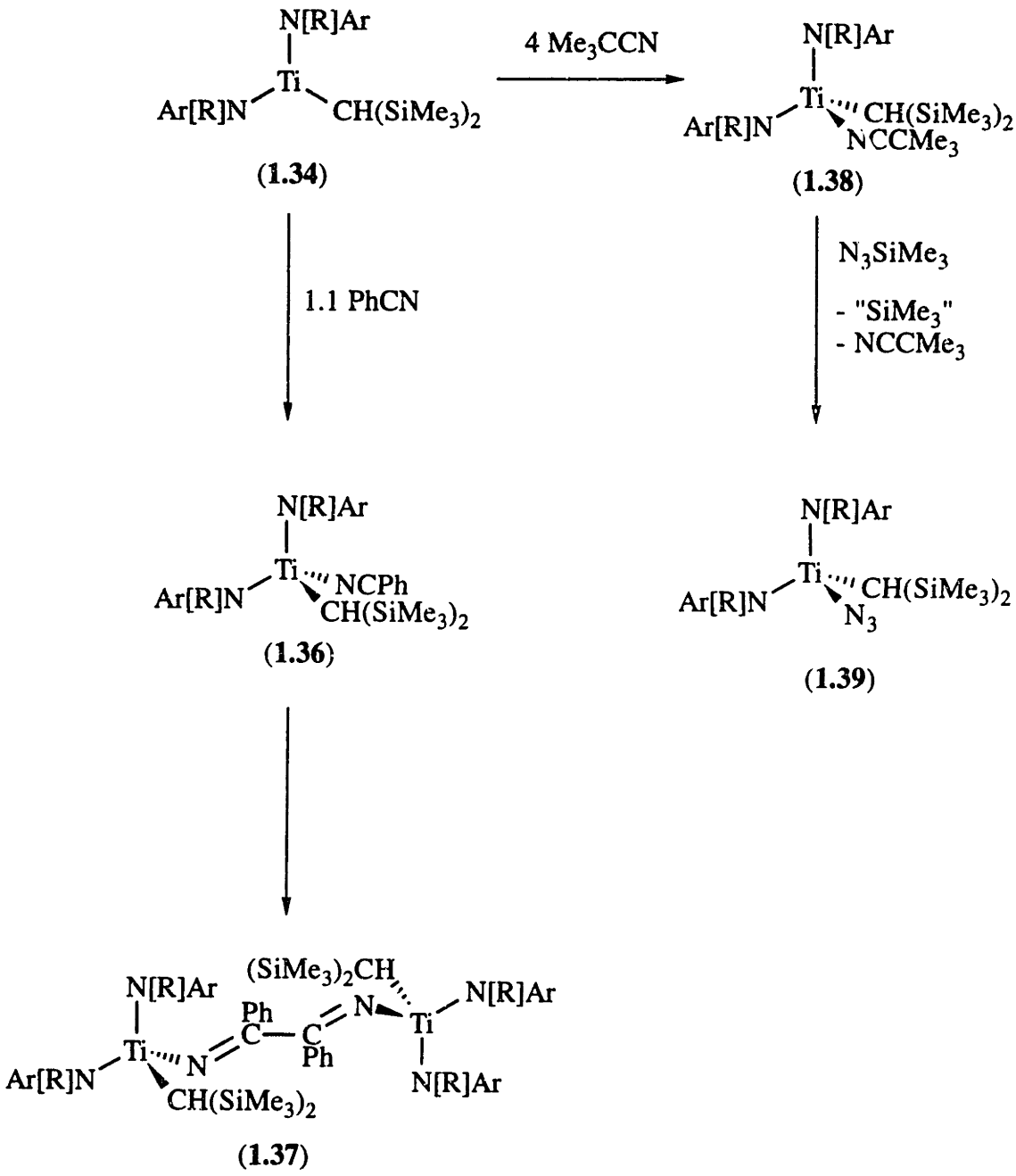

Scheme 1.8: Reaction Chemistry of $Ti(N[R]Ar)_2(CH[SiMe_3]_2)$

References begin on page 81

In an attempt to temper the reactivity of **1.35** with azide reagents, the three-coordinate titanium center is masked by the addition of several equivalents of *tert*-butylnitrile. This results in a lightening of the reaction solution to very pale green, but no subsequent reaction occurs. The adduct is formulated analogously to **1.36**, but $Ti(N[R]Ar)_2(CH[SiMe_3]_2)(NCCMe_3)$ (**1.38**) has not been isolated in pure form as the nitrile ligand is labile. When Me_3SiN_3 is added to the adduct at -35 °C, the solution gradually changes to an orange-yellow color over about two hours. A light orange powder is obtained in 37% yield by recrystallization from pentane. Proton NMR spectroscopy suggests that the product is formed high yield, but it is very soluble in organic solvents. NMR evidence is consistent with the desired imide complex, with the methyne proton resonance appearing at 2.50 ppm and the aryl methyl resonance appearing at 2.21 ppm in the ^1H NMR spectrum. However, the complex exhibits a strong IR stretch at 2107 cm^{-1}, indicative of an azido functionality. Elemental analysis data are consistent with the formulation of the product as the terminal azide $Ti(N[R]Ar)_2(CH[SiMe_3]_2)(N_3)$ (**1.39**). It has not yet been possible to convert azide **1.39** to the desired alkyl imide complex either through thermolysis or photolysis; these conditions instead lead to considerable decomposition.

Section 1.10: Conclusion

In general, the synthetic goals outlined at the beginning of this chapter have been met. A heteroleptic titanium(III) alkyl complex stabilized with amide ligands containing a deuterium spectroscopic handle has been synthesized, and its initial reactivity has been presented. However, in order to stabilize the alkyl complex enough to allow for its isolation and characterization, the unique alkyl group $CH(SiMe_3)_2$ must be used. This alkyl is large, preventing dimerization and disproportionation, but limits the approach of reagents to the titanium center. Also, the inductive electron withdrawing effect of two

References begin on page 81

silicon substituents on the α-carbon may significantly reduce the Ti-C bond reactivity. As a result of these limitations, the reactivity of **1.35** is essentially identical to $Ti(silox)_3$ or the more recently prepared $Ti(N[R]Ar)_3$. More work needs to be done in this area to develop the three-electron chemistry initially envisioned for such complexes.

A large number of new organometallic complexes of both Ti(III) and Ti(IV) with *N-tert*-alkyl anilide ligation have been prepared, such as the alkyls prepared from $Ti(N[R]Ar)_2(I)_2$ (**1.10**) and $Ti(N[R]Ar_F)_2(NMe_2)(I)$ (**1.14**) as well as the chiral-at-metal C-, N-, O-, and I- ligated species **1.20**, **1.21** and **1.27**. The steric requirements for titanium(III) alkyl complexes have been explored through the synthesis of these derivatives, showing that too little steric protection leads to decomposition, while too much leads to cyclometallation.

Additionally, the use of dimethylamide groups as protecting groups, or coordination site place holders, has proven to be an incredibly useful synthetic technique for the selective delivery of ancillary ligands to a titanium center. The dimethylamide is readily removed with methyl iodide, leaving a halide for further chemical modification. This protocol allows for the synthesis of molecular species, for example, $Ti(N[R]Ar)_2(I)_2$ (**1.10**), which cannot be accessed in synthetically useful amounts through normal means. The extensive use of this transformation demonstrates an attractive feature of the N[R]Ar ligand set: electronic tunability. This is seen in the substituent effects on the degree of completion of dimethylamide group replacement in the reactions of **1.9**, **1.13**, **1.15**, **1.18**, and **1.23** with methyl iodide. From these reactions, the relative electron donating ability of the ligand set is determined to decrease in the order $Ti(N[R]Ar)_2 \approx Ti(N[R]Ar)(OAr') > Ti(N[R_{ph}]Ar)(OAr'') > Ti(N[R]Ar_F)_2$, as measured by electrophilicity at titanium.

References begin on page 81

Section 1.11: Experimental

1.11.1 General Considerations

Unless otherwise stated, all operations were performed in a Vacuum Atmospheres dry box under an atmosphere of purified nitrogen, or using standard Schlenk techniques. Anhydrous diethyl ether, tetrahydrofuran, and toluene were purchased from Mallinckrodt; 1,2-dimethoxyethane was obtained from Fisher Scientific; benzene was purchased from J. T. Baker; *n*-pentane and *n*-hexane were purchased from EM Science. The ethereal solvents (diethyl ether, tetrahydrofuran, 1,2-dimethoxyethane) were distilled, under nitrogen, from purple sodium benzophenone ketyl. The aliphatic hydrocarbons and benzene were distilled, under nitrogen, from very dark blue to purple sodium benzophenone ketyl solubilized with a small quantity of tetraglyme. Toluene was refluxed over molten sodium for at least two days, then distilled under nitrogen. Chloroform was refluxed over potassium carbonate for at least two days before being distilled under nitrogen. Distilled solvents were transferred under vacuum into bombs before being pumped into a Vacuum Atmospheres dry box. Benzene-d_6 was degassed and dried over blue sodium benzophenone ketyl and transferred under vacuum into a storage vessel. Chloroform-*d* was degassed and dried over 4 Å sieves. Tetramethylethylenediamine (TMEDA), methyl iodide and trimethylacetonitrile were degassed and distilled from calcium hydride. 2,6-di-*iso*-propylphenol was degassed and distilled. 2,6-di-*tert*-butylphenol was crystallized from diethyl ether. 4 Å sieves and alumina were dried *in vacuo* overnight at a temperature above 150 °C. $Ar_FN{=}C(CD_3)_2$ (**1.4**),[54] $HN[R]Ar_F$ (**1.5**),[54] $Et_2O{\cdot}LiN[R]Ar_F$ (**1.6**),[54] $TiCl_3(THF)_3$,[66] $TiCl(NMe_2)_3$,[67] $Ti(Cl)_2(NMe_2)_2$,[67] and $LiCH(SiMe_3)_2$[85] were prepared by standard procedures. Other chemicals were used as received. Magnetic susceptibilities were measured by NMR techniques.[75] ^1H and ^{13}C NMR spectra were recorded on Varian XL-300, Varian Unity-300 or Brucker AC-250 spectrometers. Chemical shifts are reported with respect to internal solvent (7.15 ppm and 128.0 ppm).

References begin on page 81

^2H chemical shifts are reported with respect to external C_6D_6. Infrared measurements were carried out on a Bio-Rad FTS-135 spectrometer. UV-vis spectra were recorded on a Hewlett-Packard 8453 diode array spectrophotometer. EPR spectra were recorded on a Brucker ESP-300 spectrometer in sealed quartz tubes in toluene at either ambient temperature or low temperature by using a liquid nitrogen cooled nitrogen stream. Spectra were simulated using the program EPR-NMR.[76] CHN analyses were performed by Oneida Research Services. Melting points were obtained in sealed glass capillaries and are uncorrected.

1.11.2 SQUID Magnetic Measurements

Measurements were made using a Quantum Design SQUID magnetometer. The magnetometer uses the MPMSR2 software (Magnetic Property Measurement System Revision 2). Data were recorded at a field strength of 5000 G. Gel caps (Gelatin Capsule #4 Clear) and straws were ordered from Quantum Design, Inc. Samples of **1.34** for magnetic measurements were placed into a gel cap and Parafilm was inserted above it to keep it in place. The loaded gel cap was mounted in a straw, and the straw was placed in an airtight vessel for transport to the magnetometer. After inserting the sample, the field and temperature were adjusted to 5000 G and 5 K, respectively. Once the temperature had equilibrated and the field was stable, the sample was centered. This was done by running a full length DC scan, adjusting the position automatically, and then recentering using a DC centering scan. During the run, measurements were taken over the following temperature ranges with the indicated increments: 5-10 K (one data point every 1 K), 12-20 K (one data point every 2 K), 23-50 (one data point every 3 K), 55-100 (one data point every 5 K), 110-200 (one data point every 10 K), 220-300 (one data point every 20 K). The run required approximately 5 h.

The data for **1.34** fit the Curie-Weiss law in the temperature range 5-300 K (R = 0.99999). The calculated curve (Figure 1.4) is the best least-squares fit of the observed

References begin on page 81

susceptibility data to the equation $\chi_M(obs) = ((\mu^2)/(7.997584\times(T-\theta)))-C$. The value of μ obtained in this manner was 1.66 μ_B, to be compared with the spin-only value for one unpaired electron, 1.73 μ_B. In the least-squares fit, carried out using the General curve-fitting routine included with the program Kaleidagraph, both θ and C were treated as variable parameters. The obtained value of θ, the Weiss constant, was –0.195 K. The value of the constant C, included to represent the sum of all temperature-independent contributions to the total observed susceptibility, including the diamagnetic correction and t.i.p., was $-2.41\cdot10^{-4}$.

1.11.3 Synthesis of Complexes

(i) $ArN=C(CD_3)_2$ (1.1):[44] By the method of Eaton,[63] freshly distilled 3,5-dimethylaniline (48.24 g, 398.1 mmol), 4 Å molecular sieves (dried under vacuum at >140 °C overnight, 90 g), and acetone-d_6 (200 mL, 2.72 mol) were added to a 500 mL round bottom flask and placed under a partial vacuum at 4 °C for 4 days with occasional stirring. The molecular sieves were removed by filtration of the reaction mixture through a sintered glass frit, and the excess acetone-d_6 was removed by vacuum transfer leaving the desired imine as a pale yellow oil. More imine was obtained by immersing the sieves in pentane (100 mL) overnight followed by filtration and removal of solvent under vacuum. Yield: 64.60 g (97%). ^{1}H NMR (300 MHz, C_6D_6): δ = 6.60 (s, 1H, para); 6.44 (s, 2H, ortho); 2.15 (s, 6H, aryl CH_3). ^{13}C NMR (75 MHz, C_6D_6): δ = 166.66 ($C(CD_3)_2$); 152.65 (ipso); 138.41 (meta); 124.72 (aryl); 117.51 (aryl); 27.60 (CD_3); 21.37 (aryl CH_3); 19.40 (CD_3). High resolution mass spec. Calcd. mass (167.158), measured mass (167.158).

References begin on page 81

(ii) HN[R]Ar (1.2):[44,62] a solution of MeLi (1.4 M in diethyl ether, 300 mL, 420 mmol) in a 500 mL Erlenmeyer flask was frozen solid in a liquid nitrogen filled cold well and allowed to thaw until magnetic stirring was just possible. A solution of $ArN{=}C(CD_3)_2$ (**1.1**, 26.00 g, 155.7 mmol) in diethyl ether (ca. 20 mL) at -35 °C was added via pipet over 10 minutes. The reaction mixture was allowed to stir for 18 hours, at which point it was quenched by removing the flask from the glove box to a fume hood, and carefully pouring the reaction mixture onto ice (300 mL) in a 1 L Erlenmeyer flask. The mixture was extracted with hexanes (2 x 150 mL) and flushed through a column of oven dried alumina (2 x 25 cm). The column was washed with hexanes to give a total volume of 950 mL. The solvent was removed under vacuum resulting in a canary yellow oil. This oil was shown (by ^1H NMR spectroscopy) to be a 1:1 mixture of $ArN{=}C(CD_3)(CD_2H)$ and the desired product. Water (200 mL) was added to the oil, and with vigorous stirring, concentrated HCl (25 mL) was added via pipet over a 10 minute period. A large quantity of a white flocculent precipitate formed. Stirring was continued for 3 hours, at which point the pH of the solution was brought to 12-14 with a concentrated NaOH solution (~ 5 M). The mixture was extracted with hexanes (2 x 200 mL) and flushed through a column of oven dried alumina (2 x 25 cm). Additional hexanes were used to wash the column to give a total volume of 800 mL. The solvent was removed *in vacuo* leaving a yellow oil. The oil was used as prepared, or distilled (45 °C, ~10^{-1} torr). Yield 15.54 g (55%). M.p. ~-30 °C. ^1H NMR (300 MHz, C_6D_6): δ = 6.43 (s, 1H, para); 6.33 (s, 2H, ortho); 3.06 (s, 1H, N*H*); 2.18 (s, 6H, aryl CH_3); 1.16 (s, 3H, $C(CD_3)_2CH_3$). ^{13}C NMR (75 MHz, C_6D_6): δ = 147.53 (s, ipso); 138.19 (q, meta); 120.62 (d, aryl); 115.96 (d, aryl); 50.74 (s, $C(CD_3)_2CH_3$); 30.08 (q, $C(CD_3)_2CH_3$); 29.56 (m, $C(CD_3)_2CH_3$); 21.70 (q, aryl CH_3). MS (70 eV): *m/z*(%): 183.2(37)[*M*+]. High resolution mass spec. Calcd. mass (183.189), measured mass (183.189). Anal. Calcd. for $C_{12}H_{13}D_6N$: C, 78.62; H, 10.45; N,7.64. Found: C, 78.12; H, 10.77; N, 7.16.

References begin on page 81

(iii) Et_2O·LiN[R]Ar (1.3):[44] A solution of HN(R)Ar (**1.2**, 13.5 g, 73.7 mmol) in pentane (100 mL) was frozen solid in a liquid nitrogen filled cold well and allowed to thaw until magnetic stirring was just possible. A solution of *n*-BuLi (49 mL, 1.6 M in hexane, 78 mmol) was slowly added via pipet over a 10 minute period. The reaction mixture was stirred for 5 hours, at which point the volume was reduced to 60 mL and diethyl ether (8.30 g, 112 mmol, 1.6 eq.) was added, forming a white precipitate. The volume was further reduced to 30 mL, and the product was collected by filtration and dried under vacuum. Yield 13.0 g (96%). ^{1}H NMR (300 MHz, C_6D_6,): δ = 6.54 (s, 2H, ortho); 6.13 (s, 1H, para); 3.17 (q, 4H, OCH_2CH_3); 2.30 (s, 6H, aryl CH_3); 1.60 (s, 3H, $C(CD_3)_2CH_3$); 0.95 (t, 6H, OCH_2CH_3). ^{13}C NMR (75 MHz, C_6D_6): δ = 159.48 (ipso); 138.24 (meta); 116.42 (aryl); 113.47 (aryl); 65.34 (OCH_2CH_3); 52.13 ($C(CD_3)_2CH_3$); 31.72 ($C(CD_3)_2CH_3$); 31.00 ($C(CD_3)_2CH_3$); 22.14 (aryl CH_3); 14.87 (OCH_2CH_3).

(iv) $HN[R_{ph}]Ar$ (1.7): Phenyl lithium (145 mL of a 1.8 M solution in cyclohexane/ether, 261 mmol) was frozen solid in a liquid nitrogen cooled cold well and allowed to thaw. Just as the solution began stirring, $(CD_3)_2C$=NAr (**1.1**, 15.4 g, 92.2 mmol) in Et_2O (20 mL) at -35 °C was added. The reaction mixture was stirred for 23 hours and then slowly poured over ice (~300 mL) in a 1 L Erlenmeyer flask. The organic layer was separated and the aqueous layer was extracted with petroleum ether (~200 mL). The organics were run through a column of alumina (2 x 25 cm) and the solvent was removed *in vacuo* leaving a thick brown oil (**1**, 16.75 g, 68.3 mmol, 74%). ^{1}H NMR (300 MHz, $CDCl_3$): δ = 7.50 (d, 2H); 7.32 (t, 2H); 7.20 (m, 1H); 6.25 (s, 1H, para); 5.98 (s, 2H, orthos); 3.92 (s, 1H, N*H*); 2.10 (s, 6H, ArCH_3).

(v) Et_2O·LiN[R_{ph}]Ar (1.8): HN[R_{ph}]Ar (**1.7**, 16.75 g, 68.25 mmol) was dissolved in pentane (60 mL) and chilled to -35 °C. n-Butyllithium (47 mL of a 1.6 M solution in hexanes, 75.7 mmol) was added via pipet as the solution was stirred. A thick brown oil

References begin on page 81

precipitated 20 minutes after the addition. Addition of Et_2O (5.50g, 74.3 mmol) caused the formation of a white precipitate which was collected on a frit (**2**, 9.24 g, 28.45 mmol, 42%). ^1H NMR (300 MHz, C_6D_6): δ = 7.6 (br s, 2H); 7.15 (br s, 2H); 7.05 (s, 1H); 6.38 (br s, 2H); 5.95 (br s, 1H); 3.10 (q, 4H, $O(CH_2CH_3)_2$); 2.05 (br s, 6H, $ArCH_3$); 0.94 (t, 6H, $O(CH_2CH_3)_2$).

(vi) $Ti(N[R]Ar)_2I_2$ (1.10): $Ti(NMe_2)_2Cl_2$ (0.40 g, 1.96 mmol) was slurried in ether (10 mL) and cooled to -35 °C. Et_2O·LiN[R]Ar (**1.3**, 1.02 g, 3.88 mmol) was added all at once to the stirred solution, which immediately became a mustard yellow color. The reaction mixture was stirred overnight and then filtered to remove LiCl, leaving $Ti(N[R]Ar)_2(NMe_2)_2$ (**1.9**). Methyl iodide (6.78 g, 24 eq) was added to the dark yellow solution, and a white precipitate (Me_4NI) formed immediately. After 43 hours, solvent and excess methyl iodide were removed *in vacuo*. The solid was extracted with pentane (10 mL) and the solution was filtered. The $[NMe_4]I$ was washed with an additional 10 mL portion of pentane, and the combined pentane extractions were stored at -35 °C for 24 hours yielding a dark brown/black crystalline solid. The remaining solution was reduced in volume to ca. 2 mL and stored at -35 °C overnight yielding more dark solid (0.88 g, 1.17 mmol, 60%). M.p. 114-6 °C; ^1H NMR (250 MHz, C_6D_6): δ 7.07 (s, 4H, ortho); 6.86 (s, 2H, para); 2.11 (s, 12H, $ArCH_3$); 1.39 (s, 6H, $C(CD_3)_2CH_3$). ^{13}C NMR (75 MHz, $CDCl_3$): δ 138.693, 134.076, 132.132, 130.903, 67.555, 29.880, 29.5, 21.344; MS (70 eV): *m/z*(%): 666.2 (5.19). Anal. Calcd for $C_{24}H_{24}D_{12}N_2I_2Ti$: C, 43.26; H, 5.45; N, 4.20. Found: C, 43.24; H, 5.60; N, 4.13.

(vii) $Ti(N[R]Ar)_2(I)(CH_2SiMe_3)$ (1.11): $Ti(N[R]Ar)_2I_2$ (**1.10**, 0.3000 g, 0.4504 mmol) was dissolved in ether (15 mL) and frozen. Upon thawing, a solution of $LiCH_2SiMe_3$ (0.0424 g, 0.4504 mmol) in ether (5 mL) was added dropwise. The solution gradually changed to a light brown red color with a white precipitate. After stirring for one

References begin on page 81

hour, the solvent was removed *in vacuo* and the residue was extracted with pentane. The solution was filtered and reduced in volume to a dark red brown oil (0.29 g) which was ~95 % pure by ^{1}H NMR (250 MHz, $CDCl_3$): δ = 7.00 (s, 2H, para); 6.832 (s, 4H, ortho); 2.340 (s, 12 H, ArCH_3); 1.736 (s, 2H, CH_2); 1.307 (s, 6H, $CCH_3(CD_3)_2$); -0.134 (s, 9H, $SiMe_3$). Reduction in benzene gave no observable paramagnetic products although NaI was observed. Reduction in THF caused the formation of a vivid olive green solution which turned brown during the workup (< 50 minutes). ^{1}H NMR of the isolated material showed at least 5 products.

(viii) Ti(N[R]Ar)$_2$(I)(nph) (1.12): Ti(N[R]Ar)$_2$I$_2$ (**1.10**, 0.4995 g, 0.7498 mmol) was dissolved in pentane (30 mL) and cooled to -30 °C. Neophyl lithium (0.1055 g, 0.7528 mmol) was added as a solid. The solution changed to a red-brown color with a white precipitate in five minutes. After stirring for one hour, the solution was filtered and reduced in volume to a dark red oil (0.40 g) which was ~90 % pure by ^{1}H NMR (250 MHz, CDC_3): δ = 7.17 (m, 5H, aryl); 7.149 (s, 4H, ortho); 7.107 (s, 2H, para); 2.3 (s, 2H, CH_2); 2.253 (s, 12H, ArCH_3); 1.455 (s, 6H, $CH_2C(CH_3)_2Ph$); 1.334 (s, 6H, $CCH_3(CD_3)_2$). Reduction with sodium amalgam in benzene gave no observable paramagnetic products although NaI was observed.

(ix) Ti(N[R]Ar$_F$)$_2$(NMe$_2$)$_2$ (1.13): A solution of Et_2O·LiN[R]Ar$_F$ (3.00 g, 11.24 mmol) in ether (20 mL) at -30 °C was added to a stirring slurry of Ti(NMe$_2$)$_2$Cl$_2$ (1.16 g, 5.61 mmol) in ether (40 mL) at -30 °C. The solution changed from brown-red to yellow with a large amount of white precipitate. The reaction was stirred for 14 hours at 30 °C. Lithium chloride was removed by filtration through glass fibers to give a dark yellow solution, which was evaporated *in vacuo* and reconstituted in pentane (15 mL). Very large yellow-orange crystals were collected in two crops (2.20 g, 4.33 mmol, 77.2%). M.p. 127-129 °C. ^{1}H NMR (300 MHz, C_6D_6): δ = 6.98 (d, 1H, aryl); 6.90 (dd, 1H, aryl);

References begin on page 81

6.65 (m, 1H, aryl); 3.075 (br s, 6H, N*Me*$_2$); 2.220 (s, 3H, Ar*Me*); 1.068 (s, 3H, C(CD$_3$)$_2$C*H*$_3$)). ^{13}C NMR (75 MHz, $CDCl_3$): δ = 158.252 (d, J_{CF} = 239 Hz, C_1); 138.297 (d, $^2J_{CF}$ = 12.9 Hz, C_2); 134.16 (d, J_{CH} = 159 Hz, C_6 or C_4); 131.640 (s, C_5); 125.343 (d, J_{CH} = 158.9, C_4 or C_6); 114.902 (dd, J_{CF} = 23.4 Hz, J_{CH} = 160.1 Hz, C_3); 60.796 (s, N*C*(CD$_3$)$_2$CH$_3$); 45.146 (q, J = 131 Hz, N*Me*$_2$); 29.797 (q, J = 125.1 Hz, NC(CD$_3$)$_2$*C*H$_3$); 29.3 (m, *C*D$_3$); 20.855 (q, J = 126.3, Ar*Me*). Anal. Calcd. for $C_{26}H_{30}D_{12}N_4F_2Ti$: C, 61.40; H, 8.32; N, 11.02. Found C, 61.76; H, 8.73; N, 11.06.

(x) Ti(N[R]Ar$_F$)$_2$(I)(NMe$_2$) (1.14): To a stirring yellow solution of Ti(N[R]Ar$_F$)$_2$(NMe$_2$)$_2$ (**1.13**, 1.91 g, 3.76 mmol) in THF (40 mL) was added MeI (5.63 g, 39.6 mmol). The reaction mixture slowly changed to a bright cherry red over 18 hours. ^{1}H NMR spectroscopy was used to determine the extent of reaction by monitoring the disappearance of the dimethylamido peak at 3.075 ppm. The THF was removed *in vacuo*, and the red solid remaining was reconstituted in ether (10 mL). [NMe$_4$]I was removed by filtration through glass fibers, and the red solution was concentrated to a minimum amount. Two crops of crystals were collected (1.58 g, 2.67 mmol, 71%). M.p. 115-118 °C. ^{1}H NMR (300 MHz, C_6D_6): δ = 6.933 (m, 1H, aryl); 6.830 (dd, 1H, aryl); 6.637 (m, 1H, aryl); 3.057 (s, 6H, N*Me*$_2$); 2.057 (s, 6H, Ar*Me*); 1.392 (s, 6H, C(CD$_3$)$_2$C*H*$_3$). ^{13}C NMR (75 MHz, C_6D_6): δ = 132.59 (s, para); 115.93 (d, $^2J_{CF}$ = 23.2 Hz, ipso); ortho and metas broadened into baseline; 63.62 (s, N*C*(CD$_3$)$_2$CH$_3$); 49.00 (s, N*Me*$_2$); 30.106 (s, C(CD$_3$)$_2$*C*H$_3$); 29.589 (m, C(*C*D$_3$)$_2$CH$_3$); 20.652 (s, Ar*Me*). Anal. Calcd. for $C_{24}H_{24}D_{12}F_2N_3ITi$: C, 48.74; H, 6.14; N, 7.10. Found: C, 48.98; H, 6.44; N, 6.98.

(xi) Ti(N[R]Ar$_F$)$_2$(CH$_2$SiMe$_3$)(NMe$_2$) (1.15): Ti(N[R]Ar$_F$)$_2$(I)NMe$_2$ (**1.14**, 0.5011 g, 0.8473 mmol) was dissolved in pentane (25 mL) and cooled to -30 °C. LiCH$_2$SiMe$_3$ (0.85 mL, 1 M in pentane, 0.85 mmol) was added dropwise to the stirring solution. Precipitation of LiI with a concomitant color change to yellow orange occurred

References begin on page 81

over three hours. LiI was removed with a medium frit, and the resulting dark yellow oil was lyophilized from benzene (4 mL) leaving a solid which was recrystallized from pentane (2 mL). Mustard yellow sheets were collected in two crops (0.33 g, 0.60 mmol, 70%). M.p. 68-71 °C. ^{1}H NMR (250 MHz, C_6D_6): δ = 6.92 (m, 1H, aryl); 6.87 (d, 1H, aryl); 6.65 (m, 1H, aryl); 3.08 (s, 6H, N*Me*$_2$); 2.12 (s, 6H, Ar*Me*); 1.31 (s, 6H,C(CD$_3$)$_2$C*H*$_3$); 1.19 (s, 2H, C*H*$_2$SiMe$_3$); 0.11 (s, 9H, Si(C*H*$_3$)$_3$). ^{13}C NMR (75 MHz, C_6D_6): δ = 157.934 (d, J_{CF} = 242.4 Hz, C_2); 135.863 (s, aryl); 134.098 (s, aryl); 132.502 (s, aryl); 127.214 (s, aryl); 115.894 (s, aryl); 61.587 (s, *C*(CD$_3$)$_2$CH$_3$ or *C*H$_2$SiMe$_3$); 61.521 (s, *C*(CD$_3$)$_2$CH$_3$ or *C*H$_2$SiMe$_3$); 46.563 (s, N*Me*$_2$); 30.262 (s, NC(CD$_3$)$_2$*C*H$_3$); 29.75 (m, NC(*C*D$_3$)$_2$CH$_3$); 20.769 (s, Ar*Me*); 3.408 (s, Si*Me*$_3$). Anal. Calcd. for $C_{28}H_{35}D_{12}N_3F_2SiTi$: C, 60.95; H, 8.59; N, 7.62. Found: C, 61.18; H, 8.53; N, 7.37.

(xii) Ti(N[R]Ar$_F$)$_2$(I)(CH$_2$SiMe$_3$) (1.16): Ti(N[R]Ar$_F$)$_2$(NMe$_2$)(CH$_2$SiMe$_3$) (**1.15**, 0.21 g, 0.38 mmol) was dissolved in THF (ca. 10 mL). MeI (1.08 g, 7.61 mmol, 30 eq.) was added and the solution was stirred for 22 hours. A white precipitate was observed and the solution changed from golden yellow to orange-red. The NMe$_4$I was removed by filtration, the solvent was removed *in vacuo*, and the resulting oil was triturated with hexane to give a thick orange oil (0.20 g, 0.32 mmol, 84%). ^{1}H NMR (250 MHz, C_6D_6): δ = 6.6-6.8 (m, 6H, aryl); 2.11 (s, 6H, Ar*Me*); 1.38 (br s, 8H, NC(CD$_3$)$_2$C*H*$_3$ and C*H*$_2$SiMe$_3$); 0.143 (s, CH$_2$Si(C*H*$_3$)$_3$).

(xiii) Ti(N[R]Ar)(OAr')(I)$_2$ (1.19): TiCl(NMe$_2$)$_3$ (1.64 g, 7.63 mmol) was dissolved in Et$_2$O (40 mL) and chilled to -35 °C. Et$_2$O·LiN[R]Ar (**1.3**, 2.00 g, 7.60 mmol) was added as a solid causing a color change to greenish brown in about 30 seconds. After three hours, LiCl was removed by filtration and the solvent was removed *in vacuo* yielding a mobile dark brown oil (Ti(N[R]Ar)(NMe$_2$)$_3$, **1.17**, 2.81 g) which was judged to be ~95% pure by ^{1}H NMR (300 MHz, CDCl$_3$): δ = 6.65 (s, 1H, para); 6.58 (s, 2H,

References begin on page 81

ortho); 2.91 (s, 18H, N*Me*$_2$); 2.28 (s, 6H, Ar*Me*); 1.16 (s, 3H, C(CD$_3$)$_2$C*H*$_3$). The oil was dissolved in fresh Et_2O (5 mL). To it was added a solution of 2,6-diisopropylphenol (1.35 g, 7.58 mmol) in Et_2O (5 mL). The resulting solution was stirred for 18 hours and then the solvent was removed *in vacuo* yielding a thick dark brown oil (Ti(N[R]Ar)(OAr')(NMe$_2$)$_2$, **1.18**, 4.29 g) which was judged to be ~95% pure by ^{1}H NMR (250 MHz, $CDCl_3$): δ = 7.02 (d, 2H, OAr' meta); 6.8 (t, 1H, OAr' para); 6.68 (s, 1H, para); 6.59 (s, 2H, ortho); 3.45 (sep, 2H, C*H*(CH$_3$)$_2$); 3.04 (s, 12H, N*Me*$_2$); 2.25 (s, 6H, Ar*Me*); 1.19 (m, 15H, NC(CD$_3$)$_2$C*H*$_3$ and CH(C*H*$_3$)$_2$). The oil was dissolved in THF (50 mL) at 30 °C. MeI (10.70 g, 75.4 mmol) was added and the reaction mixture was stirred for nine hours. The reaction mixture gradually turned from dark brown to a blood red color. THF was removed *in vacuo*, and the resulting solids were triturated three times with hexane. [NMe_4]I was removed by filtration, solvent was removed *in vacuo*, and the resulting solid was recrystallized from ether to give bright red/purple faceted crystals. Second and third crops were collected from pentane as dark red crystals (3.28 g, 4.96 mmol, 65%). M.p. 130-134 °C. ^{1}H NMR (300 MHz, $CDCl_3$): δ = 7.21 (br s, 1H, aryl); 7.09 (br s, 2H, aryl); 7.08 (s, 2H, aryl); 7.07 (s, 1H, aryl); 3.66 (m, 2H, C*H*(CH$_3$)$_2$); 2.38 (s, 6H, Ar*Me*); 1.33 (s, 3H, C(CD$_3$)$_2$C*H*$_3$); 1.27 (d, 12H, CH(C*H*$_3$)$_2$). ^{13}C NMR (75 MHz, $CDCl_3$): δ = 165.329 (s), 139.185 (s), 138.366 (d), 133.330 (d), 132.004 (d), 131.943 (s), 124.037 (d), 123.194 (d), 69.877 (s, *C*(CD$_3$)$_2$CH$_3$); 29.375 (q, C(CD$_3$)$_2$*C*H$_3$); 28.9 (m, C(*C*D$_3$)$_2$CH$_3$); 27.1925 (d, *C*H(CH$_3$)$_2$); 23.8621 (q, CH(*C*H$_3$)$_2$); 21.2091 (q, Ar*Me*). Anal. Calcd. for $C_{24}H_{29}D_6NOI_2Ti$: C, 43.59; H, 5.33; N, 2.12. Found: C, 43.98; H, 5.47; N, 1.92.

(xiv) Ti(N[R]Ar)(OAr')(CH$_2$SiMe$_3$)(I) (1.20): To a stirring solution of Ti(N[R]Ar)(OAr')I_2 (**1.19**, 0.3004 g, 0.4545 mmol) in hexane (10 mL) at -35 °C was added $LiCH_2SiMe_3$ (0.0428 g, 0.4546 mmol) in hexane (5 mL). The solution rapidly turned orange with the formation of a white precipitate. The reaction was stirred for 20

References begin on page 81

minutes, filtered, and concentrated to a minimum volume. Tiny micro crystals were obtained in low yield, though the reaction appeared quantitative by NMR. ^{1}H NMR (250 MHz, $CDCl_3$): δ = 7.1 (m, 6H, aryls); 3.72 (sep, 2H, C*H*$(CH_3)_2$); 2.39 (s, 6H, Ar*Me*); 2.24 (d, 1H, C*Ha*HbSiMe$_3$); 1.38 (d, 6H, CH(C*H*$_3)_2$); 1.22 (m, 7H, CH(C*H*$_3)_2$ and CHa*Hb*SiMe$_3$); 1.10 (s, 3H, C(CD$_3)_2$C*H*$_3$); -0.09 (s, 9H, SiMe$_3$).

(xv) Ti(N[R]Ar)(OAr')(CH_2CMe_2Ph)(I) (1.21): Ti(N[R]Ar)(OAr')I_2 (**1.19**, 1.04 g, 1.57 mmol) was dissolved in hexane (25 mL) and chilled to -30 °C. Neophyllithium (0.2205 g, 1.573 mmol) was added, causing an immediate color change to a light red brown. After 15 minutes of stirring, LiI was removed as a gray solid with a frit. The mother liquor was pumped to dryness *in vacuo*, leaving a thick orange-red oil. The oil was lyophilized from benzene and crystallized from pentane to give red orange waxy crystals (0.5161 g, 49.3 %). M.p. 75-77 °C. ^{1}H NMR (300 MHz, $CDCl_3$): δ = 7.3 (br s, 1H, ortho); 7.05 (m, 9H, aryl); 6.7 (br s, 1H, ortho); 3.82 (sep, 2H, C*H*$(CH_3)_2$); 2.41 (br s, 6H, Ar*Me*); 2.35 (d, 1H, C*Ha*HbC$(CH_3)_2$Ph); 2.07 (d, 1H, CHa*Hb*C$(CH_3)_2$Ph); 1.36 (d, 6H, CH(C*H*$_3)_2$-a); 1.32 (s, 3H, CHaHbC(C*H*$_3)_2$Ph); 1.24 (s, 3H, CHaHbC(C*H*$_3)_2$Ph); 1.09 (s, 3H, C(CD$_3)_2$C*H*$_3$); 1.21 (d, 6H, CH(C*H*$_3)_2$-b).

(xvi) Ti(N[R_{ph}]Ar)(NMe_2)$_3$ (1.22): $TiCl(NMe_2)_3$ (1.50 g, 6.97 mmol) was dissolved in THF (50 mL) and chilled to -35 °C. Et_2O·LiN[R_{ph}]Ar (**2**, 2.27 g, 6.98 mmol) was added as a powder. The solution changed from brown to a darker greenish brown. The reaction mixture was stirred for 12 hours, and the solvent was removed *in vacuo*. The mixture was reconstituted in pentane (~50 mL) and filtered through a frit, leaving a yellow brown solution which was evaporated to dryness, leaving a thin oil. Lyophilization twice from benzene to remove residual THF followed by recrystallization from pentane (8 mL) afforded a greenish brown powder (2.445 g, 5.76 mmol, 82.6%). M.p. 32.5-33.5 °C. ^{1}H NMR (300 MHz, $CDCl_3$): δ = 7.21 (d, 2H); 7.06 (t, 2H); 6.95

References begin on page 81

(t, 1H); 6.29 (s, 1H); 5.96 (s, 2H); 2.77 (s, 18H, N*Me*$_2$); 1.88 (s, 6H, Ar*Me*). ^{13}C NMR (75 MHz, $CDCl_3$): δ = 151.056, 148.716, 136.578, 127.64, 126.44, 125.48, 124.09, 123.57. 45.09, 30.64, 21.46. MS (70 eV): *m/z*(%): 424(0.9)[*M*+]. Anal. Calcd. for $C_{23}H_{32}D_6N_4Ti$: C, 65.08; H, 9.02; N, 13.20. Found: C, 65.29; H, 9.02; N, 13.17.

(xvii) Ti(N[R$_{ph}$]Ar)(OAr")(NMe$_2$)$_2$ (1.23): Ti(N[R_{ph}]Ar)(NMe_2)$_3$ (**1.22**, 1.4274 g, 3.3622 mmol) was dissolved in Et_2O (20 mL) and cooled to -35 °C in a round bottom flask. 2,6-Di-*tert*-butylphenol (0.6937 g, 3.362 mmol) was dissolved in Et_2O (10 mL), cooled to -35 °C and then added to the solution. The greenish brown reaction mixture changed to a reddish orange color after three hours. ^{1}H NMR spectroscopy at this point showed considerable starting material. After 19.5 hours of reaction, the solvent was removed *in vacuo* to give a bright cherry red foam. The foam was redissolved in pentane (about 3 mL), resulting in crystallization of the desired product as an orange powder at room temperature. A second crop of powder resulted upon cooling a concentrated solution for several days at -35 °C (1.626 g, 2.776 mmol, 82.6%). M.p. 130-131 °C. ^{1}H NMR (300 MHz, $CDCl_3$): δ = 7.593 (d, 2H, *J* = 7.58 Hz); 7.3450 (t, 2H, *J* = 7.56 Hz); 7.25 (t, 3H, *J* = 7.8 Hz); 6.799 (t, 1H, *J* = 7.8 Hz); 6.5057 (s, 1H, para); 6.4372 (s, 2H, ortho); 3.0153 (s, 12H, N*Me*$_2$); 1.9116 (s, 6H, Ar*Me*); 1.4842 (s, 18H, C(C*H*$_3$)$_3$). ^{13}C NMR (75 MHz, $CDCl_3$): δ = 164.565 (s), 150.438 (s), 146.383 (s), 140.229 (s), 138.920 (s), 127.922 (d), 126.513 (d), 125.745 (d), 125.254 (d), 124.379 (d), 120.755 (d), 119.236 (d), 65.8920 (s, *C*(CD$_3$)$_2$C$_6$H$_5$), 47.9519 (q, N*Me*$_2$), 35.4817 (s, *C*(CH$_3$)$_3$), 31.6 (m, *C*D$_3$), 31.0918 (q, C(*C*H$_3$)$_3$), 21.5033 (q, Ar*Me*). MS (70 eV): *m/z*(%): 585(0.5)[*M*+]. Anal. Calcd. for $C_{35}H_{47}D_6N_3OTi$: C, 71.77; H, 9.12; N, 7.17. Found: C, 72.25; H, 8.94; N, 6.75.

(xviii) Ti(N[R$_{ph}$]Ar)(OAr")(I)(NMe$_2$) (1.24): Ti(N[R_{ph}]Ar)(OAr")(NMe_2)$_2$ (**1.23**, 0.7363 g, 1.257 mmol) was dissolved in Et_2O (45 mL) and cooled to -35 °C in a

References begin on page 81

round bottom flask. MeI (1.92 g, 13.5 mmol) was added, the flask was stoppered, and the reaction was stirred overnight. Monitoring by ^{1}H NMR showed almost no conversion to product. It was thought that MeI was escaping from the stoppered flask. The reaction mixture was transferred to a glass reaction bomb, additional MeI was added and the reaction was stirred (and monitored by ^{1}H NMR) for 48 hours. A large amount of white precipitate formed, but there was no noticeable color change. The solvent was then removed *in vacuo*, the product extracted with pentane, and [NMe_4]I was removed by filtration through a medium frit. The solution was concentrated down to about 4 mL, when small microcrystals became apparent in the solution. Cooling overnight at -35 °C yielded a cake of orange microcrystalline powder (0.7952 g, 1.189 mmol, 94.6 %). M.p. 57-9 °C. ^{1}H NMR (300 MHz, $CDCl_3$): δ = 7.4 (tm, J ~ 5.4 Hz, 2H); 7.331 (d, J = 7.8 Hz, 2H); 7.237 (dm, J ~ 4.2 Hz, 3H); 6.912 (t, J = 7.8 Hz, 1H); 6.850 (s, 1H, para); 6.408 (s, 2H, ortho); 2.859 (s, 6H, N*Me*$_2$); 2.180 (s, 6H, Ar*Me*); 1.620 (s, 18H, C(C*H*$_3$)$_3$). ^{13}C NMR (75 MHz, $CDCl_3$): δ = 165.424, 144.226, 142.433, 138.998, 137.546, 129.049, 128.891, 127.820, 127.145, 126.979, 125.765, 120.894, 68.955 (*C*(CD$_3$)$_2$C$_6$H$_5$), 49.836 (N*Me*$_2$), 35.730 (*C*(CH$_3$)$_3$), 32.414 (C(*C*H$_3$)$_3$), 31.0 (*C*D$_3$), 21.101 (Ar*Me*). MS (70 eV): *m/z*(%): 667.9 (0.19)[*M*+]. Anal. Calcd for $C_{33}H_{41}D_6IN_2OTi$: C, 59.29; H, 7.09; N, 4.19. Found: C, 58.98; H, 7.34; N, 3.88.

(xix) Ti(N[R$_{ph}$]Ar)(O-2,6-C$_6$H$_3$[CMe$_3$][CH$_2$CMe$_2$-])(I) (1.27): A solution of Ti(N[R_{ph}]Ar)(OAr")(I)(NMe_2) (**1.24**, 1.3206 g, 1.9752 mmol) in pentane (40 mL) was chilled to -40 °C. Neopentyllithium (0.1543 g, 1.9761 mmol) was added as a solution in ether. The reaction mixture changed from red to yellow over about five minutes. After the solution was stirred for 18 hours, the yellow brown solution was filtered to remove lithium iodide. Proton NMR spectroscopy showed a relatively clean conversion to the desired alkyl complex Ti(N[R_{ph}]Ar)(OAr")(CH_2CMe_3)(NMe_2) (**1.25**), but crystallization proved to be impossible. The ether was removed *in vacuo* and THF (40 mL) was added.

References begin on page 81

The mixture was heated at 65 °C for two hours. Proton NMR spectroscopy showed 50% conversion to the cyclometallated dimethylamide compound Ti(N[R_{ph}]Ar)(O-2,6-C_6H_3[CMe_3][CH_2CMe_2-])(NMe_2) (**1.26**). Further heating at 65 °C gave a clean conversion. The THF was removed *in vacuo* and ether (60 mL) and MeI (2.90 g, 20.4 mmol, 10.3 eq) were added. No reaction occurred at room temperature, so the mixture was heated to 70 °C for 21 hours. A precipitate was observed, but there was no color change. A proton NMR spectrum showed no starting dimethylamide peak. Solvent was removed *in vacuo* leaving a solid, which was reconstituted in pentane. [NMe_4]I was removed by filtration and the solution was concentrated to a minimum volume. Crystals were obtained after storage overnight at -35 °C (0.7668 g, 1.230 mmol, 62.3%). M.p. 102-103 °C. ^{1}H NMR (300 MHz, $CDCl_3$): δ = 7.78 (d, *J* = 7.59 Hz, 2H); 7.393 (t, *J* = 7.04 Hz, 2H); 7.295 (t, *J* = 6.7 Hz, 1H); 7.174 (d, *J* = 7.71 Hz, 1H); 7.0235 (d, *J* = 7.71 Hz, 1H); 6.90 (s, 1H, para); 6.879 (t, *J* ~ 10 Hz, 1H); 6.708 (s, 2H, ortho); 2.202 (s, 6H, Ar*Me*); 1.470 (d, *J* = 11.7 Hz, 1H, CH_2-a); 1.320 (s, 9H, $C(CH_3)_3$); 0.9836 (s, 6H, $C(CH_3)_2$Ar); 0.833 (d, *J* = 11.7 Hz, CH_2-b). ^{13}C NMR (125 MHz, $CDCl_3$): δ = 162.818, 146.038, 143.338, 139.764, 139.345, 136.051, 130.326, 129.281, 127.914, 126.766, 124.759, 124.577, 122.270, 122.070, 65.842, 46.410, 35.304, 32.578, 32.046, 30.603, 28.2, 25.455, 21.202. 15.259. Anal. Calcd for $C_{31}H_{34}D_6INOTi$: C, 59.72; H, 6.47; N, 2.25. Found: C, 60.19; H, 6.98; N, 1.92.

(xx) Ti(N[R_{ph}]Ar)$_2$($Cl)_2$ (1.29): $TiCl_3(THF)_3$ (1.00 g, 2.70 mmol) and TMEDA (1.94 g, 16.7 mmol) were added to THF (100 mL) to form a bright blue solution. Et_2O·Li(N[R_{ph}]Ar) (1.76 g, 5.41 mmol) was added causing the solution to become olive green. The solvent was removed *in vacuo*, the solids were reconstituted in ether and filtered to remove LiCl. Yellow green crystals of Ti(N[R_{ph}]Ar)$_2$(μ-Cl)$_2$Li(TMEDA)$_3$ (**1.28**) were collected from a concentrated solution at -35 °C (2.28 g, 2.37 mmol, 87.7%). ^{2}H NMR (46 MHz, C_6H_6): δ($\Delta\nu_{1/2}$): 4.84(46.5). A large excess of chloroform (1.48 g)

References begin on page 81

was added to an olive green ether solution of the solid (0.17 g, 0.18 mmol). The solution turned blood red. Proton NMR spectroscopy showed three equivalents of TMEDA. The solvent was removed *in vacuo* and the product was extracted with benzene. The solution was filtered through glass fibers and evaporated to dryness yielding a dark red microcrystalline powder (0.10 g, 0.16 mmol, 91%). The red solid was recrystallized by vapor diffusion of pentane into toluene followed by cold storage overnight. M.p. 155-160 °C (dec). ^{1}H NMR (300 MHz, $CDCl_3$): δ = 7.45 (d, 4H, phenyl ortho); 7.28 (m, 6H, phenyl meta, para); 6.56 (s, 2H, para); 5.62 (s, 4H, ortho); 1.93 (s, 12H, Ar*Me*). ^{13}C NMR (75 MHz, $CDCl_3$): δ = 147.700, 143.119, 137.286, 128.699, 127.812, 126.841 (may be 2 carbons), 123.475, 71.2 ($C(CD_3)_2Ar$); 28.7 (CD_3); 21.094 (Ar*Me*). Anal. Calcd. for $C_{34}H_{28}D_{12}Cl_2N_2Ti$: C, 67.22; H, 6.64; N, 4.61. Found: C, 67.00; H, 6.69; N, 4.28.

(xxi) Ti(N[R]Ar)$_2$(μ-Cl)$_2$Li(TMEDA) (1.30): $Cl_3Ti(THF)_3$ (1.00 g, 2.70 mmol) was slurried in THF (100 mL). TMEDA (1.92 g, 6.13 eq) was added, forming a blue solution. A solution of Et_2O·LiN[R]Ar (1.43 g, 5.44 mmol) was dissolved in THF (50 mL) and added, causing an rapid color change to bright green. After five minutes, the green color faded to olive. The THF was removed *in vacuo* and the resulting oil was triturated twice with pentane, extracted with pentane and filtered to remove LiCl. The solution was stored at -30 °C overnight, giving bright green needles (0.93 g, 56.9%). M.p. 137-138 °C. ^{2}H NMR (46 MHz, C_6H_6): $\delta(\Delta\nu_{1/2})$ = 3.809(18.5). μ_{eff} (300 MHz, C_6D_6, 25 °C) 2.219 μ_B. Uv-vis (hexane): $\lambda_{max}(\varepsilon)$ 780 nm (188 $M^{-1}cm^{-1}$). EPR (298 K, toluene): g = 1.95. EPR (103 K, toluene): g_1 = 1.980, g_2 = 1.964, g_3 = 1.930; this spectrum is approximately axial with broad linewidths (~25 G) that merge g_1 and g_2 into one feature. Anal. Calcd for $C_{30}H_{40}D_{12}Cl_2N_2LiTi$: C, 59.40; H, 8.64; N, 9.24. Found: C, 58.97; H, 8.44; N, 8.46.

References begin on page 81

(xxii) $Ti(N[R]Ar)_2(Cl)_2$ (1.31): A small amount of $Ti(N[R]Ar)_2(\mu\text{-}Cl)_2Li(TMEDA)$ (**1.30**) was added to $CDCl_3$, causing the solution to turn red. ^1H NMR (250 MHz, $CDCl_3$): δ = 6.877 (s, 2H, paras); 6.363 (s, 4H, orthos); 2.262 (s, 12H, ArMe); 1.263 (s, 6H, d_6-*t*-Bu); 2.389 (s, 4H, TMEDA methylene); 2.20 (s, 12H, TMEDA methyls).

(xxiii) $Ti(N[R]Ar)_2(CH_2SiMe_3)_2$ (1.32): To a solution of $Ti(N[R]Ar)_2I_2$ (**1.10**, 0.101 g, 0.152 mmol) in pentane was added a solution of $LiCH_2SiMe_3$ (0.0297 g, 0.315 mmol) to give a final volume of 10 mL. The solution immediately changed from dark brown to orange, and became yellow over the period of one hour. The solution was filtered and solvent was removed *in vacuo* to yield an orange/yellow semi-solid which was judged to be ~95% pure by ^1H NMR (0.0751 g, 0.128 mmol, 84%). ^1H NMR (300 MHz, C_6D_6): δ = 6.958 (s, 4H, ortho), 6.77 (s, 2H, para), 2.243 (s, 12H, Ar*Me*), 1.595 (s, 4H, CH_2SiMe_3), 1.344 (s, 6H, $CCH_3(CD_3)_2$), 0.180 (s, 18H, $SiMe_3$). ^{13}C NMR (75 MHz, $CDCl_3$): δ = 144.821 (s, ipso), 137.358 (q, ^2J = 6.5 Hz, meta), 129.511 (d, J = 156.7 Hz, ortho), 127.577 (d, J = 142.1, para), 79.867 (t, J = 106.8 Hz, CH_2), 60.872 (s, $CCH_3(CD_3)_2$), 30.483 (q, J = 127.2 Hz, $CCH_3(CD_3)_2$), 29.992 (m, $CCH_3(CD_3)_2$), 21.285 (q, J = 125.8 Hz, Ar*Me*), 2.474 (q, J = 117.9 Hz, $SiMe_3$).

(xxiv) $Ti(N[R]Ar)_2(CH_2CMe_2Ph)_2$ (1.33): To a solution of $Ti(N[R]Ar)_2I_2$ (**1.10**, 0.100 g, 0.150 mmol) in pentane was added a solution of $LiCH_2CMe_2Ph$ (0.0425 g, 0.303 mmol) to give a final volume of 10 mL. The solution immediately turned from dark brown to yellow and changed to a brownish red color over one hour. The solution was filtered and solvent was removed *in vacuo* to yield a dark brown oil which was judged to be ~95% pure by proton NMR (0.0968 g, 0.1426 mmol, 95%). ^1H NMR (300 MHz, C_6D_6): δ = 7.24 (m, 6H, alkyl ortho/meta); 7.07 (m, 2H, alkyl para); 6.985 (s, 4H, ortho); 6.787 (s, 2H, para); 2.248 (s, 12H, ArMe); 1.839 (s, 4H, CH_2CMe_2Ph); 1.334 (s, 6H,

References begin on page 81

$CCH_3(CD_3)_2$); 1.266 (s, 12H, $CH_2C(CH_3)_2Ph$). ^{13}C NMR (75 MHz, $CDCl_3$): δ = 153.211 (s, alkyl ipso); 146.700 (s, ipso); 137.502 (q, ^2J = 5.9 Hz, meta); 129.947 (d, J = 164.6 Hz); 127.645 (d, J = 161.1 Hz); 127.567 (d, J ~ 160 Hz); 125.418 (d, J ~ 157 Hz); 124.696 (d, J = 160.0 Hz); 107.206 (t, J = 110.3 Hz, CH_2CMe_2Ph); 60.832 (s, $CCH_3(CD_3)_2$); 43.787 (s, CH_2CMe_2Ph); 32.777 (q, J = 125.4 Hz, $CH_2C(CH_3)_2Ph$)); 32.520 (q, J = 124.5 Hz, $CCH_3(CD_3)_2$); 30.044 (m, $CCH_3(CD_3)_2$); 21.322 (q, J = 126.4 Hz, Ar*Me*).

(xxv) $Ti(N[R]Ar)_2(CH[SiMe_3]_3)$ (1.34): $Ti(N[R]Ar)_2(\mu\text{-}Cl)_2Li(TMEDA)$ (**1.30**, 1.1385 g, 1.8770 mmol) in pentane (50 mL) was cooled to -35 °C. $LiCH(SiMe_3)_2$ (0.3123 g, 1.877 mmol) was added as a solid. The reaction mixture became dark green on addition. The reaction was stirred for 15 minutes, and then filtered to remove LiCl (0.1348 g, 3.186 mmol, 1.7 eq). The resulting dark green solution was concentrated to about 20 mL and stored at -35 °C. Dark green block-like crystals were obtained in two crops (0.7755 g, 1.356 mmol, 72.3 %). M.p. 134-135 °C. ^2H NMR (46 MHz, C_6H_6): δ = 3.968; $\Delta\nu_{1/2}$ 17.9 Hz. μ_{eff} (300 MHz, C_6D_6, 25 °C) 2.213 μ_B. UV-Vis (ether): $\lambda_{max}(\varepsilon)$ = 663 nm (407 $M^{-1}cm^{-1}$). EPR (298 K, toluene): g = 1.95. EPR (95 K, toluene): g_1 = 1.997; g_2 = 1.962; g_3 = 1.918. Anal. Calcd. for $C_{31}H_{43}D_{12}N_2Si_2Ti$: C, 65.10; H, 9.69; N, 4.90. Found: C, 65.36; H, 9.76; N, 4.67.

(xxvi) $Ti(N[R]Ar)_2(CH[SiMe_3]_2)(I)$ (1.35): $Ti(N[R]Ar)_2(CH[SiMe_3]_2)$ (**1.34**, 0.4034 g, 0.7054 mmol) was dissolved in benzene (5 mL). Iodine (0.0900 g, 0.3546 mmol, 0.5 eq) was slurried in benzene (5 mL) and the slurry was added to the alkyl. The reaction mixture became dark orange-red. The solvent was removed *in vacuo* giving a light orange powder. Crystals were obtained from a concentrated ether solution (0.3329 g, 0.4764 mmol, 67.5 %). M.p. 175-176 °C. ^1H NMR (300 MHz, C_6D_6): δ = 6.938 (br d, J = 71.9 Hz, 4H, ortho); 6.710 (s, 2H, para); 3.466 (s, 1H, $CH(SiMe_3)_2$); 2.184 (s, 12H,

References begin on page 81

Ar*Me*); 1.404 (s, 6H, $C(CD_3)_2CH_3$); 0.393 (s, 18H, Si*Me*$_3$). ^{13}C NMR (125 MHz, $CDCl_3$): δ = 145.972 (s, ipso), 137.682 & 137.085 (s, meta), 128.594 & 127.971 (d, ortho and meta); 112.023 (d, para), 104.010 (d, *J* = 90.6 Hz, $CH(SiMe_3)_2$); 65.306 (s, $C(CD_3)_2CH_3$), 30.394 (q, $C(CD_3)_2CH_3$); 30.074 (m, $C(CD_3)_2CH_3$), 21.274 (q, Ar*Me*), 5.857 (q, Si*Me*$_3$). Anal. Calcd. for $C_{31}H_{43}D_{12}IN_2Si_2Ti$: C, 53.28; H, 7.93; N, 4.01. Found: C, 53.66; H, 7.90; N, 3.84. **Alternate preparation from 1.10:** Alkylation of $Ti(N[R]Ar)_2I_2$ with $LiCH(SiMe_3)_2$ in pentane was exceedingly slow, and led to some decomposition. However, the major product after 48 hours was complex **1.35**.

(xxvii) $[Ti(N[R]Ar)_2(CH[SiMe_3]_2)(NCPh)]_2$ (1.37):

$Ti(N[R]Ar)_2(CH[SiMe_3]_2)$ (**1.34**, 0.4257 g, 0.7444 mmol) was dissolved in ether (20 mL) and cooled to -35 °C. Benzonitrile (100 mL, 0.7534 mmol) was added over approximately 5 minutes causing a rapid color change to the deep dark blue of $Ti(N[R]Ar)_2[CH(SiMe_3]_2(NCPh)$ (**1.36**). ^2H NMR (46 MHz, Et_2O): $\delta(\Delta\nu_{1/2})$ = 4.671(20), 1.86(17). The diamagnetic peak grew in noticeably over a 10 minute period. After 17 hours of stirring, an orange powder which precipitated was collected on a frit (0.4212 g, 0.6130 mmol, 82%). The powder was essentially insoluble in pentane and ether but could be recrystallized from hot THF. M.p. 180 °C (dec). ^1H NMR (300 MHz, C_6D_6): δ = 8.039 (br s, 2H); 7.28 (m, 8H); 6.587 (s, 4H); 6.397 (br s, 8H); 2.159 (s, 24H, Ar*Me*); 1.439 (s, 2H, $CH(SiMe_3)_2$); 1.210 (s, 12H, $C(CD_3)_2CH_3$); 0.443 (s, 36H, Si*Me*$_3$). ^{13}C NMR (75 MHz, $CDCl_3$): δ = 173.115 (s, *C*=N); 148.112 (s); 143.462 (s); 135.773 (s); 129.878 (d); 129.441 (d); 128.037 (d); 127.458 (d); 127.140 (d); 77.206 (d, $CH(SiMe_3)_2$); 62.380 (s, $C(CD_3)_2CH_3$); 30.628 (q, $C(CD_3)_2CH_3$); 30.065 (m, $C(CD_3)_2CH_3$); 21.408 (q, Ar*Me*); 6.181 (q, Si*Me*$_3$). Anal. Calcd. for $C_{76}H_{96}D_{24}N_6Si_4Ti_2$: C, 67.61; H, 8.96; N, 6.22. Found: C, 68.05; H, 9.26; N, 6.13.

References begin on page 81

(xxviii) $Ti(N[R]Ar)_2(CH[SiMe_3]_2)(N_3)$ (1.39): $Ti(N[R]Ar)_2(CH[SiMe_3]_2)$ (**1.34**, 0.7124 g, 0.1.245 mmol) was dissolved in pentane (40 mL). *tert*-Butyl nitrile (575 mL, 5.20 mmol, 4 eq) was added, causing a color change to a light green. Trimethylsilylazide (230 mL, 0.1.733 mmol, 1.4 eq) was then added and the solution was stirred overnight (after about 2 hours the solution changed to an orange/yellow color). The pentane was removed *in vacuo*, and the waxy solid thus obtained was recrystallized from pentane to give a light orange powder (0.2852 g, 0.4645 mmol, 37%). M.p. 147-148 °C (dec. with bubbling). ^1H NMR (300 MHz, C_6D_6): δ = 6.839 (br s, 4H, ortho); 6.708 (s, 2H, para); 2.50 (s, 1H, $CH(SiMe_3)_2$); 2.213 (s, 12H, Ar*Me*); 1.251 (s, 6H, $C(CD_3)_2CH_3$); 0.222 (s, 18H, $SiMe_3$). ^{13}C NMR (75 MHz, $CDCl_3$): δ = 146.815 (s, ipso); 137.629 (s, meta); 128.247 (d, J = 157.3 Hz); 128.201 (d, J = 157.4 Hz); 98.1749 (d, J = 90.85 Hz, $CH(SiMe_3)_2$); 63.6716 (s, $C(CD_3)_2CH_3$); 30.3523 (q, J = 125.9 Hz, $C(CD_3)_2CH_3$); 29.8439 (m, $C(CD_3)_2CH_3$); 21.3200 (q, J = 126.4 Hz, Ar*Me*); 4.2006 (q, J = 118.2 Hz, $SiMe_3$). IR (16 scans, 2.0 cm^{-1}, THF): $\nu(N_3)$ 2107 cm^{-1}. Anal. Calcd for $C_{31}H_{43}D_{12}N_5Si_2Ti$: C, 60.64; H, 9.03; N, 11.41. Found: C, 60.75; H, 9.07; N, 11.05.

1.11.4 X-ray Structure of $Ti(N[R]Ar)_2(CH[SiMe_3]_2)$ (1.34). A crystal of approximate dimensions 0.50 × 0.23 × 0.20 mm was obtained from a chilled ether solution. The crystal was mounted on a glass fiber. Data were collected at –86 °C on an Enraf-Nonius CAD-4 diffractometer with graphite-monochromated Mo Kα radiation. A total of 4774 reflections were collected to a 2θ value of 44.9 °, 4446 of which were unique (R_{int} = 0.098); equivalent reflections were merged. The structure was solved by direct methods. Non-hydrogen atoms were refined anisotropically, except C26 which was refined isotropically. The final cycle of least-squares refinement was based on 2735 observed reflections (I > 3.00σ(I)) and 320 variable parameters and converged (largest parameter shift was 0.01 times its esd) with R = 0.075 and R_w = 0.065. A final difference Fourier map showed no chemically significant features. Crystal data: a = 10.644(2) Å, b =

References begin on page 81

10.844(2) Å, c = 16.718(4) Å, V = 1713(2) Å^3, α = 100.48(3) °, β = 95.86(3) °, γ = 113.11(3) °, space group $P\bar{1}$ (No. 2), Z = 2, M_r = 571.92 for $C_{31}H_{43}D_{12}N_2Si_2Ti$, and ρ(calcd) = 1.109 g/cm^3. See Tables 1.1 and 1.2 for metrical parameters, Table 1.3 for positional parameters and U(eq), and Figure 1.5 for an ORTEP diagram.

References begin on page 81

References

1) Wailes, P. C.; Coutts, R. S. P.; Weigold, H. *Organometallic Chemistry of Titanium, Zirconium, and Hafnium*; Academic Press Inc.: New York, 1974.
2) Collman, J. P.; Hegedus, L. S.; Norton, J. R.; Finke, R. G. *Principles and Applications of Organotransition Metal Chemistsry*; University Science Books: Mill Valley, California, 1987.
3) Mitchell, J. P.; Hajela, S.; Brookhart, S. K.; Hardcastle, K. I.; Henling, L. M.; Bercaw, J. E. *J. Am. Chem. Soc.* **1996**, *118*, 1045.
4) Margl, P.; Lohrenz, J. C. W.; Ziegler, T.; Blöchl, P. E. *J. Am. Chem. Soc.* **1996**, *118*, 4434.
5) Willoughby, C. A.; Buchwald, S. L. *J. Am. Chem. Soc.* **1992**, *114*, 7562-4.
6) McMurry, J. E.; Siemers, N. O. *Tet. Lett.* **1993**, *34*, 7891-4.
7) Buchwald, S. L.; Nielsen, R. B. *J. Am. Chem. Soc.* **1989**, *111*, 2870-74.
8) Jeffery, J.; Lappert, M. F.; Luong-Thi, N. T.; Webb, M.; Atwood, J. L.; Hunter, W. E. *J. Chem. Soc. Dalton* **1981**, 1593-1605.
9) Wild, F. R. W. P.; Wasiucionek, M.; Huttner, G.; Brintzinger, H. H. *J. Organometal. Chem.* **1985**, *288*, 63.
10) Wild, F. R. W. P.; Zsolnai, L.; Huttner, G.; Brintzinger, H. H. *J. Organomet. Chem.* **1982**, *232*, 233-47.
11) Herrmann, W. A.; Morawietz, M. J. A. *J. Organometal. Chem.* **1994**, *482*, 169.
12) Shapiro, P. J.; Cotter, W. D.; Schaefer, W. P.; Labinger, J. A.; Bercaw, J. E. *J. Am. Chem. Soc.* **1994**, *116*, 4623-40.
13) Borkowsky, S. L.; Baenziger, N. C.; Jordan, R. F. *Organometallics* **1993**, *12*, 486.
14) Alelyunas, Y. W.; Guo, Z. Y.; Lapointe, R. E.; Jordan, R. F. *Organometallics* **1993**, *12*, 544.
15) LaPointe, R. E.; Wolczanski, P. T.; Mitchell, J. F. *J. Am. Chem. Soc.* **1986**, *108*, 6382-4.
16) Neithamer, D. R.; LaPointe, R. E.; Wheeler, R. A.; Richeson, D. S.; Van Duyne, G. D.; Wolczanski, P. T. *J. Am. Chem. Soc.* **1989**, *111*, 9056-72.
17) Miller, R. L.; Toreki, R.; LaPointe, R. E.; Wolczanski, P. T.; Van Duyne, G. D.; Roe, D. C. *J. Am. Chem. Soc.* **1993**, *115*, 5570-88.
18) Covert, K. J.; Wolczanski, P. T.; Hill, S. A.; Krusic, P. J. *Inorg. Chem.* **1992**, *31*, 66-78.
19) Covert, K. J.; Neithamer, D. R.; Zonnevylle, M. C.; LaPointe, R. E.; Schaller, C. P.; Wolczanski, P. T. *Inorg. Chem.* **1991**, *30*, 2494-2508.
20) Neithamer, D. R.; Pákányi, L.; Mitchell, J. F.; Wolczanski, P. T. *J. Am. Chem. Soc.* **1988**, *110*, 4421-3.
21) Eppley, D. F.; Wolczanski, P. T.; Van Duyne, G. D. *Angew. Chem. Int. Ed. Engl.* **1991**, *30*, 584-5.
22) Covert, K. J.; Wolczanski, P. T. *Inorg. Chem.* **1989**, *28*, 4565-7.
23) Wolczanski, P. T. *Polyhedron* **1995**, *14*, 3335-3362.
24) Visciglio, V. M.; Fanwick, P. E.; Rothwell, I. P. *Inorganica Chimica Acta* **1993**, *211*, 203-9.
25) Hill, J. E.; Fanwick, P. E.; Rothwell, I. P. *Organometallics* **1991** *10*, 15-16.
26) Hill, J. E.; Balaich, G.; Fanwick, P. E.; Rothwell, I. P. *Organometallics* **1993**, *12*, 2911-24.
27) Dick, D. G.; Duchateau, R.; Edema, J. J. H.; Gambarotta, S. *Inorg. Chem.* **1993**, *32*, 1959-62.
28) Hagadorn, J. R.; Arnold, J. *J. Am. Chem. Soc.* **1996**, *118*, 893-4.
29) Bradley, D. C.; Copperthwaite, R. G. *Inorg. Synth.* **1978**, *18*, 112.
30) Bradley, D. C.; Hursthouse, M. B.; Malik, K. M. A.; Möseler, R. *Transition Met. Chem.* **1978**, *3*, 253-4.

References begin on page 81

31) Andersen, R. A.; Wilkinson, G. *Inorg. Synth.* **1979**, *19*, 262-4.
32) Andersen, R. A. *Inorg. Chem.* **1979**, *18*, 2928-32.
33) Andersen, R. A.; Faegri, K.; Green, J. C.; Haaland, A.; Lappert, M. F.; Leung, W.-P.; Rypdal, K. *Inorg. Chem.* **1988**, *27*, 1782-6.
34) Bradley, D. C.; Chisholm, M. H. *Accts. Chem. Res.* **1976**, *9*, 273.
35) Berno, P.; Moore, M.; Minhas, R.; Gambarotta, S. *Can. J. Chem.* **1996**, *74*, 1930-1935.
36) Gambarotta, S. *J. Organometal. Chem.* **1995**, *500*, 117-126.
37) Song, J.-I.; Berno, P.; Gambarotta, S. *J. Am. Chem. Soc.* **1994**, *116*, 6927-6928.
38) Hoffman, D. M.; Rangarajan, S. P. *Acta Crystallogr C-Cryst Str* **1996**, *52*, 1616-1618.
39) Scoles, L.; Minhas, R.; Duchateau, R.; Jubb, J.; Gambarotta, S. *Organometallics* **1994**, *13*, 4978-83.
40) Airoldi, C.; Bradley, D. C. *Inorg. Nucl. Chem. Letters* **1975**, *11*, 155.
41) Duchateau, R.; Williams, A. J.; Gambarotta, S.; Chiang, M. Y. *Inorg. Chem.* **1991**, *30*, 4863-4866.
42) Pattiasina, J. W.; Heeres, H. J.; van Bolhuis, F.; Meetsma, A.; Teuben, J. H. *Organometallics* **1987**, *6*, 1004-10.
43) La Mar, G. N.; Horrocks Jr., W. D.; Holm, R. H. *NMR of Paramagnetic Molecules*; Academic Press: New York, 1973.
44) Laplaza, C. E.; Davis, W. M.; Cummins, C. C. *Organometallics* **1995**, *14*, 577-580.
45) Fickes, M. G.; Davis, W. M.; Cummins, C. C. *J. Am. Chem. Soc.* **1995**, *117*, 6384-6385.
46) Laplaza, C. E.; Davis, W. M.; Cummins, C. C. *Angew. Chem. Int. Ed. Engl.* **1995**, *34*, 2042-2044.
47) Laplaza, C. E.; Odom, A. L.; Davis, W. M.; Cummins, C. C.; Protasiewicz, J. D. *J. Am. Chem. Soc.* **1995**, *117*, 4999.
48) Laplaza, C. E.; Cummins, C. C. *Science* **1995**, *268*, 861-863.
49) Laplaza, C. E.; Johnson, M. J. A.; Peters, J. C.; Odom, A. L.; Kim, E.; Cummins, C. C.; George, G. N.; Pickering, I. J. *J. Am. Chem. Soc.* **1996**, *118*, 8623-8638.
50) Laplaza, C. E.; Johnson, A. R.; Cummins, C. C. *J. Am. Chem. Soc.* **1996**, *118*, 709-710.
51) Odom, A. L.; Cummins, C. C. *J. Am. Chem. Soc.* **1995**, *117*, 6613-6614.
52) Odom, A. L.; Cummins, C. C. *Organometallics* **1996**, *15*, 898-900.
53) Peters, J. C.; Johnson, A. R.; Odom, A. L.; Wanandi, P. W.; Davis, W. M.; Cummins, C. C. *J. Am. Chem. Soc.* **1996**, *118*, 10175.
54) Stokes, S. L.; Davis, W. M.; Odom, A. L.; Cummins, C. C. *Organometallics* **1996**, *15*, 4521-4530.
55) Wanandi, P. W.; Davis, W. M.; Cummins, C. C.; Russell, M. A.; Wilcox, D. E. *J. Am. Chem. Soc.* **1995**, *117*, 2110-11.
56) a) Kim, E.; Cummins, C. C. **1996**, Unpublished Results. b) Sharp, P. R. and Schrock, R. R. *J. Am. Chem. Soc.* **1983**, *102*, 1430. c) Schrock, R. R., Sturgeoff, L. G. and Sharp, P. R. *Inorg. Chem.* **1983**, *22*, 2801. d) Chisholm, M. H. Eichhorn, B. W., Folting, K., Huffman, J. C., Ontiverus, C. D., Streib, W. E. and Van Der Sluys, W. G. *Inorg. Chem.* **1987**, *26*, 3182.
57) Wanandi, P. W.; Cummins, C. C. **1996**, Unpublished Results.
58) Johnson, A. R.; Wanandi, P. W.; Cummins, C. C.; Davis, W. N. *Organometallics* **1994**, *13*, 2907-2909.
59) Baumann, R.; Davis, W. M.; Schrock, R. R. *J. Am. Chem. Soc.* **1997**, *119*, 3830-3831.

References begin on page 81

60) Johnson, A. R.; Davis, W. M.; Cummins, C. C. *Organometallics* **1996**, *15*, 3825-3835.
61) Johnson, A. R.; Cummins, C. C. *Inorg. Synth.* **1997**, *32*, In Press.
62) Hunter, D. H.; Racok, J. S.; Rey, A. W.; Ponce, Y. Z. *J. Org. Chem.* **1988**, *53*, 178-1281.
63) Eaton, D. R.; Tong, P. K. *Inorg. Chem.* **1980**, *19*, 740-4.
64) Stokes, S. L.; Cummins, C. C. **1996**, Unpublished Results.
65) Fickes, M. G.; Odom, A. L.; Stokes, S. L. **1996**, Personal communication.
66) Manzer, L. E. *Inorg. Synth.* **1982**, *21*, 135.
67) Benzing, E.; Kornicker, W. *Chem. Ber.* **1961**, *94*, 2263.
68) Schulz, H.; Folting, K.; Huffman, J. C.; Streib, W. E.; Chisholm, M. H. *Inorg. Chem.* **1993**, *32*, 6056-66.
69) Kim, E.; Cook, J.; Cummins, C. C. **1997**, Manuscript in Preparation.
70) Latesky, S. L.; Keddington, J.; McMullen, A. K.; Rothwell, I. P.; Huffman, J. C. *Inorg. Chem.* **1985**, *24*, 995-1001.
71) Odom, A. L. **1997**, Unpublished Results.
72) Latesky, S. L.; McMullen, A. K.; Rothwell, I. P.; Huffman, J. C. *J. Am. Chem. Soc.* **1985**, *107*, 5981-5987.
73) Chamberlain, L. R.; Rothwell, I. P.; Huffman, J. C. *J. Am. Chem. Soc.* **1986**, *108*, 1502-1509.
74) Chamberlain, L.; Keddington, J.; Rothwell, I. P.; Huffman, J. C. *Organometallics* **1982**, *1*, 1538-40.
75) Sur, S. K. *J. Magnetic Resonance* **1989**, *82*, 169-73.
76) Mombourquette, M. J.; Weil, J. A.; McGavin, D. G. *Computer Program EPR-NMR*; University of Saskatchewan, Canada: Department of Chemistry, 1993.
77) Minhas, R. K.; Scoles, L.; Wong, S.; Gambarotta, S. *Organometallics* **1996**, *15*, 1113-1121.
78) Barker, G. K.; Lappert, M. F. *J. Organometal. Chem.* **1974**, *76*, C45.
79) Barker, G. K.; Lappert, M. F.; Howard, J. A. K. *J. Chem. Soc. Dalton* **1978**, 734-40.
80) Davies, C. E.; Gardiner, I. M.; Green, J. C.; Green, M. L. H.; Grebenik, P. D.; Mtetwa, V. S. B.; Prout, K. *J. Chem. Soc., Dalton Trans.* **1985**, 669.
81) Luinstra, G. A.; ten Cate, L. C.; Heeres, H. J.; Pattiasina, J. W.; Meetsma, A.; Teuben, J. H. *Organometallics* **1991**, *10*, 3227.
82) Luker, T.; Whitby, R. J.; Webster, M. *J. Organometal. Chem.* **1995**, *492*, 53-7.
83) LaMonica, G.; Cenini, S. *J. Chem. Soc., Dalton Trans.* **1980**, 1145-9.
84) Nugent, W. A.; Mayer, J. M. *Metal-Ligand Multiple Bonds*; John Wiley & Sons: New York, 1988, pp 76-78.
85) Davidson, P. J.; Harris, D. H.; Lappert, M. F. *J. Chem. Soc., Dalton Trans.* **1976**, 2268-74.

References begin on page 81

Chapter II: Molybdenum(V) and -(VI) Chalcogenide Complexes*

* Reprinted in part with permission from *J. Am. Chem. Soc.*, submitted for publication (© 1997 American Chemical Society).

References begin on page 184

Section 2.1: Introduction

Transition metal complexes with a terminal chalcogen atom in the coordination sphere currently are being studied in order to develop new chalcogen atom transfer reagents. The field of oxygen atom transfer has been reviewed,[1,2] but there is much less precedent for the transfer of the heavier chalcogens.[3,4] Transition metal complexes of the heavier chalcogens are rare,[5,6] and their chemistry is dominated by single bonding.[7,8] Complexes which support double bonding to tellurium have only recently become available,[9] but since that time, other complexes containing the terminal tellurido functionality have appeared.[8,10-17] Further study of chalcogenido complexes may uncover novel reactivity and interesting periodic trends. [5]

A variety of synthetic routes to the tellurolate anion (RTe^-) are being examined by Arnold, and these groups can be converted to the terminal telluride by using appropriate procedures. Elemental tellurium inserts into a lithium alkyl bond to form the lithium tellurolate, which is used in substitution reactions to generate transition metal tellurolates.[18] $HTeSi(SiMe_3)_3$ reacts with $Zr(Bz)_4$ to liberate toluene and generate $Zr(TeSi[SiMe_3]_3)_4$. Addition of the bridging phosphine dmpe initially forms $Zr(TeSi[SiMe_3]_3)_4(dmpe)$ and then $Zr(Te)(TeSi[SiMe_3]_3)_2(dmpe)_2$ with the loss of $Te(Si[SiMe_3]_3)_2$.[13] Tellurium also inserts into transition metal-alkyl bonds. Cp_2ScR reacts with elemental Te to give the tellurolate Cp_2ScTeR. The corresponding reaction with Cp^*_2TiH results in the loss of dihydrogen, and a complex with a μ_2 bridging tellurium between two Cp^*_2Ti centers is the isolated product.[19] A similar reaction occurs between $Cp^*_2Ta(H)(CH_2)$ and tellurium in the presence of PMe_3. Tellurium adds across the metal carbon double bond to form the tantalum adduct of telluroformaldehyde, $Cp^*_2Ta(\eta^2\text{-}CH_2Te)(H)$, which is stable at room temperature. Heating above 130 °C causes a tautomerization to form the methyl telluride complex $Cp^*_2Ta(Te)(Me)$.[8] The corresponding addition reaction does not occur with O and S atom sources, although $Cp^*_2TaH_3$ reacts with Se to form the *cyclo*-diselenide $Cp^*_2Ta(\eta^2\text{-}Se_2)(H)$. This species reacts with MeI at 80 °C to give the selenide iodide

References begin on page 184

$Cp^*_2Ta(Se)(I)$.[20] $Cp^*_2Zr(CO)_2$ reacts with Se to give the terminal Zirconium(IV) chalcogenide $Cp^*_2Zr(Se)(CO)$.[21]

$V(N_3N)$ (N_3N = $[Me_3SiNCH_2CH_2]_3N$) reacts with a variety of oxo donors (propylene oxide, pyridine-*N*-oxide, N_2O, DMSO) to generate the oxo; S_8 and episulfides to generate the sulfido; elemental Se to generate the selenide; and trimethylphosphine telluride to generate the terminal telluride, which is only observed spectroscopically.[10] $V(N_3N)$ does not react with elemental tellurium, however. $TaCl_2(N_3N)$ reacts with two equivalents of either $LiSeSi(SiMe_3)_3$ or $LiTeSi(SiMe_3)_3$ to generate $ETa(N_3N)$ and $E(Si[SiMe_3]_3)$.[14] Sharp bands for the selenide (507 cm^{-1}) and telluride (460 cm^{-1}) are observed in the Raman spectrum.

The periodic trends of the chalcogenide series on a variety of transition metals are being studied by Parkin. In group four, $Cp^*_2M(CO)_2$ (M = Zr, Hf) reacts with elemental sulfur, selenium or tellurium in the presence of pyridine at 80-100 °C to give the terminal chalcogenide pyridine complex $Cp^*_2M(E)(py)$. The telluride reacts with N_2O to give the oxo complex.[11,22] $Mo(PMe_3)_4$ reacts with H_2S, H_2Se, Se and Te to give the *trans*-dichalcogenide complexes $Mo(E)_2(PMe_3)_4$,[16] and $W(PMe_3)_4(H)(\eta^2\text{-}CH_2PMe_2)$ reacts with H_2S, H_2Se and Te to give, again, the *trans* species $W(E)_2(PMe_3)_4$.[5]. Neither the corresponding tungsten nor molybdenum oxo complex has been made.

$Mo(N[R]Ar)_3$ (**2.1**, R = $C(CD_3)_2CH_3$, Ar = 3,5-$C_6H_3Me_2$) is an extremely reactive three-coordinate trigonal planar complex.[23] The complex is a powerful three electron reductant, capable of reducing dinitrogen[24] and effecting nitrogen atom transfer from $Mo(N)(O\text{-}t\text{-}Bu)_3$.[25] Interest in chalcogenide chemistry with complex **2.1** stems from the unusual selectivity in its reaction with N_2O, giving exclusively the terminal nitrido and nitrosyl complexes $NMo(N[R]Ar)_3$ and $(ON)Mo(N[R]Ar)_3$ rather than the terminal oxo complex $OMo(N[R]Ar)_3$.[23] There are a number of examples of N_2O acting as an O-atom donor,[26-29] and this makes thermochemical sense as the N-N bond dissociation enthalpy is 84.4 kcal·mol^{-1} while the N-O enthalpy is only 38.6 kcal·mol^{-1},[30,31] and the liberation of

References begin on page 184

dinitrogen is entropically favorable. There are therefore only a few examples of N-N bond cleavage in N_2O.[31-33] In the molybdenum tris-anilide system, the reverse cleavage is rationalized by the fact that two strong Mo-N triple bonds are formed in the products, but it seems counterintuitive that the Mo(V) oxo complex is not formed, thereby liberating dinitrogen. This species is never observed even in small quantities during the reaction, a fact initially attributed to thermodynamic or kinetic instability.

This chapter describes the preparation and characterization of the entire series of paramagnetic Mo(V) terminal chalcogenido complexes with the N[R]Ar ancillary ligand environment, definitively showing that the terminal oxo species is not an unstable complex. This is the first full series of terminal chalcogenido complexes of molybdenum, although a partial series does exist.[16] Estimates of the Mo-O and Mo-S bond dissociation enthalpies determined by calorimetry and further verified by high level theoretical calculations further demonstrate the high stability of these Mo(V) d^1 complexes. All four complexes undergo a thermal C-N bond homolysis reaction, generating a series of diamagnetic Mo(VI) chalcogenide complexes. Extensive studies examining chalcogen atom abstraction from a wide variety of organic and inorganic substrates are also described.

Section 2.2: Mo(V) Chalcogenide Complexes

(i) Synthesis and Characterization of $OMo(N[R]Ar)_3$ (2.2)

Simple mixing of the reactive d^1 complex $Ti(N[R]Ar)_3$ with the vanadium oxo complex $OV(O\text{-}t\text{-}Bu)_3$ forms the heterodinuclear μ-oxo species $(Ar[R]N)_3TiOV(O\text{-}t\text{-}Bu)_3$ in good yield.[34] With the more reducing $Mo(N[R]Ar)_3$ (**2.1**) the reaction should lead to complete atom transfer, generating the terminal Mo(V) oxo species $OMo(N[R]Ar)_3$ (**2.2**). Simple mixing of ethereal solutions of the two reagents in fact leads to a marked color change to dark brown. Examination of the reaction mixture by ^2H NMR spectroscopy shows a single peak at approximately 7.2 ppm, indicative of a d^1 species in this system.[35]

References begin on page 184

Unfortunately, the resulting vanadium product is not easily separated from the molybdenum complex, though fractional crystallization does lead to a purified fraction of the oxo complex. The putative [V(O-*t*-Bu)$_3$] fragment is an intractable dark oil which exhibits four to five broad resonances in its ^{1}H NMR spectrum and no signal by ^{51}V NMR spectroscopy. EI-MS is inconclusive, as the compound has not been entirely purified, and the molecular ion is intermediate between the V(III) complex and the corresponding dimer V$_2$(O-*t*-Bu)$_6$. For preparative scale reactions to generate **2.2**, pyridine *N*-oxide serves as an efficient oxo donor (Scheme 2.1). Addition of the solid reagent to a solution of **2.1** causes a rapid color change to reddish brown in a matter of minutes. The complex is highly crystalline and is isolated from ether in yields in excess of 70%.

Compound **2** exhibits a single resonance in the ^{2}H NMR spectrum at 7.6 ppm in toluene with a peak width at half height of 30 Hz. The corresponding ^{1}H NMR spectrum exhibits only two resonances in the range ± 100 ppm: 7.2 ppm for the *tert*-butyl group, and 0 ppm for the aryl methyl group. The other resonances are apparently too broad to be observed. The complex has a strong infrared stretch at 893 cm^{-1} attributable to $\nu_{Mo\text{-}O}$. Labeling the complex with ^{18}O has not yet been attempted. An Evans method[36] measurement of μ_{eff} gives a value of 2.19 μ_B, higher than the spin only value of 1.73 μ_B as is typical for d^1 complexes using this method.[37] The magnetic susceptibility data of solid **2.2** determined over the temperature range 5 to 300 K using a SQUID magnetometer are consistent with simple paramagnetic behavior, obeying the Curie law over the entire temperature range. The data and least squares fit, shown in Figure 2.1, give a value for μ of 1.66 μ_B, corresponding well to the expected spin only value of 1.73 μ_B. A room temperature EPR spectrum of **2.2** in toluene gives an isotropic g value of 1.96 with a six line coupling pattern to the s = 5/2 nuclei ^{95}Mo and ^{97}Mo of 35.7 Gauss. This six line pattern is approximately 25% of the area of the central peak, reflecting the natural abundance of $^{95/97}$Mo.[38] Due to the similar gyromagnetic ratios of the two s = 5/2 molybdenum nuclei, separate couplings are not seen, nor are they expected.[16,38] A frozen

References begin on page 184

glass EPR spectrum in toluene shows a poorly resolved rhombic spectrum with g values of 1.990, 1.967 and 1.937 (Figure 2.2); the g values are obtained through simulation of the spectrum.[39] The corresponding couplings to ^{95}Mo and ^{97}Mo are not resolved in this spectrum. An ORTEP diagram of complex **2.2** derived from single crystal X-ray data is shown in Figure 2.3. Pertinent bond distances and angles are given in Tables 2.1 and 2.2, and positional parameters and U(eq.) are listed in Table 2.3. The molybdenum oxygen bond distance of 1.706(2) Å in **2.2** is at the long end of the range typical for Mo(V) oxo complexes.[6] The other bond distances are typical, although the arrangement of the three anilide ligands is unique in that the complex is neither pseudo-C_3 nor pseudo-C_s, the two common arrangements for tris-anilide complexes. As seen from the O-Mo-N-C(*tert*) dihedral angles (Table 2.2) one anilide is tilted by about 40°, larger by 10-20° than that usually seen in anilide complexes of this sort,[23,34,37,40] one by 3° and the third by 62°. This third anilide ligand also is slightly pyramidalized towards the site trans to the oxo ligand, with the sum of the angles about nitrogen being 356.2°. The other two nitrogen atoms are planar. Although the three anilide ligands are quite different in the solid state, in solution there is no differentiation on the ^{2}H NMR timescale.

References begin on page 184

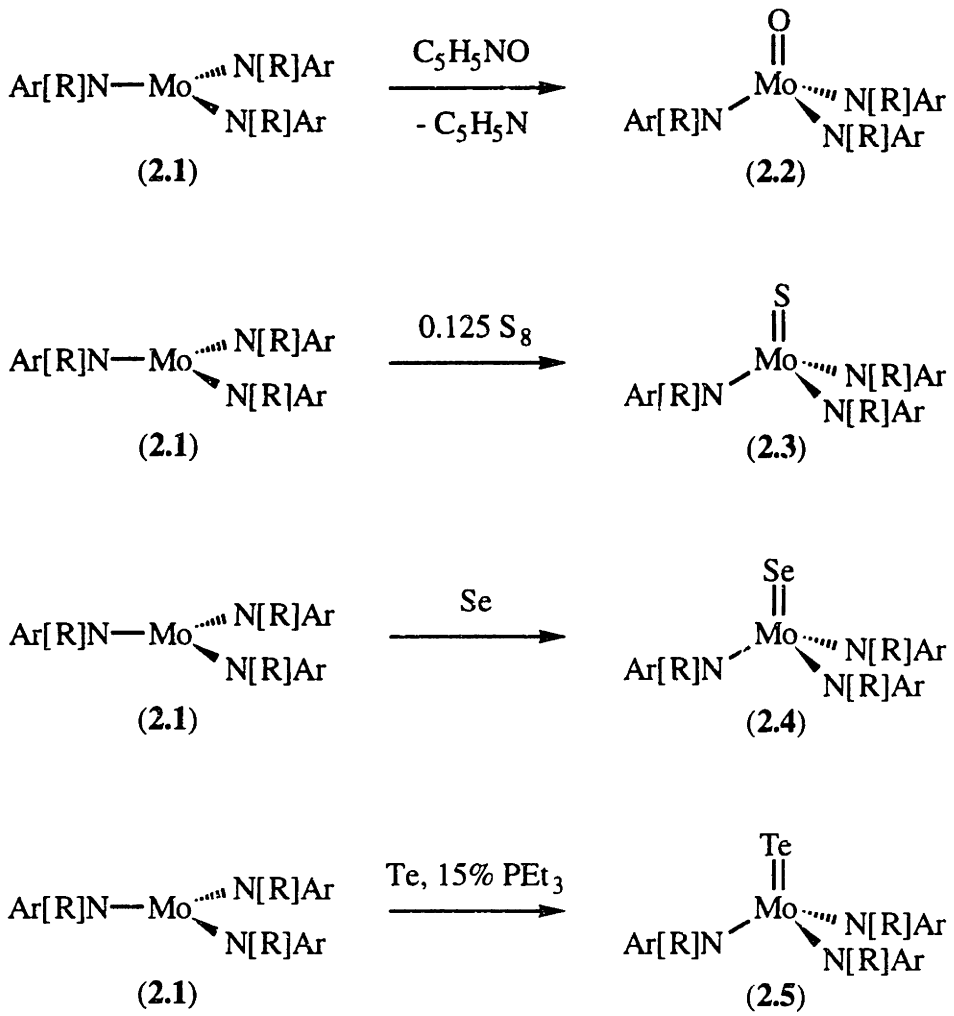

Scheme 2.1: Preparation of Mo(V) Chalcogenide Complexes

References begin on page 184

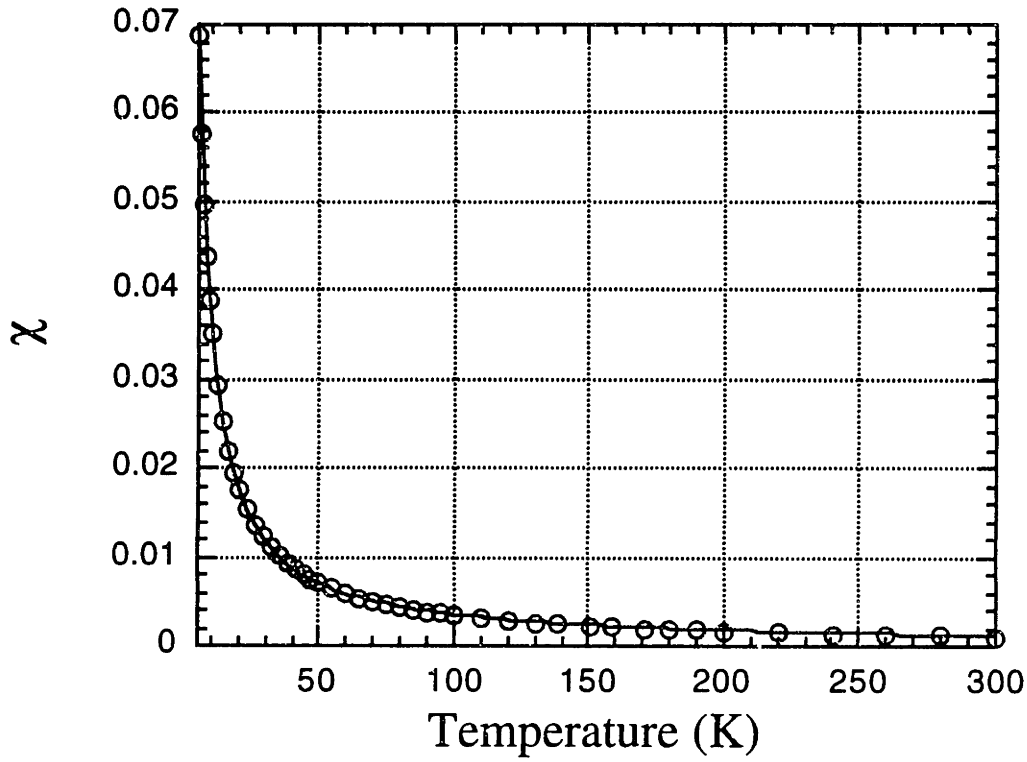

Figure 2.1: SQUID magnetic susceptibility data for solid $OMo(N[R]Ar)_3$ (**2.2**) from 5 to 300 K fit to the Curie law ($\mu = 1.66\ \mu_B$).

References begin on page 184

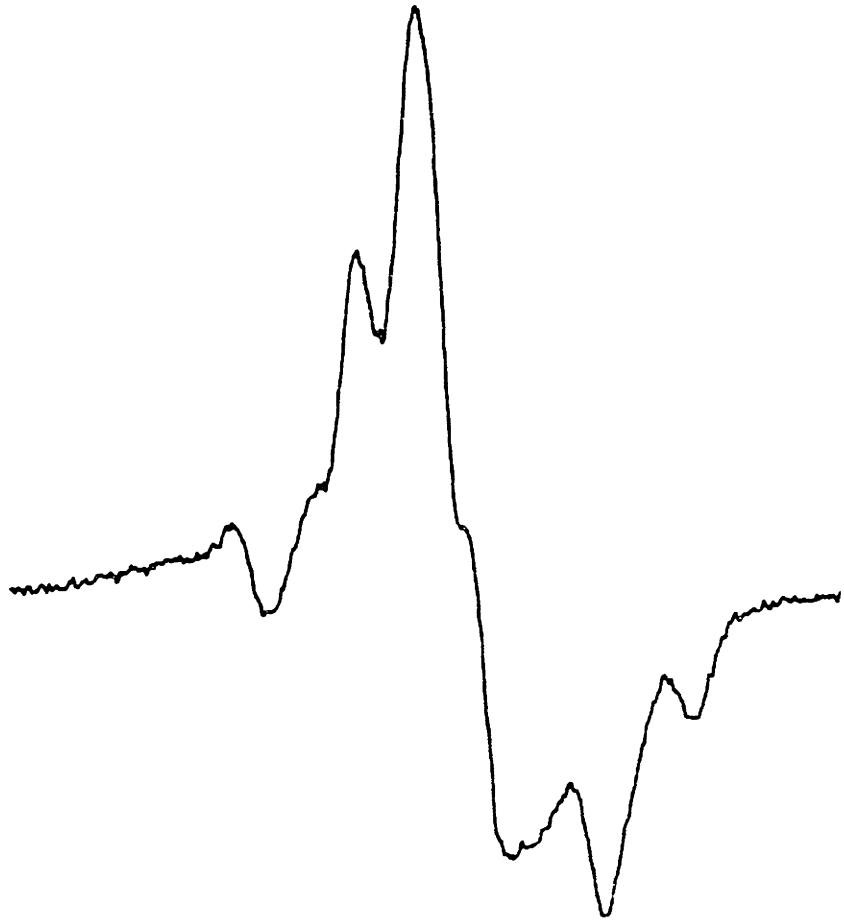

Figure 2.2: EPR spectrum (100 K, toluene) of $OMo(N[R]Ar)_3$ (**2.2**) with $g_1 = 1.990$, $g_2 = 1.967$, $g_3 = 1.937$.

References begin on page 184

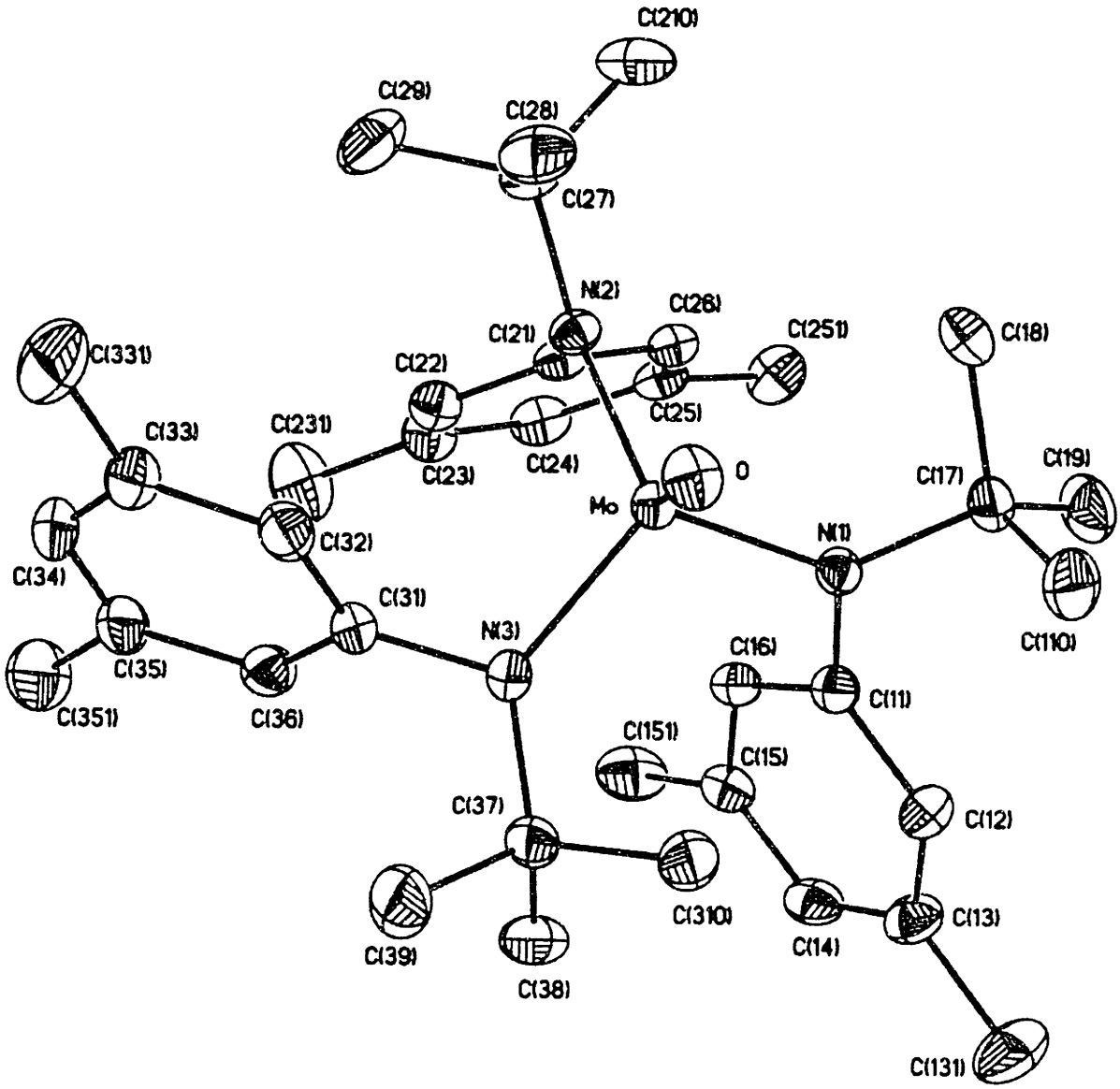

Figure 2.3: ORTEP diagram of $OMo(N[R]Ar)_3$ (**2.2**) with ellipsoids at the 30% probability level.

References begin on page 184

Table 2.1: Selected Bond Lengths (Å) for $OMo(N[R]Ar)_3$ (**2.2**).

Mo-O	1.706(2)	N2-C27	1.506(4)
Mo-N(1)	1.990(2)	N3-C37	1.518(4)
Mo-N(2)	1.980(2)	N1-C11	1.431(4)
Mo-N(3)	1.973(2)	N2-C21	1.447(4)
N1-C17	1.514(4)	N3-C31	1.441(4)

Table 2.2: Selected Bond Angles (°) for $OMo(N[R]Ar)_3$ (**2.2**).

O-Mo-N1	108.56(10)	C21-N2-Mo	114.6(2)
O-Mo-N2	115.53(10)	C27-N2-Mo	130.2(2)
O-Mo-N3	103.22(10)	C21-N2-C27	115.2(2)
N1-Mo-N2	109.13(10)	C31-N3-Mo	113.7(2)
N2-Mo-N3	111.60(9)	C37-N3-Mo	127.5(2)
N3-Mo-N1	108.50(9)	C31-N3-C37	115.1(2)
C11-N1-Mo	121.5(2)	O-Mo-N1-C17	39.0
C17-N1-Mo	119.7(2)	O-Mo-N2-C27	2.7
C11-N1-C17	118.3(2)	O-Mo-N3-C37	61.9

References begin on page 184

Table 2.3: Positional Parameters (x 10^4) and U(eq.) ($Å^2$ x 10^3) for the Non-Hydrogen Atoms of $OMo(N[R]Ar)_3$ (**2.2**).

Atom	x	y	z	U(eq.)
Mo	1135(1)	3120(1)	2423(1)	24(1)
O	1056(2)	4799(2)	2520(1)	37(1)
N2	-478(3)	1437(3)	2818(1)	28(1)
N3	3190(3)	3680(3)	2843(1)	28(1)
N1	1049(3)	2474(3)	1454(1)	27(1)
C18	-1442(4)	2459(4)	1296(2)	44(1)
C12	3032(4)	2627(4)	696(2)	37(1)
C17	6(3)	2703(4)	962(2)	34(1)
C11	2090(3)	1972(3)	1198(1)	29(1)
C31	3208(3)	3413(3)	3529(1)	31(1)
C21	-453(3)	-3(3)	2691(2)	30(1)
C26	-1157(3)	-960(3)	2094(2)	32(1)
C14	4153(3)	960(4)	758(2)	39(1)
C32	2612(4)	4083(4)	3989(2)	40(1)
C35	3800(4)	2248(4)	4416(2)	46(1)
C13	4061(4)	2128(4)	474(2)	41(1)
C16	2229(3)	806(3)	1473(2)	31(1)
C27	-1738(4)	1415(4)	3217(2)	37(1)
C28	-1548(4)	3020(4)	3366(2)	47(1)
C15	3246(3)	282(3)	1255(2)	36(1)
C36	3792(3)	2493(4)	3751(2)	38(1)
C22	334(3)	-421(3)	3143(2)	35(1)
C19	-493(4)	1521(5)	339(2)	54(1)
C37	4718(3)	4799(3)	2636(2)	34(1)
C23	431(4)	-1769(4)	3003(2)	41(1)
C38	5586(4)	3954(4)	2377(2)	47(1)
C351	4491(5)	1288(5)	4659(2)	68(1)
C25	-1043(3)	-2290(3)	1938(2)	35(1)
C24	-257(4)	-2679(3)	2403(2)	39(1)
C34	3156(4)	2900(5)	4857(2)	52(1)
C151	3323(4)	-1005(4)	1560(2)	55(1)
C310	4462(4)	5635(4)	2089(2)	42(1)
C110	759(4)	4328(4)	781(2)	52(1)
C210	-3295(4)	410(4)	2823(2)	53(1)
C251	-1690(4)	-3240(4)	1268(2)	50(1)
C29	-1664(5)	829(5)	3885(2)	58(1)
C33	2562(4)	3813(5)	4654(2)	50(1)
C39	5687(4)	5991(4)	3223(2)	57(1)
C231	1311(5)	-2193(5)	3503(2)	68(1)
C131	5080(5)	2880(5)	-58(2)	66(1)
C331	1880(6)	4535(6)	5138(2)	81(1)

References begin on page 184

(ii) Synthesis and Characterization of $SMo(N[R]Ar)_3$ (2.3)

It is also possible to synthesize homologues of oxo complex **2.2** with the heavier elements of group 16, starting with sulfur. An ethereal solution of $Mo(N[R]Ar)_3$ (**2.1**) reacts with a slight excess of elemental sulfur to give a dark greenish brown solution (Scheme 1.1). Monitoring the reaction by ^2H NMR spectroscopy shows that all the starting material is consumed over approximately an 18 hour period, being converted to a single product. The excess sulfur is removed by filtration, and the terminal sulfido complex $SMo(N[R]Ar)_3$ (**2.3**) is obtained by recrystallization from ether in 63% yield. Complex **2.1** also reacts with ethylene sulfide to give complex **2.3**; the reaction is complete in only a few minutes.

The ^2H NMR spectrum of **2.3** in ether exhibits a single resonance at 6.5 ppm with a peak width at half height of 22 Hz. The corresponding ^1H NMR spectrum exhibits two broad resonances: one at 6.0 ppm for the *tert*-butyl group and one at 1.1 ppm for the aryl methyl group. As is the case with the oxo species, none of the other resonances are observed. The complex has a strong infrared stretch due to $\nu_{Mo\text{-}S}$ at 492 cm^{-1}. The solution magnetic susceptibility measurements again give an anamolously high value for μ_{eff} of 2.21 μ_B. A measurement of the magnetic susceptibility by SQUID magnetometry from 5 to 300 K is again consistent with simple paramagnetic behavior. A fit of the data to the Curie law gives μ = 1.63 μ_B; the data and fit are shown in Figure 2.4. An EPR spectrum of **2.3** at room temperature in toluene gives an isotropic g value of 1.96 with coupling to the s = 5/2 nuclei $^{95/97}Mo$ of 28.5 Gauss. A frozen glass EPR spectrum in toluene shows a rhombic pattern with g values of 1.996, 1.970 and 1.922 (Figure 2.5). In this spectrum, the anisotropic couplings to g_1 and g_3 are partially resolved as 25 G and 54 G respectively. Again, these assignments are obtained through spectrum simulation.[39]

References begin on page 184

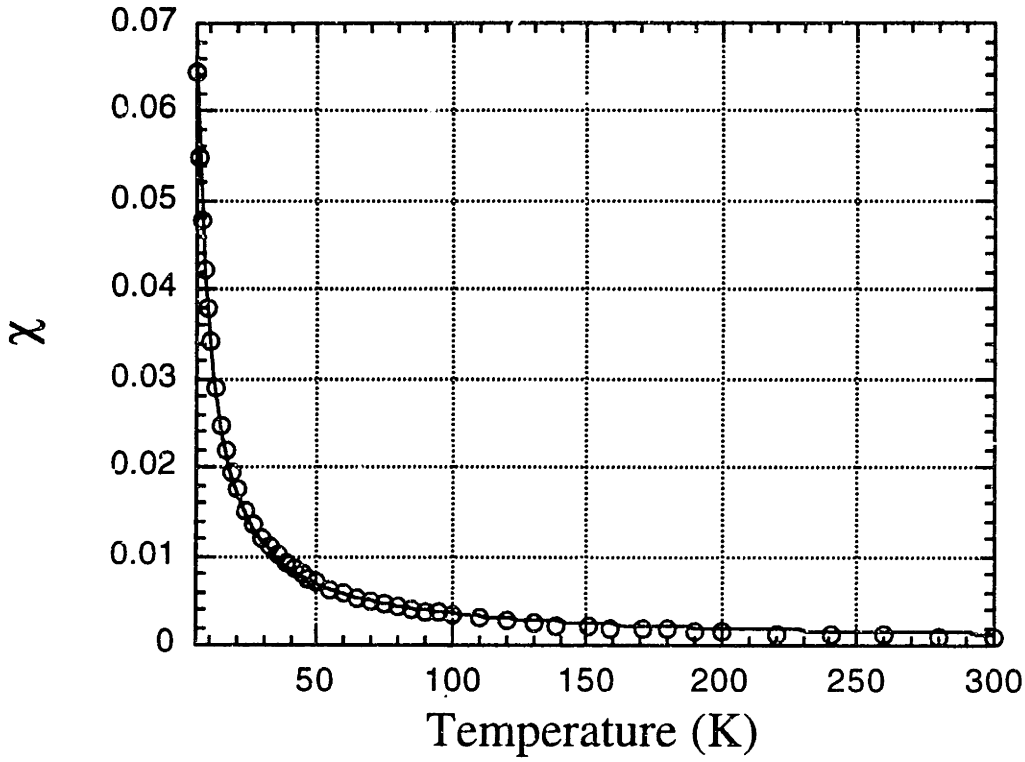

Figure 2.4: SQUID magnetic susceptibility data for solid $SMo(N[R]Ar)_3$ (**2.3**) from 5 to 300 K fit to the Curie law ($\mu = 1.63\ \mu_B$)

References begin on page 184

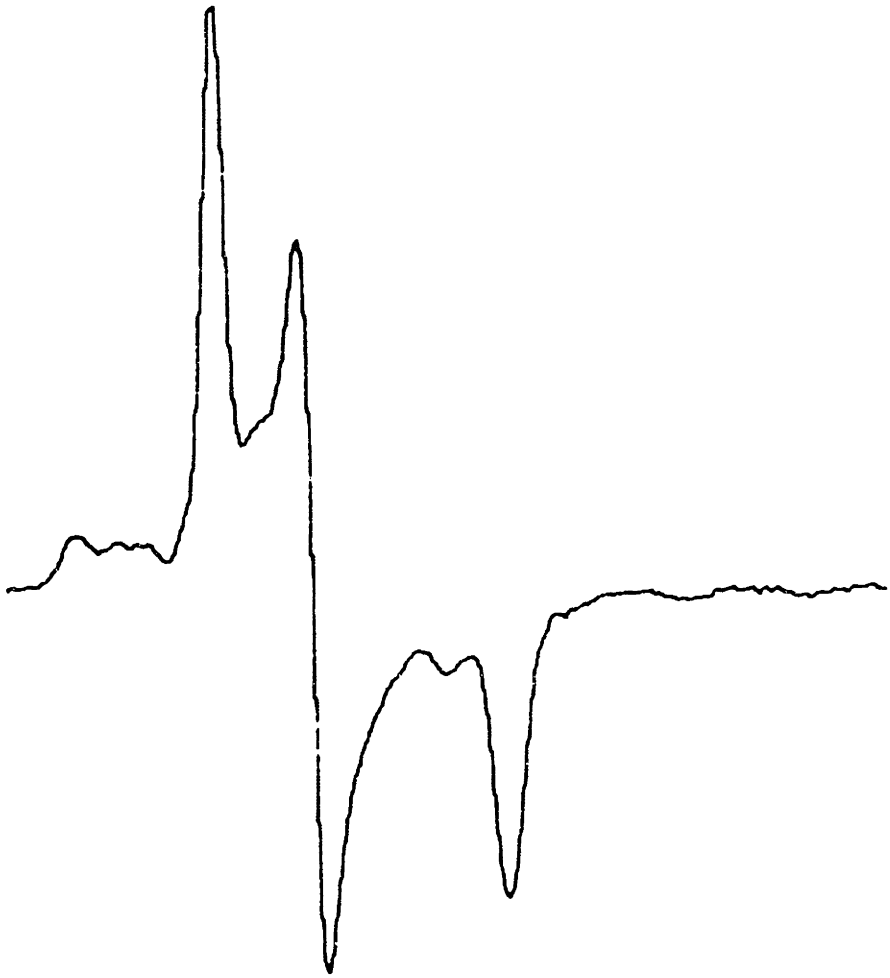

Figure 2.5: EPR spectrum (100 K, toluene) of $SMo(N[R]Ar)_3$ (**2.3**) with $g_1 = 1.996$, $g_2 = 1.970$, $g_3 = 1.922$, $A_1 = 25$ G and $A_3 = 54$ G.

References begin on page 184

An X-ray crystal structure determination on complex **2.3** shows it to have pseudo-C_s symmetry, and an ORTEP diagram of the structure is shown in Figure 2.6. Selected bond lengths and angles are listed in Tables 2.4 and 2.5, and positional parameters and U(eq.) are given in Table 2.6. The molybdenum sulfur distance is 2.1677(12) Å. This distance is 0.09 Å shorter than those reported for *d*(Mo-S) in *trans*-$Mo(S)_2(PR_3)_4$,[16] but this is best explained by the increased Mo-S π bonding possible in **2.3** relative to the bis sulfide complex. $Mo(S)_2(PR_3)_4$ has at most a Mo-S double bond, while complex **2.3** has a Mo-S bond order of 2.5 (see Section 2.3 for further details). Tungsten complexes with doubly bonded sulfur exhibit bond distances on the order of 2.25 Å, while those with a bond order of 2.5 to sulfur have lengths near 2.19 Å.[5] As Mo and W have similar radii, this places the Mo-S bond distance in **2.3** in the 2.5 bond order regime. The other bond distances in the sulfide complex are normal. The pseudo-C_s arrangement of the anilides is identical to that seen in the d^1 tris anilide complex $ClNb(N[R]Ar)_3$.[41] Two of the anilides engage in a π stacking arrangement with the *tert*-butyl groups splayed away from the center of the molecule, while the third is oriented in a more typical upright arrangement with a S-Mo-N-C(*tert*) dihedral angle of 7° and is nearly bisected by the pseudo-mirror plane.

References begin on page 184

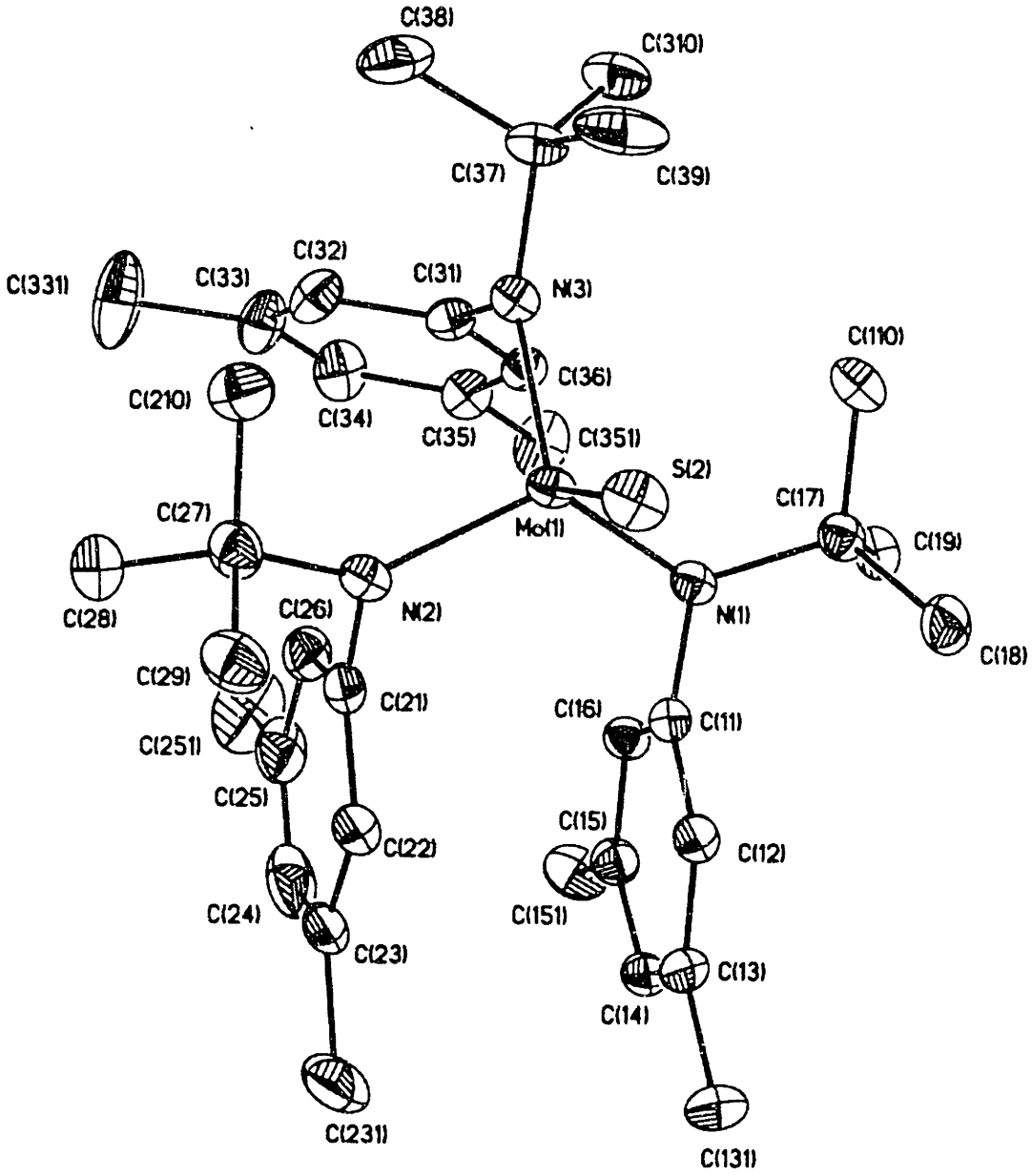

Figure 2.6: ORTEP diagram of $SMo(N[R]Ar)_3$ (**2.3**) with ellipsoids at the 30% probability level.

References begin on page 184

Table 2.4: Selected Bond Lengths (Å) for $SMo(N[R]Ar)_3$ (**2.3**).

Mo-S	2.1677(12)	N2-C27	1.525(6)
Mo-N1	1.963(4)	N3-C37	1.515(6)
Mo-N2	1.947(4)	N1-C11	1.439(6)
Mo-N3	1.976(3)	N2-C21	1.439(6)
N1-C17	1.516(5)	N3-C31	1.449(5)

Table 2.5: Selected Bond Angles (°) for $SMo(N[R]Ar)_3$ (**2.3**).

S-Mo-N1	103.62(10)	C21-N2-Mo	118.2(3)
S-Mo-N2	105.81(11)	C27-N2-Mo	126.5(3)
S-Mo-N3	116.94(11)	C21-N2-C27	115.0(4)
N1-Mo-N2	115.9(2)	C31-N3-Mo	109.0(3)
N2-Mo-N3	104.0(2)	C37-N3-Mo	135.7(3)
N3-Mo-N1	110.97(14)	C31-N3-C37	115.3(3)
C11-N1-Mo	119.8(3)	S-Mo-N1-C17	62.9
C17-N1-Mo	126.0(3)	S-Mo-N2-C27	49.2
C11-N1-C17	112.5(3)	S-Mo-N3-C37	6.7

References begin on page 184

Table 2.6: Positional Parameters (x 10^4) and U(eq.) ($Å^2$ x 10^3) for the Non-Hydrogen Atoms of $SMo(N[R]Ar)_3$ (**2.3**).

Atom	x	y	z	U(eq.)
Mo	7581(1)	1227(1)	966(1)	26(1)
S	7498(1)	502(1)	-14(1)	40(1)
N1	8780(3)	2031(3)	969(2)	27(1)
N2	6402(3)	2028(3)	1018(2)	31(1)
N3	7575(3)	296(3)	1751(2)	28(1)
C11	8741(3)	3131(3)	851(2)	28(1)
C12	8636(3)	3526(4)	201(2)	30(1)
C13	8682(3)	4588(4)	82(2)	39(1)
C14	8816(3)	5245(4)	629(2)	37(1)
C15	8887(3)	4881(4)	1284(2)	36(1)
C16	8840(3)	3818(4)	1385(2)	31(1)
C17	9783(3)	1591(4)	915(2)	31(1)
C18	10113(4)	1696(4)	197(2)	46(1)
C19	10499(3)	2148(4)	1393(2)	39(1)
C21	6482(3)	3117(4)	1170(2)	34(1)
C22	6442(3)	3854(4)	664(3)	45(1)
C23	6439(4)	4911(4)	818(4)	57(2)
C24	6518(4)	5197(5)	1490(4)	68(2)
C27	5379(3)	1646(4)	850(2)	40(1)
C28	4682(4)	2190(5)	1304(3)	54(2)
C29	5102(4)	1881(4)	118(2)	50(1)
C31	7504(3)	916(3)	2351(2)	29(1)
C32	6655(3)	993(4)	2680(2)	40(1)
C331	5614(4)	1717(7)	3567(3)	83(2)
C34	7357(4)	2228(4)	3452(2)	46(1)
C35	8216(3)	2180(4)	3132(2)	36(1)
C25	6564(4)	4483(5)	1999(3)	57(2)
C26	6546(3)	3436(4)	1836(3)	43(1)
C36	8283(3)	1516(3)	2586(2)	31(1)
C37	7614(4)	-865(4)	1862(2)	39(1)
C38	6690(4)	-1291(5)	2152(3)	70(2)
C39	7766(5)	-1414(4)	1209(3)	62(2)
C110	9784(4)	451(4)	1101(2)	42(1)
C131	8585(4)	5011(4)	-624(2)	52(2)
C210	5322(4)	487(4)	969(2)	45(1)
C231	6376(5)	5698(5)	265(4)	85(2)
C251	6664(5)	4822(6)	2733(3)	90(2)
C310	8446(4)	-1111(4)	2365(3)	51(1)
C33	6570(4)	1632(5)	3231(2)	46(1)
C151	9020(4)	5606(4)	1865(3)	54(2)
C351	9064(4)	2832(5)	3374(3)	55(2)

References begin on page 184

(iii) Synthesis and Characterization of $SeMo(N[R]Ar)_3$ (2.4)

Synthesis of the terminal selenide complex is straightforward. Again, simple mixing of a solution of $Mo(N[R]Ar)_3$ (**2.1**) and excess elemental selenium results in a slow color change over about 11 hours to dark brown (Scheme 2.1). The excess selenium is removed by filtration and the product, $SeMo(N[R]Ar)_3$ (**2.4**), is collected by crystallization from ether in 80% yield.

The ^2H NMR spectrum of **2.4** in ether exhibits a single resonance at 7.0 ppm, with a peak width at half height of 31 Hz. The ^1H NMR spectrum is similar to those observed for complexes **2.3** and **2.2**, with resonances at 6.5 ppm for the *tert*-butyl group and -1.5 ppm for the aryl methyl group. The complex exhibits a fairly strong peak at 342 cm^{-1} in the Far-IR spectrum which is due to $\nu_{Mo\text{-}Se}$. Measurement of the magnetic moment by SQUID magnetometry from 5 to 300 K gives a μ value of 1.75 μ_B and a θ value of -1.45 K when fit to the Curie-Weiss Law; the SQUID data and fit are presented in Figure 2.7. An EPR spectrum of **2.4** in toluene at room temperature exhibits an isotropic g value of 1.97, with isotropic coupling to ^{95}Mo and ^{97}Mo of 30.5 G. The frozen glass EPR spectrum has well resolved g values of 2.030, 1.986 and 1.899 (Figure 2.8). The separation allows the anisotropic couplings for g_1 and g_3 to be observed at 29 and 48 G respectively. The g values and *A* couplings are verified by simulation.[39] Complex **2.4** is isostructural to the sulfide **2.3**, with pseudo-C_s symmetry, as determined by single crystal X-ray diffraction; an ORTEP diagram is shown in Figure 2.9. Selected bond distances and angles are listed in Tables 2.7 and 2.8, and positional parameters and U(eq.) are listed in Table 2.9. The Mo-Se distance is 2.3115(6) Å. Tungsten complexes with bond orders of two to selenium have W-Se bond distances of approximately 2.38 Å while those with a bond order of 2.5 have bond lengths near 2.32 Å,[5] suggesting a bond order of 2.5 in the selenide complex.

References begin on page 184

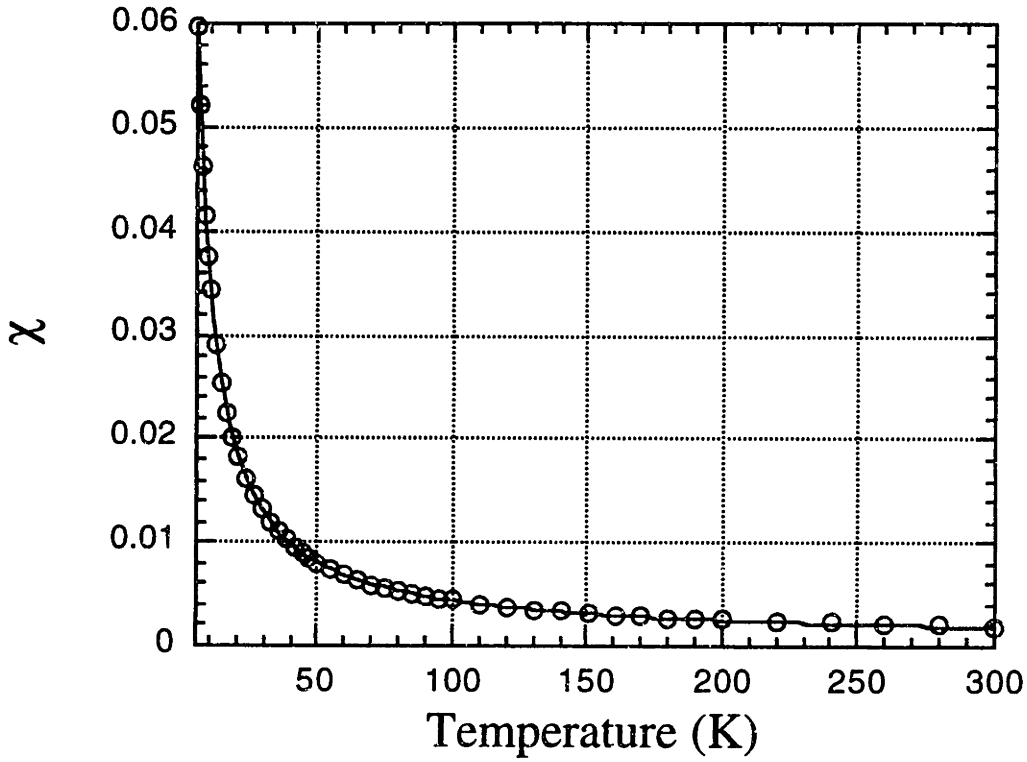

Figure 2.7: SQUID magnetic susceptibility data for solid $SeMo(N[R]Ar)_3$ (**2.4**) from 5 to 300 K fit to the Curie-Weiss law (μ = 1.75 μ_B; θ = -1.45 K)

References begin on page 184

Figure 2.8: EPR spectrum (100 K, toluene) of SeMo(N[R]Ar)$_3$ (**2.4**) with $g_1 = 2.030$, $g_2 = 1.986$, $g_3 = 1.899$, $A_1 = 29$ G and $A_3 = 48$ G.

References begin on page 184

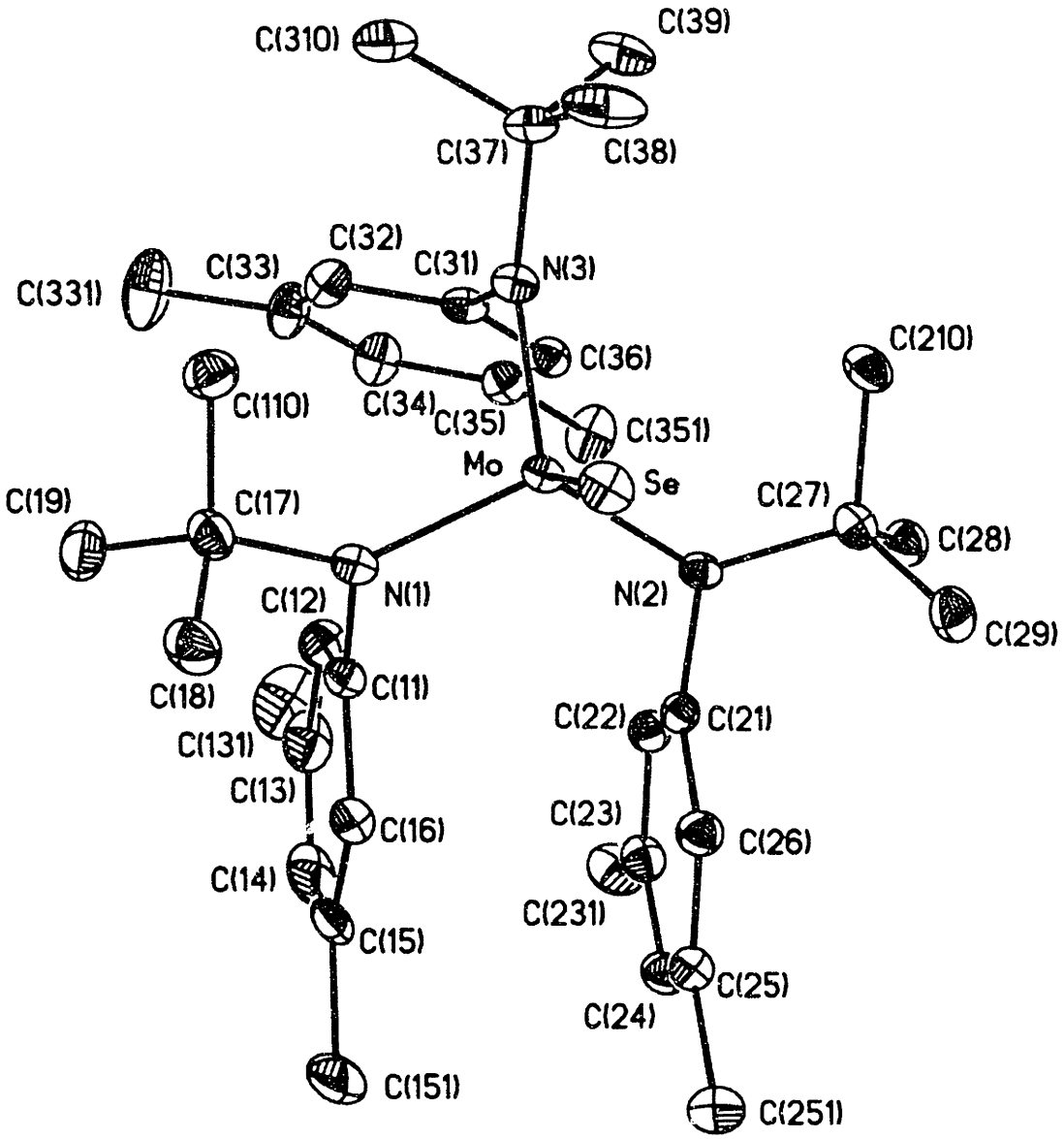

Figure 2.9: ORTEP diagram of $SeMo(N[R]Ar)_3$ (**2.4**) with ellipsoids at the 30% probability level.

References begin on page 184

Table 2.7: Selected Bond Distances (Å) for $SeMo(N[R]Ar)_3$ (**2.4**).

Mo-Se	2.3115(6)	N2-C27	1.522(6)
Mo-N(1)	1.948(4)	N3-C37	1.520(6)
Mo-N(2)	1.967(4)	N1-C11	1.453(6)
Mo-N(3)	1.976(3)	N2-C21	1.451(6)
N1-C17	1.529(6)	N3-C31	1.459(6)

Table 2.8: Selected Bond Angles (°) for $SeMo(N[R]Ar)_3$ (**2.4**).

Se-Mo-N1	105.49(11)	C21-N2-Mo	119.1(3)
Se-Mo-N2	103.33(10)	C27-N2-Mo	126.7(3)
Se-Mo-N3	117.03(10)	C21-N2-C27	112.4(3)
N1-Mo-N2	116.6(2)	C31-N3-Mo	108.4(3)
N2-Mo-N3	110.7(2)	C37-N3-Mo	136.5(3)
N3-Mo-N1	104.1(2)	C31-N3-C37	115.1(3)
C11-N1-Mo	117.6(3)	Se-Mo-N1-C17	50.9
C17-N1-Mo	127.6(3)	Se-Mo-N2-C27	63.0
C11-N1-C17	114.6(4)	Se-Mo-N3-C37	6.2

References begin on page 184

Table 2.9: Positional Parameters (x 10^4) and U(eq.) ($Å^2$ x 10^3) for the Non-Hydrogen Atoms of $SeMo(N[R]Ar)_3$ (**2.4**).

Atom	x	y	z	U(eq.)
Mo	7575(1)	1215(1)	964(1)	19(1)
Se	7488(1)	460(1)	-89(1)	28(1)
N1	6392(3)	2008(3)	1020(2)	24(1)
N2	8778(3)	2016(3)	968(2)	21(1)
N3	7574(3)	270(3)	1744(2)	22(1)
C11	6476(3)	3106(4)	1179(2)	28(1)
C12	6549(4)	3414(4)	1842(3)	33(1)
C13	6586(4)	4463(4)	2017(3)	45(1)
C14	6518(4)	5178(4)	1502(4)	50(2)
C15	6439(4)	4902(4)	832(3)	45(2)
C16	6433(3)	3846(4)	670(3)	34(1)
C17	5364(3)	1631(4)	869(2)	30(1)
C18	5071(4)	1875(4)	132(2)	38(1)
C19	4675(4)	2161(4)	1335(3)	40(1)
C21	8733(3)	3127(3)	853(2)	21(1)
C22	8833(3)	3804(4)	1393(2)	26(1)
C23	8879(3)	4873(4)	1292(2)	30(1)
C24	8809(3)	5245(4)	639(3)	33(1)
C25	8680(3)	4593(4)	85(2)	30(1)
C26	8641(3)	3529(4)	202(2)	28(1)
C27	9787(3)	1583(4)	911(2)	25(1)
C28	10496(3)	2141(4)	1402(2)	30(1)
C29	10121(4)	1696(4)	197(2)	33(1)
C31	7502(3)	895(3)	2350(2)	23(1)
C32	6638(3)	960(4)	2681(2)	30(1)
C33	6568(4)	1601(4)	3236(2)	35(1)
C34	7360(4)	2189(4)	3461(2)	34(1)
C35	8222(3)	2147(4)	3136(2)	29(1)
C36	8284(3)	1492(3)	2580(2)	25(1)
C37	7610(4)	-896(3)	1859(2)	29(1)
C38	7783(5)	-1453(4)	1208(3)	49(2)
C39	8436(4)	-1144(4)	2372(3)	42(1)
C110	5311(4)	463(4)	982(2)	33(1)
C131	6676(5)	4790(5)	2741(4)	72(2)
C151	6366(5)	5699(5)	277(4)	67(2)
C210	9789(4)	435(4)	1095(2)	31(1)
C231	9012(4)	5595(4)	1887(3)	44(1)
C251	8595(4)	5029(4)	-622(3)	42(1)
C310	6680(4)	-1321(4)	2142(3)	52(2)
C331	5624(4)	1685(6)	3579(3)	59(2)
C351	9075(4)	2799(4)	3381(3)	42(1)

References begin on page 184

(iv) Synthesis and Characterization of TeMo(N[R]Ar)$_3$ (2.5)

The synthesis of the terminal telluride completes the series of Mo(V) chalcogenido complexes (Scheme 2.1).[42] Treating Mo(N[R]Ar)$_3$ (**2.1**) with a slight excess of elemental tellurium in ether causes an extremely slow conversion to dark brown TeMo(N[R]Ar)$_3$ (**2.5**) as shown by ^{2}H NMR spectroscopy. After 72 hours at room temperature, there is significant decomposition, on the order of 35%, as well as about 5% unreacted **2.1**. In order to circumvent the slow reaction time, a soluble form of tellurium is required. Phosphine tellurides effectively deliver tellurium atoms to appropriate substrates,[8,10,43] and compound **2.1** does not react with triethyl phosphine as shown by ^{2}H NMR spectroscopy, so triethyl phosphine telluride seems a good delivery agent. Rather than synthesizing the phosphine telluride directly, a catalytic amount of phosphine (ca. 15 mol%) is added to the reaction mixture of **2.1** and tellurium, resulting in conversion to the desired telluride **2.5** over approximately 18 hours. When prepared this way, there is typically about 12% decomposed, diamagnetic material as determined by ^{2}H NMR spectroscopy. After removing the solvent and phosphine by evaporation, the reaction mixture is extracted with THF and filtered to remove excess tellurium. The telluride complex is much less soluble in ether than the lighter homologues but recrystallizes from ether in 73% yield.

The ^{2}H NMR spectrum of **2.5** exhibits a single resonance at 8.1 ppm with a peak width at half height of 23 Hz. The ^{1}H NMR spectrum is unsurprising, with resonances at 8 ppm for the *tert*-butyl group and -2 ppm for the aryl methyl group. A determination of the magnetic moment by SQUID magnetometry gives a μ value of 1.86 μ_B and a θ value of -5.1 K when fit to the Curie-Weiss law over the temperature range 5-170 K. The data and fit are shown in Figure 2.10. The frozen glass EPR spectrum is very well resolved as seen in Figure 2.11, with g values and their associated A (^{95,97}Mo) couplings (G) of 2.130 (28), 1.970 (24) and 1.850 (48). The best simulation of this spectrum is obtained using the values g_1 = 2.1302, A_1 = 25, g_2 = 1.9717, A_2 = 22, g_3 = 1.8481 and A_3 = 41. The isotropic spectrum shows a g value of 1.98, but is extremely broad and obscures the

References begin on page 184

smaller peaks due to the s = 5/2 nuclei. Complex **2.5** is isostructural to complexes **2.3** and **2.4**, with pseudo-C_s symmetry relating the two parallel and π-stacked aryl rings. An ORTEP diagram of the structure is shown in Figure 2.12, selected bond distances and angles are listed in Tables 2.10 and 2.11 and positional parameters and U(eq.) for the structure are given in Table 2.12. The Mo-Te distance is 2.5353(6) Å, and all other bond distances are normal. Tungsten complexes with bond orders of two to Te have bond lengths of around 2.60 Å, while those with a bond order of 2.5 have lengths of 2.53 Å,[5] indicating the higher bond order in complex **2.5**.

Table 2.10: Selected Bond Distances (Å) for TeMo(N[R]Ar)$_3$ (**2.5**).

Mo-Te	2.5353(6)	N2-C27	1.528(4)
Mo-N1	1.978(2)	N3-C37	1.521(4)
Mo-N2	1.938(2)	N1-C11	1.455(4)
Mo-N3	1.958(2)	N2-C21	1.443(4)
N1-C17	1.518(4)	N3-C31	1.450(4)

Table 2.11: Selected Bond Angles (°) for TeMo(N[R]Ar)$_3$ (**2.5**).

Te-Mo-N1	116.72(7)	C21-N2-Mo	117.1(2)
Te-Mo-N2	104.78(7)	C27-N2-Mo	129.0(2)
Te-Mo-N3	102.37(7)	C21-N2-C27	113.8(2)
N1-Mo-N2	104.64(10)	C31-N3-Mo	118.9(2)
N2-Mo-N3	117.69(10)	C37-N3-Mo	127.8(2)
N3-Mo-N1	111.03(10)	C31-N3-C37	112.1(2)
C11-N1-Mo	107.7(2)	Te-Mo-N1-C17	6.0
C17-N1-Mo	137.8(2)	Te-Mo-N2-C27	52.0
C11-N1-C17	114.5(2)	Te-Mo-N3-C37	64.7

References begin on page 184

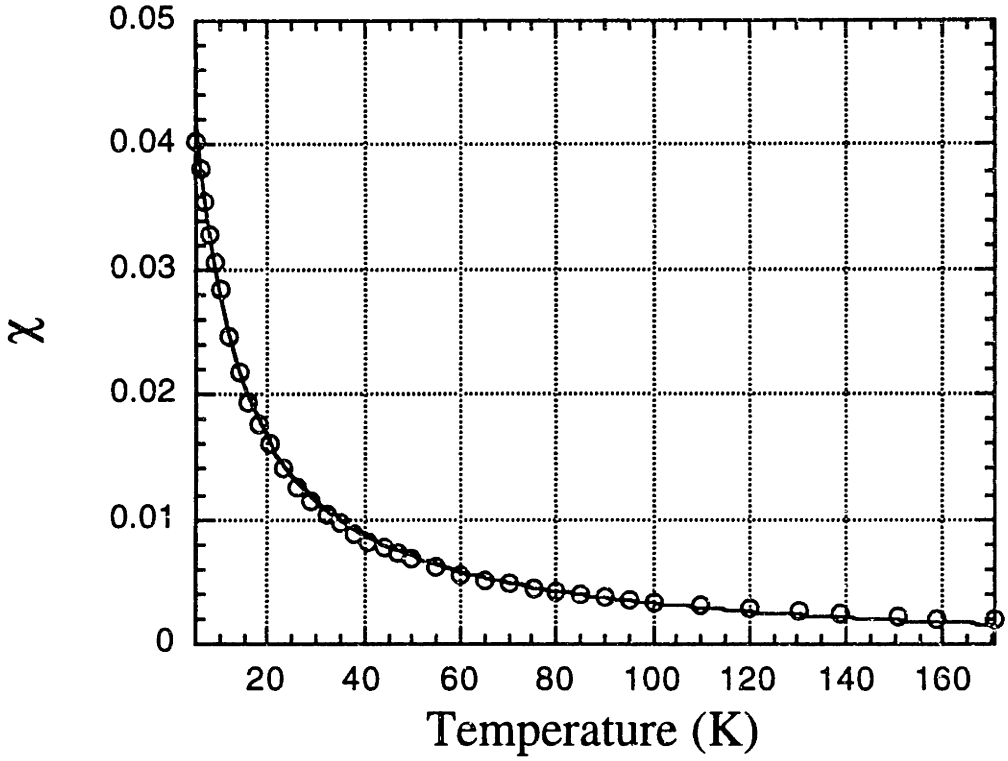

Figure 2.10: SQUID magnetic susceptibility data for solid $TeMo(N[R]Ar)_3$ (**2.5**) from 5 to 170 K fit to the Curie-Weiss law (μ = 1.86 μ_B; θ = -5.1 K)

References begin on page 184

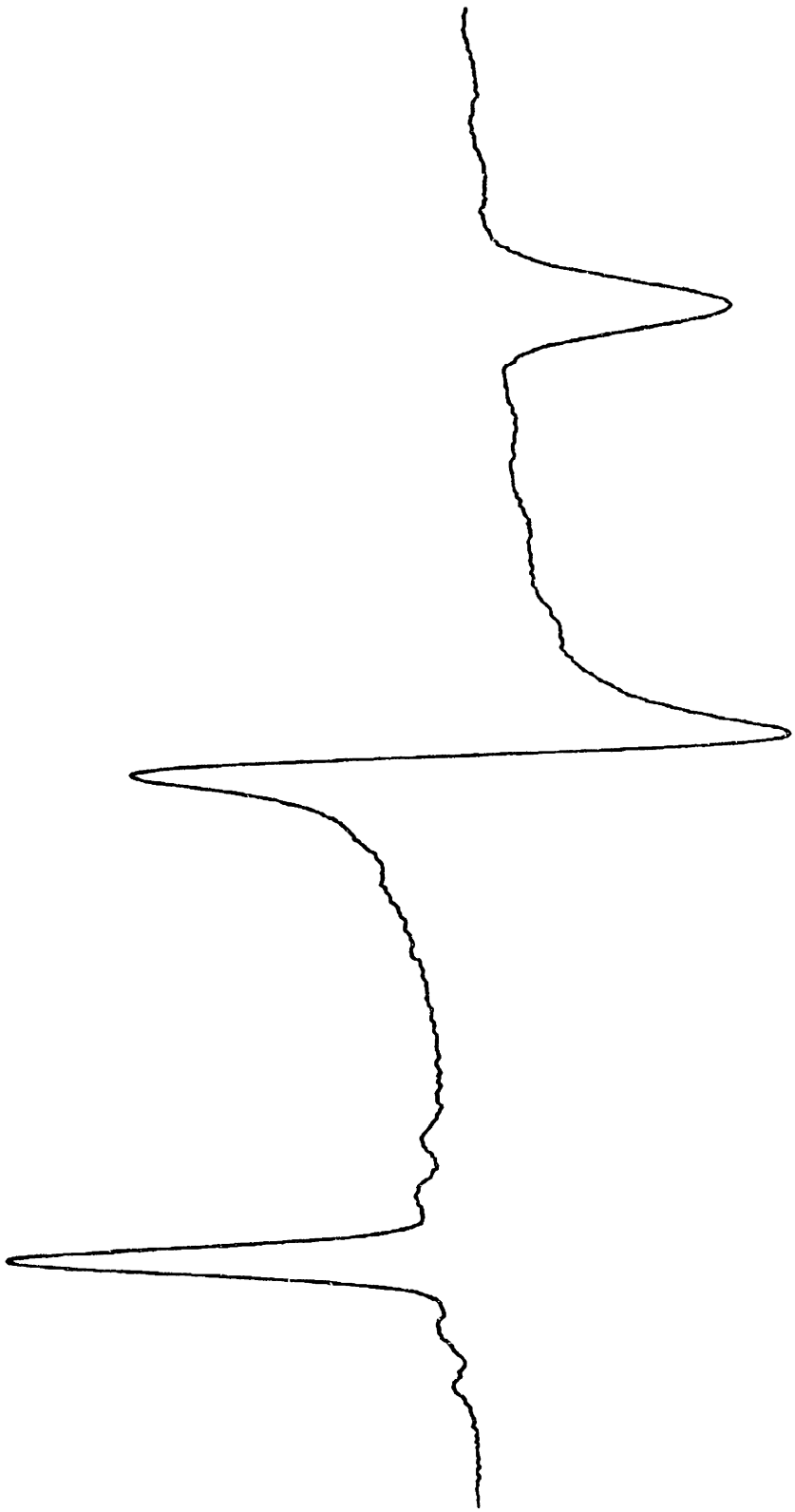

Figure 2.11: EPR spectrum (100 K, toluene) of TeMo(N[R]Ar)$_3$ (**2.5**) with $g_1 = 2.130$, $g_2 = 1.970$, $g_3 = 1.850$, $A_1 = 28$ G, $A_2 = 24$ G and $A_3 = 48$ G.

References begin on page 184

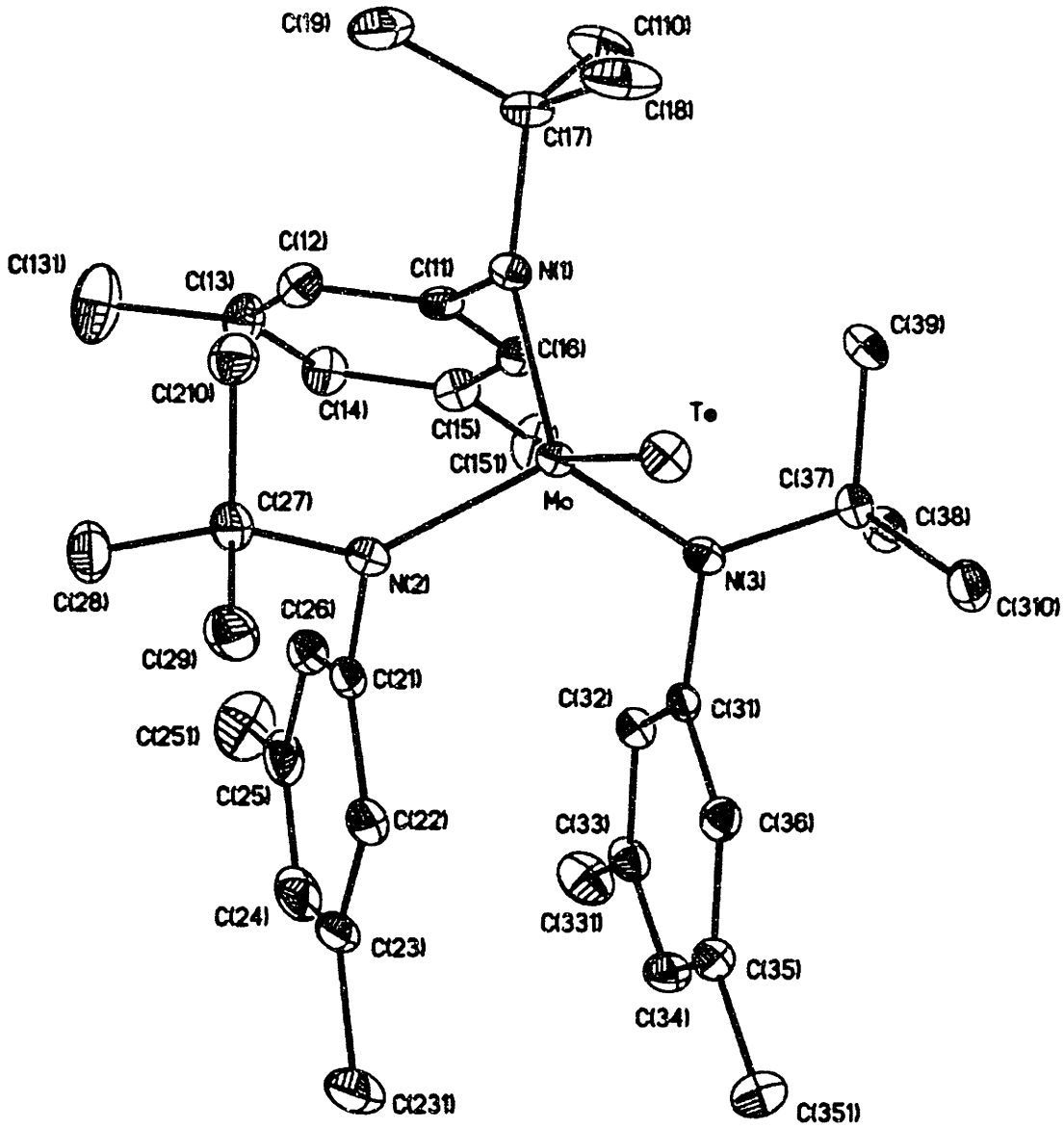

Figure 2.12: ORTEP diagram of $TeMo(N[R]Ar)_3$ (**2.5**) with ellipsoids at the 30% probability level.

References begin on page 184

Table 2.12: Positional Parameters (x 10^4) and U(eq.) ($Å^2$ x 10^3) for the Non-Hydrogen Atoms of $TeMo(N[R]Ar)_3$ (**2.5**).

Atom	x	y	z	U(eq.)
Mo	7430(1)	1198(1)	-984(1)	16(1)
Te	7524(1)	377(1)	167(1)	24(1)
N1	7423(2)	226(2)	-1751(1)	20(1)
N2	8601(2)	1980(2)	-1039(1)	21(1)
N3	6244(2)	1993(2)	-973(1)	19(1)
C32	6186(2)	3790(2)	-1409(2)	23(1)
C22	8562(2)	3833(3)	-695(2)	29(1)
C36	6377(2)	3534(2)	-223(2)	23(1)
C21	8520(2)	3080(2)	-1198(2)	23(1)
C35	6321(2)	4612(3)	-118(2)	28(1)
C31	6287(2)	3115(2)	-865(2)	19(1)
C110	6569(3)	-1185(3)	-2374(2)	40(1)
C38	4549(2)	2131(3)	-1409(2)	27(1)
C17	7383(2)	-949(2)	-1870(2)	26(1)
C16	6719(2)	1443(2)	-2583(2)	22(1)
C210	9676(2)	429(3)	-1008(2)	29(1)
C331	5994(3)	5584(3)	-1916(2)	42(1)
C14	7621(2)	2139(3)	-3467(2)	29(1)
C29	9938(2)	1867(3)	-183(2)	34(1)
C28	10287(2)	2142(3)	-1383(2)	39(1)
C15	6774(2)	2098(3)	-3140(2)	27(1)
C26	8429(2)	3395(3)	-1861(2)	29(1)
C11	7495(2)	851(2)	-2352(1)	20(1)
C37	5243(2)	1567(2)	-922(2)	22(1)
C27	9621(2)	1611(3)	-902(2)	26(1)
C12	8339(2)	915(3)	-2690(2)	26(1)
C34	6192(2)	5261(3)	-671(2)	30(1)
C13	8404(2)	1552(3)	-3251(2)	31(1)
C351	6397(3)	5059(3)	577(2)	40(1)
C19	8297(3)	-1381(3)	-2149(2)	49(1)
C25	8402(3)	4451(3)	-2034(2)	38(1)
C231	8629(3)	5716(3)	-315(2)	54(1)
C33	6131(2)	4866(2)	-1321(2)	27(1)
C18	7204(3)	-1522(3)	-1223(2)	47(1)
C24	8469(3)	5186(3)	-1525(2)	42(1)
C23	8557(2)	4898(3)	-860(2)	38(1)
C131	9331(3)	1630(4)	-3596(2)	55(1)
C39	5236(2)	408(2)	-1097(2)	27(1)
C151	5926(3)	2744(3)	-3378(2)	39(1)
C310	4909(2)	1699(3)	-209(2)	30(1)
C251	8301(3)	4776(3)	-2758(2)	60(1)

References begin on page 184

(v) Cyclic Voltammetry[44]

The cyclic voltammetry data for the four Mo(V) chalcogenide complexes are shown in Table 2.13. The $E_{1/2}$ values for the electrochemically reversible oxidations, obtained in CH_2Cl_2 with saturated Bu_4NPF_6 as the supporting electrolyte, are reported relative to the Fc/Fc^+ couple.[45] The data clearly show that the oxo complex **2.2** is a more powerful reductant than the other chalcogenide complexes; this result is supported by experimental data. There is no reaction when $[Mo(O)(N[R]Ar)_3][OTf]$ **2.12** (see section 2.5) is mixed with a solution of the other chalcogenide complexes **2.3-2.5**. It is not possible to test the reverse reaction of adding a cationic chalcogenide species to **2.2**, as the heavier cations are not isolable.

Table 2.13: Cyclic Voltammetry of $EMo(N[R]Ar)_3$ species in CH_2Cl_2 solution.

Species	$E_{1/2}$ rel. to Fc/Fc^+ (V)
$OMo(N[R]Ar)_3$	-0.92
$SMo(N[R]Ar)_3$	-0.73
$SeMo(N[R]Ar)_3$	-0.64
$TeMo(N[R]Ar)_3$	-0.63

(vi) Thermochemistry[46]

Estimates of the solution bond dissociation enthalpies for both the Mo-O and the Mo-S bonds in complexes **1.2** and **1.3** are determined based on thermochemical experiments carried out by Steve Nolan and Scafford Serron at the University of New Orleans; details are presented in the experimental section. The heat of reaction of **2.1** with pyridine *N*-oxide (equation 2.1) is -83.5 ± 1.4 kcal·mol^{-1}. The bond dissociation enthalpy of pyridine *N*-oxide (equation 2.2) is 72.11 ± 0.67 kcal·mol^{-1}.[47] Combination of these two values (equation 2.3 = eq. 2.2 - eq. 2.1) leads to the bond dissociation enthalpy for the Mo-O bond in **2.2** of 155.6 ± 1.6 kcal·mol^{-1}.

References begin on page 184

2.1) $Mo(N[R]Ar)_3 + py\text{-}O \rightarrow OMo(N[R]Ar)_3 + py$; $\Delta H_r = -83.5 \pm 1.4$ kcal·mol^{-1}

2.2) $py\text{-}O \rightarrow [O] + py$; $\Delta H_r = 72.11 \pm 0.67$ kcal·mol^{-1}

2.3) $OMo(N[R]Ar)_3 \rightarrow [O] + Mo(N[R]Ar)_3$; $\Delta H_r = 155.6 \pm 1.6$ kcal·mol^{-1}

Similarly, the heat of reaction of **2.1** with ethylene sulfide (equation 2.4) is 45.2 ± 1.2 kcal·mol^{-1}. The heat of reaction of ethylene sulfide to give ethylene and sulfur atoms (equation 2.5) is calculated to be 59.15 ± 0.33 kcal·mol^{-1}.[48,49] Finally, combination of the two reactions (equation 2.6 = eq. 2.5 - eq. 2.4) leads to the bond dissociation enthalpy for the Mo-S bond in **2.3** of 104.4 ± 1.2 kcal·mol^{-1}.

2.4) $Mo(N[R]Ar)_3 + SC_2H_4 \rightarrow SMo(N[R]Ar)_3 + C_2H_4$; $\Delta H_r = -45.2 \pm 1.2$ kcal·mol^{-1}

2.5) $SC_2H_4 \rightarrow [S] + C_2H_4$; $\Delta H_r = 59.15 \pm 0.33$ kcal·mol^{-1}

2.6) $SMo(N[R]Ar)_3 \rightarrow [S] + Mo(N[R]Ar)_3$; $\Delta H_r = 104.4 \pm 1.2$ kcal·mol^{-1}

The small contribution due to solvation effects is accounted for where possible; the heat of solvation of complex **2.1**, which is included in the above calculations, is 8.9 ± 0.2 kcal·mol^{-1}. A major assumption which must be made in the above interpretation is that the measured heats of reaction in equations 2.1 and 2.4 correspond closely to the bond dissociation enthalpies of interest. This seems reasonable, as the only bonds being made or broken during the reaction are element-chalcogen bonds. Changes in enthalpy on structural reorganization from the C_3 symmetric **1.1** to the pseudo-C_s symmetric chalcogenide complexes are expected to be on the order of 6 kcal·mol^{-1}.[50]

References begin on page 184

The value for the Mo-O bond dissociation enthalpy in complex **1.2** of 155 kcal·mol^{-1} represents one of the strongest transition metal-oxo bond strengths known when compared to an extensive list tabulated by Holm for the purposes of investigating biological oxo transfer.[51] There are many fewer data corresponding to metal-sulfur interactions, so it is assumed that the Mo-S bond in complex **1.3** is comparably strong.

Section 2.3: Theoretical Description of Mo(V)-E Complexes

(i) Extended Hückel MO Analysis

The electronic structures of the Mo(V) chalcogenides are examined through an extended Hückel analysis using the computer program CACAO.[52,53] Further discussion of this method is presented in Appendix I of this thesis. The calculations are simplified by using the model complex $SMo(NH_2)_3$. The ground state structure of $Mo(NH_2)_3$ is known to be of C_{3h} symmetry from high level theoretical calculations.[54] By bringing in a sulfur atom at an appropriate distance (2.168 Å), an interaction diagram between the two entities in the point group C_3 is constructed. This diagram is shown in Figure 2.13. The Cartesian coordinates used for the calculations are shown in Table 2.14. The lowest energy orbitals (4a and 3e) are primarily Mo-N in plane bonding. Orbital 4e is a mixture of Mo-E and Mo-N π bonding, and 5a is Mo-E σ bonding. Orbital 6a is a ligand based lone pair consisting of in-phase in-plane p orbitals on all three nitrogens and 5e is the metal based d_{xy} and $d_{x^2-y^2}$. The 6e orbital is a singly occupied degenerate Mo-E π^* orbital. A CACAO generated diagram of this degenerate orbital set, MO 14 and 15, is shown in Figure 2.14. Orbitals 7e and 7a are empty, and correspond to Mo-N π^* and Mo-E σ^* interactions respectively. The net Mo-S bond order predicted from these calculations is 2.5, in agreement with the structural data given in Section 2.2.

References begin on page 184

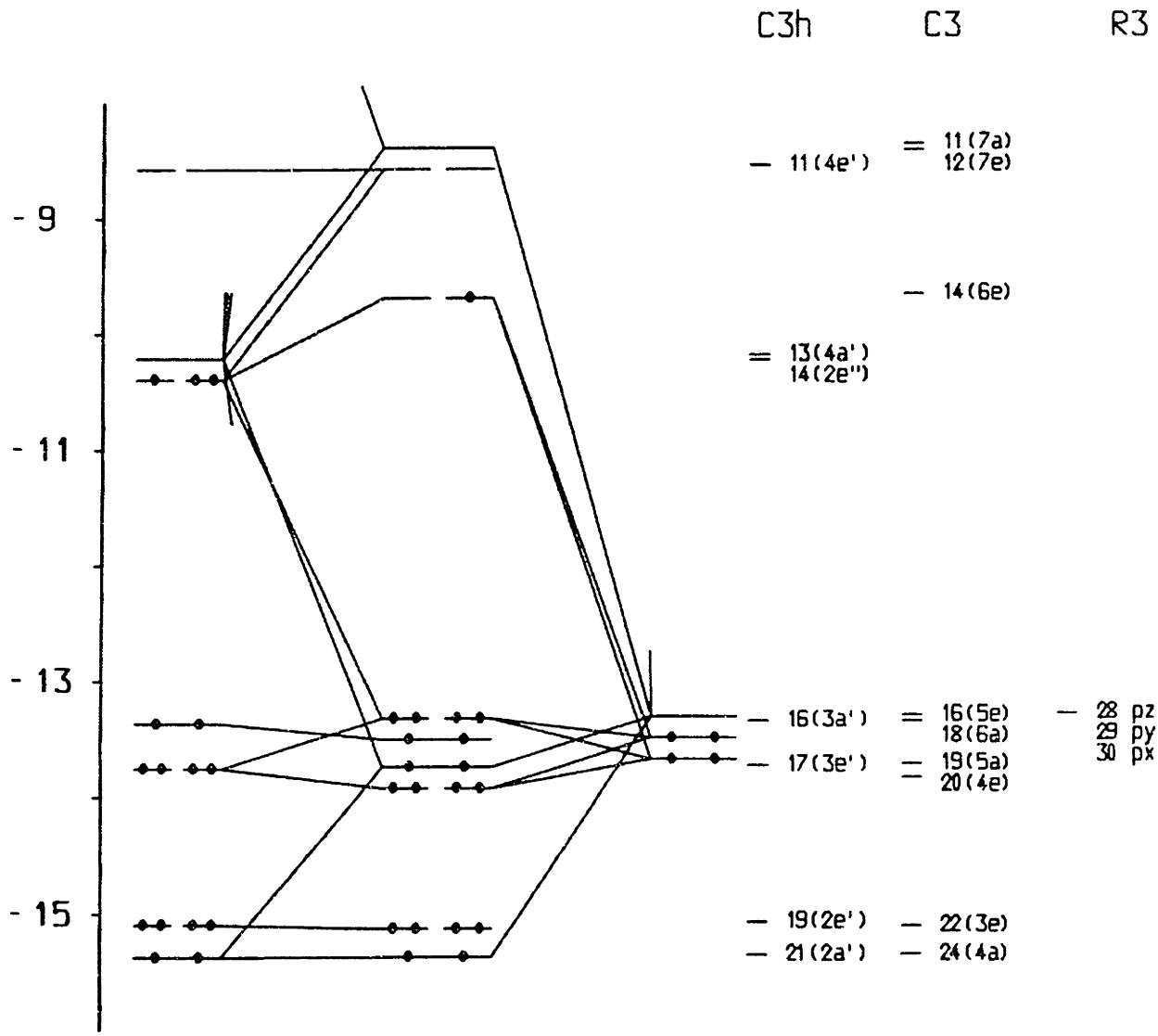

Figure 2.13: Diagram in C_3 for the Interaction of $Mo(NH_2)_3$ in C_{3h} with a sulfur atom at 2.168 Å.

References begin on page 184

Table 2.14: Cartesian Coordinates for $SMo(NH_2)_3$ in C_3.

Atom	x	y	z
Mo	0.000	0.000	0.000
N1	1.980	0.000	0.000
H11	2.558	0.156	-0.827
H12	2.558	0.156	0.827
N2	-0.990	1.715	0.000
H21	-1.414	2.137	-0.827
H22	-1.414	2.137	0.827
N3	-0.990	-1.715	0.000
H31	-1.144	-2.294	-0.827
H32	-1.144	-2.294	0.827
S	0.000	0.000	2.168

Table 2.15: Cartesian Coordinates for $SMo(NH_2)_3$ with coordinates derived from X-ray data (pseudo-C_s).

Atom	x	y	z
Mo	0.000	0.000	0.000
N1	1.612	-1.023	-0.461
H11	1.527	-2.007	-0.747
H12	2.579	-0.759	-0.234
N2	-1.694	-0.796	-0.531
H21	-1.674	-1.609	-1.159
H22	-2.633	-0.482	-0.255
N3	0.000	1.762	-0.895
H31	-0.128	1.623	-1.906
H32	0.104	2.739	-0.595
S	0.000	0.000	2.168

References begin on page 184

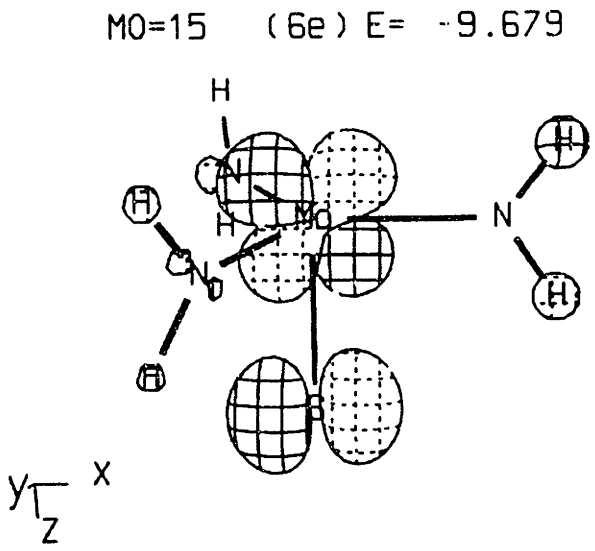

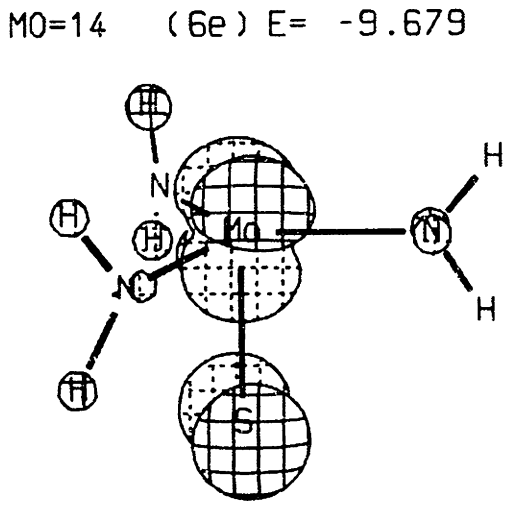

Figure 2.14: The singly occupied degenerate HOMO (orbitals 14 and 15) in C_3 for the calculated structure of $Mo(NH_2)_3$ (C_{3h}) with a sulfur atom at 2.168 Å.

References begin on page 184

This C_3 symmetric structure would be expected to undergo a Jahn-Teller type distortion in order to break the degeneracy of the partially filled π^* orbital, and in fact, this is what is observed in the crystal structures of the four chalcogen complexes, which approximate C_s symmetry. An interaction diagram of $SMo(NH_2)_3$ constructed using coordinates derived from the X-ray structure of complex **2.3** is shown in Figure 2.15. The Cartesian coordinates used for the calculations are listed in Table 2.15. Most of the orbitals in this diagram roughly correspond to the same type of interaction as in the C_3 diagram. The largest difference is the singly occupied 6e orbital from the C_3-symmetric structure which splits significantly in energy upon distorting to the C_s geometry. The orbital partner which lowers in energy and is half filled is primarily Mo-E π^* in character, MO 15 in Figure 2.16, while the partner which rises in energy and remains empty is primarily Mo-N π^* in character, MO 14 in Figure 2.16. This analysis helps to explain the experimentally observed distortion. In pseudo-C_s symmetry, the unpaired electron is able to occupy an orbital with minimal Mo-N π^* character, reducing the unfavorable interaction with the strongly electron-donating nitrogen lone pairs which exist before the distortion.

References begin on page 184

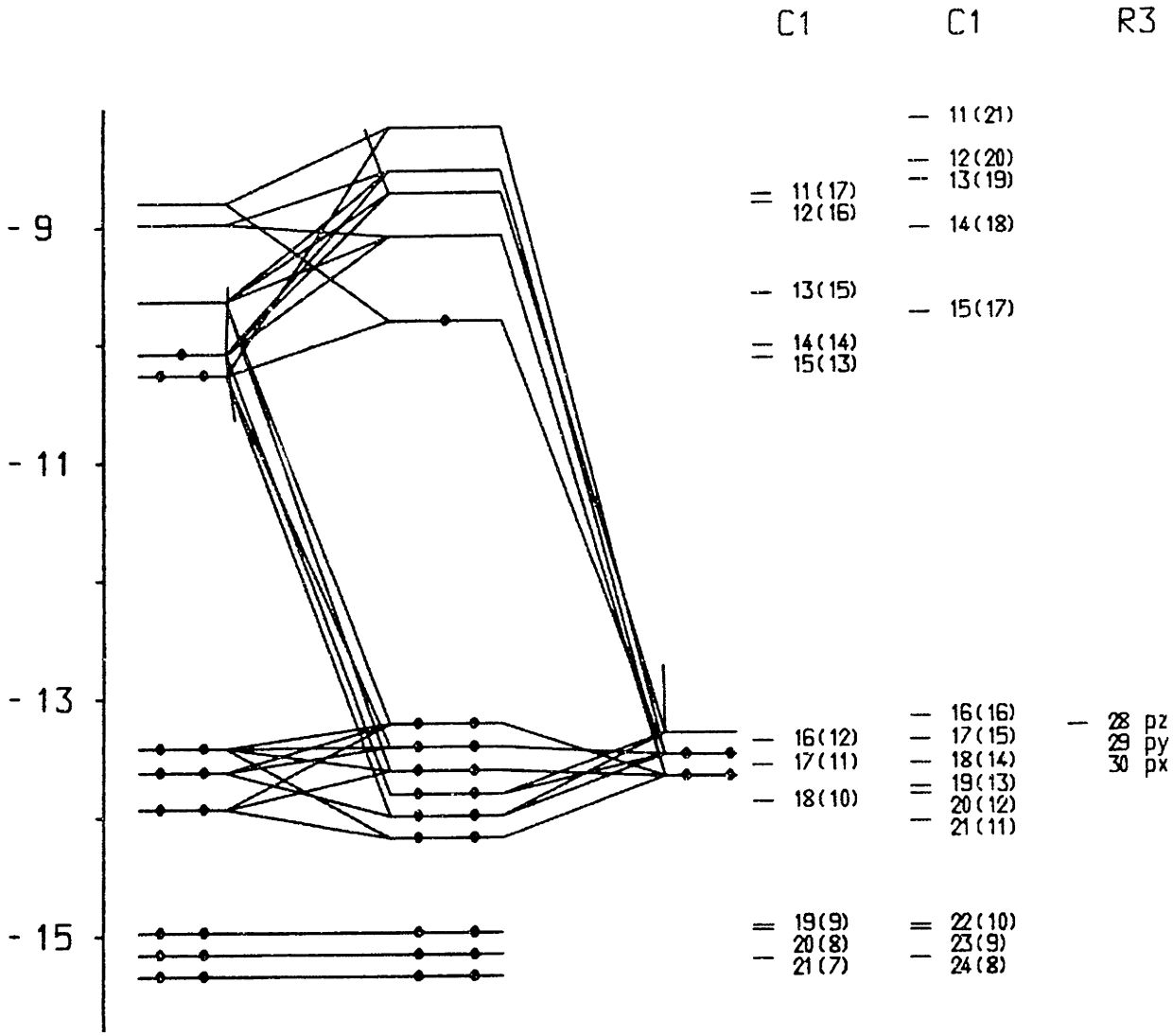

Figure 2.15: Interaction diagram for the model complex $SMo(NH_2)_3$ derived from the X-ray coordinates of $SMo(N[R]Ar)_3$ (**2.3**).

References begin on page 184

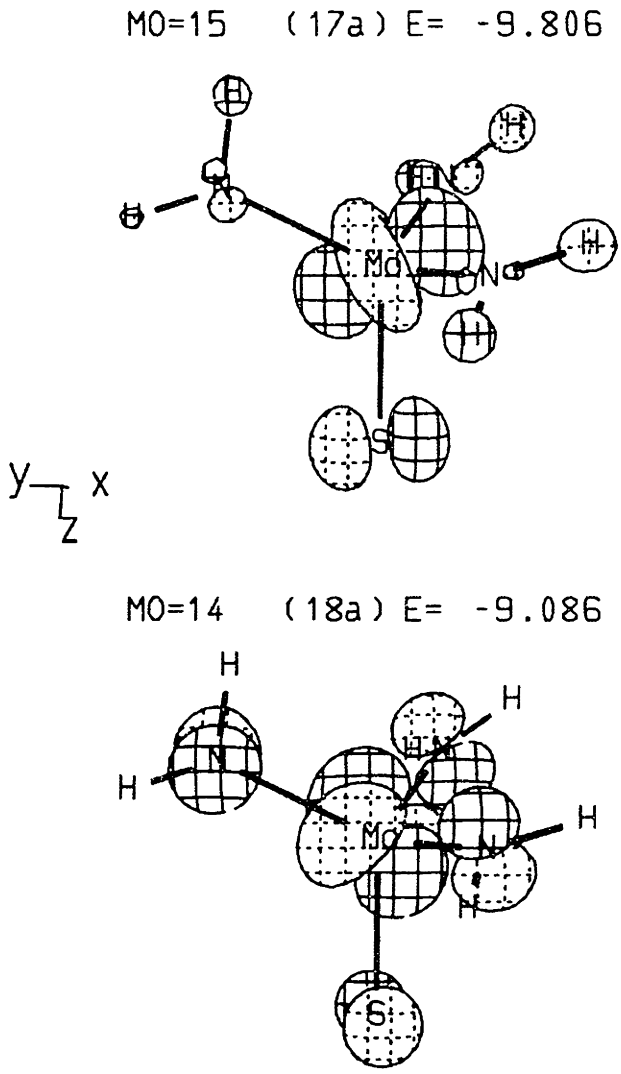

Figure 2.16: The LUMO (orbital 14) and SOMO (orbital 15) for the model complex $SMo(NH_2)_3$ derived from the X-ray coordinates of $SMo(N[R]Ar)_3$ (**2.3**).

References begin on page 184

(ii) Density Functional Calculations[55]

Quantum chemical calculations have been carried out on the model complexes $EMo(NH_2)_3$ by Jamal Musaev and Keiji Morokuma at Emory University in order to further elucidate the electronic and geometrical structures as well as thermodynamic parameters of the $EMo(N[R]Ar)_3$ complexes. These calculations use the hybrid density functional B3LYP method[56-58] in conjunction with the double-ζ plus polarization quality basis set lanl2dz + d_E (α_d = 0.85, 0.503, 0.364 and 0.252 for O,[59] S, Se and Te atoms,[60] respectively), which for heavy atoms (S, Se, Te and Mo) uses the Hay and Wadt effective core potential (ECP) including the relativistic effects for Mo and Te.[61,62] All calculations were performed by the GAUSSIAN-94 package.[63]

Gradient-corrected density functional methods such as B3LYP are quite reliable both in geometry and in energies.[54,64,65] For instance, the B3LYP method describes the geometry of the model complex $(\mu\text{-}N_2\{Mo[N(HNCH_2CH_2)_3]\}_2$ very well in comparison with the experimental structure of the real system $(\mu\text{-}N_2\{Mo[N(t\text{-}BuMe_2SiNCH_2CH_2)_3]\}_2$, with the N-N distance of 1.22 Å (calculated) vs. 1.20 Å (X-ray), the Mo-N(*trans* to N_2) distance of 2.30 Å (calculated) vs. 2.29 Å (X-ray) and the other Mo-N distances of 1.97 Å (calculated) vs. 2.01 Å (average, X-ray).[66]

As mentioned previously, the ground state of the $Mo(NH_2)_3$ complex is the quartet A' state in C_{3h} symmetry with three unpaired electrons in the [d_{xz} and d_{yz}] (e") and sd_σ (a') orbitals. The doublet A' state is calculated to be about 14.5 kcal·mol^{-1} higher.[54] In C_3 symmetry, the addition of an O, S, Se or Te atom in the ^3S state with two unpaired electrons to the quartet $Mo(NH_2)_3$ gives the doublet $EMo(NH_2)_3$ complex with a Mo-E bonding interaction consisting of one σ- and a net 1.5 π-component. The interaction diagram obtained is qualitatively identical to the one calculated from extended Hückel methods shown in Figure 2.13.

References begin on page 184

(iii) Density Functional Structures

The Jahn-Teller effect should distort the structure from a C_3 symmetry into one of the two C_s conformations **A** or **B**, shown in Figure 2.17. Both conformations distort from C_3 symmetry to C_s symmetry, but conformation **A** has one horizontal amide and two vertical amides, while conformation **B** has one vertical amide and two horizontal amides. The primary orbital considerations for this type of distortion are demonstrated in Figures 2.13-2.16. Geometry optimization on the model complexes $EMo(NH_2)_3$ converges to the conformation **A** for all four E ligands.

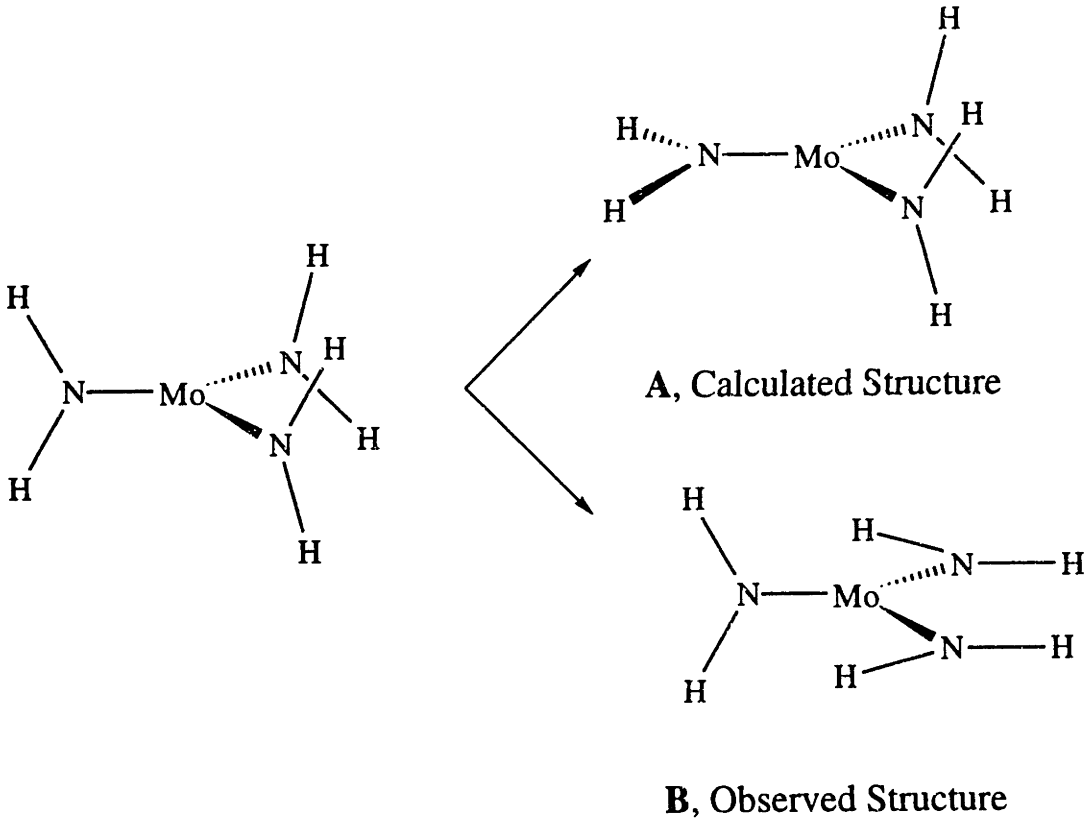

Figure 2.17: Two Possible Conformations of C_s $EMo(NH_2)_3$ Resulting from Jahn-Teller Distortion of the C_3 Structure.

References begin on page 184

$OMo(NH_2)_3$ is calculated to have C_1 symmetry, albeit only slightly distorted from C_s, with a doublet A ground state, while the other homologues are calculated to have true C_s symmetry with a doublet A" ground state. The Cartesian coordinates of the calculated structures are given in Tables 2.16-2.19 for the four chalcogen complexes. PLUTO diagrams of the calculated structures are shown in Figures 2.18-2.21. Pertinent bond distances are presented in Table 2.20. The conformation **B** is not a local minimum, though the energy of **B** relative to that of **A** is less than 2 kcal·mol^{-1}.

Table 2.16: Cartesian Coordinates for $OMo(NH_2)_3$ calculated at the B3LYp/lanl2dz + d_E level.

Atom	x	y	z
Mo	0.051336	-0.060178	0.076809
N1	-0.778661	1.715789	1.715789
H11	-0.279780	2.569753	0.300558
H12	-1.790249	1.850962	0.300558
N2	1.749471	0.072696	-0.900824
H21	2.6062421	-0.374157	-0.574599
H22	1.887584	0.573086	-1.778714
N3	-1.373144	-0.989457	-0.904877
H31	-2.012385	-0.528050	-1.552834
H32	-1.574391	-1.983869	-0.805781
O	0.227902	0.646683	1.678742

Table 2.17: Cartesian Coordinates for $SMo(NH_2)_3$ calculated at the B3LYp/lanl2dz + d_E level.

Atom	x	y	z
Mo	0.179436	0.000082	-0.027536
N1	1.029367	-0.001585	1.726113
H11	1.146214	-0.849149	2.283940
H12	1.145700	0.844644	2.286071
N2	0.771342	-1.628121	-0.915302
H21	0.179833	-2.171355	-1.543204
H22	0.178944	2.174308	-1.539189
N3	0.770779	1.630015	-0.912502
H31	1.721413	-1.996133	-0.852842
H32	1.720800	1.998089	-0.849738
S	-1.976853	-0.000375	0.130208

References begin on page 184

Table 2.18: Cartesian Coordinates for $SeMo(NH_2)_3$ calculated at the B3LYp/lanl2dz + d_E level.

Atom	x	y	z
Mo	-0.575906	0.000029	-0.025397
N1	-1.353124	-0.000822	1.758983
H11	-1.449969	0.845979	2.321967
H12	-1.450057	-0.848135	2.321177
N2	-1.184751	-1.625677	-0.900086
H21	-0.612744	2.165538	-1.547989
H22	-0.612993	-2.164159	-1.549909
N3	-1.184854	-1.625677	-0.900086
H31	-2.135465	1.989536	-0.815950
H32	-2.135638	-1.988591	-0.817604
Se	1.724824	-0.000043	0.042173

Table 2.19: Cartesian Coordinates for $TeMo(NH_2)_3$ calculated at the B3LYp/lanl2dz + d_E level.

Atom	x	y	z
Mo	0.923899	0.000010	-0.020664
N1	1.683733	-0.000049	1.769876
H11	1.782080	-0.847408	2.331885
H12	1.781527	0.847081	2.332324
N2	1.517578	-1.623813	-0.90599
H21	0.943622	-2.158933	-1.556052
H22	0.943636	2.159192	-1.555754
N3	1.517624	1.623856	-0.905306
H31	2.474178	1.976490	-0.841796
H32	2.474027	-1.976698	-0.841701
Te	-1.581449	-0.000002	0.024707

Table 2.20: Calculated Bond distances (Å) at the B3LYP lanl2dz + d_E level of theory for the complexes $Mo(NH_2)_3$ and $EMo(NH_2)_3$ where E = O, S, Se and Te.

Complex	Symmetry, Ground State	Mo-E	Mo-N_1	Mo-N_2	Mo-N_3
$Mo(NH_2)_3$	C_{3h}, $^4A'$	---	1.980	1.980	1.980
$OMo(NH_2)_3$	C_1, ^2A	1.715	1.956	1.956	1.960
$SMo(NH_2)_3$	C_s, $^2A''$	2.162	1.949	1.947	1.947
$SeMo(NH_2)_3$	C_s, $^2A''$	2.302	1.946	1.944	1.944
$TeMo(NH_2)_3$	C_s, $^2A''$	2.506	1.945	1.942	1.942

The experimental structures for the complexes $EMo(N[R]Ar)_3$ have the **B** conformation for E = S, Se and Te, and a distorted **B** conformation for E = O. This discrepancy between theory and experiment is attributable mainly to the steric effect of the bulky N[R]Ar ligands which could reasonably overshadow the small electronic energy difference between the two conformations. This steric effect would also be expected to

References begin on page 184

enforce significant differences in bond angles, and therefore, only bond distances in the calculated structures have any real meaning.

Table 2.20 shows that addition of an O, S, Se or Te atom should shorten the Mo-N distance by 0.02-0.03 Å from 1.98 Å in C_{3h} $Mo(NH_2)_3$. The calculated Mo-N distances are in good agreement with those observed experimentally. The distance between Mo and the added O, S, Se and Te atom is calculated to be 1.715, 2.162, 2.302, and 2.506 Å, which is in excellent agreement with the experimental values, 1.706, 2.168, 2.312 and 2.535 Å .

(iv) Density Functional Bond Energies

As seen in Table 2.21, the $EMo(NH_2)_3$ binding energies calculated at the B3LYP/lanl2dz + d_E level are 140.2, 94.1, 82.5 and 64.5 kcal·mol^{-1} for E = O, S, Se and Te, respectively. At this level of theory, the calculated values for $OMo(NH_2)_3$ and $SMo(NH_2)_3$ are 10% smaller than the experimentally determined ones, 155.6 ± 1.6 and 104.3 ±1.2 kcal·mol^{-1}, respectively. The errors, in part due to the approximations used in the calculations and in part due to the difference between the real and model systems, are expected to be systematic. Therefore, the $SeMo(N[R]Ar)_3$ and $TeMo(N[R]Ar)_3$ bond energies are best estimated by scaling up the calculated values for $SeMo(NH_2)_3$ and $TeMo(NH_2)_3$ by 10% to be 91 and 71 kcal·mol^{-1}, respectively.

Table 2.21: The calculated and experimental $EMoL_3$ binding energies (in kcal/mol), where E = O, S, Se, and Te and L = NH_2 (calculated) and N[R]Ar (experimental, R = $C(CD_3)_2CH_3$ and Ar = 3,5-$Me_2C_6H_3$).

E	Symmetry, Ground State	D_e (Mo-E)		
		B3LYP lanl2dz + d_E	Best estimated[a]	Experiment
O	C_1, ^2A	140.2	--	155.61 ± 1.6
S	C_s, $^2A''$	94.1	--	104.35 ± 1.2
Se	C_s, $^2A''$	82.5	91.0	----
Te	C_s, $^2A''$	64.5	71.0	----

a) See text for more detail.

References begin on page 184

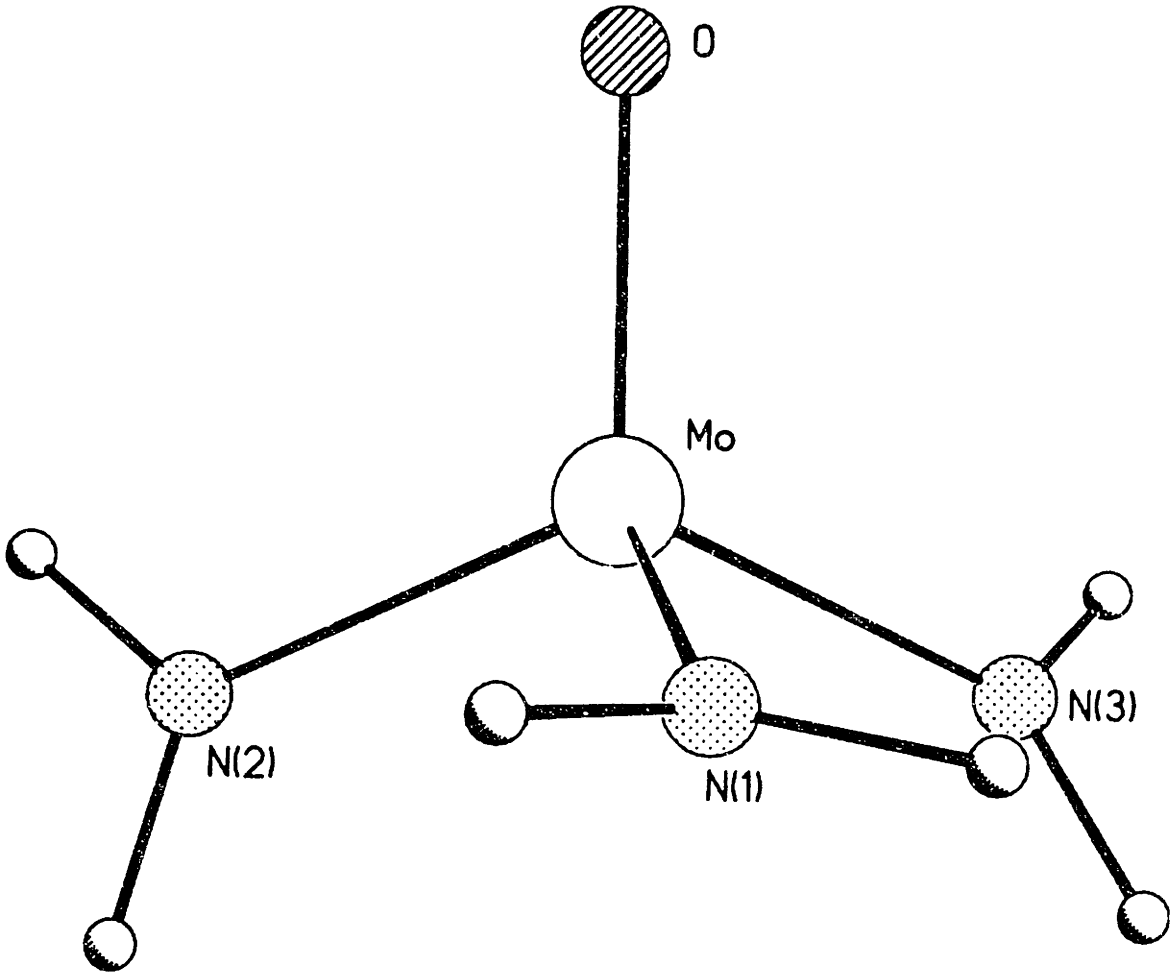

Figure 2.18: PLUTO diagram of the calculated structure for $OMo(NH_2)_3$ (C_1, ^2A) at the B3LYP/lanl2dz + d_E level.

References begin on page 184

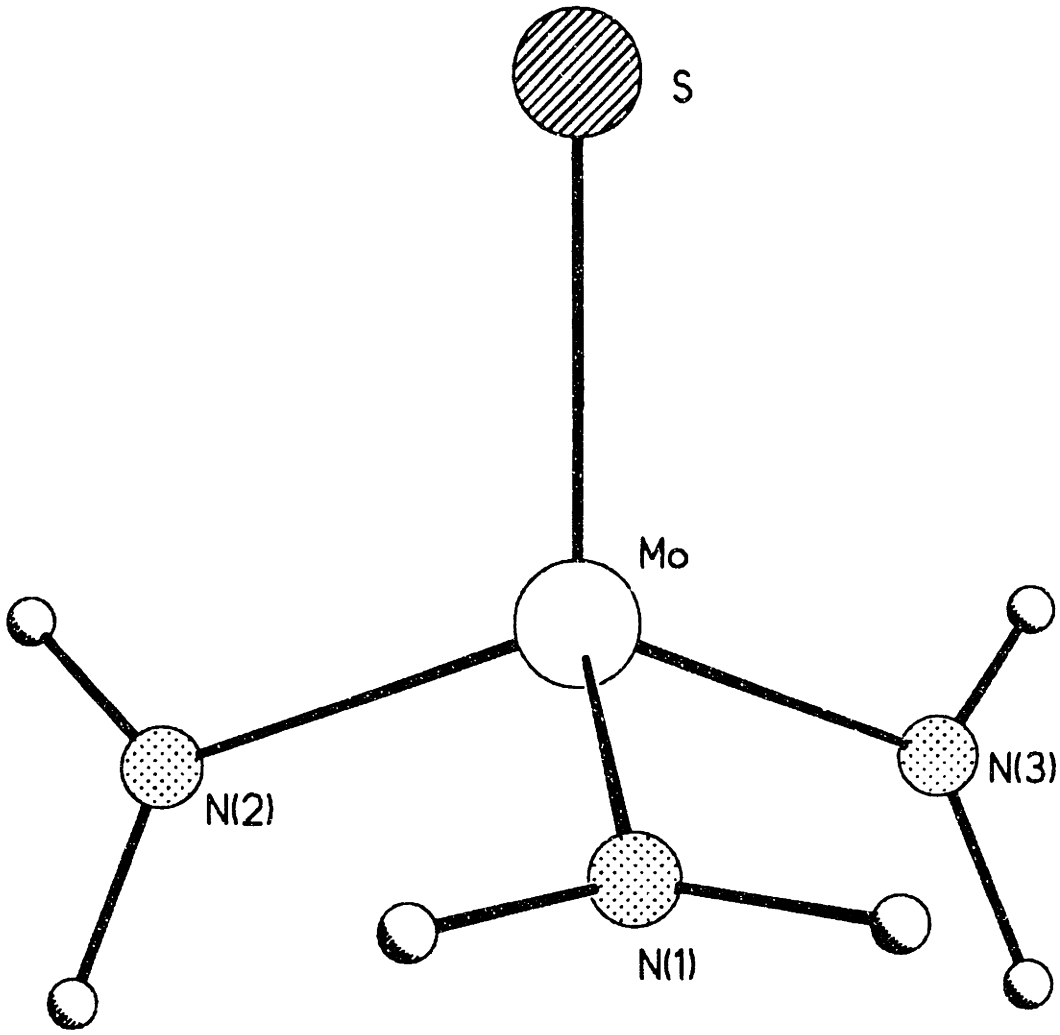

Figure 2.19: PLUTO diagram of the calculated structure for $SMo(NH_2)_3$ (C_s, $^2A''$) at the B3LYP/lanl2dz + d_E level.

References begin on page 184

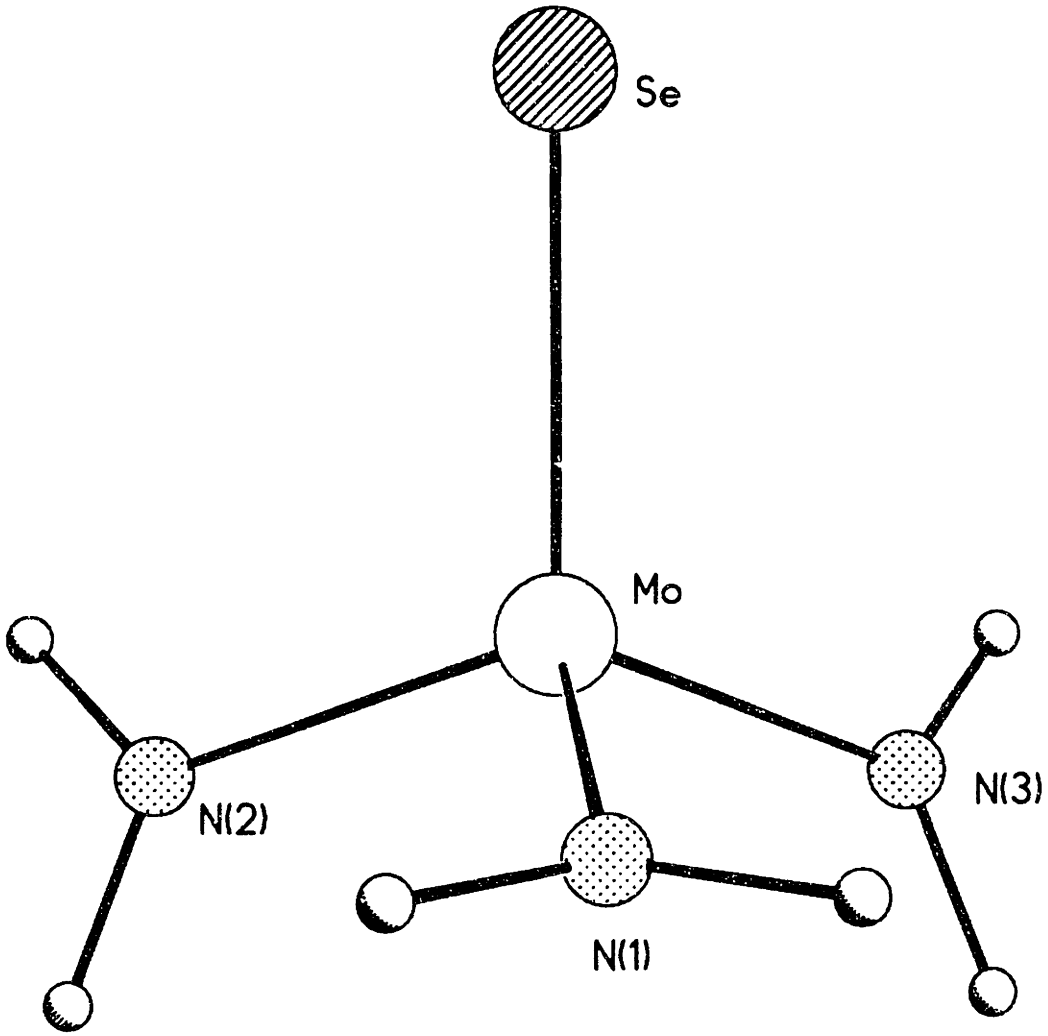

Figure 2.20: PLUTO diagram of the calculated structure for $SeMo(NH_2)_3$ (C_s, $^2A''$) at the B3LYP/lanl2dz + d_E level.

References begin on page 184

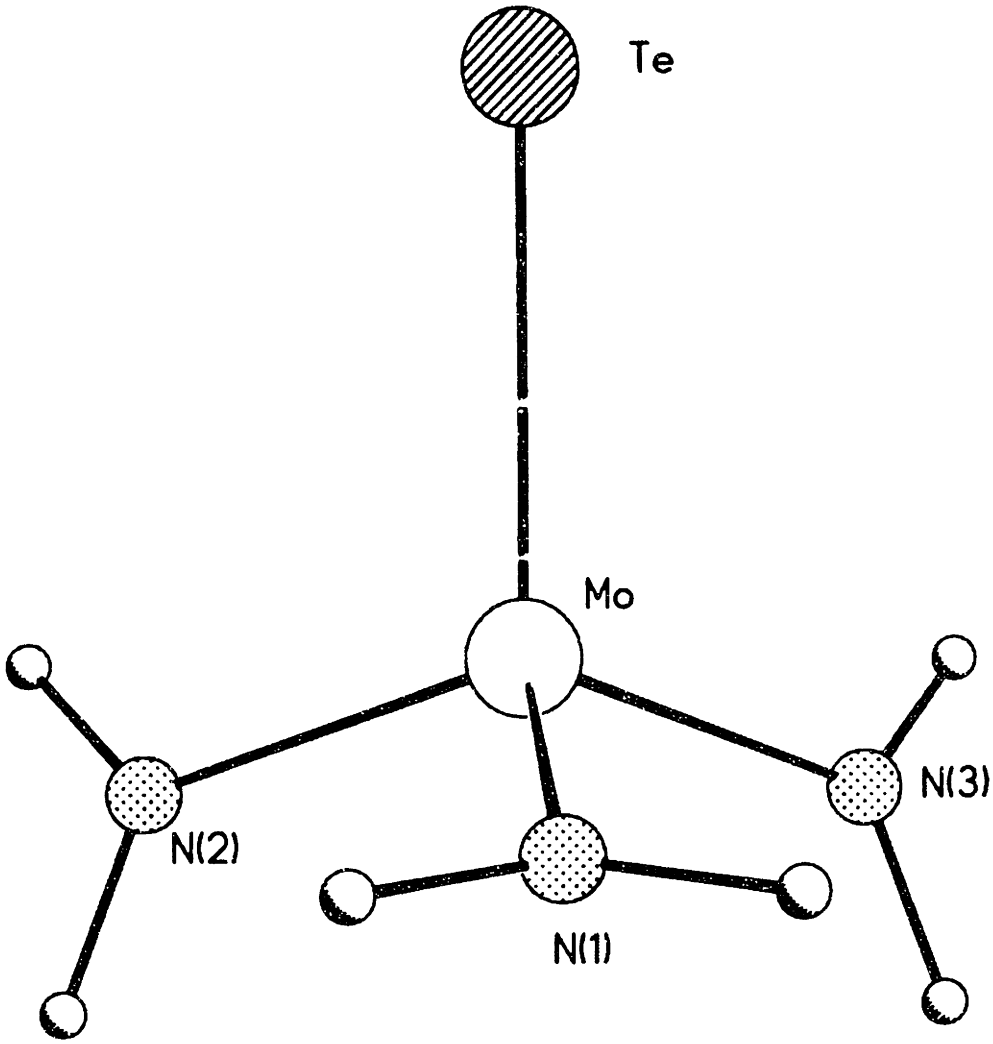

Figure 2.21: PLUTO diagram of the calculated structure for $TeMo(NH_2)_3$ (C_s, $^2A''$) at the B3LYP/lanl2dz + d_E level.

References begin on page 184

(v) Population Analysis and Metal-Ligand Bond Character

The above mentioned trends in the energies and geometries of the calculated complexes are best explained in terms of the electronegativity and the size of valence s and p orbitals of the O, S, Se and Te atoms. The atomic electronegativity decreases in the order O > S > Se > Te, and the size of valence s and p orbitals increases in the same order. Therefore, the electrostatic character of the Mo-E bond decreases and its covalent character increases in the order of E: O-S-Se-Te. As seen in Table 2.22 in the Mulliken population analysis, both the positive charge of the metal center, +1.35, +1.16, +1.10, and +1.04 e, and the absolute value of the negative charge of the atom E, -0.46, -0.38, -0.32, and -0.29 e, decrease in the same order, confirming that the ionic character of the Mo-E bond decreases in the above order. At the same time, the overlap population Q between the Mo and E atoms, 0.68, 0.81, 0.86 and 0.87 e increases in the same order, confirming that the covalent character of the Mo-E bond increases in this order.

Table 2.22: The Mulliken atomic charges (Z*), overlap population (Q) and spin density (all in e) of $EMo(NH_3)_3$, where E = O, S, Se and Te.

	Z*		Q(X-Mo)	Spin Density	
E	E	Mo		E	Mo
O	-0.46	+1.35	0.68	0.06	0.87
S	-0.38	+1.16	0.81	0.16	0.81
Se	-0.32	+1.10	0.86	0.17	0.80
Te	-0.29	+1.04	0.87	0.21	0.78

The Mulliken spin density in Table 2.22 confirms that the unpaired electron in the Mo-E π^* orbital is localized more on the molybdenum atom. The extent of localization decreases as the ligand E goes down the periodic table. As E changes in this order, the lower electronegativity of E as well as the larger Mo d_π-E p_π overlap increases the contribution of the E p_π orbital in the π^* orbital, resulting in more delocalization and smaller spin density on molybdenum.

References begin on page 184

Section 2.4: Mo(VI) Chalcogenide Complexes

(i) Synthesis and Characterization of $OMo(NAr)(N[R]Ar)_2$ (2.6)

Prolonged thermolysis of the Mo(V) oxo complex **2.2** at temperatures exceeding 65 °C leads to disappearance of the starting material and clean appearance of a new diamagnetic product as determined by ^1H and ^2H NMR spectroscopies. The color of the solution also changes from dark brown to a very light yellow-brown. When the reaction is carried out in C_6D_6 and the volatiles are examined by ^1H NMR spectroscopy, isobutylene, isobutane and hexamethylethane are observed. Close examination of the reaction by ^2H NMR spectroscopy shows the presence of isobutylene at around 4.8 ppm. The fact that these organic products are observed in both the deuterium and the proton NMR spectra leads to the conclusion that the reaction in question is *tert*-butyl radical elimination of a d_6-*tert*-butyl group.[67-69] Recent reports describe a similar type of reaction involving *tert*-butyl radical elimination from a *tert*-butoxy group.[35] Scheme 2.2 shows the reaction in question. Carrying out the thermolysis reaction on a large scale results in formation of the oxo imide species **2.6**. Unfortunately, this complex proves to be an oil, contaminated with 5-10% HN[R]Ar, which resists purification. Carrying out the thermolysis reaction at higher temperatures leads to shorter reaction times, but the resulting product is less pure: there is a higher degree of free aniline production, and higher temperatures cause a disproportionation reaction (see below for details).

References begin on page 184

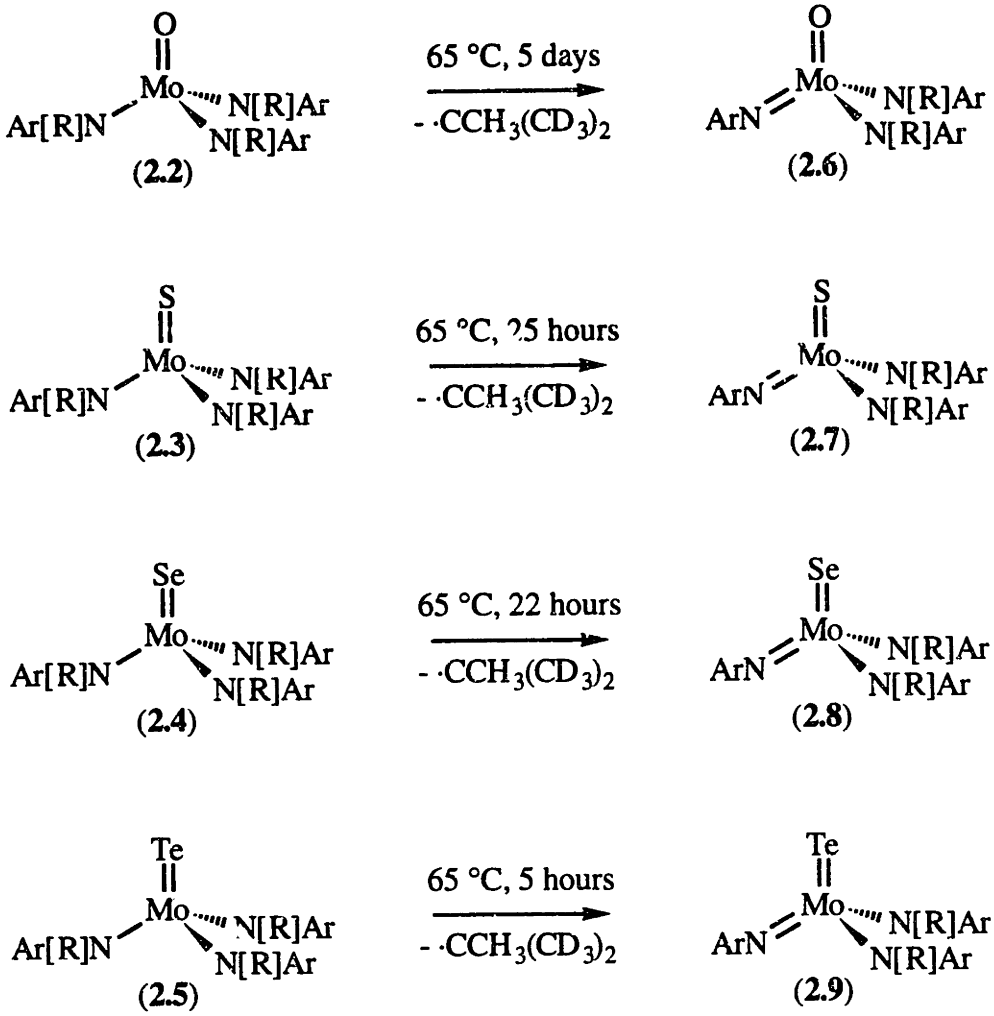

Scheme 2.2: Preparation of Mo(VI) Chalcogenide Complexes through Radical C-N Bond Homolysis

References begin on page 184

^{1}H NMR spectroscopy is not sufficient to distinguish between two possible structures, the oxo imide $OMo(NAr)(N[R]Ar)_2$, or the aryloxide nitrido species $NMo(OAr)(N[R]Ar)_2$ which could result from the migration of an aryl group. The migration of an N-bound substituent to oxygen is precedented in a related system.[35] Other characterization data (HRMS, ^{13}C NMR) are consistent with either connectivity. Hydrolysis of the isolated material followed by analysis by GC-MS shows HN[R]Ar and H_2NAr, but no HOAr, consistent with the formulation of **2.6** as $OMo(NAr)(N[R]Ar)_2$. Complex **2.6** reacts with benzaldehyde to the extent of about 10% to the products shown in Scheme 2.3 suggesting a terminal oxo ligand in **2.6**. Both imine PhC(H)=NAr and the dioxo complex $O_2Mo(N[R]Ar)_2$ **2.12** (see section 2.5) are observed spectroscopically (see experimental section for details). Prolonged storage of complex **2.6** at room temperature, or thermolysis of the complex in solution at high temperatures leads to disproportionation of **2.6** to a mixture of **2.6**, **2.12** and the presumed bis-imide complex $Mo(NAr)_2(N[R]Ar)_2$. This reaction appears to be an equilibrium mixture, with $K_{eq} \approx 1$. The most convincing evidence obtained for the formulation of the product as the oxo imide is the intense IR stretch at 913 cm^{-1} due to ν_{Mo-O}. This band is at slightly higher energy than the stretch observed for oxo complex **2.2**, as would be expected for the increase in oxidation state of the molybdenum center.

References begin on page 184

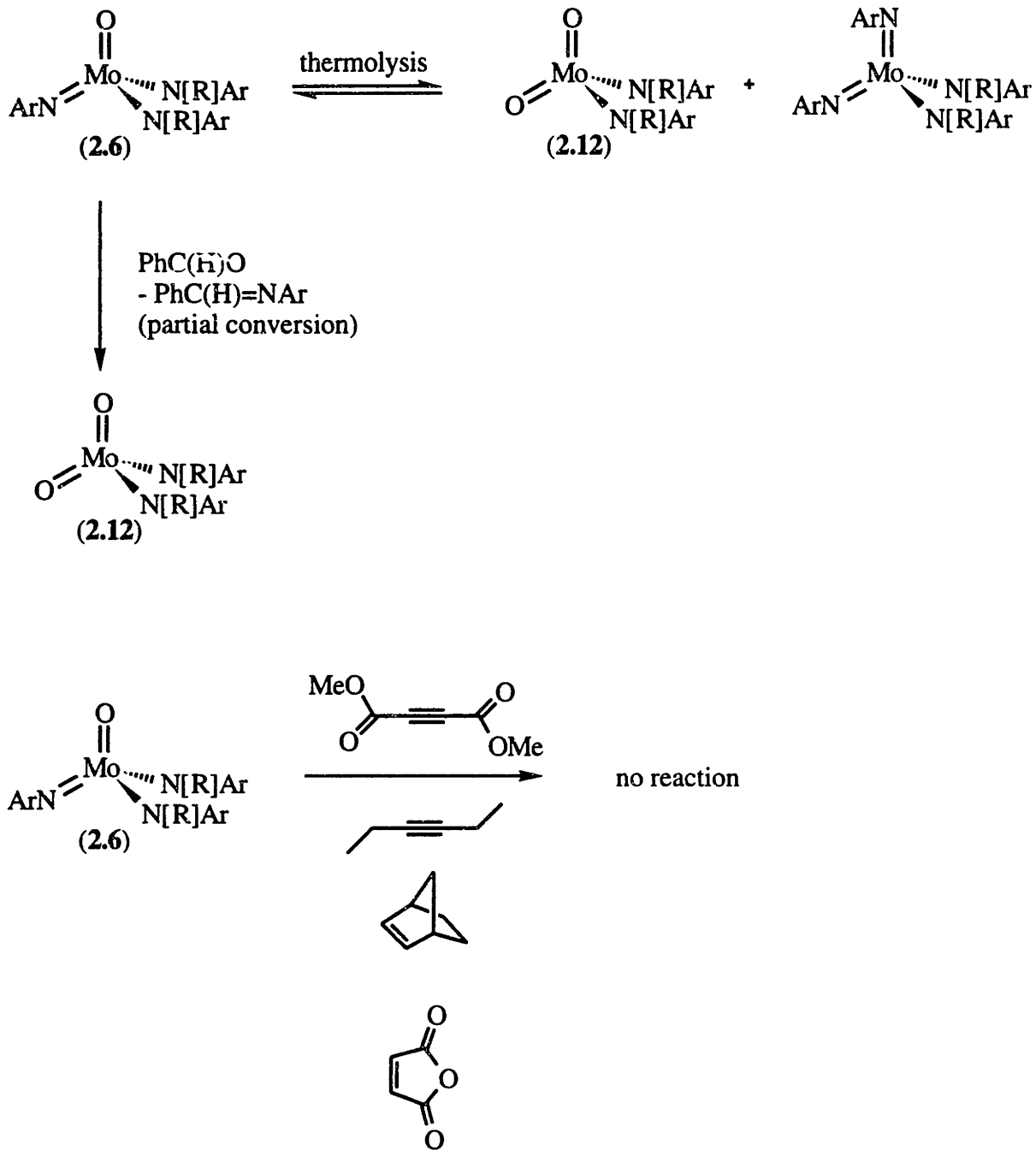

Scheme 2.3: Reactions of $OMo(NAr)(N[R]Ar)_2$ (**2.6**)

(ii) Synthesis and Characterization of $SMo(NAr)(N[R]Ar)_2$ (2.7)

Thermolysis of sulfide **2.3** causes a color change from dark brown to a much lighter reddish brown (Scheme 2.2). The reaction also results in the formation of

References begin on page 184

isobutylene, isobutane and hexamethylethane (observed by ^1H and ^2H NMR spectroscopy) due to *tert*-butyl radical elimination from the Mo(V) complex. The sulfide imide **2.7** is recrystallized from ether as an orange powder in 84% yield.

Again, spectroscopic evidence does not differentiate between the two possible connectivities (sulfide imide or thiophenoxide nitride). Crystals suitable for an X-Ray diffraction experiment have not been obtained. Complex **2.7** reacts with benzaldehyde and spectroscopic evidence for gradual production of the imine PhC(H)=NAr in small quantities suggests that the sulfide is terminal like the oxo ligand in **2.6**. Prolonged thermolysis of the complex leads primarily to decomposition. The complex exhibits a strong stretch in the IR at 506 cm^{-1} which has a slightly higher ν_{Mo-S} than that observed for the Mo(V) sulfide complex **2.3**, supporting the proposed terminal sulfide formulation.

(iii) Synthesis and Characterization of SeMo(NAr)(N[R]Ar)$_2$ (2.8)

Thermolysis of selenide **2.4** at 65 °C for 22 hours gives a diamagnetic product, as determined by ^1H NMR spectroscopy, generating isobutane, isobutylene and hexamethylethane as side products (Scheme 2.2). The color of the reaction mixture changes from dark brown to a lighter red-orange. The selenide imide **2.8** is orangeish brown in color and is isolated in 64% yield as a powder.

Spectroscopic evidence is consistent with its formulation as the terminal chalcogenide imide like complexes **2.6** and **2.7**. Investigation of the complex by ^{77}Se NMR spectroscopy shows a broad resonance at 1923.4 ppm ($\Delta\nu_{1/2}$ = 46.2 Hz); molybdenum satellites are not observed. The ^{77}Se NMR chemical shifts for transition metal selenides are extremely dependent on the chemical environment, but there are some general trends. Terminal selenides exhibit resonances appearing between 800 and 2400 ppm,[5,14,70] with the majority falling in the 1900-2300 ppm range.[5,16] Alkyl selenides have resonances in the region from 200 to 1100 ppm,[71-74] although this latter number is of a very deshielded complex. The chemical shift in **2.8** is therefore more consistent with a

References begin on page 184

terminal selenido than an organoselenolate functionality. The complex exhibits a strong peak in the Far-IR at 355 cm^{-1}, attributable to $\nu_{Mo\text{-}Se}$, which is at slightly higher energy than that observed for the Mo(V) selenide, lending further support to the formulation as a terminal selenide.

(iv) Synthesis and Characterization of TeMo(NAr)(N[R]Ar)$_2$ (2.9)

Telluride **2.5** eliminates a *tert*-butyl radical at 65 °C to generate a diamagnetic product which is much more thermally sensitive than the lighter homologues (Scheme 2.2). Prolonged heating gives rise to peaks in the NMR spectrum suggesting a disproportionation reaction similar to that seen for the oxo complex **2.6** in Scheme 2.3. This decomposition reaction occurs at a rate comparable to product formation, and there is also substantial formation of free HN[R]Ar. As a consequence, the thermolysis is only carried out for about five hours at 65 °C. The reaction (as monitored by ^2H NMR spectroscopy) is approximately 80% complete after this time period. Recrystallization of TeMo(NAr)(N[R]Ar)$_2$ (**2.9**) from ether gives a dark brown powder in around 40% yield, but it has not been obtained analytically pure.

Spectroscopic evidence is analogous to that reported for **2.6**, **2.7** and **2.8**, consistent with its formulation as the terminal telluride imide. The complex exhibits an extremely broad ^{125}Te NMR resonance at 2459.3 ppm ($\Delta\nu_{1/2}$ = 250 Hz) and Mo satellites are not observed. Terminal tellurides tend to have ^{125}Te chemical shifts in the window from 2700[8] to 3300[16] ppm, though they can appear below this region.[14] Alkyl tellurides of tin[75] and iron[76] have chemical shifts of approximately -1200 ppm. There is a scarcity of tellurium NMR data in the literature, but it is possible to correlate selenium and tellurium chemical shifts in related systems.[5] The chemical shift for **2.9** is more consistent with a terminal telluride function than an aryltellurolate. The complex exhibits a strong peak in the Far-IR at 291 cm^{-1}, which is at slightly higher energy for $\nu_{Mo\text{-}Te}$ than that observed for the Mo(V) telluride, lending further support to the terminal telluride formulation.

References begin on page 184

(v) General Features of Mo(VI) Chalcogenide Complexes

The molybdenum(VI) chalcogenide imide complexes **2.6-2.9** are quite unreactive. For example, **2.6** fails to react with even the strained or activated unsaturated hydrocarbons shown in Scheme 2.3. The chemistry of these molecules remains to be explored further.

The thermolysis of Mo(V) chalcogenide complexes to give Mo(VI) chalcogenide imide complexes takes advantage of the stability of the *tert*-butyl radical. This relatively high degree of stability also explains the ease of *tert*-butyl radical ejection from *tert*-butoxide ligands.[35] Alternatively, this reaction shows a potential weakness of the N[R]Ar ligand framework. The ejection of *tert*-butyl radicals from the N[R]Ar ligand to form aryl imides is also an observed decomposition pathway in niobium chemistry. The Nb(III) reduction product of $ClNb(N[R]Ar)_3$ is not isolated or even spectroscopically observed as it decomposes via a *tert*-butyl radical expulsion to give the Nb(IV) dimer $[Nb(N[R]Ar)_2(\mu\text{-}NAr)]_2$.[41] The thermolysis reaction represents a new synthesis of imides that, although not expected to be general in scope, may have some synthetic utility.

(vi) Kinetics of C-N Bond Homolysis

Measuring the kinetics of the thermolysis reactions (Scheme 2.2) by UV-visible spectroscopy has been hampered by the lack of suitable absorption differences between the starting materials and products, and also by the presumed disproportionation reaction of the chalcogenide imide complexes at higher temperatures. The deconvolution of UV-vis spectroscopic data using suitable computer programs has been unsuccessful.[77]

The kinetics of the thermolysis reaction of oxo **2.2** are determined between 65 °C and 105 °C by monitoring the disappearance of the starting material relative to an internal sealed reference capillary of D_2O/THF by ^2H NMR spectroscopy (see experimental section for details). The reaction is cleanly first order over this temperature range, and the observed first order rate constants are given in Table 2.23. An Eyring plot of the data is

References begin on page 184

shown in Figure 2.22, clearly showing a good fit to first order kinetics. The first order activation parameters derived from the fit are shown in Table 2.24. The $\Delta H^{\ddagger}$ value of 28.85 ± 0.07 kcal·mol^{-1} suggests bond breaking in the transition state, while the $\Delta S^{\ddagger}$ value of 3.10 ± 0.08 cal·mol^{-1}·K^{-1} is very small and not indicative of a substantial entropy contribution to the rate.

Table 2.23: Kinetics of EMo(N[R]Ar)$_3$ Decomposition.

OMo(N[R]Ar)$_3$		SMo(N[R]Ar)$_3$	
T (K)	k (x 10^5 sec $^{-1}$)	T (K)	k (x 10^4 sec $^{-1}$)
335.9	0.586 ± 0.067	339.1	1.32 ± 0.27
345.7	1.86 ± 0.37	343.3	2.25 ± 0.23
355.7	6.50 ± 2.09	348.5	3.86 ± 0.62
365.8	22.8 ± 4.0	355.9	8.94 ± 1.87
377.0	67.4 ± 10.8	366.0	20.1 ± 3.8

Table 2.24: Heats (kcal·mol^{-1}) and enthalpies (cal·mol^{-1}·K^{-1}) of activation for the thermolysis of EMo(N[R]Ar)$_3$.

Species	$\Delta H^{\ddagger}$	$\Delta S^{\ddagger}$
OMo(NRAr)$_3$	28.85 ± 0.07	3.10 ± 0.08
SMo(NRAr)$_3$	24.39 ± 0.13	-4.53 ± 0.06

References begin on page 184

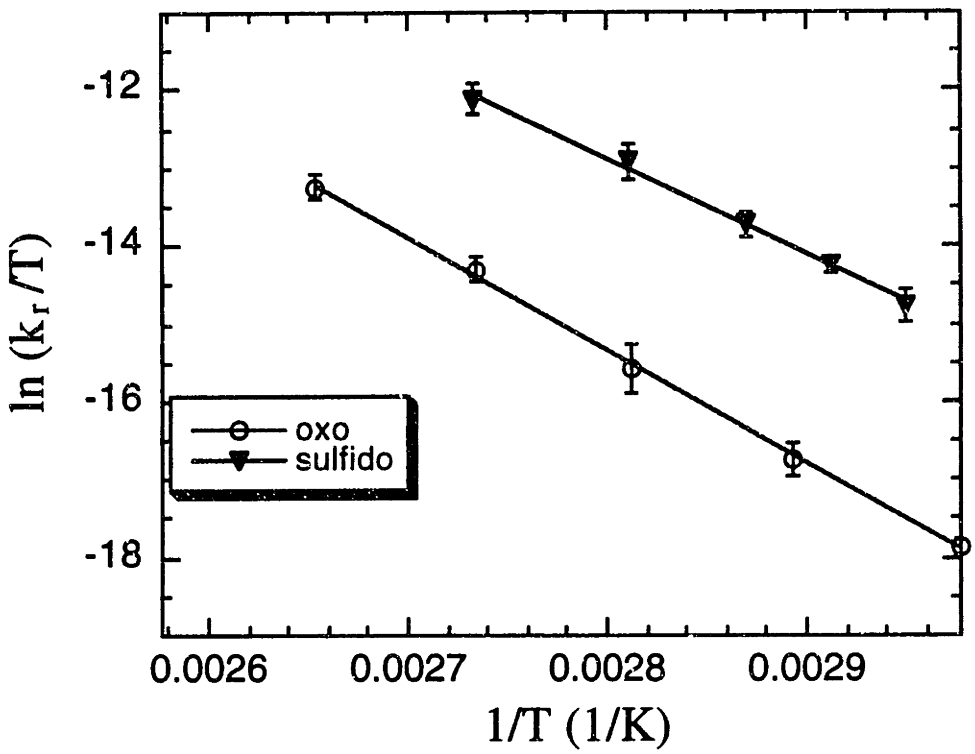

Figure 2.22: Logarithmic least-squares fit of first-order rate constants [ln ($k_r \cdot T^{-1}$)] versus reciprocal temperature [K^{-1}] using the Eyring equation [ln ($k_r \cdot T^{-1}$) = $-\Delta H^{\ddagger} \cdot R^{-1} \cdot T^{-1}$ + C] for the thermal conversion of $OMo(N[R]Ar)_3$ (**2.2**) and $SMo(N[R]Ar)_3$ (**2.3**) to $OMo(NAr)(N[R]Ar)_2$ (**2.6**) and $SMo(NAr)(N[R]Ar)_2$ (**2.7**) with *tert*-butyl radical loss. Data are shown with 95% confidence limit intervals.

References begin on page 184

The kinetics of the thermolysis reaction leading to **2.7** are determined over the temperature range from 65 °C to 95 °C in an analogous manner. The reaction is cleanly first order over this temperature range, but the rate is too fast to be measured accurately using this method above 95 °C. The observed first order rate constants are approximately an order of magnitude larger than those for the oxo thermolysis, and the two sets of numbers are compared in Table 2.23. An Eyring plot of the data is given in Figure 2.22, clearly showing a good fit to first order kinetics. The first order activation parameters derived from the fit are shown in Table 2.24. The $\Delta H^{\ddagger}$ value of 24.39 ± 0.13 kcal·mol^{-1} suggests bond breaking in the transition state. The $\Delta S^{\ddagger}$ value of -4.53 ± 0.06 cal·mol^{-1}·K^{-1} is opposite in sign to the one measured for the oxo thermolysis reaction, but again, it is very small and not indicative of substantial entropy contribution to the rate.

(vii) Extended Hückel Description of Thermolysis

The thermolysis reaction is readily examined in more detail by carrying out extended Hückel calculations on a model complex which undergoes plausible deformations along the reaction coordinate. This analysis sheds light on mechanistic aspects of the reaction, despite the limited attempts to find a minimum energy surface. Step one in this simplistic scheme is the C_s symmetric $SMo(NH_2)_3$, with one vertical amide and two horizontal amides, derived from slight distortions of the experimentally determined solid state structure. Steps two through ten retain C_s symmetry, but one N-H bond on the unique amide is graudally lengthened along the original NH vector to 2 Å, suggesting its loss as a radical, while the Mo-N-H angle for the remaining hydrogen is increased from 107° to 180°. The Cartesian coordinates of step one and step ten used for these calculations are given in Table 2.25 and 2.26. This simplistic pathway ignores any changes in the pertinent Mo-N distance, and assumes that all other atoms in the molecule remain stationary. It is expected that the molecule represented in step ten would undergo significant distortions to lower its energy, but these distortions are ignored in this analysis.

References begin on page 184

Table 2.25: Cartesian Coordinates used in Extended Hückel calculations for step one of the model transformation of $SMo(NH_2)_3$ to $SMo(NH)(NH_2)_2$.

Atom	x	y	z
Mo	0.000	0.000	0.000
N1	1.767	0.000	0.889
H11	2.751	0.000	0.616
H12	1.607	0.000	0.616
N2	-0.949	1.644	0.438
H21	-1.929	1.588	0.720
H22	-0.660	2.603	0.242
N3	-0.949	-1.644	0.438
H31	-0.660	-2.603	0.242
H32	-1.929	-2.603	0.720
S	0.000	0.000	-2.167

Table 2.26: Cartesian Coordinates used in Extended Hückel calculations for step ten of the model transformation of $SMo(NH_2)_3$ to $SMo(NH)(NH_2)_2$.

Atom	x	y	z
Mo	0.000	0.000	0.000
N1	1.767	0.000	0.889
H11	2.679	0.000	1.348
H12	2.895	0.000	2.960
N2	-0.949	1.644	0.438
H21	-1.929	1.588	0.720
H22	-0.660	2.603	0.242
N3	-0.949	-1.644	0.438
H31	-0.660	-2.603	0.242
H32	-1.929	-2.603	0.720
S	0.000	0.000	-2.167

Despite the simplistic model, mechanistic conclusions are obtained which give a deeper understanding of the reaction pathway than the single headed arrow mechanism that is usually drawn for a radical elimination reaction. A Walsh diagram depicting the transformation is shown in Figure 2.23. The total energy of the system is shown as a dashed line in the Figure, which rises to a maximum in step seven and then begins dropping. However, as mentioned previously, the model complex described by step ten should undergo significant distortions to lower its energy. In Step one, the interaction diagram is, not surprisingly, essentially identical to that shown in Figure 2.15. During the course of this reaction coordinate, all of the orbitals depicted in the interaction diagram

References begin on page 184

remain unchanged in either directionality or energy except orbitals 10, 13, 15, 22, 24 and 26 of Step one, which make significant changes in these areas. Orbital 10 starts as an N-H σ^* orbital in the upright amide, and drops substantially in energy, becoming a Mo-N π^* orbital in step ten. Orbital 13 is primarially a Mo-N π^* orbital to the two horizontal amides, but gains some Mo-N π^* to the upright amide at the expense of a Mo-N σ^* interaction, thereby lowering its energy. Orbital 15, which in step one contains the unpaired electron in a Mo-E and Mo-N π^* interaction, drops in energy along the reaction coordinate as it gains a significant amount of electron density on the departing hydrogen atom, suggesting its departure as a radical. Two orbitals representing the starting and ending points of this transformation are shown in Figure 2.24a. Orbital 22 is a Mo-N σ orbital in step one, and it transforms into a Mo-N π interaction by step ten, thereby raising slightly in energy. Two orbitals which show this transformation are shown in Figure 2.24b. Orbital 24 is a Mo-N σ interaction to all three nitrogens in step one, but loses most of the σ interaction to the upright amide nitrogen by step ten, and raises only slightly in energy. Finally, orbital 26 starts in step one as a N-H σ orbital in the upright amide which changes into a Mo-N σ orbital in step ten while slightly increasing its energy. Two orbitals which show this transformation are depicted in Figure 2.24c.

Mechanistically, this analysis suggests that the *tert*-butyl radical elimination reaction depicted in Scheme 2.2 involves the smooth transfer of a metal based electron into a carbon centered orbital. As this orbital becomes filled, it supports the formation of a new Mo-N π bond at the expense of the Mo-N σ bond, and a new Mo-N σ bond at the expense of the N-C σ bond which is lost with the loss of an alkyl radical. This is in agreement with the observed thermochemical parameters presented in Table 2.24 which suggest bond-breaking in the transition state and a minimal entropy contribution. In the experimental system, the preferred (more stable) radical to be lost is the *tert*-butyl radical, which explains the selectivity in the thermolysis reaction for formation of an aryl imide rather than a *tert*-butyl imide.

References begin on page 184

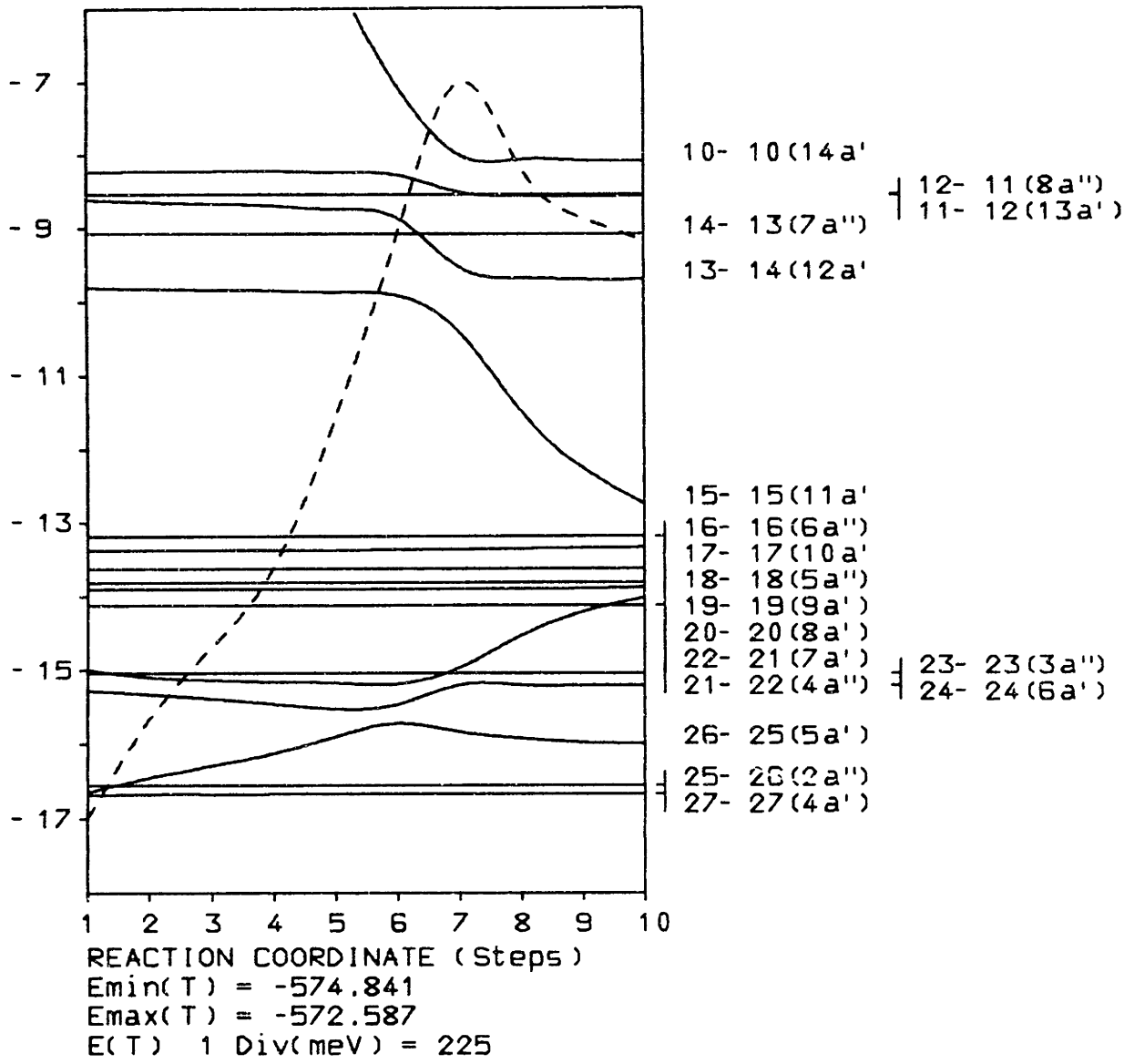

Figure 2.23: Walsh diagram for the model transformation of $EMo(NH_2)_3$ to $EMo(NH)(NH_2)_2$. See text for further details.

References begin on page 184

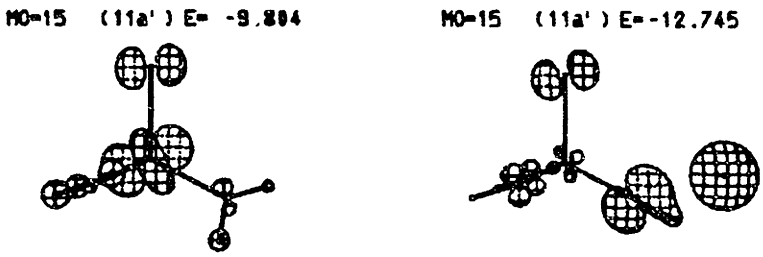

a) Transformation of Orbital 15

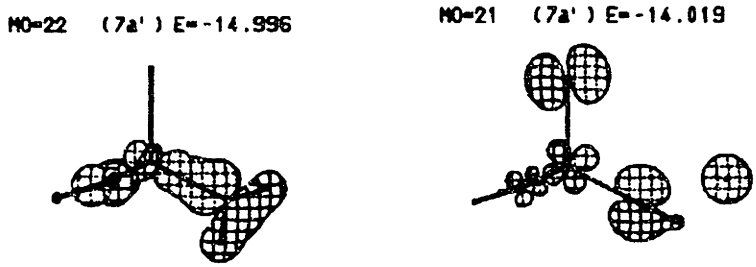

b) Transformation of Orbital 22

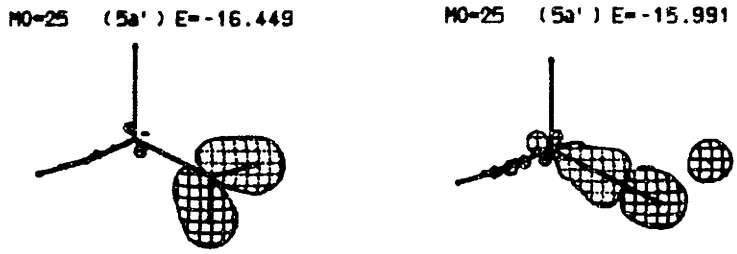

c) Transformation of Orbital 26

Figure 2.24: a) Orbital 15 of step one transforms from a Mo based π^* orbital to a hydrogen radical. b) Orbital 22 of step one transforms from a Mo-N σ bond to a Mo-N π bond. c) Orbital 26 of step one transforms from a N-H σ bond to a Mo-N σ bond. See text for further details.

References begin on page 184

Section 2.5: Oxidation of $OMo(N[R]Ar)_3$ (2.2)

(i) One Electron Oxidants

$OMo(N[R]Ar)_3$ is oxidized to a Mo(VI) cation with either ferrocenium triflate $[(C_5H_5)_2Fe(O_3SCF_3)]$[78] or iodine to generate the corresponding triflate $[OMo(N[R]Ar)_3][OTf]$ (**2.10**) or iodide complex $[OMo(N[R]Ar)_3][I]$ (**2.11**) (Scheme 2.4). Adding FcOTf to a solution of the oxo **2.2** causes the slow precipitation of an orange brown solid over 15 hours. This complex is isolated in 71% yield. The IR spectrum of this complex shows a strong peak at 972 cm^{-1} for the ν_{Mo-O} stretch, and peaks indicative of an ionic rather than a covalently bound triflate.[79] Adding one-half equivalent of iodine to **2.2** causes rapid precipitation of an orange solid which is isolated in 88% yield. This complex exhibits a strong stretch in the IR spectrum at 975 cm^{-1}, ascribable to ν_{Mo-O}. Both complexes decompose slightly during recrystallization (THF, CH_2Cl_2); the iodide is especially sensitive to decomposition in solution, precluding its analysis by ^{13}C NMR spectroscopy. As a result, combustion analytical data are poor.

The syntheses of cations of **2.3**, **2.4**, and **2.5** by similar methodology is not possible, as mentioned in Section 2.2.v, as the salts are unstable. The complex $[SMo(N[R]Ar)_3][OTf]$ is spectroscopically observable but it is not isolable. Addition of either ferrocenium triflate or iodine to the telluride complex **2.5** results in rapid decomposition. Presumably the cationic species forms and decomposes rapidly to unknown products.

References begin on page 184

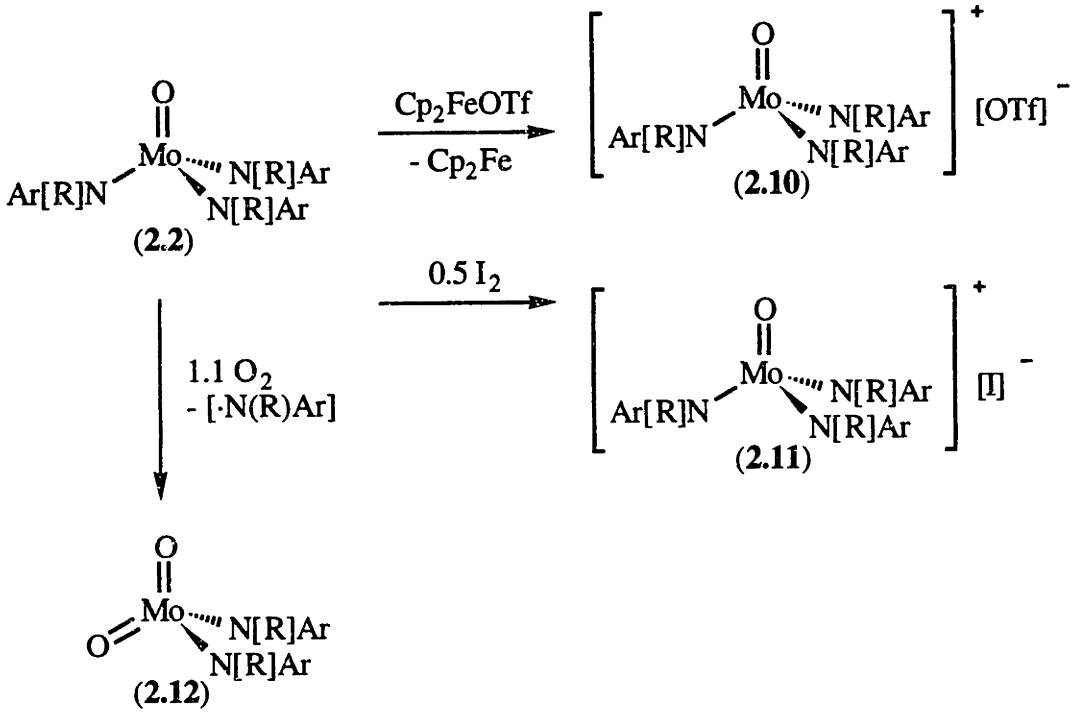

Scheme 2.4: Oxidations of $OMo(N[R]Ar)_3$ (**2.2**)

(ii) Dioxygen: Synthesis of $O_2Mo(N[R]Ar)_2$ (2.12)

Treating $OMo(N[R]Ar)_3$ with 1.1 equivalents of dioxygen causes a gradual color change from dark brown to a much darker brown (Scheme 2.4). After approximately 12 hours, the reaction mixture is deep red-brown. Analysis of the reaction mixture by ^1H NMR spectroscopy shows the formation of HN[R]Ar and $O_2Mo(N[R]Ar)_2$ (**2.12**) in an approximate two to one molar ratio. The dioxo complex **2.12** is crystallized away from the aniline in low yield as bright yellow crystals. The complex exhibits two strong $\nu_{Mo\text{-}O}$ peaks in the IR at 943 and 920 cm^{-1}, which correspond well to those reported in the literature for the related dioxo complex $O_2Mo(O\text{-}t\text{-}Bu)_2$.[80] The use of excess dioxygen is essential; if $OMo(N[R]Ar)_3$ is treated with one half equivalent of dioxygen over a similar time period, ^2H NMR spectroscopy shows approximately 50% starting oxo complex. Complex **2.12** also forms, non-reproducibly and in low yield, from the reaction of oxo **2.2** with Me_2SO, or from the reaction of **2.1** with dioxygen. This reactivity is starkly

References begin on page 184

different than that observed in the analogous chromium system. $Cr(N[R]Ar)_3$ reacts immediately with even a large excess of dioxygen to generate $O_2Cr(N[R]Ar)_2$ in essentially quantitative yield.[81] The reaction of **2.1** with dioxygen is complex, generating $OMo(N[R]Ar)_3$ and $O_2Mo(N[R]Ar)_2$ in some cases, but in general resulting in complete destruction of the $Mo(N[R]Ar)_3$ framework with formation of HN[R]Ar. The reaction of oxo imide **2.6** with benzaldehyde to generate the dioxo complex **2.12** is described in detail in section 2.4.

Section 2.6: Reactions of $Mo(N[R]Ar)_3$ With Chalcogen Donors

(i) Carbon Dioxide

From the list of bond enthalpies tabulated by Holm,[51] a prediction of the thermodynamic favorability of an oxo transfer reaction is possible. For example, since the bond strength of the oxo ligand in **2.2** is 155 kcal·mol^{-1}, and the oxo bond strength in Me_2SO is 87 kcal/mol, **2.2** should be able to deoxygenate Me_2SO with ΔH_r of 68 kcal·mol^{-1}. To this end, a variety of potential chalcogen atom donors are allowed to react with $Mo(N[R]Ar)_3$ in an attempt to map out thermodynamic favorability and its relation to kinetic barriers. Several reactions of **2.1** which are thermodynamically feasible have turned out to be kinetically non-viable (Scheme 2.5). There is no reaction of **2.1** with CO_2 (either 1 eq, 10 eq or 1 atm) in a sealed reaction bomb, even though this reaction should be exothermic by almost 30 kcal·mol^{-1}.

References begin on page 184

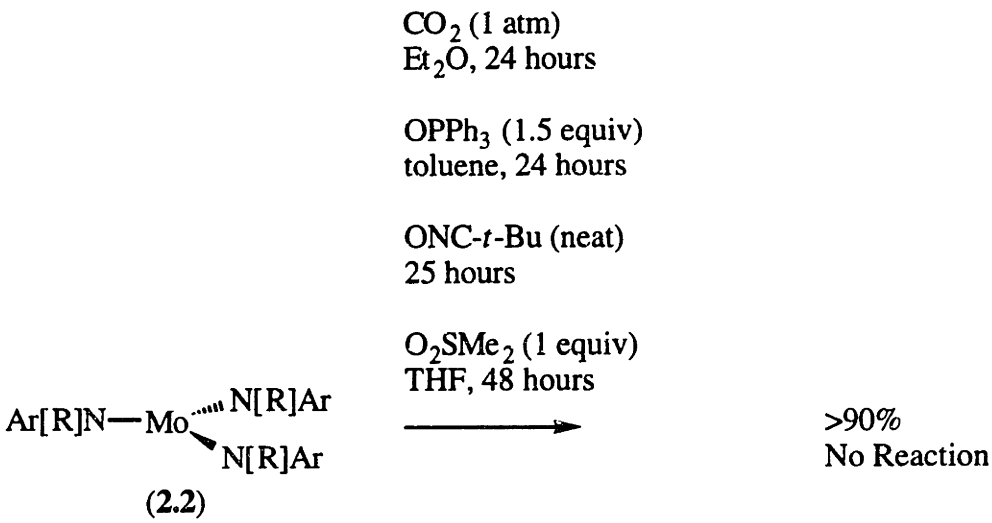

Scheme 2.5: Oxygen Donors Unreactive towards $Mo(N[R]Ar)_3$ (**2.2**)

(ii) Triphenylphosphine Oxide

The reaction of **2.1** with Ph_3PO is enthalpically downhill by 22 kcal·mol^{-1}, but again, no reaction is observed. In this case, it may be the steric bulk of the two reactants which prevents oxo transfer. As a control experiment, oxo **2.2** and Ph_3P are mixed and no reaction is observed.

(iii) *tert*-Butyl Isocyanate

The deoxygenation of MeNCO with **2.1** is calculated to be exothermic by 46 kcal·mol^{-1}. When **2.1** is treated with the related *t*-BuNCO, only a very small amount of oxo **2.2** and $Mo(NC\text{-}t\text{-}Bu)(N[R]Ar)_3$ are observed over a 24 hour time period. The latter isonitrile adduct is detected by ^2H NMR spectroscopy, and is presumably analogous to the known $(OC)Mo(N[R]Ar)_3$.[82]

(iv) Dimethylsulfone

The enthalpy for the reaction of **2.1** with Me_2SO_2 is calculated to be favorable by 43 kcal·mol^{-1}. This reaction is intriguing, in that the second deoxygenation of the oxidant

References begin on page 184

(deoxygenation of Me_2SO) is more favorable at 68 kcal·mol^{-1} as mentioned previously. Therefore, for each molecule of Me_2SO_2 which reacts, two equivalents of $OMo(N[R]Ar)_3$ are expected. However, over a 48 hour period, there is essentially no oxygen atom transfer from Me_2SO to **2.1**. The lack of reactivity for Me_2SO_2 is likely due to its insolubility in hydrocarbon solvents in which **2.1** is soluble.

(v) Dimethylsulfoxide

Some oxygen atom donors do react with complex **2.1**, and these are shown in Scheme 2.6. $Mo(N[R]Ar)_3$ is thermodynamically capable of deoxygenating Me_2SO as predicted at the beginning of this section. Simply treating **2.1** with Me_2SO forms a dark brown product in about 10 minutes. ^2H NMR spectroscopy shows greater than 90% conversion to oxo **2.2**.

(vi) Nitrogen Dioxide

Complex **2.1** is thermodynamically competent to reduce NO_2, with a reaction enthalpy of -82 kcal·mol^{-1}. When $Mo(N[R]Ar)_3$ is treated with 0.5 equiv. NO_2, the color changes to brown over a 10 minute period. Examination of the reaction mixture shows the clean production of the oxo complex **2.2**, as well as the known terminal nitrosyl complex $(ON)Mo(N[R]Ar)_3$[23] in a 1:1 molar ratio as determined by both ^2H and ^1H NMR spectroscopies.

References begin on page 184

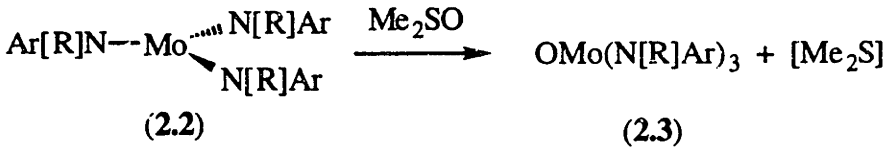

(2.2) (2.3)

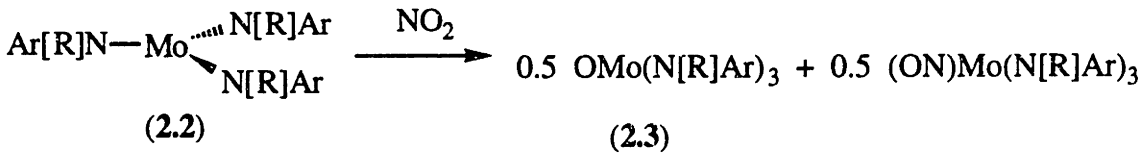

(2.2) (2.3)

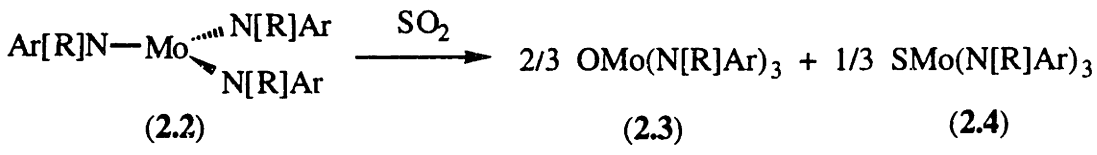

(2.2) (2.3) (2.4)

Scheme 2.6: Oxygen Donors Reactive towards $Mo(N[R]Ar)_3$ (**2.2**)

(vii) Sulfur Dioxide

Complex **2.1** is also thermodynamically competent to remove one oxygen from SO_2 with an enthalpy of reaction of -24 kcal·mol^{-1}. $Mo(N[R]Ar)_3$ reacts with 0.6 equivalent of gaseous SO_2 to give an immediate color change to dark brown. Analysis of the reaction mixture by ^2H NMR spectroscopy shows clean conversion to the oxo complex **2.2** and the sulfide complex **2.3** in a two to one molar ratio. This reaction is a rare example of clean activation of SO_2 to give sulfido and oxo ligands where the fate of all the reactants and product distribution is known.[83-85] Oxidation of the crude reaction mixture with iodine shows conversion to the oxo iodide **2.11** and the decomposition products observed when **2.3** is oxidized with iodine.

References begin on page 184

(viii) Carbon Disulfide: Synthesis of $(N[R]Ar)_3Mo(\mu\text{-}CS)Mo(N[R]Ar)_3$ (2.13)

Addition of one equivalent of CS_2 to $Mo(N[R]Ar)_3$ results in a rapid darkening of the solution to greenish brown (Scheme 2.7). Analysis of the reaction mixture by ^2H NMR spectroscopy at this point shows complete conversion of the starting material to two products, paramagnetic $SMo(N[R]Ar)_3$ (**2.3**) and diamagnetic $(N[R]Ar)_3Mo(\mu\text{-}CS)Mo(N[R]Ar)_3$ (**2.13**) in a 1:1 molar ratio. Separation of the two complexes is difficult; the best analytical data for **2.13** are given in the experimental section. Activation of CS_2 by transition metals is the subject of a fairly dated review,[86] but this article does not describe the formation of bridging thiocarbonyl complexes, though some are known.[87-89] The complex does not have a distinct band in its IR spectrum corresponding to $\nu_{C\text{-}S}$. The stretching frequency for this functional group is expected to be in the range 1150-1230 cm^{-1}.[89] Proton NMR spectroscopy shows two distinct ligand environments corresponding to the inequivalent halves of the molecule. The thiocarbonyl carbon is strongly deshielded, appearing at 293.51 ppm in the ^{13}C NMR spectrum.

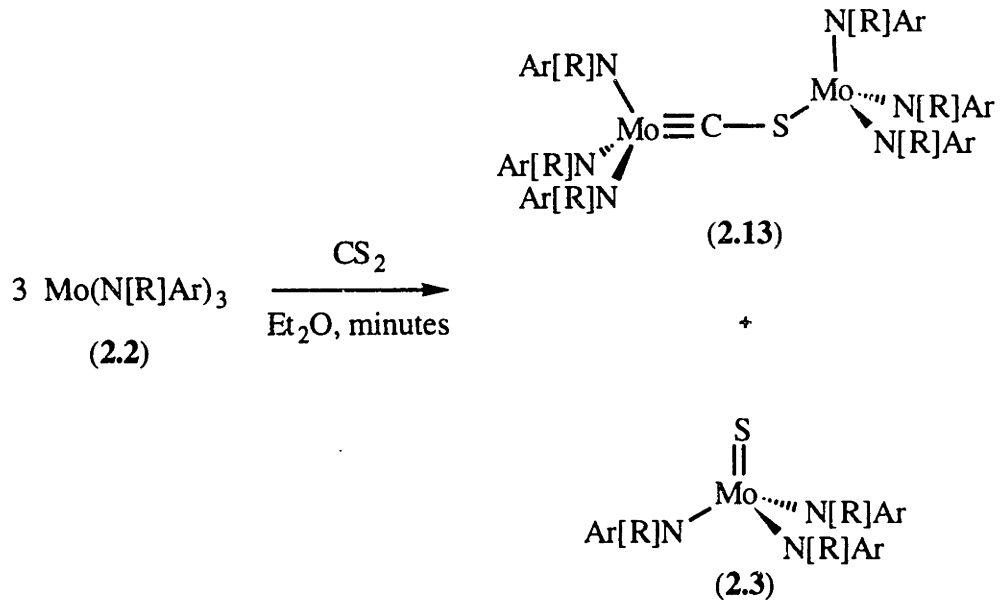

Scheme 2.7: Synthesis of $(Ar[R]N)_3Mo(\mu\text{-}CS)Mo(N[R]Ar)_3$ (**2.13**)

References begin on page 184

A single crystal X-ray structural determination of bridging thiocarbonyl complex **2.13** is of marginal quality due to a disordered *tert*-butyl group in the molecule (modeled with 1/2 occupancy at two positions), as well as two disordered diethyl ether molecules in the asymmetric unit, but it clearly shows the atomic connectivity. Selected bond lengths and angles are given in Tables 2.27 and 2.28, positional parameters and U(eq.) are listed in Table 2.29, and an ORTEP diagram is shown in Figure 2.25. The μ-CS linkage is clearly bent at sulfur, with a C-S-Mo(2) angle of 130.5(5)° indicative of lone pair character on sulfur. The sulfur is presumed to act as a 1σ-, 1π-donor of 3 e^- to molybdenum, forcing the Mo(IV) center to be low spin d^2 and diamagnetic. The Mo(1)-C-S angle of 162.7° is approximately linear, indicative of sp hybridization at carbon. The Mo-C bond distance of 1.751(12) Å and the Mo-S bond distance of 2.289(3) Å are similar to those reported for $(\eta^6\text{-}C_6H_5Me)(CO)_2Cr(\mu\text{-}CS)Cr(CO)_5$, where the Cr-C bond distance is 1.747(5) Å and the Cr-S distance is 2.486(2) Å.[89] This chromium complex is the only other structurally characterized end to end bridging thiocarbonyl complex found in a search of the Cambridge Structural Database.

The bond lengths in **2.13** are indicative of Mo-C triple bonding and Mo-S single bonding. The molecule is unique in that it exhibits the two most common arrangements for the N[R]Ar ligand in a single molecule. There is a pseudo-C_3 symmetric half, that containing Mo(1) and the carbon atom, and a pseudo-C_s symmetric half, that containing Mo(2) and the sulfur atom. The dihedral angles between the Mo-C and N-C vectors are 18.0, 23.0 and 32.5°, while the corresponding angles to the Mo-S vector are 1.0, 38.8 and 50.8°. This type of arrangement seems to be general. Molecules which have a molybdenum in a high formal oxidation state (i.e. no lone pairs or unpaired electrons) like $NMo(N[R]Ar)_3$,[24] $(ON)Mo(N[R]Ar)_3$[23] or $PMo(N[R]Ar)_3$[90] have pseudo-C_3 propeller arrangements of the anilide ligands. Meanwhile, molecules which have unpaired electrons, like the Mo(V) chalcogenido complexes, or lone pairs have pseudo-C_s symmetry.

References begin on page 184

Table 2.27: Selected Bond Distances (Å) for $(Ar[R]N)_3Mo(\mu\text{-}CS)Mo(N[R]Ar)_3$ (**2.14**).

Mo1-C	1.751(12)	N3-C37	1.49(2)
Mo1-N1	1.968(10)	N1-C11	1.43(2)
Mo1-N2	1.938(2)	N2-C21	1.43(2)
Mo1-N3	1.999(11)	N3-C31	1.46(2)
Mo2-S	2.289(3)	N4-C47	1.52(2)
Mo2-N4	1.990(10)	N5-C57	1.50(2)
Mo2-N5	1.959(11)	N6-C67	1.53(2)
Mo2-N6	1.960(10)	N4-C41	1.44(2)
N1-C17	1.52(2)	N5-C51	1.44(2)
N2-C27	1.49(2)	N6-C61	1.42(2)

Table 2.28: Selected Bond Angles (°) for $(Ar[R]N)_3Mo(\mu\text{-}CS)Mo(N[R]Ar)_3$ (**2.14**).

C-Mo1-N1	104.5(5)	N3-Mo1-N1	113.2(4)
C-Mo1-N2	104.3(5)	C47-N4-C41	113.1(10)
C-Mo1-N3	102.9(5)	C47-N4-Mo2	138.0(8)
S-Mo2-N4	102.3(3)	Mo2-N4-C41	108.9(8)
S-Mo2-N5	110.2(3)	C57-N5-C51	114.6(10)
S-Mo2-N6	106.8(3)	C57-N5-Mo2	128.9(8)
S-C-Mo1	162.7(8)	Mo2-N5-C51	116.6(8)
C-S-Mo2	130.5(5)	C67-N6-C61	113.4(9)
C17-N1-C11	114.2(10)	C67-N6-Mo2	126.3(7)
C17-N1-Mo1	134.1(8)	Mo2-N6-C61	120.2(8)
Mo1-N1-C11	111.3(8)	N4-Mo2-N5	107.3(4)
C27-N2-C21	114.0(10)	N5-Mo2-N6	116.7(4)
C27-N2-Mo1	134.1(8)	N6-Mo2-N4	112.7(4)
Mo1-N2-C21	111.8(8)	C-Mo1-N1-C17	18.0
C37-N3-C31	115.8(10)	C-Mo1-N2-C27	32.5
C37-N3-Mo1	133.9(8)	C-Mo1-N3-C37	23.0
Mo1-N3-C31	109.3(8)	S-Mo2-N4-C47	1.0
N1-Mo1-N2	117.0(4)	S-Mo2-N5-C57	38.8
N2-Mo1-N3	113.0(4)	S-Mo2-N6-C67	50.8

References begin on page 184

Table 2.29: Positional Parameters (x 10^4) and U(eq.) ($Å^2$ x 10^3) for the Non-Hydrogen Atoms of $(Ar[R]N)_3Mo(\mu\text{-}CS)Mo(N[R]Ar)_3$ (**2.14**).

Atom	x	y	z	U(eq.)
Mo1	2314(1)	9960(1)	2686(1)	21(1)
Mo2	5740(1)	7655(1)	3561(1)	20(1)
C	3345(9)	9271(9)	3074(6)	22(3)
S	4099(2)	8652(2)	3678(2)	25(1)
N1	2907(7)	10287(7)	1776(5)	26(3)
N2	1512(8)	9135(7)	2782(5)	30(3)
N3	1644(7)	11078(7)	3234(6)	30(3)
N4	5876(7)	7096(7)	4490(5)	21(3)
N5	5955(7)	6617(7)	3025(5)	25(3)
N6	6549(7)	8449(7)	3230(5)	19(3)
C11	2252(10)	11156(10)	1493(6)	25(3)
C12	2351(10)	12019(10)	1532(6)	30(4)
C13	1740(11)	12889(10)	1250(7)	34(4)
C14	991(10)	12847(11)	937(7)	40(4)
C15	878(10)	12014(11)	877(7)	29(4)
C16	1511(10)	11175(10)	1162(7)	35(4)
C17	3932(10)	9885(10)	1350(7)	33(4)
C18	4566(11)	10454(11)	1398(9)	53(5)
C19	3802(11)	9930(14)	631(7)	66(6)
C21	1040(9)	9269(9)	2217(6)	20(3)
C22	1558(10)	8794(10)	1656(7)	30(4)
C23	1136(11)	8898(10)	1095(7)	34(4)
C24	152(11)	9502(10)	1102(7)	35(4)
C25	-402(10)	9991(9)	1662(7)	30(4)
C26	51(10)	9887(10)	2205(6)	28(4)
C27	1332(10)	8393(10)	3299(7)	32(4)
C28	1680(12)	8447(11)	3936(8)	48(4)
C29	1900(12)	7413(10)	3036(8)	54(5)
C31	564(9)	11388(9)	3275(7)	25(3)
C32	101(10)	11998(10)	2762(7)	33(4)
C33	-941(10)	12292(10)	2780(7)	33(4)
C34	-1483(10)	11946(11)	3322(7)	36(4)
C35	-1038(11)	11358(11)	3841(7)	38(4)
C36	-25(10)	11086(10)	3816(7)	32(4)
C37	1992(9)	11528(9)	3678(7)	28(4)
C38	1330(10)	12577(10)	3716(8)	47(4)
C39	3063(10)	11448(10)	3393(8)	41(4)
C41	6864(10)	6382(9)	4490(6)	27(3)
C42	7692(9)	6634(9)	4395(6)	26(3)
C43	8677(11)	5989(11)	4380(7)	38(4)
C44	8790(10)	5046(12)	4452(7)	45(4)
C45	8016(13)	4733(11)	4541(8)	52(5)
C46	7033(11)	5406(10)	4549(6)	33(4)
C47	5227(11)	7180(10)	5174(7)	37(4)
C48	4224(20)	7961(23)	5175(14)	39(9)
C49	5150(21)	6269(20)	5507(14)	49(10)
C51	6889(9)	6304(9)	2573(6)	22(3)
C52	6965(11)	6556(9)	1909(7)	33(4)

References begin on page 184

Table 2.29 Continued.

Atom	x	y	z	U(eq.)
C53	7848(12)	6201(11)	1462(7)	36(4)
C54	8687(11)	5530(10)	1710(7)	38(4)
C55	8661(10)	5278(9)	2399(7)	32(4)
C56	7737(10)	5670(9)	2825(7)	26(4)
C57	5284(10)	6080(10)	3029(7)	33(4)
C58	4692(11)	6492(11)	2444(8)	49(4)
C59	4540(10)	6148(10)	3672(7)	36(4)
C61	7265(10)	8249(9)	2636(6)	21(3)
C62	8255(9)	7644(9)	2646(7)	25(3)
C63	8988(9)	7524(9)	2084(6)	26(3)
C64	8696(10)	8013(10)	1487(7)	35(4)
C65	7715(10)	8596(9)	1440(7)	31(4)
C66	7009(10)	8698(10)	2022(7)	31(4)
C67	6455(9)	9345(8)	3526(6)	21(3)
C68	5894(11)	10219(10)	3108(7)	39(4)
C69	5899(10)	9377(10)	4234(7)	38(4)
C110	4474(10)	8849(10)	1515(7)	43(4)
C131	1889(12)	13787(11)	1274(8)	53(5)
C151	75(10)	12003(11)	529(7)	46(4)
C210	217(11)	8542(11)	3481(8)	46(4)
C231	1724(13)	8377(13)	473(8)	66(5)
C251	-1502(11)	10606(12)	1669(8)	56(5)
C310	1961(12)	11026(11)	4385(7)	42(4)
C331	-1423(11)	12959(11)	2228(7)	46(4)
C351	-1653(11)	11026(12)	4431(7)	49(4)
C410	5831(20)	7488(19)	5654(13)	39(9)
C431	9557(10)	6288(14)	4261(9)	73(6)
C451	8175(14)	3664(12)	4595(9)	76(6)
C510	5911(11)	5019(10)	2947(8)	46(4)
C531	7943(13)	6481(13)	729(7)	58(5)
C551	9557(10)	4590(10)	2680(8)	46(4)
C610	7506(10)	9342(10	3540(8)	39(4)
C631	10069(9)	6866(10)	2089(7)	39(4)
C651	7428(11)	9099(12)	788(7)	51(5)

References begin on page 184

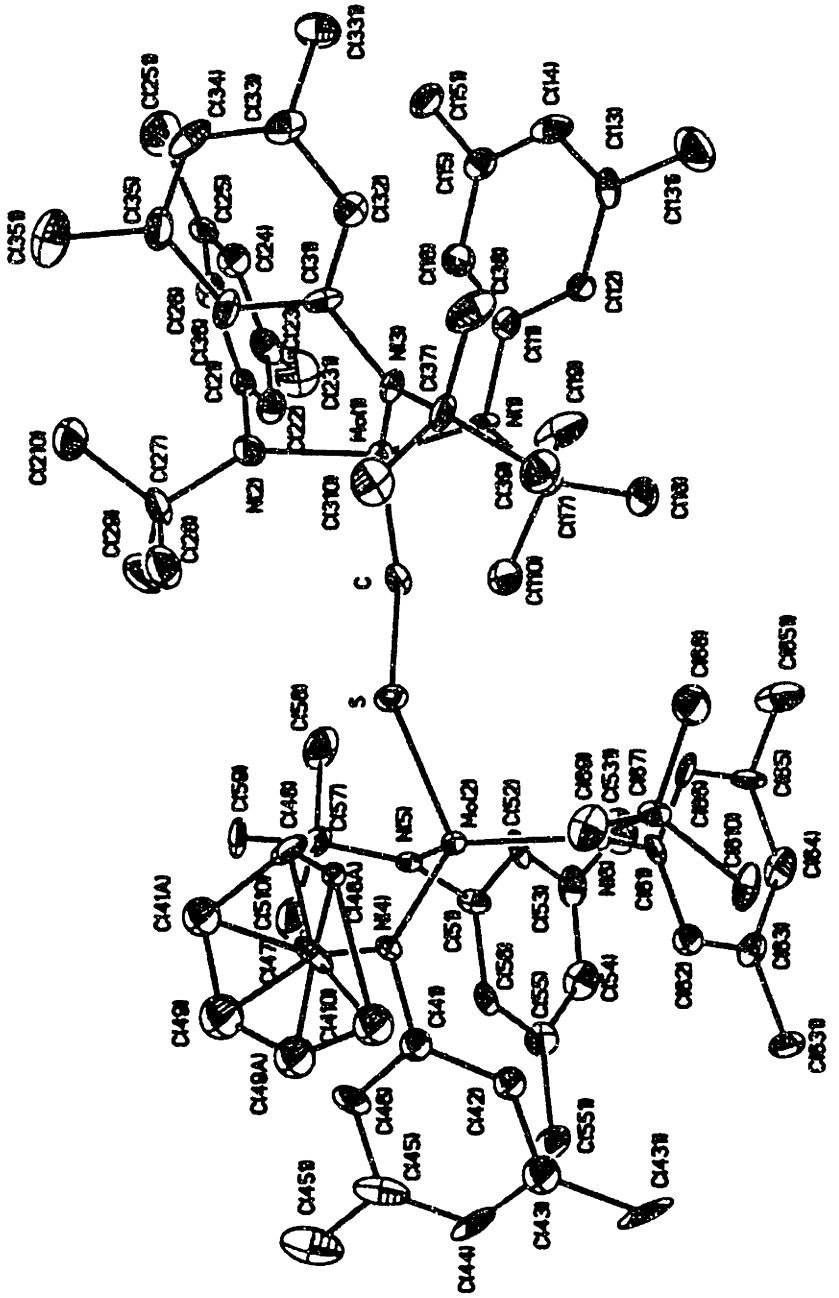

Figure 2.25: Partial ORTEP diagram of $(Ar[R]N)_3Mo(\mu\text{-}CS)Mo(N[R]Ar)_3$ (**2.14**) with ellipsoids at the 30% probability level (two disordered solvent molecules have been removed for clarity).

References begin on page 184

Extended Hückel calculations performed on the model complex $(H_2N)_3Mo(\mu\text{-}CS)Mo(NH_2)_3$ with coordinates derived from the X-ray structure, give the electronic structure of the μ-CS linkage. The Cartesian coordinates used for the calculations are listed in Table 2.30. CACAO[52,53] drawings of some pertinent orbitals are shown in Figure 2.26. The second and third HOMOs, of which only one is shown (MO 32), are Mo-C π bonding and C-S π*, with a weaker Mo-S π interaction. This result is consistent with the experimentally observed short Mo-C bond and long C-S bond. The HOMO (MO 31) is best described as an lone pair on sulfur, as expected from the bent structure. The LUMO (MO 30) is largely Mo-S π*, while the second and third LUMOs (of which only one is shown, MO 29) are mostly Mo-C π* in character.

Table 2.30: Cartesian Coordinates for $(H_2N)_3Mo(\mu\text{-}CS)Mo(NH_2)_3$ with coordinates derived from X-ray data.

Atom	x	y	z
Mo1	-3.108	-0.391	-0.050
N1	-3.600	-1.200	-1.098
N2	-3.600	-0.391	1.877
N3	-3.556	2.108	-0.972
H1	-4.500	-1.093	-1.524
H2	-3.112	-2.030	-1.360
H3	-4.431	-0.143	2.050
H4	-3.185	0.778	2.703
H5	-4.384	2.497	-0.565
H6	-3.065	2.702	-1.612
Mo2	2.251	-0.331	-0.043
N4	3.614	0.948	0.639
N5	2.200	-1.845	1.200
N6	2.495	-0.757	-1.941
H7	4.500	-.483	-.684
H8	3.647	1.889	0.981
H9	2.609	-2.702	0.878
H10	1.836	-1.881	2.132
H11	2.608	-1.708	-2.233
H12	2.465	-0.107	-2.703
C	-1.357	0.391	-0.050
S	0.320	0.886	0.117

References begin on page 184

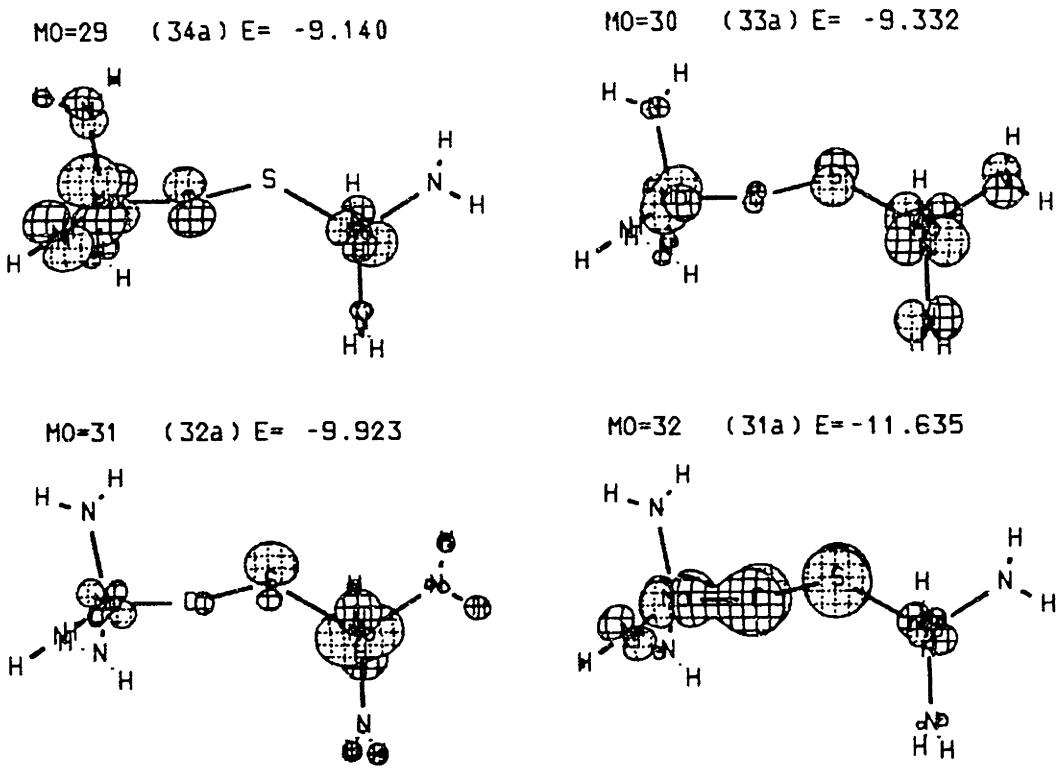

Figure 2.26: Frontier molecular orbitals calculated for $(Ar[R]N)_3Mo(\mu\text{-}CS)Mo(N[R]Ar)_3$ (**2.14**). Orbitals 29 and 30 are unoccupied, while orbitals 31 and 32 are filled.

References begin on page 184

(ix) Diphenyl Diselenide: Synthesis of (PhSe)Mo(N[R]Ar)$_3$ (2.14)

Addition of one half equivalent Ph_2Se_2 to Mo(N[R]Ar)$_3$ results in the formation of a brilliant blue-green diamagnetic complex, (PhSe)Mo(N[R]Ar)$_3$ (**2.14**), which is isolated in 72% yield, Scheme 2.8. The complex exhibits an extremely broad ^{77}Se NMR chemical shift of 1006.3 ppm ($\Delta\nu_{1/2}$ = 600 Hz). This chemical shift falls in the predicted region for alkyl selenides,[71-74] though it is towards the low-field end of the range. The diamagnetism of the molecule suggests that the Mo-Se-C vector is bent, as seen in the Mo-S-C angle in **2.13**, but no structural data is available for the selenolate complex.

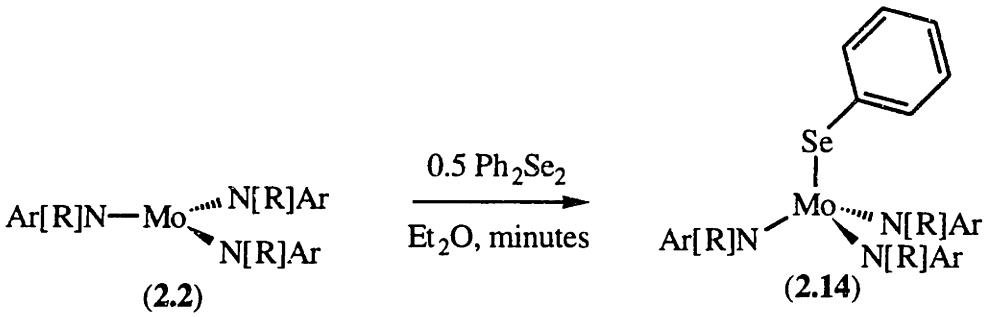

Scheme 2.8: Synthesis of (PhSe)Mo(N[R]Ar)$_3$ (**2.14**)

Section 2.7: Conclusion

This chapter addresses the question of the stability of Mo(V) chalcogenido complexes with N[R]Ar ligation initially raised by the reaction of Mo(N[R]Ar)$_3$ with N_2O. Theoretical and experimental observations suggest that the Mo-E bond is very strong. Theoretical calculations explain the Jahn-Teller distortion of the chalcogenide complexes from C_3 symmetry to pseudo-C_s symmetry in the observed structures. The complexes are, in fact, quite stable, but do undergo a C-N bond homolysis at elevated temperatures, resulting in *tert*-butyl radical elimination and the formation of Mo(VI) chalcogenide imide complexes. A mechanistic analysis of this thermolysis reaction suggests smooth transfer of the unpaired electron into an N-H σ^* orbital, causing a rearrangement of the complex and

References begin on page 184

the formation of a new Mo-N π bond. The reaction, or lack thereof, of a variety of chalcogenido donors with $Mo(N[R]Ar)_3$ lays the groundwork for chalcogen atom transfer reactions with this system. The potential for $Mo(N[R]Ar)_3$ to act as a chalcogen atom acceptor is generally high for the donors which have been tested.

Section 2.8: Experimental

2.8.1 General Considerations

General experimental details are as described in Chapter I. Ether was dried according to a procedure by Grubbs.[91] Other solvents were distilled, under nitrogen, from sodium benzophenone ketyl. Toluene which was used for EPR spectroscopy was vacuum transferred from *tert*-butyllithium. $Mo(N[R]Ar)_3$[23] was prepared by standard procedures. Other chemicals were purified and dried by standard procedures[92] or used as received. Magnetic susceptibilities were measured by NMR spectroscopy.[36] ^1H and ^{13}C NMR spectra were recorded on Varian XL-300, Varian Unity-300 or Brucker AC-250 spectrometers. Chemical shifts are reported with respect to internal solvent (7.15 ppm and 128.0 ppm). ^2H chemical shifts are reported with respect to external C_6D_6. ^{77}Se NMR spectra were recorded on a Varian Unity-300 or a Varian VXR-500 spectrometer and are referenced to Me_2Se (0 ppm) by comparing to external PhSeSePh ($CDCl_3$, 460 ppm)[5,93,94]. ^{125}Te NMR spectra were recorded on a Varian VXR-500 spectrometer and referenced to Me_2Te (0 ppm) by comparing to external $TeCl_4$ (HCl/H_2O, 1237 ppm).[94] EPR spectra were recorded on a Brucker ESP-300 spectrometer in sealed quartz tubes in toluene at either ambient temperature or low temperature by using a liquid nitrogen cooled nitrogen stream. Spectra were simulated using the program EPR-NMR.[39] Infrared measurements were carried out on a Bio-Rad FTS 135 spectrometer. Far-IR measurements were carried out on a Mattson Instruments IR-10110 spectrometer. UV-vis spectra were recorded on a Hewlett-Packard 8453 diode array spectrophotometer. Electrochemical

References begin on page 184

measurements were carried out at room temperature in a glove box with ~1 x 10^{-3} M methylene chloride solutions containing saturated *n*-Bu_4NPF_6 as the supporting electrolyte. The standard three electrode system consisted of platinum working and counter electrodes with a silver reference electrode. Platinum electrodes were pretreated by polishing with diamond paste. Potentials are referred to the ferrocene/ferrocenium couple.[45,95] CHN analyses were performed by Oneida Research Services (Whitesboro, NY) or Microlytics (South Deerfield, MA). Melting points were obtained in sealed glass capillaries and are uncorrected.

2.8.2 SQUID Magnetic Measurements

Data were acquired as reported in Chapter I using a Quantum Design SQUID magnetometer.[37] The calculated curves are the best least-squares fits of the observed susceptibility data to either the Curie Law, with the equation $\chi_M(obs) = ((\mu^2)/(7.997584\times(T))-C$, or the Curie Weiss law, with the equation $\chi_M(obs) = ((\mu^2)/(7.997584\times(T-\theta)))-C$.

2.8.3 Kinetics Measurements

A sample of $OMo(N[R]Ar)_3$ or $SMo(N[R]Ar)_3$ (ca. 0.02 M in C_6H_6) was placed in an NMR tube along with a sealed capillary filled with a D_2O/THF solution (1:20 by weight). The tube was flame sealed and stored at 4 °C. Constant temperature oil baths were employed for the thermolysis reaction. NMR tubes were placed in the oil bath for a measured time interval, and then immediately placed in an ice water slurry. The decay of starting material was measured by comparing integrals of peaks in the ^2H NMR spectrum. The oxo peak was integrated from 9.2 ppm to 5.2 ppm, the sulfido peak was integrated from 7.8 to 4.8 ppm, and the D_2O peak was integrated from 3.6 to 4.6 ppm (relative to external C_6D_6). The tubes were then replaced in the oil bath and this process was repeated for 3 to 4 half lives. Plots of [oxo (or sulfido) area]/[D_2O area] versus time were obtained

References begin on page 184

and fit to the equation $Y = M_1 + M_2\exp(-M_3 \cdot X)$. Alternatively, linear fits could be obtained from plots of ln(relative area) versus time. The measured first order rate constants (M_3) are reported with their respective 95% confidence intervals. Activation parameters were obtained from the relation of the derived first order rate constants with temperature using the following equations: $\ln (k_r \cdot T^{-1}) = -\Delta H^{\ddagger} \cdot R^{-1} \cdot T^{-1} + C$; and $\Delta S^{\ddagger} = \Delta H^{\ddagger} \cdot T^{-1} + R \cdot \ln(h \cdot k_r \cdot k^{-1} \cdot T^{-1})$ where h is Planck's constant, k is Boltzmann's constant and T is absolute temperature.[96]

2.8.4 Synthesis of Complexes

(i) OMo(N[R]Ar)$_3$ (2.2): Mo(N[R]Ar)$_3$ (**2.1**, 0.5844 g, 0.9090 mmol) was dissolved in ether (15 mL) and pyridine-*N*-oxide (0.1014 g, 0.9467 mmol) was added. The slurry was stirred for 3.5 hours, at which time all the oxidant had dissolved and the solution had turned dark brown. The solvent was removed, the product was extracted with fresh ether and the solution was filtered. Crystallization from ether yielded dark brown faceted crystals (0.4311 g, 0.6543 mmol, 72%). M.p. 134-135 °C (dec.). ^{2}H NMR (46 MHz, toluene): δ = 7.62; $\Delta\nu_{1/2}$ = 30 Hz. ^{1}H NMR (300 MHz, C_6D_6): δ = ~7.2 (br s, 9H, $C(CD_3)_2CH_3$), 0.0895 (br s, 18H, Ar*Me*). IR (benzene/KBr, 2 cm^{-1}): $\nu_{Mo\text{-}O}$ = 891 cm^{-1}. UV/Vis (ether): $\lambda_{max}(\varepsilon)$ = 212(53000). EPR (toluene, 25 °C): g = 1.96, $A(^{95/97}Mo)$ = 35.7 G; (toluene, 101 K): g_1 = 1.990, g_2 = 1.967, g_3 = 1.937. MS (70 eV): *m/z*(%): 654.5(3.8)[*M*+]. μ_{eff} (300 MHz, C_6D_6, 22.6 °C): 2.19 μ_B. SQUID (5-300K): μ = 1.664 μ_B. CV (CH_2Cl_2/Bu_4NPF_6): $E_{1/2}$ = -0.92 V. Anal. Calcd. for $C_{36}H_{39}D_{15}MoN_3O$: C, 65.93; H, 8.30; N, 6.41. Found: C, 66.22; H, 8.50; N, 6.19.

(ii) SMo(N[R]Ar)$_3$ (2.3): Mo(N[R]Ar)$_3$ (**2.1**, 0.4303 g, 0.6693 mmol) in ether (6 mL) was added to a slurry of S_8 (0.0322 g, 0.1255 mmol, 1.5 eq) in ether (5 mL) causing a rapid color change to purple and then brown after about five minutes. The reaction was

References begin on page 184

stirred overnight and the ether was removed *in vacuo*. The product was extracted with pentane, the solution was filtered, and crystals were obtained from ether (3 mL) at -35 °C (0.2865 g, 0.4245 mmol, 63%). M.p. 110-112 °C (dec.). ^{2}H NMR (46 MHz, ether): δ = 6.545; $\Delta\nu_{1/2}$ = 22.0 Hz. ^{1}H NMR (300 MHz, C_6D_6): δ = ~6.0 (br s, 9H, $C(CD_3)_2CH_3$), ~-1.1 (br s, 18H, Ar*Me*). IR (benzene/KBr, 2 cm^{-1}): $\nu_{Mo\text{-}S}$ = 491 cm^{-1}. EPR (toluene, 25 °C): g = 1.96 $A(^{95,97}Mo)$ = 28.5 G; (toluene, 107 K): g_1 = 1.996, $A_1(^{95/97}Mo)$ = 25 G, g_2 = 1.970, g_3 = 1.922, $A_3(^{95/97}Mo)$ = 54 G. MS (70 eV): *m/z*(%): 671 (0.22)[*M*$^+$]. μ_{eff} (300 MHz, C_6D_6, 22.3 °C): 2.21 μ_B. SQUID (5-300K): μ = 1.630 μ_B. CV (CH_2Cl_2/Bu_4NPF_6): $E_{1/2}$ = -0.73 V. Anal. Calcd. for $C_{36}H_{42}D_{12}MoN_3S$: C, 64.64; H, 8.14; N, 6.28. Found: C, 64.94; H, 8.31; N, 6.23.

(iii) SeMo(N[R]Ar)$_3$ (2.4): Mo(N[R]Ar)$_3$ (**2.1**, 0.5008 g, 0.7790 mmol) and Se (0.0810 g, 0.790 mmol) were combined in ether (10 mL) and the resulting mixture was stirred for 11 hours. The solution was filtered to remove excess Se and the filtrate was concentrated. Three crops of crystals were collected from ether at -35 °C (0.4519 g, 0.6260 mmol, 80.4%). M.p. 128-130 °C. ^{2}H NMR (46 MHz, Et_2O): δ = 7.036; $\Delta\nu_{1/2}$ = 30.7 Hz. ^{1}H NMR (300 MHz, C_6D_6): δ = ~6.5 (br s, 9H, $C(CD_3)_2CH_3$), -1.412 (br s, 18H, Ar*Me*). IR (benzene/polyethylene, 2 cm^{-1}): $\nu_{Mo\text{-}Se}$ = 342 cm^{-1}. EPR (toluene, 25 °C): g = 1.97, $A(^{95/97}Mo)$ = 30.5 G; (toluene, 98 K): g_1 = 2.030, $A_1(^{95/97}Mo)$ = 29 G, g_2 = 1.986, g_3 = 1.899, $A_3(^{95/97}Mo)$ = 48 G. UV/Vis (Ether): $\lambda(\varepsilon)$ = 403(6270); 487(2410). MS (70 eV): *m/z*(%): 658.2(18.11)[*M*$^+$ - d_6-*tert*-Bu]. SQUID (5-300 K): μ = 1.75 μ_B; θ = −1.45 K. CV (CH_2Cl_2/Bu_4NPF_6): $E_{1/2}$ = -0.64 V. Anal. Calcd. for $C_{36}H_{36}D_{18}MoN_3Se$: C, 59.90; H, 7.54; N, 5.82. Found: C, 60.25; H, 7.41; N, 5.68.

(iv) TeMo(N[R]Ar)$_3$ (2.5): Mo(N[R]Ar)$_3$ (**2.1**, 0.5035 g, 0.7832 mmol) and Te (0.1188 g, 0.9310 mmol) were mixed in ether (10 mL). PEt_3 (20 µl, 0.14 mmol, 0.17 eq) was then added and the solution was stirred for 18 hours. The solution gradually turned a

References begin on page 184

dark brown color. The ether was removed *in vacuo*, the product was extracted with THF, and the extract was filtered. The product was recrystallized from ether (ca. 25 mL) at -35 °C (2 crops, 0.4422 g, 0.5739 mmol, 73%). M.p. 127-128 °C (dec.). ^{2}H NMR (46 MHz, ether): δ = 8.120; $\Delta\nu_{1/2}$ = 22.9 Hz. ^{1}H NMR (300 MHz, C_6D_6): δ = ~8 (br S, 9H, $NC(CD_3)_2CH_3$), -1.9 (br s, 18H, Ar*Me*). IR (benzene/polyethylene, 2 cm^{-1}): $\nu_{Mo\text{-}Te}$ = 286 cm^{-1}. EPR (toluene, 25 °C): g = 1.977; (toluene, 105 K): g_1 = 2.130, $A_1(^{95/97}Mo)$ =28 G, g_2 = 1.970, $A_2(^{95/97}Mo)$ = 24 G, g_3 = 1.850, $A_3(^{95/97}Mo)$ = 48 G. UV-Vis (ether): $\lambda_{max}(\varepsilon)$ = 486(6314). MS (70 eV): *m/z*(%): 707.3(38.24)[*M*+ -d_6-*tert*-Bu]. SQUID (5-180 K): μ = 1.86 μ_B; θ = -5.1 K. CV (CH_2Cl_2/Bu_4NPF_6): $E_{1/2}$ = -0.63 V. Anal. Calcd. for $C_{36}H_{42}D_{12}MoN_3Te$: C, 56.12; H, 7.06; N, 5.45. Found: C, 56.50; H, 7.33; N, 5.17.

(v) OMo(NAr)(N[R]Ar)$_2$ (2.6): OMo(N[R]Ar)$_3$ (**2.2**, O.4422 g, 0.6879 mmol) was heated at 65 °C in benzene (10 mL) until the dark brown color faded to a much lighter yellow (ca. 5 days). Solvent was removed *in vacuo* yielding a yellow oil in quantitative yield. Proton NMR spectroscopy showed it to be approximately 85-90% pure, contaminated with HN[R]Ar. ^{1}H NMR (300 MHz, C_6D_6): δ = 6.912 (s, 4H, orthos); 6.885 (s, 2H, paras); 6.712 (s, 2H, imide orthos); 6.52 (s, 1H, imide para); 2.139 (s, 12H, Ar*Me*); 2.026 (s, 6H, imide Ar*Me*); 1.340 (s, 6H, $C(CD_3)_2CH_3$). ^{13}C NMR (75 MHz, $CDCl_3$): δ = 156.365 (s, NAr ipso); 150.510 (s, N[R]Ar ipso); 137.712 (s, NAr meta); 137.560 (s, N[R]Ar meta); 128.304 (d, J_{CH} = 158.2, N[R]Ar ortho); 127.373 (d, J_{CH} = 155.0, NAr ortho); 120.702 (d, J_{CH} ~160, NAr para); 120.008 (d, J_{CH} = 160.7, N[R]Ar para); 60.555 (s, $NC(CH_3)_2CD_3$); 31.496 (q, J_{CH} = 125.9, $C(CD_3)_2CH_3$); 30.990 (m, $NC(CD_3)_2CH_3$); 21.237 (q, J_{CH} = 126.1, N[R]Ar Ar*Me*); 21.143 (q, J_{CH} ~ 126, NAr Ar*Me*). IR (benzene/KBr, 2 cm^{-1}): $\nu_{Mo\text{-}O}$ = 913 cm^{-1}. MS (70 eV): *m/z*(%): 594.3(1.77)[*M*+]. HRMS (70 ev): calcd. mass (597.3370); found mass (597.3371).

References begin on page 184

(vi) PhCHNAr for spectroscopic characterization: Benzaldehyde (8.12 g, 76.5 mmol) and 3,5-dimethylaniline (10.23 g, 84.43 mmol) were mixed in benzene (30 mL) and heated to reflux for 6 hours. Water was collected with a Dean-Stark trap (1.2 mL, .87 eq) yielding a thick yellow oil (16.22 g) which was 95% pure by ^{1}H NMR spectroscopy. ^{1}H NMR (300 MHz, C_6D_6): δ = 8.284 (s, 1H, N=C*H*C_6H_5); 7.923 (m, 2H, phenyl); 7.196 (m, 3H, phenyl); 6.946 (s, 2H, aryl ortho); 6.786 (s, 1H, aryl para); 2.223 (s, 6H, Ar*Me*). ^{13}C NMR (75 MHz, $CDCl_3$): δ = 159.934 (d, J_{CH} = 158.2, aryl para); 152.176 (d, $^2J_{CH}$ = 9.7, ipso); 138.795 (q, $^2J_{CH}$ = 5.8, aryl meta); 136.446 (s, ipso); 131.288 (dt, $^1J_{CH}$ = 160.6, $^2J_{CH}$ = 7.7, phenyl para); 128.800 (d, J_{CH} = 163.8, phenyl meta); 127.729 (d, J_{CH} = 155.2, ortho); 118.753 (d, J_{CH} = 157.5, ortho); 113.204 (d, J_{CH} ~ 170, N=*C*HC_6H_5); 21.3884 (q, J_{CH} = 126.5, Ar*Me*). MS (70 eV): *m/z*(%): 209.2(100)[*M*+]. HRMS (70 ev): calcd. mass (209.1205); found mass (209.1204).

(vii) SMo(NAr)(N[R]Ar)$_2$ (2.7): SMo(N[R]Ar)$_3$ (**2.3**, 0.1640 g, 0.2430 mmol) was dissolved in benzene (10 mL) and heated at 62.5 °C in a sealed bomb for 25 hours. The solution changed from dark brown to reddish brown. The benzene was removed *in vacuo* and an orange powder was obtained by recrystallization from Et_2O (0.1250 g, 0.2043 mmol, 84.1%). M.p. 183-4 °C. ^{1}H NMR (300 MHz, C_6D_6): δ = 7.204 (s, 2H, N[R]Ar para); 7.15 (s, 4H, N[R]Ar orthos); 6.710 (s, 2H, NAr orthos); 6.587 (s, 1H, NAr para); 2.145 (s, 12H, N[R]Ar Ar*Me*); 2.041 (s, 6H, NAr Ar*Me*); 1.310 (s, 6H, C(CD_3)$_2$C*H*$_3$). ^{13}C NMR (75 MHz, $CDCl_3$): δ = 157.545 (s, NAr ipso); 151.53 (s, N[R]Ar ipso); 138.27 (s, NAr meta); 137.87 (s, N[R]Ar meta); 129.77 (d, J_{CH} = 150.6 Hz, ortho); 128.60 (br d, J_{CH} = 156.6 Hz, ortho); 127.711 (d, J_{CH} = 155.6 Hz, para); 119.87 (d, J_{CH} = 162.3 Hz, para); 62.385 (s, *C*(CD_3)$_2$CH_3); 31.957 (q, J_{CH} = 126.5 Hz, C(CD_3)$_2$*C*H$_3$); 31.447 (m, C(*C*D$_3$)$_2$CH$_3$); 21.481 (q, J_{CH} = 126.7 Hz, NAr and N[R]Ar Ar*Me*). IR (benzene/KBr, 2 cm^{-1}): $\nu_{Mo\text{-}S}$ = 506 cm^{-1}. MS (70 eV): *m/z*(%):

References begin on page 184

613(44.1)[*M*+]. Anal. Calcd. for $C_{32}H_{33}D_{12}MoN_3S$: C, 62.82; H, 7.41; N, 6.87. Found: C, 63.11; H, 7.56; N, 6.76.

(viii) SeMo(NAr)(N[R]Ar)$_2$ (2.8): SeMo(N[R]Ar)$_3$ (**2.4**, 0.6377 g, 0.8834 mmol) and benzene (30 mL) were loaded into a sealable glass reaction bomb which was then evacuated to autogenic pressure. The mixture was heated at 65 °C for 22 hours at which point the solution had changed from the dark brown initial color to a red-orange color. The benzene was removed *in vacuo*, and the product was precipitated from ether (~15 mL) at -35 °C as a finely divided orange brown powder in two crops (0.3733 g, 0.5667 mmol, 64%). M.p. 201.5-202 °C. ^{1}H NMR (300 MHz, C_6D_6): δ = 7.304 (2H, aryl); 7.15 (4H, N[R]Ar orthos); 6.713 (2H, aryl); 6.601 (1H, NAr para); 2.145 (12H, N[R]Ar Ar*Me*); 2.052 (6H, NAr Ar*Me*); 1.290 (6H, $C(CD_3)_2CH_3$). ^{13}C NMR (75 MHz, $CDCl_3$): δ = 157.243 (s, NAr ipso); 150.940 (s, N[R]Ar ipso); 138.027 (q, $^2J_{CH}$ = 6.14 Hz, NAr meta); 137.613 (q, $^2J_{CH}$ = 4.03 Hz, N[R]Ar meta); 129.454 (d, J_{CH} = 153.1 Hz, aryl); 128.612 (br m, N[R]Ar ortho); 127.438 (d, J_{CH} = 155.1 Hz, aryl); 119.225 (d, J_{CH} = 163.2 Hz, aryl); 62.20 (s, $C(CD_3)_2CH_3$); 31.517 (q, J_{CH} = 126.6 Hz, $C(CD_3)_2CH_3$); 31.0 (m, $C(CD_3)_2CH_3$); 21.101 (q, J_{CH} = 126.2 Hz, NAr and N[R]Ar Ar*Me*). ^{77}Se NMR (57.292 MHz, $CDCl_3$, pw = 15 µsec, d_1 = 1 sec, 16000 scans): δ = 1923.4; $\Delta\nu_{1/2}$ = 46.2 Hz. IR (benzene/polyethylene, 2 cm^{-1}): $\nu_{Mo\text{-}Se}$ = 355 cm^{-1}. UV/Vis (ether): $\lambda_{max}(\varepsilon)$ = 292(17700 M^{-1}cm^{-1}). MS (70 eV): *m/z*(%): 660(5)[*M*+]. Anal. Calcd. for $C_{32}H_{33}D_{12}MoN_3Se$: C, 58.35; H, 6.89; N, 6.38. Found: C, 58.79 H, 6.94; N, 6.24.

(ix) TeMo(NAr)(N[R]Ar)$_2$ (2.9): TeMo(N[R]Ar)$_3$ (**2.5**, 0.5085 g, 0.6600 mmol) was dissolved in benzene (25 mL) in a reaction bomb which was then evacuated to autogenic pressure. The solution was heated at 65 °C for 5 hours; no color change was observed. The benzene was removed *in vacuo* leaving a fine dark red-brown powder (0.3712 g, 0.5248 mmol, 80%) which was contaminated with about 5% HN[R]Ar. The

References begin on page 184

complex could be recrystallized from ether in low yield (~40%). M.p. 194.5-195.5 °C. ^{1}H NMR (300 MHz, $CDCl_3$): δ = 7.3 (br s, 2H, N[R]Ar ortho *a*); 7.032 (s, 2H, aryl); 6.916 (s, 1H, NAr para); 6.886 (s, 2H, aryl); 6.4 (br s, 2H, N[R]Ar ortho *b*); 2.350 (s, 6H, NAr Ar*Me*); 2.278 (s, 12H, N[R]Ar Ar*Me*); 1.131 (s, $C(CD_3)_2CH_3$). ^{13}C NMR (75 MHz, $CDCl_3$): δ = 157.624 (s, NAr ipso); 149.799 (N[R]Ar ipso); 138.412 (q, $^2J_{CH}$ = 5.8 Hz, NAr meta); 137.947 (q, $^2J_{CH}$ = 5.7 Hz, N[R]Ar meta); 131.2 (br d, J_{CH} ~ 125 Hz, N[R]Ar ortho *a*); 129.548 (d, J_{CH} = 155 Hz, aryl); 127.776 (d, J_{CH} = 155 Hz, aryl); 127.0 (br d, J_{CH} ~ 125 Hz, N[R]Ar ortho *b*); 119.116 (d, J_{CH} = 162 Hz, aryl); 62.6735 (s, $C(CD_3)_2CH_3$); 31.4322 (q, J_{CH} = 126.2 Hz, $C(CD_3)_2CH_3$); 30.9061 (m, $C(CD_3)_2CH_3$); 21.2830 (q, J_{CH} = 127.1 Hz, N[R]Ar Ar*Me*); 21.2226 (q, J_{CH} = 126.6 Hz, NAr Ar*Me*). ^{125}Te NMR (158 MHz, $CDCl_3$, pw = 12 μsec, d_1 = 1 sec, 28000 scans): δ = 2459.3; $\Delta\nu_{1/2}$ = 250 Hz. IR (benzene/polyethylene, 2 cm^{-1}): $\nu_{Mo\text{-}Te}$ = 291 cm^{-1}. UV/Vis (ether): $\lambda_{max}(\varepsilon)$ = 327(13700). MS (70 eV): *m/z*(%): 705.2(70)[*M*+]. Anal. Calcd. for $C_{32}H_{33}D_{12}MoN_3Te$: C, 54.34; H, 6.41; N, 5.94. Found: C, 51.30; H, 6.42; N, 5.39.

(x) [OMo(N[R]Ar)$_3$][OTf] (2.10): $OMo(N[R]Ar)_3$ (**2.2**, 0.0996 g, 0.1512 mmol) in ether was added to a slurry of FcOTf (0.0512 g, 0.1528 mmol) in ether to give a total volume of 5 mL. The solution was stirred for 15 hours, at which point the solution was brown and an orange brown precipitate was observed. The solid was collected on a frit and washed with ether; the washings were colorless (0.0865 g, 0.1071 mmol, 71%). The complex decomposed fairly rapidly in solvents in which it was soluble, precluding purification by recrystallization. The reported analysis is of isolated and washed material. M.p. 100-101 °C (dec). ^{1}H NMR (300 MHz, $CDCl_3$): δ = 7.094 (s, 3H, para); 5.5 (br s, 6H, ortho); 2.221 (br s, 18H, Ar*Me*); 1.428 (br s, 9H, $C(CD_3)_2CH_3$). ^{19}F NMR (282 MHz, $CDCl_3$): δ = -83.417. ^{13}C NMR (125 MHz, $CDCl_3$): 148.083, 139.397, 131.501, 125.394 (ipso), 70.547 ($C(CD_3)_2CH_3$), 31.227 ($C(CD_3)_2CH_3$), 30.739 ($C(CD_3)_2CH_3$), 21.564 (Ar*Me*). IR (Nujol/KBr 2 cm^{-1}): 1601.8, 1266.1(ionic triflate),[79]

References begin on page 184

1221.8, 1146.4, 1111.1, 1031.1(ionic triflate),[79] 971.8(ν_{Mo-O}), 698.8, 637.3, 570.7, 474.0. Anal. Calcd. for $C_{37}H_{36}D_{18}F_3MoN_3O_4S$: C, 55.00; H, 6.74; N, 5.20. Found: C, 56.67; H, 6.94; N, 4.89.

(xi) [OMo(N[R]Ar)$_3$][I] (2.11): To a solution of OMo(N[R]Ar)$_3$ (**2.2**, 0.0999 g, 0.1516 mmol) in ether was added iodine (0.0199 g, 0.0784 mmol. 0.52 eq) in ether to give a total volume of 5 mL. An orange precipitate formed immediately. The solution was stirred for 15 hours, at which point the solution was colorless. The orange solid was collected on a frit and washed with ether; the washings were colorless (0.1042 g, 0.1326 mmol, 87.5%). The complex decomposed fairly rapidly in solvents in which it was soluble, precluding characterization by ^{13}C NMR spectroscopy and purification by recrystallization. The reported analysis is of isolated and washed material. M.p. 95-97 °C (dec). ^1H NMR (300 MHz, $CDCl_3$): δ = 7.079 (s, 3H, para); 5 (br s, 6H, ortho); 2.214 (br s, 18H, Ar*Me*); 1.428 (br s, 9H, $C(CD_3)_2CH_3$). IR (Nujol/KBr 2 cm^{-1}): 1602.1, 1582.8, 1285.0, 1147.6, 1110.8, 1051.3, 1030.6, 974.5(ν_{Mo-O}), 939.1, 886.3, 701.1, 696.2. Anal. Calcd. for $C_{36}H_{36}D_{18}IMoN_3O$: C, 55.03; H, 6.93; N, 5.35. Found: C, 54.17; H, 6.99; N, 5.14.

(xii) O$_2$Mo(N[R]Ar)$_2$ (2.12): OMo(N[R]Ar)$_3$ (**2.2**, 0.2198 g, 0.3336 mmol) was dissolved in ether (15 mL) in a reaction bomb and dioxygen (45.96 mL, 150 torr, 0.3712 mmol, 1.11 eq) was added. After 80 minutes, the reaction mixture was dark brown. After 14 hours, the reaction mixture was a rich dark red brown. An aliquot was examined by ^1H NMR spectroscopy, showing the presence of O$_2$Mo(N[R]Ar)$_2$ and HN[R]Ar in a 1:2 molar ratio as the major products. Examination of the reaction mixture by ^2H NMR spectroscopy showed the consumption of all paramagnetic material. The solvent was removed *in vacuo* and the resulting oily solid was dissolved in a minimum of hexane (ca. 2 mL). A dark brown solid was collected, which could be recrystallized from hexane

References begin on page 184

yielding a dark golden yellow solid (0.0410 g, 0.0832 mmol, 25%). M.p. 129-130 °C. ^{1}H NMR (300 MHz, C_6D_6): δ = 6.761 (s, 4H, ortho); 6.666 (s, 2H, ortho); 2.074 (s, 12H, Ar*Me*); 1.227 (s, 6H, $CCH_3(CD_3)_2$). ^{13}C NMR (125 MHz, $CDCl_3$): δ = 148.390 (s, ipso); 138.369 (s, meta); 128.855 (d, J_{CH} = 154.3 Hz, para); 127.602 (d, J_{CH} = 158.0 Hz, ortho); 61.54 (s, $CCH_3(CD_3)_2$); 30.976 (q, J_{CH} = 126.4 Hz, $CCH_3(CD_3)_2$); 30.611 (m, $CCH_3(CD_3)_2$); 21.476 (q, J_{CH} = 126.4 Hz, Ar*Me*). IR (benzene, 2 cm^{-1}): ν_{Mo-O} = 943, 920 cm^{-1}. MS (70 eV): *m/z*(%): 491.8(17.6)[*M*+]. Anal. Calcd. for $C_{24}H_{24}D_{12}MoN_2O_2$: C, 58.52; H, 7.37; N, 5.69. Found: C, 58.74; H, 7.36; N, 5.64.

(xiii) $(N[R]Ar)_3Mo(\mu\text{-}CS)Mo(N[R]Ar)_3$ (2.13): CS_2 (50 μL, 0.5187 mmol, 0.66 eq) was added to a solution of $Mo(N[R]Ar)_3$ (**2.1**, 0.5034 g, 0.7831 mmol) in ether (25 mL). The solution rapidly turned a dark greenish brown color. ^{2}H NMR spectroscopy at this point showed a 1:1 molar ratio of the terminal sulfide complex and the bridging thiocarbonyl complex. Solvent was removed *in vacuo* leaving a foamy solid which was dissolved in ether (~3 mL). Upon standing for about 30 seconds, a dark solid began to precipitate. More ether was added to fully dissolve the solid (~10 mL), and the solution was stored at -35 °C. The first crop of solid was >95% diamagnetic but additional crops were contaminated with sulfide **2.3** (as determined by ^{2}H NMR spectroscopy) (0.1640 g, 0.1233 mmol, 47%). M.p. 139-140 °C. ^{1}H NMR (300 MHz, $CDCl_3$): δ = 6.711 (s, 3H, para(a)); 6.5681 (s, 3H, para(b)); 6.455 (br s, 6H, ortho(a)); 5.718 (s, 6H, ortho(b)); 2.199 (s, 18H, Ar*Me*(a)); 2.112 (s, 18H, Ar*Me*(b)); 1.285 (br s, 18H, $C(CD_3)_2CH_3$). ^{13}C NMR (125 MHz, $CDCl_3$): δ = 293.51 (br s, μ-*C*S); 153.42 (br s, ipso(a)); 151.10 (s, ipso(a)); 136.20 (m, meta(a)); 136.00 (m, meta(b)); 131.02 (d, *J* = 158.7 Hz, aryl); 127.67 (d, J = 158.4 Hz, aryl); 126.96 (d, *J* = 153.8 Hz, aryl); 126.39 (d, *J* = 152.9 Hz, aryl); 63.57 (br s, $CCH_3(CD_3)_2$(a)); 61.30 (s, $CCH_3(CD_3)_2$(b)); 33.69 (q, *J* = 125.4 Hz, $C(CD_3)_2CH_3$(a)); 33.01 (m, $C(CD_3)_2CH_3$(a)); 31.99 (q, *J* = 125.5 Hz, $C(CD_3)_2CH_3$(b)); 31.33 (m, $C(CD_3)_2CH_3$(b)); 21.69 (q, *J* = 125.9 Hz, Ar*Me*(a)); 21.60 (q, *J* = 125.7 Hz,

References begin on page 184

Ar*Me*(b)). UV/Vis (ether): λ(ε) = 363(27300); 438(9660); 582(3090). Anal. Calcd. for $C_{73}H_{72}D_{36}Mo2N_6S$: C, 65.93; H, 8.19; N, 6.32. Found: C, 64.74; H, 8.18; N, 6.18.

(xiv) (PhSe)Mo(N[R]Ar)$_3$ (2.14): Diphenyldiselenide (0.1273 g, 0.4078 mmol, 0.52 eq) was dissolved in ether (10 mL) and added to a solution of Mo(N[R]Ar)$_3$ (**2.1**, 0.5063 g, 0.7876 mmol) in ether (20 mL). The solution rapidly changed to a dark green-blue color. The solvent was removed *in vacuo*, and the resulting blue-green solid was recrystallized from ether (0.4520 g, 0.5657 mmol, 71.8%). M.p. 141-142 °C. ^{1}H NMR (300 MHz, $CDCl_3$): δ = 8.09 (d, *J* = 7.5 Hz, 2H, Ar); 7.38 (t, *J* = 7.4 Hz, 2H, Ar); 7.29 (t, *J* = 7.2 Hz, 1H, Ar); 6.48 (s, 3H, N[R]Ar para); 6.05 (br s, 6H, N[R]Ar ortho); 2.10 (s, 18H, Ar*Me*); 1.25 (s, 9H, $C(CD_3)_2CH_3$). ^{13}C NMR (75 MHz, $CDCl_3$): δ = 152.03 (s, N[R]Ar ipso); 148.5 (s, ipso); 136.04 (s, N[R]Ar ortho); 133.72 (d, *J* = 159.8 Hz, aryl); 128.33 (d, *J* = 158.5 Hz, aryl); 127.57 (br d, aryl); 126.62 (d, *J* = 154.4 Hz, aryl); 125.35 (d, *J* = 159.8 Hz, aryl); 62.67 (s, $C(CD_3)_2CH_3$); 31.11 (q, *J* = 127.6 Hz, $C(CD_3)_2CH_3$); 30.62 (m, $C(CD_3)_2CH_3$); 21.652 (q, *J* = 126.2 Hz, Ar*Me*). ^{77}Se NMR (95.4 MHz, $CDCl_3$, pw = 8 μsec, d_1 = 1 sec, 14400 scans): δ = 1006.3; $\Delta\nu_{1/2}$ ~ 600 Hz. UV/Vis (ether): λ(ε) = 255(5000); 421(5970); 582(2490). Anal. Calcd. for $C_{42}H_{41}D_{18}MoN_3Se$: C, 63.14; H, 7.44; N, 5.26. Found: C, 63.38; H, 7.67; N, 5.28.

2.8.5 Other Reactions

(i) Reaction of 2.1 with SO_2: Mo(N[R]Ar)$_3$ (0.0219 g, 0.0341 mmol) was dissolved in ether (5 mL) in an evacuated reaction bomb. SO_2 (0.50 mL, 0.020 mmol, 0.58 equiv) was added via syringe, causing a rapid color change to dark brown. Examination of the reaction mixture by ^{2}H NMR spectroscopy showed the presence of the oxo complex **2.2** (δ = 7.41) and the sulfido complex **2.3** (δ = 6.46 ppm) in

References begin on page 184

approximately a 2:1 ratio. The peaks were not baseline resolved, preventing an accurate integral to be obtained.

(ii) Reaction of 2.1 with NO_2: $Mo(N[R]Ar)_3$ (0.0203 g, 0.0316 mmol) was dissolved in ether (5 mL) in an evacuated reaction bomb. NO_2 (0.42 mL, 0.017 mmol, 0.54 equiv) was added via syringe, causing a color change to pale tan-brown over a 10 minute period. Examination of the reaction mixture by ^2H NMR spectroscopy showed the presence of the oxo complex **2.2** (δ = 7.57) and diamagnetic material (δ = 2.16) in a 1:1 molar ratio. The solvent was removed *in vacuo* and the reaction mixture was examined by ^1H NMR spectroscopy, clearly showing that the only diamagnetic product was $(ON)Mo(N[R]Ar)_3$.

(iii) Reaction of 2.1 with $OSMe_2$: $Mo(N[R]Ar)_3$ (0.0201 g, 0.0313 mmol) was dissolved in ether (3 mL) and $OSMe_2$ (2.5 µL, 0.0352 mmol, 1.1 equiv) was added. After 10 minutes, the reaction mixture was dark brown in color. Examination of the reaction mixture by ^2H NMR spectroscopy showed $Mo(N[R]Ar)_3$ **2.1** (δ = 63.95) and $OMo(N[R]Ar)_3$ **2.2** (δ = 7.59) in a 1:9 molar ratio.

(iv) Reaction of 2.1 with $OPPh_3$: $Mo(N[R]Ar)_3$ (0.0400 g, 0.0622 mmol) and $OPPh_3$ (0.0260 g, 0.0934 mmol, 1.5 equiv) were dissolved in toluene (5 mL) under an atmosphere of Ar and stored at -35 °C for 24 hours. The solution was then warmed to room temperature. Analysis of the reaction mixture by ^2H NMR spectroscopy showed the presence of $Mo(N[R]Ar)_3$ (δ = 62.99), $OMo(N[R]Ar)_3$ (δ = 7.1) and diamagnetic material (δ = 1.53) in a 5:2:1 ratio. Analysis of the reaction mixture by ^{31}P NMR showed the presence of $OPPh_3$ (δ = 25.00). The reaction was stirred at room temperature for 24 hours, at which point the ^2H NMR spectrum showed the presence of $Mo(N[R]Ar)_3$ (δ = 63.27), an unknown paramagnetic material (δ = 23.46), $OMo(N[R]Ar)_3$ (δ = 7.22) and

References begin on page 184

diamagnetic material (δ = 1.49) in a 3:1:1:1 ratio. The ^{31}P NMR again only showed the presence of $OPPh_3$ (δ = 25.00). Analysis of the reaction mixture by ^{1}H NMR showed primarily HN[R]Ar.

(v) Reaction of 2.1 with CO_2: $Mo(N[R]Ar)_3$ (0.0500 g, 0.0778 mmol) was dissolved in ether (ca. 5 mL) in a reaction bomb and CO_2 (ca. 25 mL, 1 atm, 1.0 mmol, 13 equiv) was added. After 1 hour at 0 °C, the reaction mixture was examined by ^{2}H NMR spectroscopy, showing $Mo(N[R]Ar)_3$ (δ = 64) and $OMo(N[R]Ar)_3$ (δ = 7.5) in an 18:1 molar ratio. The reaction was repeated and allowed to react at 0 °C for 24 hours. Examination of the reaction mixture by ^{2}H NMR showed $Mo(N[R]Ar)_3$ (δ = 63.6), $(OC)Mo(N[R]Ar)_3$ (δ = 10.0),[97] $OMo(N[R]Ar)_3$ and other material (δ = 7-8) and diamagnetic material (δ = 2.13) in approximately a 20:1:10:20 ratio.

(vi) Reaction of 2.1 with *tert*-BuNC: $Mo(N[R]Ar)_3$ (0.0204 g, 0.0317 mmol) was dissolved in ether (3 mL) and *tert*-BuNC (3.5 µL, 0.0309 mmol, 0.97 equiv) was added causing a rapid color change to dark red/brown. Analysis of the reaction mixture by ^{2}H NMR spectroscopy showed a peak at 11.1 ppm corresponding to the adduct Mo(CN-*t*-Bu)$(N[R]Ar)_3$.

(vii) Reaction of 2.1 with *tert*-BuNCO: $Mo(N[R]Ar)_3$ (0.0217 g, 0.0338 mmol) was dissolved in *tert*-BuNCO (0.75 g) and the reaction mixture was stirred for 24 hours. Examination of the reaction mixture by ^{2}H NMR spectroscopy showed $Mo(N[R]Ar)_3$ (δ = 64.7), paramagnetic material (δ = 29.4 and 26.4), Mo(CN-*t*-Bu)$(N[R]Ar)_3$ (δ = 11.6), $OMo(N[R]Ar)_3$ (δ = 7.8) and diamagnetic material (δ = 2.9-3) in a 60:1:5:1:3:10 ratio.

(viii) Reaction of 2.1 with O_2SMe_2: $Mo(N[R]Ar)_3$ (0.0211 g, 0.0328 mmol) was dissolved in THF (2 mL) and O_2SMe_2 (0.0030 g, 0.0319 mmol, 0.97 equiv) was added.

References begin on page 184

The reaction mixture was stirred for 48 hours, at which point is was examined by ^2H NMR spectroscopy, showing $Mo(N[R]Ar)_3$ (δ = 64.3) and diamagnetic material (δ = 2.2-1.8) in a 5:1 ratio, along with a tiny amount of $OMo(N[R]Ar)_3$ (δ = 7.5).

(ix) Reaction of 2.2 with PPh_3: $OMo(N[R]Ar)_3$ (0.0480 g, 0.0729 mmol) was dissolved in toluene and PPh_3 (0.0400 g, 0.153 mmol, 2.1 equiv) was added. The reaction was stirred for 24 hours, at which point examination by ^2H NMR spectroscopy showed only the starting oxo complex. Examination of the reaction by ^{31}P NMR spectroscopy showed only PPh_3 (δ = -4.41).

(x) Reaction of 2.2 with $OSMe_2$: $OMo(N[R]Ar)_3$ (0.0312 g, 0.0474 mmol) was dissolved in ether (5 mL) and $OSMe_2$ (8.5 mL, 0.12 mmol, 2.5 equiv) was added. The reaction was stirred for 20 hours, at which point it was examined by ^2H NMR spectroscopy, showing the presence of a significant amount of starting oxo complex. The reaction was stirred an additional 48 hours, at which point the reaction solution was red-brown. Analysis of the reaction mixture by ^1H NMR spectroscopy showed HN[R]Ar and $O_2Mo(N[R]Ar)_2$ in a 3.5:1 ratio.

(xi) Reaction of 2.1 with O_2: $Mo(N[R]Ar)_3$ (0.2200 g, 0.3422 mmol) was dissolved in ether (10 mL) and dioxygen (8.5 mL, 0.35 mmol, 1.0 eq) was added slowly over a 2 minute period. The solution became dark blue for about 10 seconds, and then green. After 30 seconds, the solution was dark brown. A ^2H NMR spectrum obtained at this point showed the presence of 1 part $OMo(N[R]Ar)_3$ and 2 parts diamagnetic material. A ^1H NMR spectrum of the material showed five products: $O_2Mo(N[R]Ar)_2$, HN[R]Ar, and $OMo(N[R]Ar)_3$ in a 2:1:1 molar ratio, as well as two additional unidentified products.

References begin on page 184

(xii) Thermolysis of OMo(NAr)(N[R]Ar)$_2$: OMo(NAr)(N[R]Ar)$_2$ (ca. 0.015 g) was dissolved in C_6D_6 (ca. 1 mL) and sealed in an NMR tube. The mixture was heated at 110 °C for 82 hours, at which point it was examined by ^{1}H NMR spectroscopy. Three products were observed: O_2Mo(N[R]Ar)$_2$, OMo(NAr)(N[R]Ar)$_2$ and a product corresponding to Mo(NAr)$_2$(N[R]Ar)$_2$ in a 1:2:1molar ratio.

(xiii) Reaction of 2.6 with benzaldehyde: OMo(NAr)(N[R]Ar)$_2$ (0.0471 g, 0.0788 mmol) and benzaldehyde (0.080 mL, 0.787 mmol, 10 eq) were dissolved in ether (3 mL) and stirred at room temperature for 72 hours. ^{1}H NMR showed primarily starting material, but also a small amount of O_2Mo(N[R]Ar)$_2$ and PhC(H)=NAr.

(xiv) Reaction of 2.1 with PEt$_3$: Several hundred milligrams of Mo(N[R]Ar)$_3$ were dissolved in C_6D_6 (1.5 mL) and triethylphosphine (ca. 10 μL) was added. Analysis of the reaction mixture by ^{2}H NMR spectroscopy showed only starting *tris*-anilide **2.1**.

2.8.6 Thermodynamic Measurements[46]

(i) General Considerations. All manipulations involving organomolybdenum complexes were performed under inert atmospheres of argon in a Vacuum Atmospheres glovebox containing less than 1 ppm oxygen and water. Calorimetric measurements were performed using a Calvet calorimeter (Setaram C-80) which was periodically calibrated using the TRIS reaction[98] or the enthalpy of solution of KCl in water.[99] The experimentally determined enthalpies for these two standard calibration reactions are the same within experimental error as the literature values. This calorimeter has been previously described[100] and typical procedures are described below. Experimental enthalpy data are reported with 95% confidence limits.

References begin on page 184

(ii) ^{2}H NMR titrations. Prior to the calorimetric experiments, an accurately weighed amount (± 0.1 mg) of the molybdenum complex was placed in an NMR tube and toluene was subsequently added. The solution was titrated with a large excess of the reagent of interest. The reactions were monitored by ^{2}H NMR spectroscopy and the reactions were found to be rapid, clean and quantitative under experimental calorimetric conditions. These conditions are necessary for accurate and meaningful calorimetric results and were satisfied for the molybdenum reactions investigated with pyridine *N*-oxide and ethylene sulfide. Only reactants and products were observed in the course of the NMR titration.

(iii) Calorimetric Measurement for Preparation of 2.2. The mixing vessels of the Setaram C-80 were cleaned, dried in an oven maintained at 120 °C, and then taken into the glovebox. A 20-30 mg sample of **2.1** was accurately weighed into the lower vessel, and it was closed and sealed with 1.5 mL of mercury. Four mL of a stock solution of pyridine N-oxide [0.5 g of pyridine N-Oxide in 25 mL of toluene] was added and the remainder of the cell was assembled, removed from the glovebox and inserted in the calorimeter. The reference vessel was loaded in an identical fashion with the exception that no organomolybdenum complex was added to the lower vessel.

After the calorimeter had reached thermal equilibrium at 30.0 °C (about 1.5 hrs), the calorimeter was inverted thereby allowing the reactants to mix. After reaching thermal equilibrium, the vessels were removed from the calorimeter, taken into the glovebox, opened, and analyzed using ^{1}H NMR spectroscopy. Conversion to $OMo(N[R]Ar)_3$ was found to be quantitative under these reaction conditions. The enthalpy of reaction, -74.6 ± 1.2 kcal/mol represents the average of five individual calorimetric determinations. The enthalpy of solution of **2.1** was then added to this value to obtain a value of -83.5 ± 1.4 kcal/mol for all species in solution.

References begin on page 184

(iv) Calorimetric Measurement for Preparation of 2.3. The mixing vessels of the Setaram C-80 were cleaned, dried in an oven maintained at 120 °C, and then taken into the glovebox. A 20-30 mg sample of **2.1** was accurately weighed into the lower vessel, and it was closed and sealed with 1.5 mL of mercury. Four mL of a stock solution of ethylene sulfide [0.5 g of ethylene sulfide in 25 mL of toluene] was added and the remainder of the cell was assembled, removed from the glovebox and inserted in the calorimeter. The reference vessel was loaded in an identical fashion with the exception that no organomolybdenum complex was added to the lower vessel.

After the calorimeter had reached thermal equilibrium at 30.0 °C (about 1.5 hrs), the calorimeter was inverted thereby allowing the reactants to mix. After reaching thermal equilibrium, the vessels were removed from the calorimeter, taken into the glovebox, opened, and analyzed using ^{1}H NMR spectrocopy. Conversion to SMo(N[R]Ar)$_3$ was found to be quantitative under these reaction conditions. The enthalpy of reaction, -36.3 ± 1.2 kcal/mol represents the average of five individual calorimetric determinations. The enthalpy of solution of **2.1** was then added to this value to obtain a value of -45.2 ± 1.2 kcal/mol for all species in solution.

(v) Calorimetric Measurement of Enthalpy of Solution of 2.1. In order to consider all species in solution, the enthalpies of solution of **2.1** had to be directly measured in the solvents utilized. This was performed by using a similar procedure as the one described above with the exception that no chalcogen reagent was added to the reaction cell. This enthalpy of solution represents the average of three individual determinations and is 8.9 ± 0.2 kcal/mol in toluene.

References begin on page 184

2.8.7 X-ray Structural Determination

(i) $OMo(N[R]Ar)_3$ (2.2)

A black needle of approximate dimensions 0.8 x 0.5 x 0.2 mm was obtained from a chilled ether solution. The crystal was mounted on a glass fiber. Data collection was carried out on a Siemens Platform goniometer with a CCD detector at 188 K using Mo Kα radiation (λ = 0.71073 Å). The total data collected were 7169 reflections ($-10 \leq h \leq 10$, $-11 \leq k \leq 10$, $-22 \leq l \leq 21$), of which 4915 were unique (R_{int} = 0.0309). Corrections applied: Semi-empirical from psi-scans. The structure was solved by direct methods (SHELXTL V5.0, G. M. Sheldrick and Siemens Industrual Automation, Inc., 1995) in conjunction with standard difference Fourier techniques. Least-squares refinement based upon F^2 converged with residuals of R_1 = 0.0341, wR_2 = 0.0959, and GOF = 1.053 based upon $I > 2\sigma(I)$. All non-hydrogen atoms were refined anisotropically, and hydrogen atoms were placed in calculated ($d_{C\text{-}H}$ = 0.96 Å) positions. The residual peak and hole electron density was 0.446 and -0.558 e $Å^{-3}$. Crystal data: triclinic, a = 9.8974(12) Å, b = 9.9883(14) Å, c = 20.254(2) Å, V = 1760.9(4) $Å^3$, α = 95.745(10)°, β = 92.324(8)°, γ = 117.356(8)°, space group P1, Z = 2, μ = 0.402 mm^{-1}, M_r = 640.76 for $C_{36}H_{54}MoN_3O$, ρ(calcd) = 1.208 g/cm^3, and F(000) = 682. See Tables 2.1 and 2.2 for metrical parameters, Table 2.3 for positional parameters and U(eq), and Figure 2.3 for an ORTEP diagram.

(ii) $SMo(N[R]Ar)_3$ (2.3)

A black needle of approximate dimensions 0.55 x 0.23 x 0.11 mm was obtained from a chilled ether solution. The crystal was mounted on a glass fiber. Data collection was carried out on a Siemens Platform goniometer with a CCD detector at 188 K using Mo Kα radiation (λ = 0.71073 Å). The total data collected were 13213 reflections ($-15 \leq h \leq 15$, $-14 \leq k \leq 7$, $-22 \leq l \leq 22$), of which 5098 were unique (R_{int} = 0.0570). No

References begin on page 184

Absorption corrections were applied. The structure was solved by direct methods (SHELXTL V5.0, G. M. Sheldrick and Siemens Industrual Automation, Inc., 1995) in conjunction with standard difference Fourier techniques. Least-squares refinement based upon F^2 converged with residuals of R_1 = 0.0527, wR_2 = 0.1015, and GOF = 1.168 based upon $I > 2\sigma(I)$. All non-hydrogen atoms were refined anisotropically, and hydrogen atoms were placed in calculated ($d_{C\text{-}H}$ = 0.96 Å) positions. The residual peak and hole electron density was 0.376 and -0.709 e Å^{-3}. Crystal data: monoclinic, a = 13.9099(8) Å, b = 12.8972(8) Å, c = 19.9860(12) Å, V = 3580.4(4) Å^3, α = 90°, β = 93.0580(10)°, γ = 90°, space group $P2_1/c$, Z = 4, μ = 0.451 mm^{-1}, M_r = 656.82 for $C_{36}H_{54}MoN_3S$, ρ(calcd) = 1.219 g/cm^3, and F(000) = 1396. See Tables 2.4 and 2.5 for metrical parameters, Table 2.6 for positional parameters and U(eq), and Figure 2.6 for an ORTEP diagram.

(iii) SeMo(N[R]Ar)$_3$ (2.4)

A black needle of approximate dimensions 0.75 x 0.32 x 0.22 mm was obtained from a chilled ether solution. The crystal was mounted on a glass fiber. Data collection was carried out on a Siemens Platform goniometer with a CCD detector at 188 K using Mo Kα radiation (λ = 0.71073 Å). The total data collected were 12674 reflections ($-7 \le h \le 15$, $-14 \le k \le 14$, $-22 \le l \le 15$), of which 5075 were unique (R_{int} = 0.0379). Corrections applied: Semi-empirical from psi-scans. The structure was solved by direct methods (SHELXTL V5.0, G. M. Sheldrick and Siemens Industrual Automation, Inc., 1995) in conjunction with standard difference Fourier techniques. Least-squares refinement based upon F^2 converged with residuals of R_1 = 0.0391, wR_2 = 0.0976, and GOF = 1.285 based upon $I > 2\sigma(I)$. All non-hydrogen atoms were refined anisotropically, and hydrogen atoms were placed in calculated ($d_{C\text{-}H}$ = 0.96 Å) positions. The residual peak and hole electron density was 0.394 and -0.501 e Å^{-3}. Crystal data: monoclinic, a = 13.9372(7) Å, b = 12.8821(7) Å, c = 19.9510(10) Å, V = 3577.4(3) Å^3, α = 90°, β = 92.9060(10)°, γ =

References begin on page 184

90°, space group $P2_1/c$, Z = 4, μ = 1.411 mm^{-1}, M_r = 703.72 for $C_{36}H_{54}MoN_3Se$, ρ(calcd) = 1.307 g/cm^3, and F(000) = 1468. See Tables 2.7 and 2.8 for metrical parameters, Table 2.9 for positional parameters and U(eq), and Figure 2.9 for an ORTEP diagram.

(iv) TeMo(N[R]Ar)$_3$ (2.5)

A black needle of approximate dimensions 0.65 x 0.48 x 0.23 mm was obtained from a chilled ether solution. The crystal was mounted on a glass fiber. Data collection was carried out on a Siemens Platform goniometer with a CCD detector at 188 K using Mo Kα radiation (λ = 0.71073 Å). The total data collected were 14461 reflections ($-12 \leq h \leq 15$, $-14 \leq k \leq 11$, $-22 \leq l \leq 22$), of which 5182 were unique (R_{int} = 0.0295). No Absorption corrections were applied. The structure was solved by direct methods (SHELXTL V5.0, G. M. Sheldrick and Siemens Industrual Automation, Inc., 1995) in conjunction with standard difference Fourier techniques. Least-squares refinement based upon F^2 converged with residuals of R_1 = 0.0256, wR_2 = 0.0634, and GOF = 1.008 based upon $I > 2\sigma(I)$. All non-hydrogen atoms were refined anisotropically, and hydrogen atoms were placed in calculated ($d_{C\text{-}H}$ = 0.96 Å) positions. The residual peak and hole electron density was 0.399 and -0.359 e $Å^{-3}$. Crystal data: monoclinic, a = 14.108(2) Å, b = 12.762(3) Å, c = 20.083(4) Å, V = 3612.2(13) $Å^3$, α = 90°, β = 92.558(11)°, γ = 90°, space group $P2_1/c$, Z = 4, μ = 1.181 mm^{-1}, M_r = 752.36 for $C_{36}H_{54}MoN_3Te$, ρ(calcd) = 1.383 g/cm^3, and F(000) = 1540. See Tables 2.10 and2.11 for metrical parameters, Table 2.12 for positional parameters and U(eq), and Figure 2.12 for an ORTEP diagram.

(v) (N[R]Ar)$_3$Mo(μ-CS)Mo(N[R]Ar)$_3$·2 Et$_2$O (2.13)

A greenish brown needle of approximate dimensions 0.40 x 0.21 x 0.18 mm was obtained from a chilled ether solution. The crystal was mounted on a glass fiber. Data collection was carried out on a Siemens Platform goniometer with a CCD detector at 188 K

References begin on page 184

using Mo Kα radiation (λ = 0.71073 Å). The total data collected were 11885 reflections ($-16 \le h \le 13$, $-16 \le k \le 12$, $-22 \le l \le 20$), of which 7493 were unique (R_{int} = 0.0673). Corrections applied: semi-empirical from psi-scans. The structure was solved by direct methods (SHELXTL V5.0, G. M. Sheldrick and Siemens Industrual Automation, Inc., 1995) in conjunction with standard difference Fourier techniques. Least-squares refinement based upon F^2 converged with residuals of R_1 = 0.1035, wR_2 = 0.2107, and GOF = 1.209 based upon $I > 2\sigma(I)$. All non-hydrogen atoms were refined anisotropically, and hydrogen atoms were placed in calculated ($d_{C\text{-}H}$ = 0.96 Å) positions. The residual peak and hole electron density was 0.920 and -0.512 e Å^{-3}. Crystal data: triclinic, a = 14.6441(3) Å, b = 15.2700(2) Å, c = 20.5956(4) Å, V = 4150.44(13) Å^3, α = 89.1990(10)°, β = 77.8370(10)°, γ = 67.6530(10)°, space group $P\bar{1}$, Z = 2, μ = 0.372 mm^{-1}, M_r = 1432.76 for $C_{81}H_{119}Mo_2N_6O_2S$, ρ(calcd) = 1.146 g/cm^3, and F(000) = 1526. See Tables 2.27 and 2.28 for metrical parameters, Table 2.29 for positional parameters and U(eq), and Figure 2.25 for an ORTEP diagram.

References begin on page 184

References

1) Bottomley, F.; Sutin, L. *Adv. Organometall. Chem.* **1988**, *28*, 399.
2) Holm, R. H. *Chem. Rev.* **1987**, *87*, 1401.
3) Berreau, L. M.; Woo, L. K. *J. Am. Chem. Soc.* **1995**, *117*, 1314-1317.
4) Woo, L. K. *Chem. Rev.* **1993**, *93*, 1125-1136.
5) Rabinovich, D.; Parkin, G. *Inorg. Chem.* **1995**, *34*, 6341-6361.
6) Nugent, W. A.; Mayer, J. M. *Metal-Ligand Multiple Bonds*; John Wiley & Sons: New York, 1988, pp 76-78.
7) Greenwood, N. N.; Earnshaw, A. *Chemistry of the Elements*; Pergamon Press Inc.: Tarrytown, New York, 1984.
8) Shin, J. H.; Parkin, G. *Organometallics* **1994**, *13*, 2147-2149.
9) Rabinovich, D.; Parkin, G. *J. Am. Chem. Soc.* **1991**, *113*, 9421.
10) Cummins, C. C.; Schrock, R. R.; Davis, W. M. *Inorg. Chem.* **1994**, *33*, 1448-1457.
11) Howard, W. A.; Parkin, G. *J. Organometal. Chem.* **1994**, *472*, C1-C4.
12) Howard, W. A.; Parkin, G. *J. Am. Chem. Soc.* **1994**, *116*, 606-615.
13) Christou, V.; Arnold, J. *J. Am. Chem. Soc.* **1992**, *114*, 6240-6242.
14) Christou, V.; Arnold, J. *Angew. Chem. Int. Ed. Engl.* **1993**, *32*, 1450.
15) Siemeling, U.; Gibson, v. C. *J. Chem. Soc., Chem. Commun.* **1992**, 1670.
16) Murphy, V. J.; Parkin, G. *J. Am. Chem. Soc.* **1995**, *117*, 3522-3528.
17) Gardner, D. R.; Fettinger, J. C.; Eichorn, B. W. *Angew. Chem., Int. Ed. Engl.* **1994**, *33*, 1859.
18) Bonasia, P. J.; Christou, V.; Arnold, J. *J. Am. Chem. Soc.* **1993**, *115*, 6777-6781.
19) Fischer, J. M.; Piers, W. E.; MacGillivray, L. R.; Zaworotko, M. J. *Inorg. Chem.* **1995**, *34*, 2499-2500.
20) Shin, J. H.; Parkin, G. *Organometallics* **1995**, *14*, 1104-1106.
21) Howard, W. A.; Trnka, T. M.; Parkin, G. *Organometallics* **1995**, *14*, 4037-4039.
22) Howard, W. A.; Parkin, G. *Organometallics* **1993**, *12*, 2363-2366.
23) Laplaza, C. E.; Odom, A. L.; Davis, W. M.; Cummins, C. C.; Protasiewicz, J. D. *J. Am. Chem. Soc.* **1995**, *117*, 4999.
24) Laplaza, C. E.; Cummins, C. C. *Science* **1995**, *268*, 861-863.
25) Laplaza, C. E.; Johnson, A. R.; Cummins, C. C. *J. Am. Chem. Soc.* **1996**, *118*, 709-710.
26) Bottomley, F. *Polyhedron* **1992**, *11*, 1707-1731.
27) Smith III, M. R.; Matsunaga, P. T.; Andersen, R. A. *J. Am. Chem. Soc.* **1993**, *115*, 7049-7050.
28) Matsunaga, P. T.; Hillhouse, G. L.; Rhenigold, A. L. *J. Am. Chem. Soc.* **1993**, *115*, 2075-2077.
29) Arzoumanian, H.; Nuel, D.; Sanchez, J. *J. Mol. Cat.* **1991**, *65*, L9-L11.
30) Okabe, H. *Photochemistry of Small Molecules*; Wiley: New York, 1978.
31) Hintz, P. A.; Sowa, M. B.; Ruatta, S. A.; Anderson, S. L. *J. Chem. Phys.* **1991**, *94*, 6446-6458.
32) Kramlich, J. C.; Linak, W. P. *Prog. Energy Combust. Sci.* **1994**, *20*, 149.
33) Yount, J. T.; Lenahan, P. M.; Krick, J. T. *J. Appl. Phys.* **1994**, *76*, 1754.
34) Wanandi, P. W.; Davis, W. M.; Cummins, C. C.; Russell, M. A.; Wilcox, D. E. *J. Am. Chem. Soc.* **1995**, *117*, 2110-11.
35) Peters, J. C.; Johnson, A. R.; Odom, A. L.; Wanandi, P. W.; Davis, W. M.; Cummins, C. C. *J. Am. Chem. Soc.* **1996**, *118*, 10175.
36) Sur, S. K. *J. Magnetic Resonance* **1989**, *82*, 169-73.
37) Johnson, A. R.; Davis, W. M.; Cummins, C. C. *Organometallics* **1996**, *18*, 3825-3835.

References begin on page 184

38) Wertz, J. E.; Bolton, J. R. *Electron Spin Resonance: Elementary Theory and Practical Applications*; McGraw-Hill: New York, 1986.
39) Mombourquette, M. J.; Weil, J. A.; McGavin, D. G. *Computer Program EPR-NMR*; Department of Chemistry: University of Saskatchewan, Canada, 1993.
40) Laplaza, C. E.; Davis, W. M.; Cummins, C. C. *Organometallics* **1995**, *14*, 577-580.
41) Fickes, M. G.; Cummins, C. C., Unpublished Results.
42) As polonium is radioactive, it is not generally included in the chalcogen series. See reference 12 for a similar disclaimer from Gerard Parkin.
43) Kuchta, M. C.; Parkin, G. *J. Chem. Soc., Chem. Commun.* **1994**, 1351.
44) All CV experiments were carried out by Marc Johnson.
45) Gritzner, G.; Kuta, J. *Pure Appl. Chem.* **1984**, *56*, 461-8.
46) Thermochemical experiments were carried out in collaboration with Steve Nolan and Scafford Serron at the University of New Orleans.
47) Shaofeng, L.; Pilcher, G. *J. Chem. Thermodynamics* **1988**, *20*, 463-5.
48) Cox, J. D.; Pilcher, G. *Thermochemistry of Organic and Organometallic Compounds*; Academic Press: New York, 1970.
49) Chase, M. W. *et. al. JANAF Thermochemical Tables* ; American Chemical Society: New York, 1986.
50) Unpublished Results by Clark Landis at the University of Wisconsin communicated by Christopher Cummins.
51) Holm, R. H.; Donahue, J. P. *Polyhedron* **1993**, *12*, 571-89.
52) Mealli, C.; Proserpio, D. M. *J. Chem. Educ.* **1990**, *67*, 399-402.
53) Mealli, C.; Proserpio, D. M. *CACAO (Computer Aided Composition of Atomic Orbitals);* 4.0 ed.Florence (Italy), 1994.
54) Cui, Q.; Musaev, D. G.; Svensson, M.; Sieber, S.; Morokuma, K. *J. Am. Chem. Soc.* **1995**, *117*, 12366.
55) Quantum calculations were carried out in collaboration with Jamal Musaev and Keiji Morokuma at Emory University.
56) Becke, A. D. *Phys. Rev. A* **1988**, *38*, 3093.
57) Becke, A. D. *J. Chem. Phys.* **1993**, *98*, 5648.
58) Lee, C.; Yang, W.; Parr, R. G. *Phys. Rev. B* **1988**, *37*, 785.
59) Dunning, J. T. H.; Hay, P. J. *Methods of Electronic Structure Theory*; Plenum Press: New York, 1977, pp 1-27.
60) Hollwarth, A.; Bohme, M.; Dapprich, S.; Ehlers, A. W.; Gobbi, A.; Jonas, V.; Kohler, K. F.; Stegmann, R.; Veldkamp, A.; Frenking, G. *Chem. Phys. Lett.* **1993**, *203*, 237.
61) Hay, P. J.; Wadt, W. R. *J. Chem. Phys.* **1985**, *82*, 284.
62) Hay, P. J.; Wadt, W. R. *J. Chem. Phys.* **1985**, *82*, 299.
63) Frisch, M. J.; Trucks, G. W.; Schlegel, H. B.; Gill, P. M. W.; Johnson, B. G.; Robb, M. A.; Cheeseman, J. R.; Keith, T. A.; Petersson, G. A.; Montgomery, J. A.; Raghavachari, K.; Al-Laham, M. A.; Zakrzewski, V. G.; Ortiz, J. V.; Foresman, J. B.; Cioslowski, J.; Stefanov, B. B.; Nanayakkara, A.; Challacombe, M.; Peng, C. Y.; Ayala, P. Y.; Chen, W.; Wong, M. W.; Andres, J. L.; Replogle, E. S.; Gomperts, R.; Martin, R. L.; Fox, D. J.; Binkley, J. S.; DeFrees, D. J.; Baker, J.; Stewart, J.; Head-Gordon, M.; Gonzales, C.; Pople, J. A. *GAUSSIAN-94*; Gaussian Inc.: Pittsburgh, PA, 1995.
64) Ricca, A.; Bauschlicher, J. C. W. *J. Phys. Chem.* **1994**, *98*, 12899.
65) Ricca, A.; Bauschlicher, J., C. W. *J. Phys. Chem.* **1995**, *99*, 5922.
66) Shin, K.; Schrock, R. R.; Kempe, R.; Davis, W. M. *J. Am. Chem. Soc.* **1994**, *116*, 8804.
67) Terry, J. O.; Futrell, J. H. *Can. J. Chem.* **1968**, 664.
68) Weydert, M.; Brennan, J. G.; Andersen, R. A.; Bergman, R. G. *Organometallics* **1995**, *14*, 3942.

References begin on page 184

69) Pryor, W. A. *Free Radicals*; McGraw-Hill: New York, 1966.
70) Rabinovich, D.; Parkin, G. *Inorg. Chem.* **1994**, *33*, 2313-2314.
71) Kraatz, H.; Boorman, P. M.; Parvez, M. *Can. J. Chem.* **1993**, *71*, 1437.
72) Fischer, H.; Zeuner, S.; Gerbing, U.; Riede, J.; Kreiter, C. J. *J. Organometal. Chem.* **1989**, *377*, 105.
73) Ansari, M. A.; Mahler, C. H.; Ibers, J. A. *Inorg. Chem.* **1989**, *28*, 2669.
74) Ball, J. M.; Boorman, P. M.; Fait, J. F.; Kraatz, H.; Richardson, J. F.; Collison, D.; Mabbs, F. E. *Inorg. Chem.* **1990**, *29*, 3290.
75) Seligson, A. L.; Arnold, J. *J. Am. Chem. Soc.* **1993**, *115*, 8214-8220.
76) Gindelberger, D. E.; Arnold, J. *Inorg. Chem.* **1993**, *32*, 5813-5820.
77) Binstead, R. A.; Zuberbühler, A. D. *SPECFIT;* 2.09 ed.; Spectrum Software Associates: Chapel Hill, NC, 1995.
78) Schrock, R. R.; Sturgeoff, L. G.; Sharp, P. R. *Inorg. Chem.* **1983**, *22*, 2801.
79) Lawrance, G. A. *Chem. Rev.* **1986**, *86*, 17-33.
80) Chisholm, M. H.; Folting, K.; Huffman, J. C.; Kirkpatrick, C. C. *Inorg. Chem.* **1984**, *23*, 1021-1037.
81) Odom, A. L.; Cummins, C. C. *Polyhedron* **1997**, submitted.
82) Peters, J. C.; Odom, A. L.; Cummins, C. C. *Chem. Com.* **1997**, submitted.
83) Kubas, G. J. *Acc. Chem. Res.* **1994**, *27*, 183-190.
84) Ellis, R.; Henderson, R. A.; Hills, A.; Hughes, D. L. *J. Organometal. Chem.* **1987**, *333*, C6.
85) Lorenz, I.; Walter, G.; Hiller, W. *Chem. Ber.* **1990**, *123*, 979.
86) Butler, I. S.; Fenster, A. E. *J. Organometal. Chem.* **1974**, *66*, 161-194.
87) Dombek, B. D.; Angelici, R. J. *Inorg. Chem.* **1976**, *15*, 2397.
88) Kolb, O.; Werner, H. *Angew. Chem.* **1982**, *94*, 207.
89) Lotz, S.; Pille, R. R.; Van Rooyen, P. H. *Inorg. Chem.* **1986**, *25*, 3053-3056.
90) Laplaza, C. E.; Davis, W. M.; Cummins, C. C. *Angew. Chem. Int. Ed. Engl.* **1995**, *34*, 2042-2044.
91) Pangborn, A. B.; Giardello, M. A.; Grubbs, R. H.; Rosen, R. K.; Timmers, F. J. *Organometallics* **1996**, *15*, 1518-1520.
92) Perrin, D. D.; Armarego, L. F. *Purification of Laboratory Chemicals*; Pergamon Press: New York, 1988.
93) Lardon, M. *J. Am. Chem. Soc.* **1970**, *92*, 5063-5066.
94) Akitt, J. W., Dixon, K. R.; Goodfellow, R. J.; Howarth, O. W.; Jameson, C. J.; Kennedy, J. D.; Mann, B. E.; Mason, J.; McFarlane, H. C. E.; McFarlane, W.; Rattle, H. W. E.; Rehder, D. *Multinuclear NMR*; Plenum: New York, 1987.
95) Bard, A. J.; Faulkner, L. R. *Electrochemical Methods*; John Wiley & Sons: New York, 1980.
96) Carey, F. A.; Sundberg, R. J. *Advanced Organic Chemistry, Part A;* 3rd ed.; Plenum Press: New York, 1990, pp 194.
97) Johnson, A. R.; Peters, J. C.; Cummins, C. C., Unpublished Results.
98) Ojelund, G. ;. W., I. *Acta Chem. Scand.* **1968**, *22*, 1691-1699.
99) Kilday, M. V. *J. Res. Natl. Bur. Stand. (U. S.)* **1980**, *85*, 467-481.
100) Nolan, S. P.; Hoff, C. D. *J. Organometal. Chem.* **1985**, *282*, 357-362.

References begin on page 184

Chapter III: Activation of a Molybdenum Nitride Derived from Molecular Nitrogen

References begin on page 209

Section 3.1: Introduction

$Mo(N[R]Ar)_3$ (**2.1**, R = $C(CD_3)_2CH_3$, Ar = 3,5-$C_6H_3Me_2$) reacts with dinitrogen at -35 °C to form a dimer with a dinitrogen bridge.[1,2] Warming the complex results in clean N-N bond scission, forming the tetrahedral $NMo(N[R]Ar)_3$ (**3.1**). Extensive experimental investigation and theoretical calculations have been reported on the mechanism and structures of the intermediates proposed in this unique reaction.[3-5] The cleavage reaction can be made to occur at room temperature by the addition of $NMo(O\text{-}t\text{-butyl})_3$ or elemental sodium, but turnover numbers are very low.[6,7] This mild and efficient fixation of dinitrogen could in principle be made catalytic if an efficient means for regeneration of the paramagnetic complex **2.1** were found. This regeneration would result in the productive formation of "fixed" nitrogen-containing molecules, with ammonia being an obvious potential target.

Potential regenerative pathways include N-atom transfer,[8,9] and nitrene transfer,[10,11] either to a transition metal complex or an organic substrate. A more elegant approach involves stepwise alkylation of the nitride, with the hopeful generation of a labile amine complex. Addition of Lewis acidic substrates to transition metal nitrides to form imido ligands is precedented for many electrophilic reagents such as boron trihalides,[12] Ph_3C^+,[13] PhC(O)Cl,[13] trifluoroacetic anhydride,[14] chlorotrimethylsilane,[15] methyl iodide[13,16-18] and others.[15,19,20] This chapter describes initial experiments designed to activate the molybdenum nitride functionality in **3.1** by methylation with methyl iodide. Also reported are the reactions of **2.1** with a variety of amines. The experiments are designed to explore the compatibility or reactivity of **2.1** with these reagents, as they would be likely targets for "fixed" nitrogen containing molecules. Related chemistry concerning the activation of a coordinated phosphorus atom in $PMo(N[R]Ar)_3$ has recently been reported.[21,22]

References begin on page 209

Section 3.2: Activation of a Molybdenum Nitride

(i) Synthesis and Characterization of Mo(NMe)(N[R]Ar)$_3$ (3.3)

Nitrido **3.1**, which is obtained from the reaction of tris-anilide **2.1** with dinitrogen or mesityl azide, is methylated by stirring in neat methyl iodide for a period of 14 hours. This reaction was first carried out by Catalina Laplaza. Removal of the excess methyl iodide results in a dark orange material, [Mo(NMe)(N[R]Ar)$_3$][I] (**3.2**) which is insoluble in hydrocarbon solvents (Scheme 3.1). The complex is purified by pentane diffusion into THF, and is isolated in greater than 90% yield. The salt is unstable in solution for long periods of time (more than a few hours) but is stable indefinitely in the solid state at -35 °C.

The ^{1}H NMR spectrum of **3.2** exhibits a resonance at 5.15 ppm which is attributed to the methyl imide functionality. The methyl imide carbon resonance cannot be definitively assigned from the ^{13}C NMR spectrum taken in chloroform as it appears to overlap the aryl methyl resonance at 21.55 ppm. The ^{13}C NMR spectrum taken in THF shows some separation of the two resonances, but the complex decomposes more rapidly in THF, precluding an analysis of the spectrum. The methyl imide ^{13}C NMR chemical shift is substantially different from those observed in [OsCp(CH_2SiMe_3)$_2$(NMe)][I], with a resonance at 61.5 ppm (CD_2Cl_2),[16] and [Os(NMe)(CH_2SiMe_3)$_4$], with a resonance at 46.2 ppm (C_6D_6).[17]

References begin on page 209

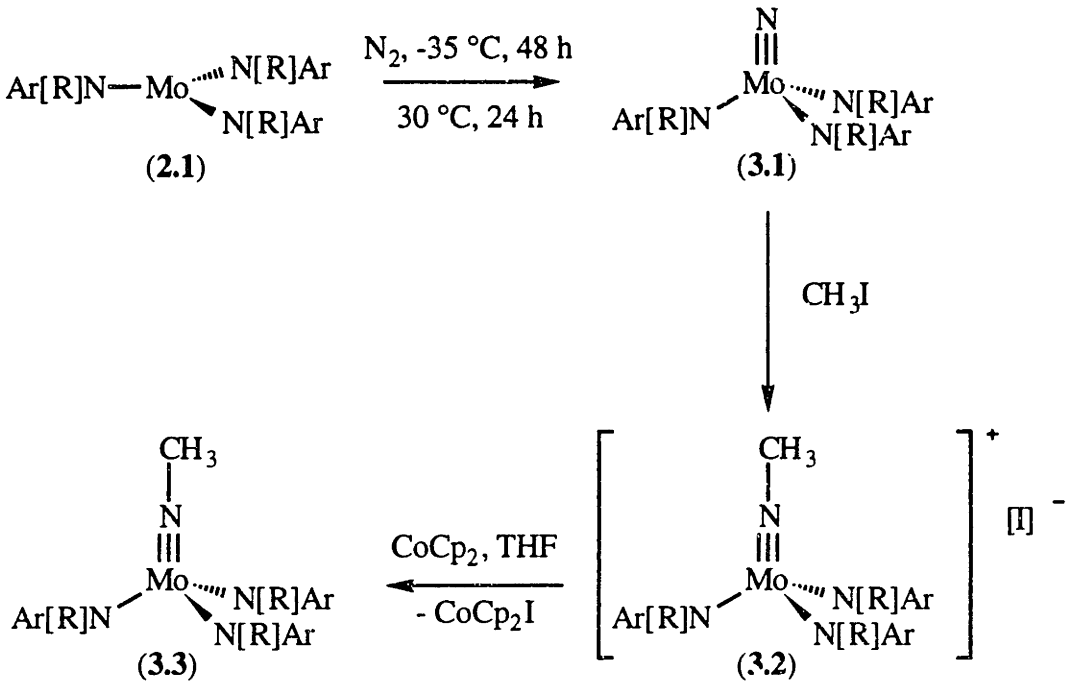

Scheme 3.1: Stepwise activation of dinitrogen to give a methylimide complex

Treatment of the cationic complex **3.2** with cobaltocene (one equivalent) results in the immediate formation of a dark brown solution and a bright yellow solid ($CoCp_2I$) which are separated by filtration (Scheme 3.1). The neutral methyl imide complex **3.3** is isolated quantitatively by dissolution in a minimum of pentane followed by precipitation with acetonitrile.[23] The complex is purified by recrystallization and isolated in ca. 50% yield. The low isolated yield is due to the extreme solubility of the complex and does not reflect low conversion to the desired complex or decomposition; the reaction is quantitative as measured by ^2H NMR spectroscopy.

Methyl imide **3.3** exhibits a single resonance in the ^2H NMR spectrum at 7.867 ppm, which corresponds well to chemical shifts observed in other d^1 molybdenum complexes with the N[R]Ar ligand framework.[24,25] The methyl resonance appears at -51.3 ppm in the ^1H NMR spectrum. The magnetic moment of the complex as measured by NMR techniques[26] is found to be 1.95 μ_B, in good agreement with the spin-only value

References begin on page 209

of 1.73 μ_B. An EPR spectrum of the complex in toluene at room temperature shows an isotropic g value of 1.949. The spectrum exhibits a six line coupling pattern which is approximately 25% of the area of the central peak, reflecting the natural abundance of the s = 5/2 nuclei ^{95}Mo and ^{97}Mo ($A(^{95,97}Mo)$ = 37 G).[27] Due to the similar gyromagnetic ratios of the two molybdenum nuclei, separate couplings to both ^{95}Mo and ^{97}Mo are not seen.[27,28] The frozen glass spectrum (102 K) exhibits a rhombic pattern, shown in Figure 3.1, with g values of 1.976, 1.956 and 1.915, but the anisotropic coupling constants are not well resolved.

(ii) Attempted Synthesis of $Mo(NMe_2)(N[R]Ar)_3$

Further functionalization of the methylimido fragment in **3.3** with additional methyl iodide could result in the formation of $[Mo(NMe_2)(N[R]Ar)_3][I]$, one step closer to removing the dinitrogen derived nitrogen atom in a productive fashion. Complex **3.3** reacts with excess methyl iodide in a fashion similar to that used for the synthesis of **3.2**, but examination of the reaction mixture by ^{1}H NMR spectroscopy after a 15 hour period shows only the presence of cationic **3.2**. Methyl iodide acts as an oxidant rather than as an electrophile in this case. The fate of the methyl radical equivalent which must form in this reaction is unknown. This result is unexpected, as from a molecular orbital point of view, the methyl imide should have nucleophilic character.[29] However, in this case the steric environment of the pocket formed by the *tert*-butyl groups dominates the reaction chemistry, blocking approach of an electrophile to the imide and forcing an electron transfer event.

References begin on page 209

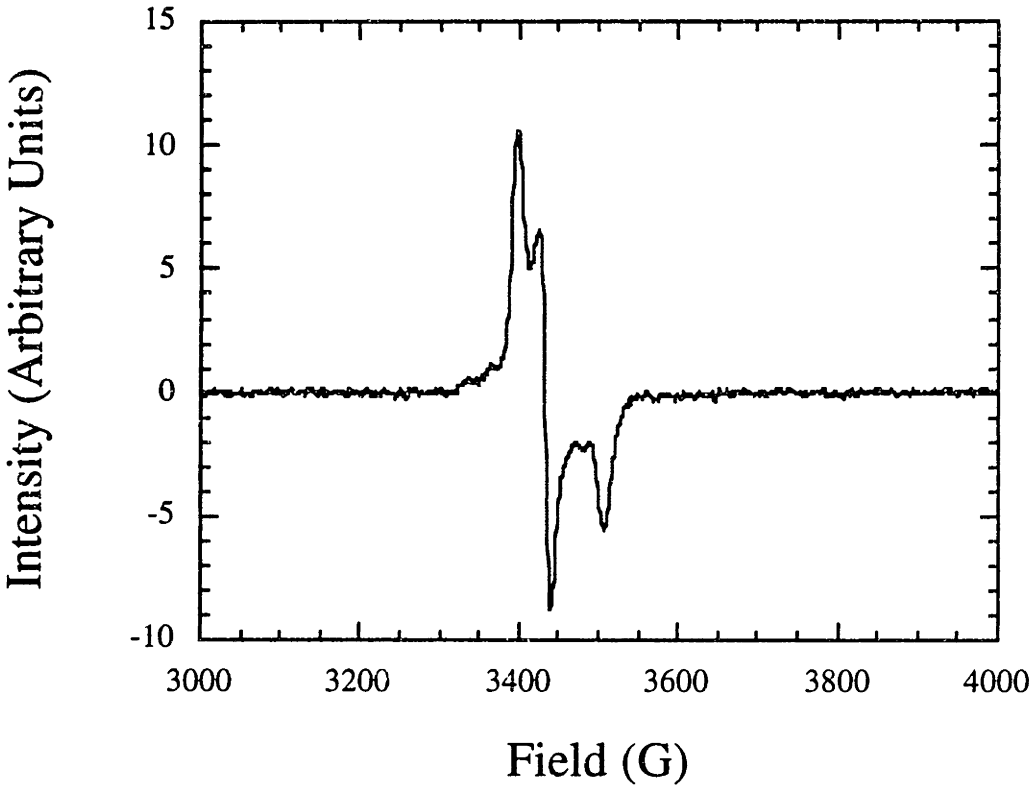

Figure 3.1: EPR spectrum (97 K, toluene) of $Mo(NMe)(N[R]Ar)_3$ (**3.3**) with $g_1 = 1.976$, $g_2 = 1.956$, $g_3 = 1.915$.

References begin on page 209

Cationic complex **3.2** also reacts with dimethylmagnesium. However, rather than addition of the methyl group to form the dimethylamide complex, reduction occurs, forming the neutral methyl imide **3.3**. Again, the electron transfer process suggests that the imide functionality is sterically protected.

(iii) Synthesis and Characterization of IMo(N[R]Ar)$_3$ (3.4)

Another potential entry into the Mo(IV) dimethylamide complex is through metathesis from a Mo(IV) halide complex. Initial experiments in this area were carried out by Catalina Laplaza. The iodide, IMo(N[R]Ar)$_3$ (**3.5**), is prepared by simple addition of one half equivalent iodine to the tris anilide **2.1** (Scheme 3.2). The addition results in a rapid color change from dark red to very dark green. The complex is obtained by crystallization from ether in 83% yield.

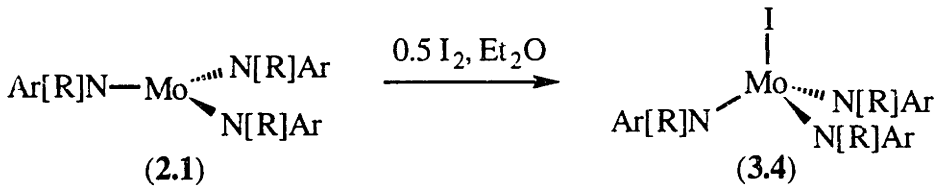

(**2.1**) (**3.4**)

Scheme 3.2: Oxidation of Mo(N[R]Ar)$_3$ (**2.1**) with Iodine

The ^{1}H NMR spectrum of **3.4** exhibits unusually sharp resonances, and the ^{2}H NMR resonance for the d_6-*tert*-butyl group is solvent dependent, appearing at 8.97 ppm in ether and 6.36 ppm in benzene. Variable temperature Evans method magnetic susceptibility measurements are suggestive of a spin equilibrium process.[30] Although the data are poor, the measured susceptibilities are so low that the diamagnetic correction factor dominates, a clear temperature dependence of μ_{eff} is observed (Figure 3.2).

References begin on page 209

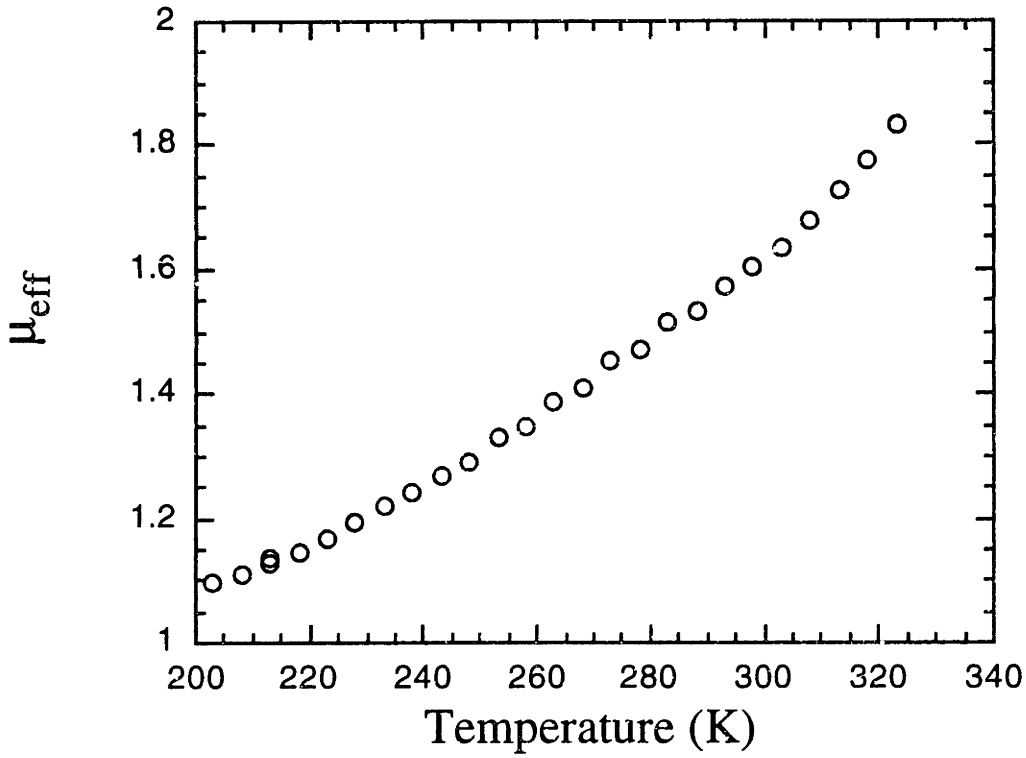

Figure 3.2: Temperature dependence of the Evans method magnetic susceptibility of complex **3.4**.

References begin on page 209

Examination of the iodide complex by SQUID magnetometry over the temperature range from 5 to 350 K, shows large fluctuations in the data over a temperature of 220 K. The SQUID data from 5 to 220 K to are presented in Figure 3.3, clearly showing a decrease in paramagnetism as measured by χ at low temperature. The dependence of μ on temperature, which is calculated from the χ values, is shown in Figure 3.4. The complex exhibits paramagnetic behavior at all temperatures, but μ approaches zero at 0 K. At 200 K, the complex is about 15% in the s = 2 state, with the remainder in the spin-paired state. It is not possible to accurately measure magnetic behavior of the complex above room temperature because the complex decomposes rapidly to unknown products when heated. Attempts to fit the data to suitable spin equilibrium models have not been successful,[30] due perhaps to the low absolute concentration of triplet spin of 15% which is observed at 220 K. EPR spectra taken at room temperature and 101 K also support a spin equilibrium. Both spectra exhibit a primary g value of 1.98, with features at g = 2.03 and 1.95, but the intensity of the low temperature spectrum is significantly reduced; the room temperature spectrum is shown in Figure 3.5.

When iodide **3.4** and lithium dimethylamide are mixed no reaction is readily observed at room temperature, and the color of the reaction solution does not change from dark green. Monitoring the reaction after 45 minutes by ^{1}H NMR spectroscopy shows unreacted starting material, tris anilide **2.1** and free HN[R]Ar, as well as decomposition products. This suggests that reduction of rather than substitution on **3.4** is the dominant mode of reactivity, a result which is also attributed to the substantial steric protection of the Mo center. There is no reaction of iodide **3.4** with the BH_3 adduct of dimethylamine in the presence of triethylamine as a base, as determined by ^{1}H NMR spectroscopy.

References begin on page 209

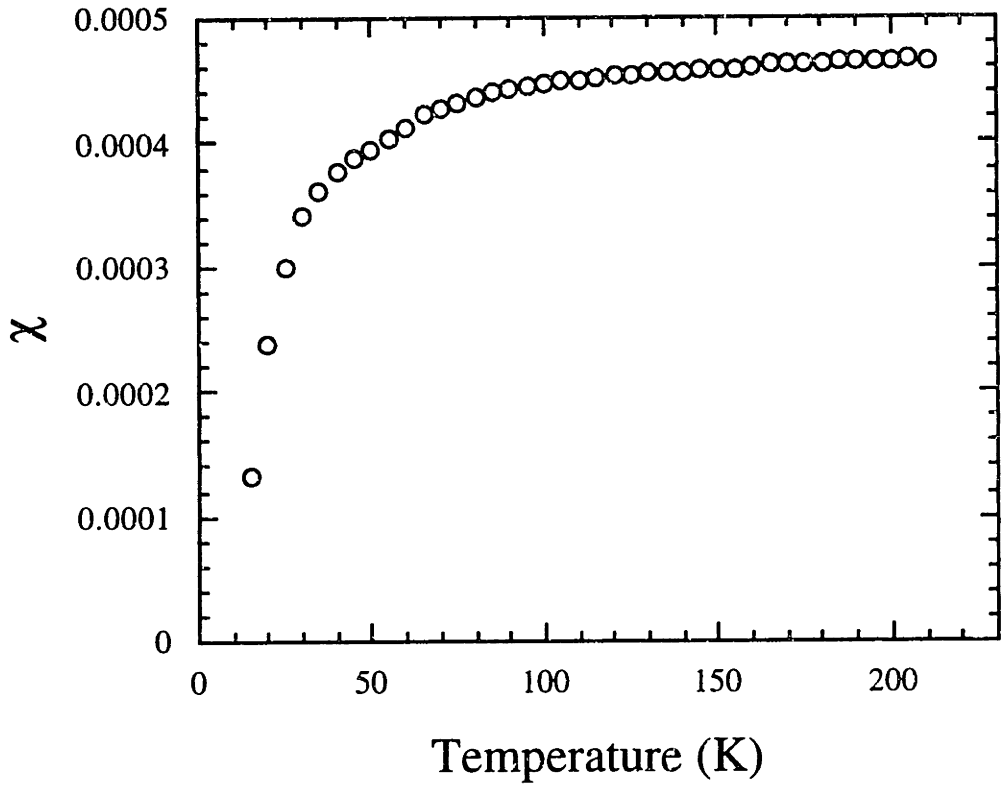

Figure 3.3: SQUID magnetic susceptibility data of complex **3.4** from 5 to 220 K.

References begin on page 209

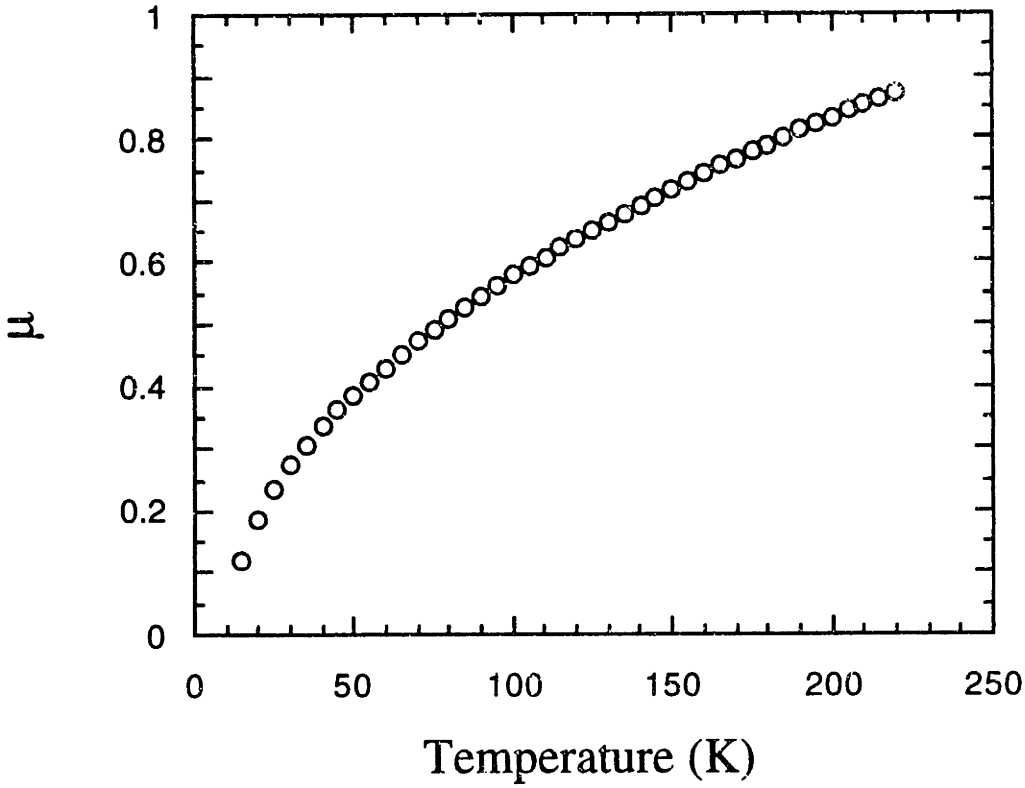

Figure 3.4: Magnetic susceptibility of complex **3.4** obtained from SQUID measurements from 5 to 220 K.

References begin on page 209

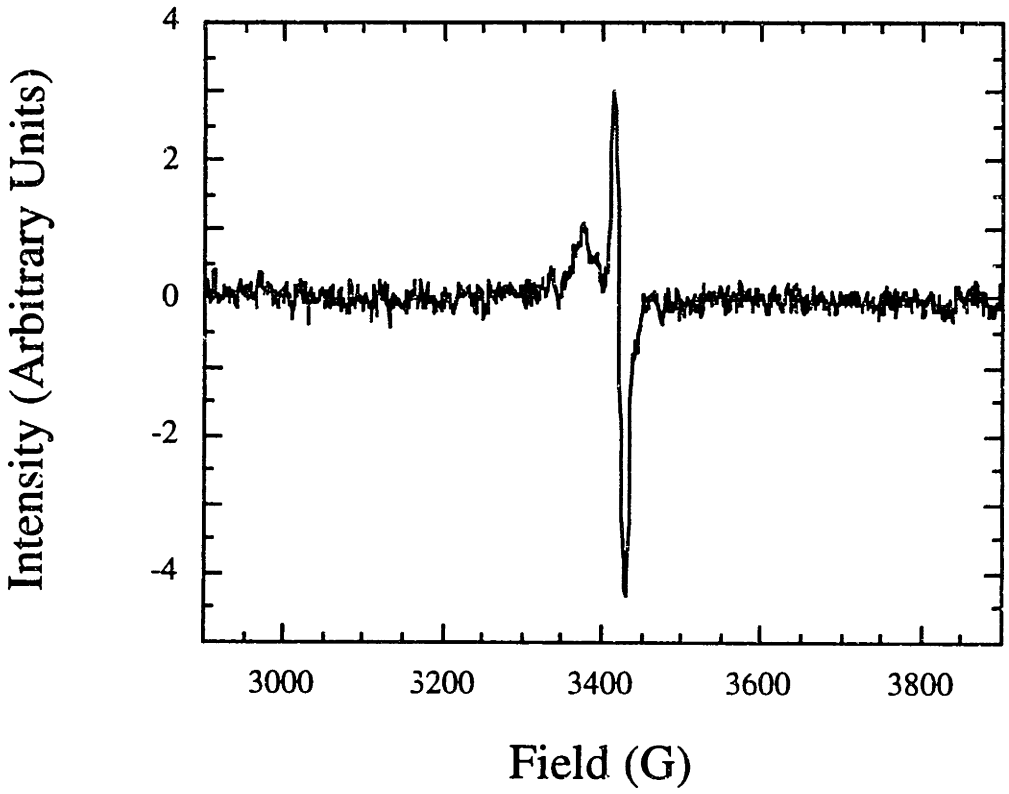

Figure 3.5: EPR spectrum (28 °C, toluene) of $IMo(N[R]Ar)_3$ (**3.4**) (See text for further details).

References begin on page 209

Section 3.3: Reactions of $Mo(N[R]Ar)_3$ (2.1) with Amines

Neither methylation of the methyl imide **3.3** nor metathesis from iodide **3.4** are productive routes into a dimethylamide complex. Therefore, the reaction of tris anilide **2.1** with a variety of amine reagents is examined in order to explore the steric and/or electronic constraints on this system with regard to the eventual synthetic goal of productive nitrogen fixation.

(i) 2-Methylaziridine

2-Methylaziridine reacts with **2.1** (Scheme 3.3); however, this does not result in the formation of $Mo(NH)(N[R]Ar)_3$, which is the expected product. Instead, nitrido **3.1** is formed, as well as an equivalent of propylene which is detected by ^1H NMR spectroscopy.[31] Free HN[R]Ar is also observed to be produced with time. No evidence for dihydrogen is observed in the ^1H NMR spectrum, and there are no observable side products, so it seems likely that the hydrogen atom is delivered to an N[R]Ar fragment resulting from some sacrificial quantity of tris-anilide complex **2.1**.

(ii) 7-Amino-7-aza-benzonorbornadiene

Tris anilide **2.1** also reacts with 7-amino-7-aza-benzonorbornadiene[32,33] (Scheme 3.3), generating an equivalent each of nitrido **3.1** and anthracene as determined by ^1H NMR spectroscopy. Approximately one equivalent of free HN[R]Ar also grows in with time, suggesting again that the hydrogen atom in the starting amine reacts with some sacrificial quantity of complex **2.1**. Repeating the reaction with the deuterated amine gives similar results. Analysis of the reaction mixture by ^2H NMR spectroscopy shows the presence of DN[R]Ar at about 3.0 ppm.

References begin on page 209

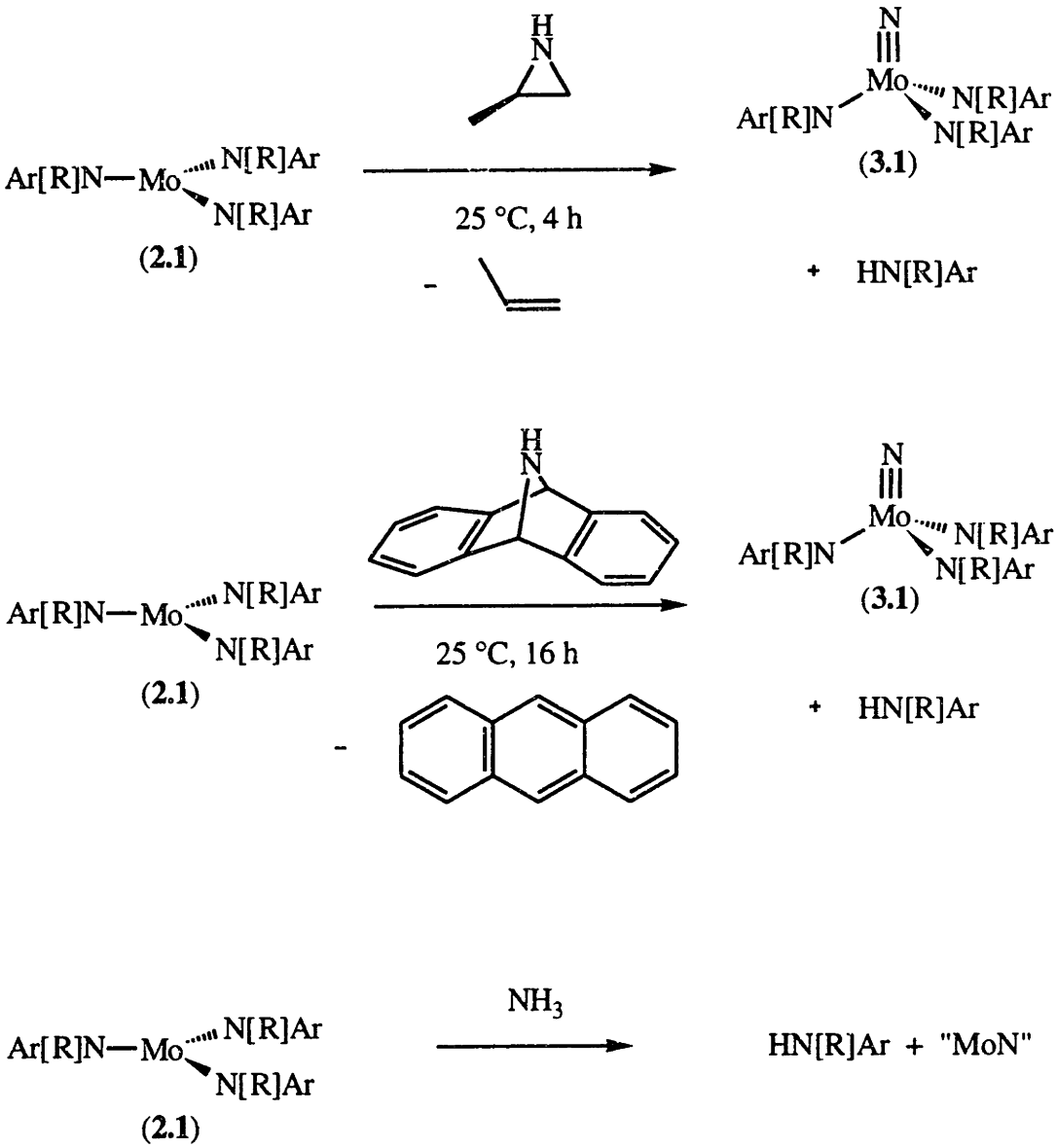

Scheme 3.3: Successful nitrogen atom transfer from organic amines to $Mo(N[R]Ar)_3$ (**2.1**).

(iii) Ammonia

Complex **2.1** reacts with one equivalent of ammonia, freshly distilled from sodium. This reaction results in complete decomposition of the starting complex **2.1**, with formation of almost 90% free HN[R]Ar. A very small amount of nitrido **3.1** is detected in

References begin on page 209

the reaction mixture. This suggests that hydrogenation or protonation of **3.1** would not result in clean formation of ammonia, counter to a predicted result.[34]

(iv) *N*-Methylaziridine

There is no reaction of complex **2.1** with a variety of other amines (Scheme 3.4). Complex **2.1** does not react with *N*-methyl aziridine to generate methyl imide complex **3.3** directly. In fact, mixing of the two reagents for 24 hours does not result in any consumption of starting material. Neither heating the reaction at 55 °C for two hours nor irradiation with UV light for 90 minutes effects the transformation. The fact that no reaction occurs suggests that tertiary amines are not capable of bonding to the tris anilide. This is most likely due to a steric effect; however, the electronic effects of a nucleophile binding to **2.1** should be considered as well. Bringing in a lone pair as a σ donor to the tris anilide would force a high-spin to low-spin conversion of complex **2.1** in order to access an empty σ-type orbital. This transformation is not very favorable as the calculated energy gap between the ground quartet (^{4}A') and first excited doublet (^{2}A') state for $Mo(NH_2)_3$ is 14-28 kcal·mol^{-1}.[35] There should therefore be an electronic barrier to amine binding as well as a steric barrier. It has been shown previously that triethylphosphine does not react with **2.1**.[24,25] This result suggests that if an tertiary amine complex of $Mo(N[R]Ar)_3$ were prepared, it would be labile and the amine would be lost, regenerating free tris anilide **2.1**.

(v) Azetidine

Complex **2.1** also does not react with azetidine. This amine would be expected to react similarly to 2-methylaziridine on a steric basis, generating nitride **3.1**. However, there does not appear to be any reaction with the four-membered amine. The reduced strain energy in this molecule may be the cause for reduced reactivity, as the two amines have similar steric profiles.

References begin on page 209

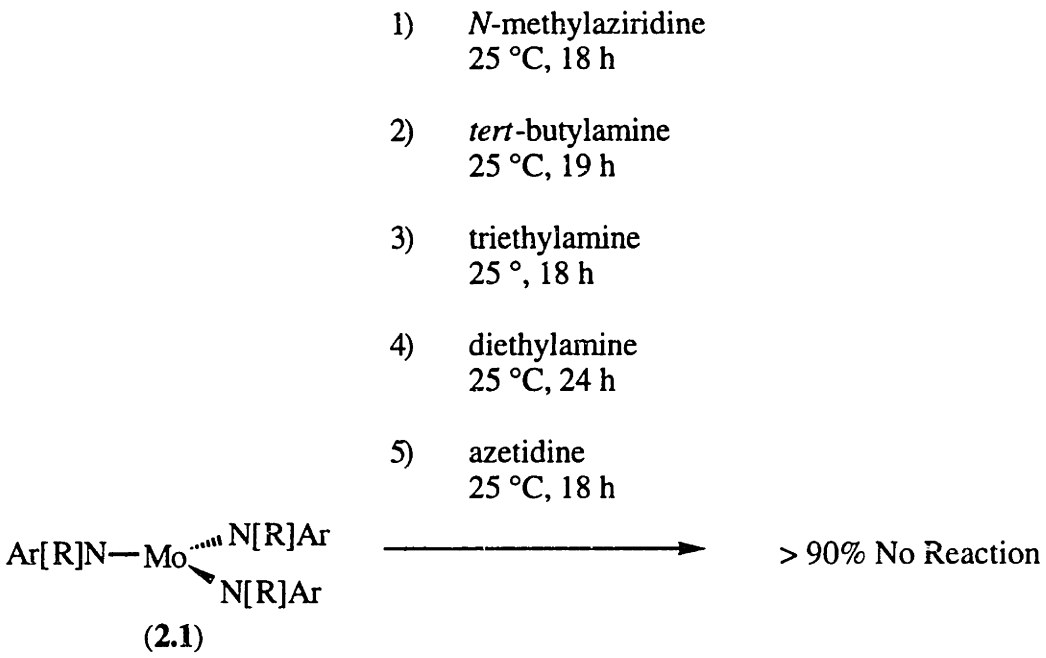

Scheme 3.4: Unsuccessful nitrogen atom transfer from organic amines to $Mo(N[R]Ar)_3$ (**2.1**).

(vi) *tert*-Butylamine, Triethylamine and Diethylamine

There is no reaction of tris anilide **2.1** with one equivalent of either *tert*-butyl amine, triethylamine or diethylamine over a period of 24 hours. The lack of reactivity with triethylamine is not surprising based on the lack of reactivity of **2.1** with triethylphosphine as mentioned in Section 2.8.

(viii) General Trends

The above results suggest reactivity for only a select class of amines with tris-anilide **2.1**. Tertiary amines seem to be prohibited from reaction on a steric ground; the bulky *tert*-butyl groups of the N[R]Ar ligand protect the molybdenum center from incoming amine reagents. Secondary amines are capable of delivering a nitrogen atom to **2.1** if the

References begin on page 209

organic fragment which must be lost is stabilized. Reorganization of 2-methylaziridine to generate propylene, or 7-amino-7-aza-benzonorbornadiene to generate anthracene, with the concomitant ejection of the [NH] fragment, occurs only through the π system, with minimal reorganization energy. Azetidine does not react because the 1,3-diradical which would form is a high-energy species which must undergo reorganization through the σ system (a 1,2-hydrogen shift) to generate propylene. Ammonia is in a special class by itself: its small size allows approach of the Mo and N atoms, and the hydrogen atoms which are lost can be transferred to N[R]Ar fragments, resulting in complete decomposition of the tris-anilide fragment.

Section 3.4: Conclusion

It is possible to begin conversion of a dinitrogen derived N-atom on a molybdenum complex to a more useful, "fixed" state. Methylation of the nitrido functionality in **3.1** results in clean, high yield formation of the methyl imide cation, which is reduced to the neutral complex with cobaltocene. It has not yet been possible to further derivatize the imido function, nor is it yet possible to observe clean metathesis reactions with the iodide **3.4**. The reactions, or lack thereof, which are observed between tris anilide complex **2.1** and a variety of amines suggest that there is a large steric barrier to reaction in the pocket at the metal center. The electronic rearrangement required to bind an amine to the molybdenum center also presents an additional barrier. Small amines such as ammonia or 2-methylaziridine are permitted to approach the complex, and those with stabilized leaving groups like 2-methylaziridine or 7-aza-dibenzonorbornadiene deliver a nitrogen atom. These results do support the idea that if a way is found to derivatize the nitrido functionality to a neutral amine complex, perhaps by making the nitride and imide functionalities more nucleophilic through changing the basal ligand set, it would be labile, resulting in regeneration of the tris anilide complex **2.1**.

References begin on page 209

Section 3.5: Experimental

3.5.1 General Considerations

General experimental details are as described in Chapters I and II. Solvents were dried and deoxygenated according to previously published procedures.[36] Diethyl ether was dried according to a procedure by Grubbs.[37] Methyl iodide was distilled from CaH_2 and stored over sieves at -35 °C. 7-Amino-7-azabenzonorbornadiene,[32,33] $Mo(N[R]Ar)_3$,[1] and $NMo(N[R]Ar)_3$,[1] were prepared according to published procedures. Iodine was sublimed prior to use. *N*-methyl aziridine was prepared from *N*-methylaminoethanol.[10,38] Other chemicals were purified and dried via standard procedures[39] or used as received.

Magnetic susceptibilities were measured by NMR spectroscopy.[26] NMR spectra were recorded on Varian XL-300, Varian Unity-300 or Varian VXR-500 spectrometers. Chemical shifts are reported with respect to internal solvent. ^2H chemical shifts are reported with respect to external C_6D_6. EPR spectra were recorded on a Brucker ESP 300 spectrometer in sealed quartz tubes in toluene at either ambient temperature or low temperature by using a liquid nitrogen cooled nitrogen stream. SQUID data were acquired as reported previously[36] using a Quantum Design SQUID magnetometer. CHN analyses were performed by Oneida Research Services (Whitesboro, NY) or Microlytics (South Deerfield, MA). Melting points were obtained in sealed glass capillaries and are uncorrected.

3.5.2 Synthesis of Complexes

(i) $[Mo(NMe)(N[R]Ar)_3][I]$ (3.2). $NMo(N[R]Ar)_3$ (**3.1**, 0.1556 g, 0.2369 mmol) was dissolved in methyl iodide (4.0 mL) and stirred for 14 hours. The color of the reaction solution gradually changed from dark brown/orange to dark yellow. The excess iodomethane was removed *in vacuo*, resulting in a dark solid material which was insoluble

References begin on page 209

in pentane and only slightly soluble in ether. The material dissolved in THF (ca. 1 mL) and was precipitated by the addition of pentane (ca. 15 mL) (0.1740 g, 0.2178 mmol, 92%). The compound is slightly unstable in both THF and $CDCl_3$ solution. M.P. 110 °C (dec). ^1H NMR (300 MHz, $CDCl_3$): δ = 6.989 (s, 3H, para); 5.620 (s, 6H, ortho); 5.151 (s, 3H, NCH_3); 2.163 (s, 18H, Ar*Me*); 1.255 (s, 9H, $C(CD_3)_2CH_3$). ^{13}C NMR (125 MHz, $CDCl_3$): δ = 145.46 (s, ipso); 138.72 (q, $^2J_{CH}$ = 6 Hz, meta); 130.88 (d, J = 155.6 Hz, para); 128.55 (d, J = 160.2 Hz, ortho); 68.22 (s, $C(CD_3)_2CH_3$); 32.10 (q, J = 126.7 Hz, $C(CD_3)_2CH_3$); 31.44 (m, $C(CD_3)_2CH_3$); 21.55 (q, J = 122.07 Hz, Ar*Me* and N*Me*). Calcd for $C_{37}H_{39}D_{18}IMoN_4$: C, 55.63; H, 7.19; N, 7.01. Found: C, 56.13; H, 7.64; N, 6.53.

(ii) Mo(NMe)(NRAr)$_3$ (3.3). [Mo(NMe)(N[R]Ar)$_3$][I] (**3.2**, 0.1740 g, 0.2178 mmol) was dissolved in THF (3.5 mL) and $CoCp_2$ (0.0409 g, 0.2163 mmol, 0.99 eq) in THF (1.5 mL) was added. The solution rapidly changed color to dark brown. The THF was removed *in vacuo* and the resulting solid was extracted with benzene, leaving behind a yellow solid which was filtered away ($CoCp_2I$). After filtration, the solvent was removed from the filtrate *in vacuo*. The solid obtained was dissolved in a minimum of pentane (ca. 1 mL) and acetonitrile (2 mL) was added, causing precipitation of a dark solid in essentially quantitative yield. Analytically pure material was obtained by recrystallization of the solid obtained from a cold ether solution (ca. 1.5 mL) (0.0753 g, 0.1121 mmol, 52%). M.p. 111-112 °C. ^2H NMR (46 MHz, ether) δ = 7.867; $\Delta\nu_{1/2}$ = 34.3 Hz. ^1H NMR (300 MHz, C_6D_6, 25 °C): δ = 7 (br s), 0.107 (br s, 18 H, Ar*Me*), 0 (br s), -51.258 (br s, 3H, N*Me*). MS (70 eV): *m/z*(%): 670(8.8)[*M*+]. μ_{eff} (300 MHz, C_6D_6, 25 °C): 1.95 μ_B. EPR (toluene, 285 K): g = 1.949, $A(^{95,97}Mo)$ = 37 G. EPR (toluene, 102 K): g_1 = 1.976, $A_1(^{95/97}Mo)$ = 25 G, g_2 = 1.956, g_3 = 1.915. Anal. Calcd for $C_{37}H_{39}D_{18}MoN_4$: C, 66.14; H, 8.55; N, 8.34. Found: C, 66.30; H, 8.70; N, 8.36.

References begin on page 209

(iii) IMo(N[R]Ar)$_3$ (3.4). Iodine (0.0706 g, 0.2782 mmol, 0.51 eq) in ether (5 mL) was added to Mo(N[R]Ar)$_3$ (**1**, 0.3494 g, 0.5435 mmol) in ether (10 mL) causing a rapid color change to deep green. The solution was stirred for 30 minutes, and the solvent was removed *in vacuo*. The product was obtained by recrystallization from ether (0.3461 g, 0.4496 mmol, 82.7%). M.p. 122-124 °C. ^{2}H NMR (46 MHz, ether): δ = 8.97; $\Delta\nu_{1/2}$ = 10.62 Hz. ^{2}H NMR (46 MHz, C_6H_6): δ = 6.363; $\Delta\nu_{1/2}$ = 11 Hz. ^{1}H NMR (300 MHz, C_6D_6): δ = 6.58 (9H, C(CD$_3$)$_2$C*H*$_3$), 4.618 (6H, ortho), 3.558 (3H, para), 1.154 (18H, Ar*Me*). EPR (toluene, 25 °C): g = 1.97 (features at g = 2.02 and 1.95); (toluene, 101 K): g = 1.98 (features at g = 2.03 and 1.95). UV/Vis (ether): $\lambda(\varepsilon)$ = 255(21400); 607(2000). μ_{eff} (300 MHz, C_6D_6, 25 °C): 1.94 μ_B. MS (70 eV): *m/z*(%): 768.2(0.6)[*M*+]. Anal. Calcd for $C_{36}H_{36}D_{18}MoN_3I$: C, 56.17; H, 7.07; N, 5.46. Found: C, 56.15; H, 6.90; N, 5.34.

3.5.3 Other Reactions

(i) Reaction of 3.3 with methyl iodide. Mo(NMe)(N[R]Ar)$_3$ (**3.3**, 0.0753 g, 0.1121 mmol) was dissolved in methyl iodide (2.0 mL) and the reaction mixture was stirred for 15 hours. The color of the reaction changed from dark brown to yellow orange over this time. The methyl iodide was removed *in vacuo*. The resulting solid (0.0854 g, 0.1069 mmol, 95%) was determined to be [Mo(NMe)(N[R]Ar)$_3$][I] (**3**) by ^{1}H NMR spectroscopy.

(ii) Reaction of 3.2 with Me$_2$Mg. [Mo(NMe)(N[R]Ar)$_3$][I] (**3.2**, 0.0854 g, 0.1069 mmol) was dissolved in THF (2 mL) and Me$_2$Mg (0.0044 g, 0.8093 mmol, 1.5 eq) in THF (2 mL) was added. The solution turned red brown on addition. The product obtained was determined to be Mo(NMe)(N[R]Ar)$_3$ (**3.3**) by ^{1}H and ^{2}H NMR spectroscopy.

References begin on page 209

(iii) Reaction of 3.4 with $LiNMe_2$. $IMo(N[R]Ar)_3$ (**3.4**, 0.1506 g, 0.1956 mmol) was dissolved in THF (5 mL) and chilled to -35 °C. A solution of $LiNMe_2$ (0.0100g, 0.196 mmol) in THF (3 mL) at -35 °C was added dropwise. The solution gradually changed to an olive green color over a 45 minute period. Solvent was removed *in vacuo*. Examination of the solid obtained by ^1H NMR spectroscopy showed the presence of $Mo(N[R]Ar)_3$, HN[R]Ar and $IMo(N[R]Ar)_3$, as well as decomposition products.

(iv) Reaction of 3.4 with BH_3NHMe_2. $IMo(N[R]Ar)_3$ (**3.4**, 0.0962 g, 0.125 mmol) was dissolved in ether (10 mL). $BH_3{\cdot}NHMe_2$ (0.0081 g, 0.14 mmol, 1.1 eq) and NEt_3 (20 µL, 0.15 mmol, 1.2 eq) in ether (2 mL) was added to the solution of **3.4**. No color change was observed. After 24 hours, the reaction mixture was examined by ^1H NMR spectroscopy, showing only starting material, as well as a small amount of HN[R]Ar.

(v) Reaction of 2.1 with 2-methylaziridine. $Mo(N[R]Ar)_3$ (**2.1**, 0.0138 g, 0.0215 mmol) was dissolved in C_6D_6 (ca. 1 mL) and 2-methylaziridine (freshly flushed through alumina, 1.6 µL, 0.023 mmol, 1.1 eq) was added via syringe. The reaction was monitored by ^1H NMR spectroscopy over about four hours, clearly showing the growth of peaks attributable to $NMo(N[R]Ar)_3$ (**2**), HN[R]Ar and propylene.

(vi) Reaction of 2.1 with 7-amino-7-aza-benzonorbornadiene. $Mo(N[R]Ar)_3$ (**2.1**, 0.0359 g, 0.0558 mmol) was dissolved in C_6D_6 (1.0 mL) and 7-amino-7-aza-benzonorbornadiene (0.0107 g, 0.0560 mmol, 1.00 eq) in C_6D_6 (0.5 mL) was added. The reaction was monitored by ^1H NMR spectroscopy after 40 minutes. At this time, there was a 4:2:1 ratio of $Mo(N[R]Ar)_3$ to $NMo(N[R]Ar)_3$ to HN[R]Ar. After 16 hours, the ratio was 1:5:3. This reaction was repeated using the deuterated amine, which was prepared by

References begin on page 209

multiple washings of the starting amine with D_2O in THF. Analysis of the reaction by ^2H NMR after 24 hours showed the presence of DN[R]Ar.

(vii) Reaction of 2.1 with ammonia. $Mo(N[R]Ar)_3$ (**2.1**, 0.0290 g, 0.0451 mmol) was dissolved in C_6D_6 (ca. 1 mL) in an NMR tube with a ground glass joint. The tube was attached to a vacuum line, and degassed with three freeze-pump-thaw cycles. Ammonia (freshly stirred over sodium until blue, 3.1 mL, 300 torr, 0.052 mmol, 1.2 eq) was condensed into the NMR tube, which was then sealed. After 80 minutes, ^1H NMR spectroscopy showed a 3:1 ratio of HN[R]Ar to $Mo(N[R]Ar)_3$ (**2.1**) and approximately 70% starting complex **2.1**. After 48 hours, ^1H NMR spectroscopy showed a greater than 10:1 ratio of HN[R]Ar to $NMo(N[R]Ar)_3$ (**3.1**), with essentially complete consumption of starting complex **2.1**. The NMR tube contained a large ammount of black insoluble solid after 48 hours, perhaps corresponding to $(MoN)_n$.[40]

(viii) Reaction of 2.1 with *N*-methylaziridine. $Mo(N[R]Ar)_3$ (**2.1**, 0.0250 g, 0.0389 mmol) was dissolved in C_6D_6 (ca. 1 mL) and *N*-methylaziridine (5 μL) was added. The reaction mixture was sealed in an NMR tube and allowed to stand at room temperature overnight. ^1H NMR spectroscopy showed no reaction after this time. The tube was heated at 55 °C for 2 hours, but a ^1H NMR spectrum obtained after this time still showed no reaction. The tube was irradiated with UV light for 90 minutes, but ^1H NMR spectroscopy showed no reaction had occurred.

(ix) Reaction of 2.1 with azetidine. $Mo(N[R]Ar)_3$ (**2.1**, 0.0163 g, 0.0254 mmol) was dissolved in C_6D_6 (1.5 mL) and azetidine (3.0 μL, 0.0495 mmol, 1.9 eq) was added. The tube was frozen and degassed and then flame-sealed. The reaction was monitored by ^1H NMR spectroscopy after 40 minutes, and again after 18 hours, showing that no reaction had occurred.

References begin on page 209

(x) Reaction of 2.1 with *tert*-butylamine. $Mo(N[R]Ar)_3$ (**2.1**, 0.0269 g, 0.0418 mmol) was dissolved in ether (1 mL) and *tert*-butyl amine (5.0 µL, 0.048 mmol, 1.1 eq) was added. ^2H NMR spectroscopy showed only the presence of starting **2.1** after 19 hours.

(xi) Reaction of 2.1 with triethylamine. $Mo(N[R]Ar)_3$ (**2.1**, 0..0220 g, 0.0342 mmol) was dissolved in C_6D_6 (1.5 mL) and trimethylamine (6.0 µL, 0.0817 mmol, 2.4 eq) was added. The reaction was monitored by ^1H NMR spectroscopy after 18 hours, showing that no reaction had occurred.

(xii) Reaction of 2.1 with diethylamine. $Mo(N[R]Ar)_3$ (**2.1**, 0.0280 g, 0.0436 mmol) was dissolved in C_6D_6 (1.5 mL) and dimethylamine (5.5 µL, 0.053 mmol, 1.2 eq) was added. The reaction was monitored by ^1H NMR spectroscopy after 24 hours, showing that no reaction had occurred.

References

1) Laplaza, C. E.; Odom, A. L.; Davis, W. M.; Cummins, C. C.; Protasiewicz, J. D. *J. Am. Chem. Soc.* **1995**, *117*, 4999.
2) Laplaza, C. E.; Cummins, C. C. *Science* **1995**, *268*, 861-863.
3) Neyman, k. M.; Nasluzov, V. A.; Hahn, J.; Landis, C. R.; Rösch, N. *Organometallics* **1997**, *16*, 995-1000.
4) Qui, Q.; Musaev, D. G.; Svensson, M.; Sieber, S.; Morokuma, K. *J. Am. Chem. Soc.* **1995**, *117*, 12366-12367.
5) Laplaza, C. E.; Johnson, M. J. A.; Peters, J. C.; Odom, A. L.; Kim, E.; Cummins, C. C.; George, G. N.; Pickering, I. J. *J Amer Chem Soc* **1996**, *118*, 8623-8638.
6) Peters, J. C.; Cummins, C. C. Unpublished results .
7) Laplaza, C. E.; Johnson, A. R.; Cummins, C. C. *J Amer Chem Soc* **1996**, *118*, 709-710.
8) Woo, L. K. *Chem. Rev.* **1993**, *93*, 1125-1136.
9) Johnson, M. J. A.; Lee, P. M.; Odom, A. L.; Davis, W. M.; Cummins, C. C. *Angew. Chem. Int. Ed. Engl.* **1997**, *36*, 87.
10) Atagi, L. M.; Over, D. E.; McAlister, D. R.; Mayer, J. M. *J. Am. Chem. Soc.* **1991**, *113*, 870-874.
11) Patrick, D. W.; Truesdale, L. K.; Biller, S. A.; Sharpless, K. B. *J. Org. Chem.* **1978**, *43*, 2628.

References begin on page 209

12) Chatt, J.; Heaton, B. T. *J. Chem. Soc. A* **1971**, 705-707.
13) Bishop, M. W.; Chatt, J.; Dilworth, J. R.; Neaves, B. D. *J. Organometal. Chem.* **1981**, *213*, 109-124.
14) Groves, J. T.; Takahashi, T. *J. Am. Chem. Soc.* **1983**, *105*, 2073-2074.
15) Wigley, D. E. *Prog. Inorg. Chem.* **1994**, *42*, 239-482.
16) Shapley, P. A.; Shusta, J. M.; Hunt, J. L. *Organometallics* **1996**, *15*, 1622-1629.
17) Shapley (Belmonte), P. A.; Own, Z.-Y.; Huffman, J. C. *Organometallics* **1986**, *5*, 1269-1270.
18) Shapley, P. A.; Own, Z. Y. *J. Organometal. Chem.* **1987**, *335*, 269-276.
19) Nugent, W. A.; Mayer, J. M. *Metal-Ligand Multiple Bonds*; John Wiley & Sons: New York, 1988, pp 76-78.
20) Dehnicke, K.; Strähle, J. *Angew. Chem. Int. Ed. Engl.* **1992**, *31*, 955-978.
21) Laplaza, C. E.; Davis, W. M.; Cummins, C. C. *Angew. Chem. Int. Ed. Engl.* **1995**, *34*, 2042-2044.
22) Johnson, M. J. A.; Odom, A. L.; Cummins, C. C. *Chem. Com.* **1997**, accepted.
23) Our laboratory is indebted to Marc Johnson for the discovery of and Jonas Peters for the implementation of this purification technique with the N[R]Ar ligand set.
24) Johnson, A. R.; Davis, W. M.; Cummins, C. C.; Serron, S.; Nolan, S. P.; Musaev, D. G.; Morokuma, K. *J. Am. Chem. Soc.* **1997**, *submitted*,
25) Also see Chapter II of this Thesis.
26) Sur, S. K. *J. Magnetic Resonance* **1989**, *82*, 169-73.
27) Wertz, J. E.; Bolton, J. R. *Electron Spin Resonance: Elementary Theory and Practical Applications*; McGraw-Hill: New York, 1986.
28) Murphy, V. J.; Parkin, G. *J. Am. Chem. Soc.* **1995**, *117*, 3522-3528.
29) Cundari, T. R. *J. Am. Chem. Soc.* **1992**, *114*, 7879.
30) Kahn, O. *Molecular Magnetism*; VCH Publishers, Inc.: New York, 1993.
31) Williams, L. F.; Bothner-By, A. A. *J. Mag. Res.* **1973**, *11*, 314-325.
32) The amine was prepared by Dan Mindiola.
33) Carpino, L. A.; Padykula, R. E.; Barr, D. E.; Hall, F. H.; Krause, J. G.; Dufresne, R. F.; Thoman, C. J. *J. Org. Chem.* **1988**, *53*, 2565.
34) Leigh, G. J. *Science* **1995**, *268*, 827-828.
35) Cui, Q.; Musaev, D. G.; Svensson, M.; Sieber, S.; Morokuma, K. *J. Am. Chem. Soc.* **1995**, *117*, 12366.
36) Johnson, A. R.; Davis, W. M.; Cummins, C. C. *Organometallics* **1996**, *15*, 3825-3835.
37) Pangborn, A. B.; Giardello, M. A.; Grubbs, R. H.; Rosen, R. K.; Timmers, F. J. *Organometallics* **1996**, *15*, 1518-1520.
38) Elderfield, R. C.; Hageman, H. A. *J. Org. Chem.* **1949**, *14*, 605-637.
39) Perrin, D. D.; Armarego, L. F. *Purification of Laboratory Chemicals*; Pergamon Press: New York, 1988.
40) Greenwood, N. N.; Earnshaw, A. *Chemistry of the Elements*; Pergamon Press Inc.: Tarrytown, New York, 1984.

References begin on page 209

Chapter IV: Group 6 Complexes with a Bulky Amide Ligand Containing β-Hydrogens- Synthesis with Mechanistic Implications

References begin on page 239

Section 4.1: Introduction

The field of low-valent, low-coordinate transition metal amide chemistry begins with the synthesis of $Cr(N(i\text{-}Pr)_2)_3$,[1,2] and $(ON)Cr(N(i\text{-}Pr)_2)_3$ by Bradley and coworkers.[3,4] In recent years, these types of complexes have exhibited diverse and fundamentally interesting reactivity. The most common amide ligands used to stabilize low-coordinate complexes, such as $-N(SiMe_3)_2$,[5-10] -N[R']Ar' (R' = *tert*-alkyl; Ar' = aryl)[11-18] and $-N(C_6H_5)_2$,[19-24] lack β-hydrogens. The β-hydrogen elimination reaction is a well known and well documented decomposition pathway for metal alkyls and alkoxides,[25] as well as late metal amides.[26-28] Some early metal amide complexes, for example those with $-N(Cy)_2$[24] and $-N(i\text{-}Pr)_2$,[29] exhibit reactivity involving formal activation of the β-hydrogen, but in general, the β-hydrogen elimination reaction is not common in metal-amide chemistry.[30] Clearly, the presence of β-hydrogens in the monomeric complex $Cr(N(i\text{-}Pr)_2)_3$ does not render it unstable.

This chapter, which describes the synthesis of a variety of group six amide complexes with the -N[2-Ad]Ar ligand (2-Ad = 2-Adamantyl, Ar = $3,5\text{-}C_6H_3Me_2$), is part of an ongoing project towards understanding the steric and electronic factors which control the reactivity of low-valent and low-coordinate metal amide complexes, especially concerning the cleavage of dinitrogen and nitrous oxide by Mo(III).[14,16] Substitution of bulkier tertiary alkyl groups for the *tert*-butyl group in the -N[R]Ar ligand (R = $C(CD_3)_2CH_3$) causes substantial reactivity differences. For example, the ligands in $Mo(N[1\text{-}Ad]Ar)_3$ (1-Ad = 1-adamantyl) are too large to allow dimerization in the transition state[14,31] required to cleave dinitrogen,[32] thereby shutting down the reaction. Other researchers have recently reported chemistry with this ligand.[33-35]

Interest in the 2-adamantyl ligand stems from the desire to activate metal-element triple bonds. The steric pocket surrounding the M-E linkage precludes approach of a reagent to the π-cloud, rendering it essentially unreactive.[36] Only recently have the Mo-N and Mo-P triple bonds been chemically modified, but the addition reactions result in

References begin on page 240

essentially linear Mo-E-X linkages with no interaction between the molybdenum atom and the added group.[37-39] By reducing the steric pocket protecting the Mo-E group, an increase in reactivity could be realized. This steric pocket would be reduced substantially by using a secondary alkyl substituent, but two potential problems are envisioned. First, a large decrease in steric protection could result in metal-metal triple bond formation,[40-42] and second, the β-hydrogen could potentially be activated by the reactive Mo(III) center.

In addition to the above mentioned $Cr(N(i\text{-}Pr)_2)_3$, there are several examples of low-coordinate metal amide or phosphide complexes with β-hydrogens, including $Ti(N(i\text{-}Pr)_2)_3$,[43] $Mo(N(i\text{-}Pr)_2)_3$,[44] $V(N(i\text{-}Pr)_2)_3$,[29] $V(P(cy)_2)_3$,[45] and $Cr(P(cy)_2)_3$,[45] but none of these latter complexes are well characterized. Therefore, it is not possible to make predictions concerning the stability of a highly reactive Mo(III) complex with such an amide ligand. The 2-adamantyl substituent potentially exhibits an *iso*-propyl-like profile, in principle opening access to the Mo-E π-bond, but retains significant steric bulk, thereby preventing dimerization. The ligand is large and is not expected to significantly reduce the steric protection of the molybdenum center, but its use tests the compatibility of the reactive metal center with β-hydrogens, opening the door for future studies with other, less bulky secondary-alkyl anilide ligands.

Section 4.2: A New Bulky Ligand with β-hydrogens

(i) Synthesis of HN[2-Ad]Ar (4.1)

The synthesis of the aniline HN[2-Ad]Ar (**4.1**) is a trivial extension of the published procedure for HN[2-Ad]Ph.[46] Simply heating 2-adamantanone with 2 equivalents each of formic acid and 3,5-dimethylaniline using Luekart conditions[47] results in the formation of aniline **4.1** in essentially quantitative yield, given that unreacted starting materials are recovered. Carrying out the synthesis using the published procedure with a five hour reflux results in good product formation, but a substantial increase in yield is

References begin on page 240

realized when the reflux is extended to 24 hours. The amine is purified by crystallization from pentane. The ^{1}H NMR spectrum of **4.1** shows the ortho and para hydrogen resonances at 6.25 and 6.41 ppm respectively, and a downfield resonance at 3.5 ppm which is due to the β-hydrogen; all other resonances are in the normal regions as expected.

(ii) Synthesis of LiN[2-Ad]Ar (4.2)

Deprotonation of **4.1** using *n*-butyllithium in a hydrocarbon solvent results in clean, quantitative formation of LiN[2-Ad]Ar (**4.2**), which precipitates directly from the reaction mixture. The lithium reagent is essentially insoluble in hydrocarbon solvents, but has good solubility in ether and THF. Isolation of the etherate of **4.2** has thus far been unsuccessful, as it has poor solubility properties, but it is not necessary to do so. The ^{1}H NMR spectrum of **4.2** in THF-d_8 shows an upfield shift of the ortho and para resonances to 5.59 and 5.35 ppm respectively, while the β-hydrogen appears at 3.31 ppm.

Section 4.3: Complexes with N[2-Ad]Ar

(i) Synthesis of Cr(N[2-Ad]Ar)$_3$ (4.3)

It is desirable to first test the properties of this ligand in a system which is expected to be well behaved in the presence of β-hydrogens. Lithium amide **4.2** reacts with $CrCl_3$ in ether, following the standard procedure for the synthesis of Cr(N[R]Ar)$_3$ complexes (Scheme 4.1).[48] After workup, the dark brown powdery material Cr(N[2-Ad]Ar)$_3$ (**4.3**) is isolated in 79% yield. The 2-adamantyl substituent significantly alters the solubility properties of the chromium complex relative to that with *tert*-butyl substitution. During filtration to remove LiCl from the crude reaction mixture, the filter cake must be washed with multiple portions of ether in order to fully dissolve **4.3**. Crystallization of the complex is difficult, and the preferred method to obtain large quantities of material is by

References begin on page 240

slurrying it in pentane to wash away the major byproduct **4.1**. This results in pure material, as shown by ^{1}H NMR spectroscopy.

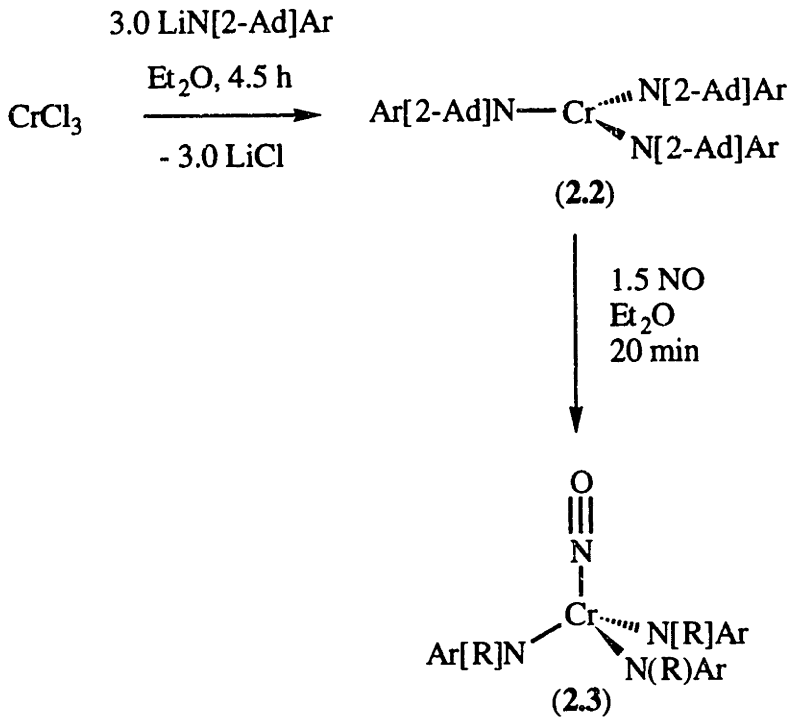

Scheme 4.1: Chromium complexes with the *N*-2-adamantyl-3,5-dimethylanilide ligand

The resonances in the ^{1}H NMR spectrum are extremely broad, and the only one that is definitively assigned is the aryl methyl resonance, appearing at -3.43 ppm. This is approximately where the aryl methyls appear in Cr(N[R]Ar)$_3$.[49] A magnetic susceptibility measurement by the Evans method[50] shows three unpaired electrons; μ_{eff} is calculated to be 3.98 μ_B, which is in good agreement with the spin-only value of 3.87 μ_B.

(ii) Synthesis of (ON)Cr(N[2-Ad]Ar)$_3$ (4.4)

Complex **4.3** reacts with an excess of nitric oxide (Scheme 4.1), following the standard procedure,[48] to form the dark red diamagnetic derivative, (ON)Cr(N[2-Ad]Ar)$_3$

References begin on page 240

(**4.4**) which is isolated in 80% yield by crystallization from ether. Crystals suitable for an X-ray diffraction study have not been obtained.

The ^{1}H NMR spectrum of the complex shows *ortho* and *para* resonances at 5.67 and 6.72 ppm respectively, with a substantially deshielded β-hydrogen resonance of 4.65 ppm. Another of the adamantyl resonances appears downfield of the aryl methyl resonance at 2.24 ppm. The IR spectrum shows a strong stretch at 1668 cm^{-1} due to $\nu_{N\text{-}O}$. It has not been possible to obtain complex **4.4** in analytically pure form, even after multiple recrystallizations; the best data are given in the experimental section. High resolution mass spectral data support the formulation proposed, and all characterization data are similar to those reported for (ON)Cr(N[R]Ar)$_3$.[48]

(iii) Synthesis of Mo(N[2-Ad]Ar)$_3$ (4.5)

The synthesis of the supposedly more reactive molybdenum complex, Mo(N[2-Ad]Ar)$_3$ (**4.5**), is also straightforward. Treating $MoCl_3(THF)_3$ with a deficiency of LiN[2-Ad]Ar (**4.2**), using standard procedures,[16] forms the desired tris-anilide complex (Scheme 4.2). The dark orange material has to be separated from an unknown dark brown impurity. This is best accomplished by allowing a fairly concentrated solution to stand at room temperature for several hours; the dark material is then simply be filtered away. Crystallization of the desired complex is difficult to initiate: solutions become supersaturated at -35 °C without significant formation of solid material. Induction of crystallization in a concentrated solution at room temperature followed by cooling to -35 °C results in the best yields. Similar solubility properties are observed with the related 1-adamantyl ligand.[33,35]

References begin on page 240

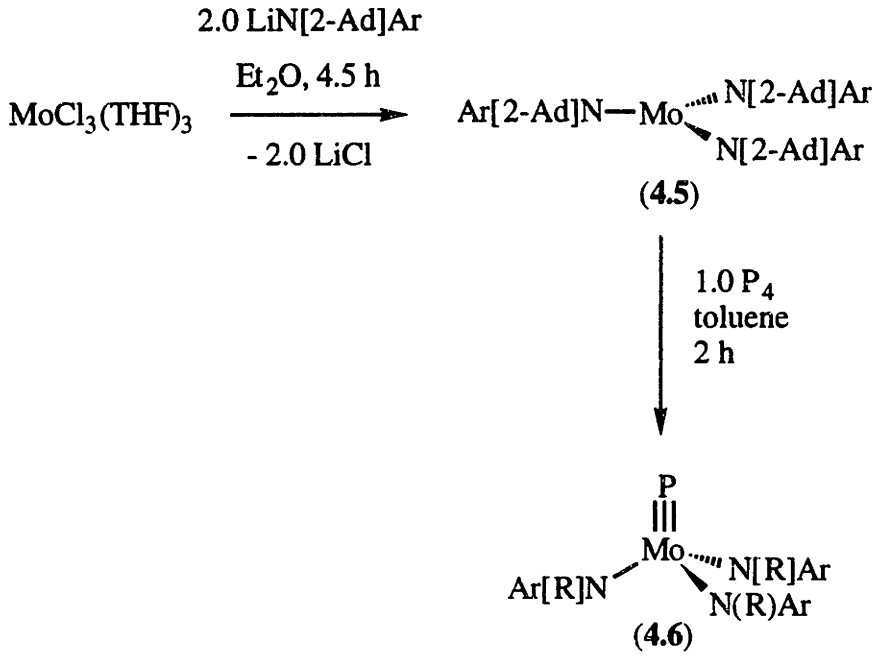

Scheme 4.2: Molybdenum complexes with the *N*-2-adamantyl-3,5-dimethylanilide ligand

The ^{1}H NMR spectrum of **4.5** is much better resolved than that of the chromium derivative **4.3**, although the resonances are still extremely broad. The aryl methyl resonance appears at -3.00 ppm. An Evans method[50] magnetic susceptibility measurement is consistent with 3 unpaired electrons (μ_{eff} = 3.88 μ_B). The increased steric bulk of the 2-adamantyl substituent relative to the *tert*-butyl substituent manifests itself during recrystallization of **4.5**. Extended storage of the purified material at -35 °C does not result in a deep purple color, and no diamagnetic material is observed to appear by ^{1}H NMR spectroscopy, suggesting that the intermolecular dinitrogen cleavage reaction is shut down in this system. This result is also observed with the 1-adamantyl derivative.[32]

Crystals suitable for X-ray diffraction are obtained from a chilled ether solution. An ORTEP diagram of **4.5** is shown in Figure 4.1, pertinent bond lengths and angles are listed in Tables 4.1 and 4.2, and positional parameters and U(eq) are listed in Table 4.3. The average Mo-N distance is 1.99 Å, the N-Mo-N angles are ca. 120°, the Mo-N-C_{ipso} angles are ca. 110°, and the Mo-N-C_α angles are ca. 130°. All metrical data are similar to

References begin on page 240

those observed with the related *tert*-butyl derivative.[16] The 2-adamantyl groups do not exhibit either the expected pseudo-*iso*-propyl or pseudo-cyclohexyl geometries, but instead are rotated by about 90° from these positions, creating a chiral C_3 propeller with significant intermeshing of the alkyl substituents. Interconversion of the two chiral rotamers is not observed spectroscopically; the adamantyl groups appear to be related by mirror symmetry on the NMR time scale.

Table 4.1. Selected Bond Lengths (Å) for Mo(N[2-Ad]Ar)$_3$ (**4.5**).

Mo-N1	2.001(3)	Mo-N2	1.990(3)
Mo-N3	1.981(3)	N1-C111	1.473(4)
N1-C11	1.426(4)	N2-C211	1.482(4)
N2-C21	1.430(4)	N3-C311	1.479(4)
N3-C31	1.429(4)		

Table 4.2. Selected Bond Angles (°) for Mo(N[2-Ad]Ar)$_3$ (**4.5**).

N1-Mo-N2	121.24(11)	N1-Mo-N3	119.92(11)
N2-Mo-N3	118.79(11)	Mo-N1-C111	128.9(2)
Mo-N1-C11	112.2(2)	C11-N1-C111	116.6(3)
Mo-N2-C211	127.4(2)	Mo-N2-C21	111.2(2)
C21-N2-C211	117.8(3)	Mo-N3-C311	132.6(2)
Mo-N3-C31	108.0(2)	C31-N3-C311	116.1(3)

References begin on page 240

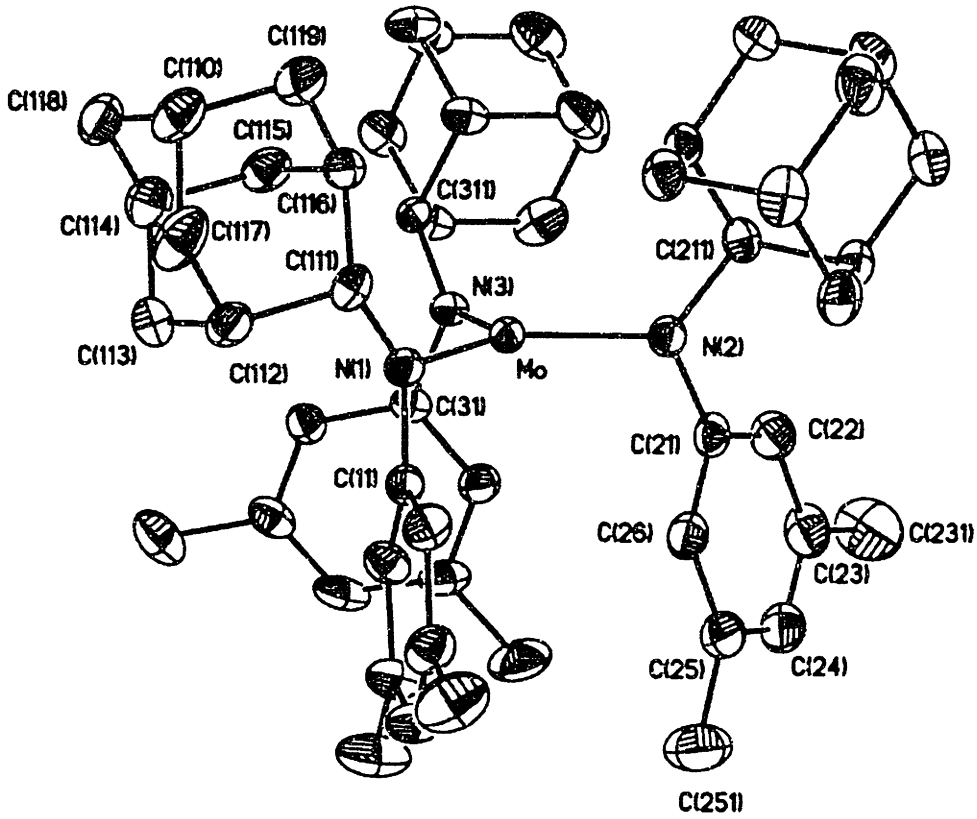

Figure 4.1: ORTEP diagram of Mo(N[2-Ad]Ar)$_3$ (**4.5**) with ellipsoids drawn at the 30% probability level.

References begin on page 240

Table 4.3: Positional Parameters (x 10^4) and U(eq.) ($Å^2$ x 10^3) for the Non-Hydrogen Atoms of $Mo(N[2\text{-}Ad]Ar)_3$ (**4.5**).

Atom	x	y	z	U(eq.)
Mo	9960(1)	3854(1)	7781(1)	29(1)
N1	10239(2)	3207(1)	8473(1)	33(1)
N2	10481(2)	4814(1)	7884(1)	36(1)
N3	9211(2)	3533(1)	6970(1)	31(1)
C11	11434(3)	3025(2)	8651(2)	33(1)
C12	12069(3)	3112(2)	9236(2)	42(1)
C13	13244(3)	2946(2)	9387(2)	46(1)
C14	13789(3)	2709(2)	8946(2)	51(1)
C15	13189(3)	2617(2)	8360(2)	49(1)
C16	12009(3)	2766(2)	8223(2)	41(1)
C21	11526(3)	4918(2)	7668(2)	38(1)
C22	11566(4)	5313(2)	7162(2)	52(1)
C23	12589(4)	5371(2)	6947(2)	61(1)
C24	13571(4)	5033(2)	7244(2)	59(1)
C25	13565(4)	4640(2)	7747(2)	54(1)
C26	12534(3)	4592(2)	7957(2)	44(1)
C31	10019(3)	3107(2)	6754(1)	33(1)
C32	11015(3)	3394(2)	6613(2)	42(1)
C33	11850(3)	2993(2)	6431(2)	53(1)
C34	11680(3)	2299(2)	6394(2)	56(1)
C35	10704(3)	1995(2)	6529(2)	46(1)
C36	9877(3)	2404(2)	6708(2)	38(1)
C110	7597(4)	2388(2)	9356(2)	56(1)
C111	9490(3)	3054(2)	8904(2)	37(1)
C112	9589(3)	2315(2)	9121(2)	48(1)
C113	9136(4)	1829(2)	8606(2)	59(1)
C114	7845(3)	1979(2)	8356(2)	54(1)
C115	7750(3)	2706(2)	8120(2)	48(1)
C116	8206(3)	3196(2)	8629(2)	42(1)
C117	8874(4)	2225(3)	9612(2)	64(1)
C118	7152(3	1893(2)	8846(2)	56(1)
C119	7494(4)	3114(2)	9123(2)	57(1)
C131	13916(4)	3023(3)	10028(2)	71(1)
C151	13782(4)	2334(3)	7882(2)	78(2)
C210	8633(4)	6425(2)	8592(2)	55(1)
C211	9763(3)	5416(2)	7950(2)	36(1)
C212	10449(3)	6011(2)	8288(2)	41(1)
C213	10952(3)	5811(2)	8935(2)	48(1)
C214	9968(4)	5628(2)	9257(2)	51(1)
C215	9308(3)	5021(2)	8930(2)	45(1)
C216	8793(3)	5216(2)	8279(2)	37(1)
C217	9620(4)	6616(2)	8275(2)	52(1)
C218	9139(4)	6235(2)	9239(2)	59(1)
C219	7964(3)	5821(2)	8268(2)	49(1)
C231	12636(6)	5795(3)	6395(3)	106(2)
C251	14659(4)	4293(3)	8078(3)	84(2)
C310	5749(3)	3885(2)	5921(2)	53(1)
C311	7981(3)	3468(2)	6659(1)	33(1)

References begin on page 240

Table 4.3 Continued

Atom	x	y	z	U(eq.)
C312	7813(3)	3549(2)	5976(2)	43(1)
C313	8096(4)	4270(2)	5818(2)	62(1)
C314	7290(4)	4766(2)	6046(2)	65(1)
C315	7471(4)	4702(2)	6724(2)	56(1)
C316	7199(3)	3977(2)	6888(2)	41(1)
C317	6548(3)	3384(2)	5690(2)	55(1)
C318	6027(4)	4605(2)	5756(2)	67(1)
C319	5932(3)	3811(2)	6601(2)	55(1)
C331	12926(4)	3321(3)	6285(3)	88(2)
C351	10553(5)	1233(2)	6496(2)	73(1)

(iv) Synthesis of PMo(N[2-Ad]Ar)$_3$ (4.6)

In order to chemically characterize **4.5**, a diamagnetic triply-bonded derivative analogous to those obtained with Mo(N[R]Ar)$_3$ is desired. Treating a solution of **4.5** with a large excess of P_4 generates the phosphide complex, PMo(N[2-Ad]Ar)$_3$ (**4.6**) in moderate yield (Scheme 4.2). Using only 1.4 equivalents of [P], the standard preparation,[15] results in significant formation of free aniline **4.1**, which is also the major contaminant in the preparation using a large excess of phosphorus. Separation of the two complexes is extremely difficult, especially given the poor solubility properties of complexes with the 2-adamantyl ligand as discussed previously. Precipitation of **4.6** from a methylene chloride solution with acetonitrile is the only way to obtain good yields of material. However, even after multiple recrystallizations from toluene, the material is not analytically pure. The best analytical data are given in the experimental section. The observed proton NMR spectrum is typical for diamagnetic complexes with the N[2-Ad]Ar ligand environment; the *ortho* and *para* protons have resonances at 5.99 and 6.65 ppm respectively, while the β-hydrogen appears at 4.70 ppm. The ^{31}P NMR spectrum has a single resonance at the extremely downfield position of 1215 ppm. This is the usual region for phosphide (P^{3-}) signals.[15,37,38,51] The high resolution mass spectrum supports the formulation presented.

A crystal suitable for X-ray diffraction is obtained from a chilled ether solution. An ORTEP diagram of **4.6** is shown in Figure 4.2, pertinent bond lengths and angles are

References begin on page 240

listed in Tables 4.4 and 4.5, and positional parameters and U(eq) are listed in Table 4.6. The Mo-P vector of the molecule sits on a three-fold axis, and the Mo-P bond length of 2.106(3) Å is comparable to those observed in other phosphido complexes.[15,38,51] The Mo-N distance is 1.987(6) Å. The phosphido complex is approximately tetrahedral, with a P-Mo-N angle of 102.6(2)° and an N-Mo-N' angle of 115.35(11)°. The most significant distortion in the molecule is the Mo-N-C111 angle of 136.2(4)°, increased by an average of 7° from complex **4.5**. This results in a compression of the C11-N-C111 angle by an average of 6° from the starting tris-anilide complex. This distortion is necessary to allow room for the phosphido fragment. The N-α-carbon vector of the 2-adamantyl group is displaced by 5° from the Mo-P vector, a significantly smaller angle than that usually observed for pseudo-C_3 symmetric complexes using the N[R]Ar ligand environment; these angles are typically 20-30°.[15,38,52,53] This is due to the large steric requirement of the 2-adamantyl group when oriented sideways in a C_3 propeller.

Table 4.4. Selected Bond Lengths (Å) for PMo(N[2-Ad]Ar)$_3$ (**4.6**).

Mo-P	2.106(3)	Mo-N	1.987(6)
N-C11	1.441(9)	N-C111	1.488(9)

Table 4.5. Selected Bond Angles (°) for PMo(N[2-Ad]Ar)$_3$ (**4.6**).

N-Mo-N'	115.35(11)	P-Mo-N	102.6(2)
Mo-N-C11	110.2(4)	Mo-N-C111	136.2(4)
C11-N-C111	110.9(6)	P-Mo-N-C111	5.0
P-Mo-N-C11	152.0		

References begin on page 240

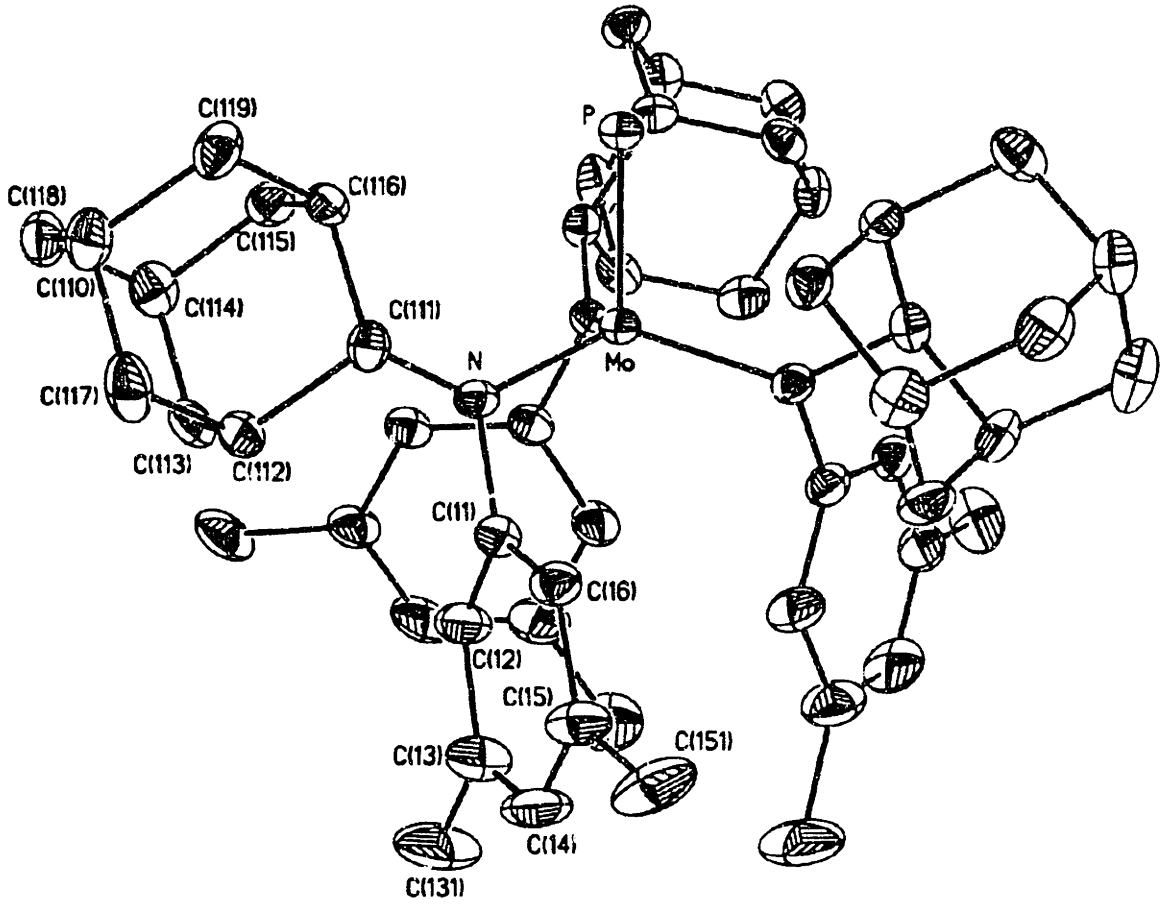

Figure 4.2: ORTEP diagram of $PMo(N[2\text{-}Ad]Ar)_3$ (**4.6**) with ellipsoids drawn at the 30% probability level.

References begin on page 240

Table 4.6: Positional Parameters (x 10^4) and U(eq.) (Å^2 x 10^3) for the Non-Hydrogen Atoms of PMo(N[2-Ad]Ar)$_3$ (**4.6**).

Atom	x	y	z	U(eq.)
Mo	1372(1)	1372(1)	1372(1)	26(1)
P	1559(1)	1559(1)	1559(1)	30(1)
N	229(5)	654(5)	3118(5)	29(1)
C11	454(7)	-83(7)	3291(7)	34(2)
C12	-131(8)	483(8)	2995(8)	46(2)
C13	55(10)	-253(10)	3217(10)	60(2)
C14	871(10)	-1515(10)	3659(9)	61(2)
C15	1483(9)	-2100(8)	3939(8)	47(2)
C16	1254(7)	-1380(7)	3771(7)	36(2)
C110	-2759(7)	853(7)	6432(7)	41(2)
C111	-519(6)	383(6)	4340(6)	31(2)
C112	-1705(7)	469(7)	5212(7)	37(2)
C113	-2601(7)	1815(8)	4684(8)	44(2)
C114	-3016(7)	2645(7)	4608(7)	41(2)
C115	-1871(7)	2578(7)	3760(7)	37(2)
C116	-952(7)	1246(7)	4253(6)	32(2)
C117	-2358(8)	31(8)	6503(7)	49(2)
C118	-3657(7)	2183(8)	5915(7)	43(2)
C119	-1592(7)	778(8)	5561(7)	42(2)
C131	-626(13)	374(12)	2932(14)	91(4)
C151	2396(10)	-3465(8)	4363(9)	67(3)

Section 4.4: Reactions of Mo(N[2-Ad]Ar)$_3$ (4.5)

(i) Mesityl Azide, Synthesis of NMo(N[2-Ad]Ar)$_3$ (4.7)

The nitride of **4.5**, NMo(N[2-Ad]Ar)$_3$ (**4.7**), is prepared by using mesityl azide as the nitrogen atom source (Scheme 4.3). Spectroscopically, the reaction generates an equivalent of free aniline **4.1**, but it is possible to isolate the nitride complex in low yield and in pure form by multiple recrystallizations from ether. The ^{1}H NMR resonances due to the N[2-Ad]Ar ligand protons are grossly similar to those observed in the chromium nitrosyl **4.4** and in the molybdenum phosphide derivative **4.6**.

References begin on page 240

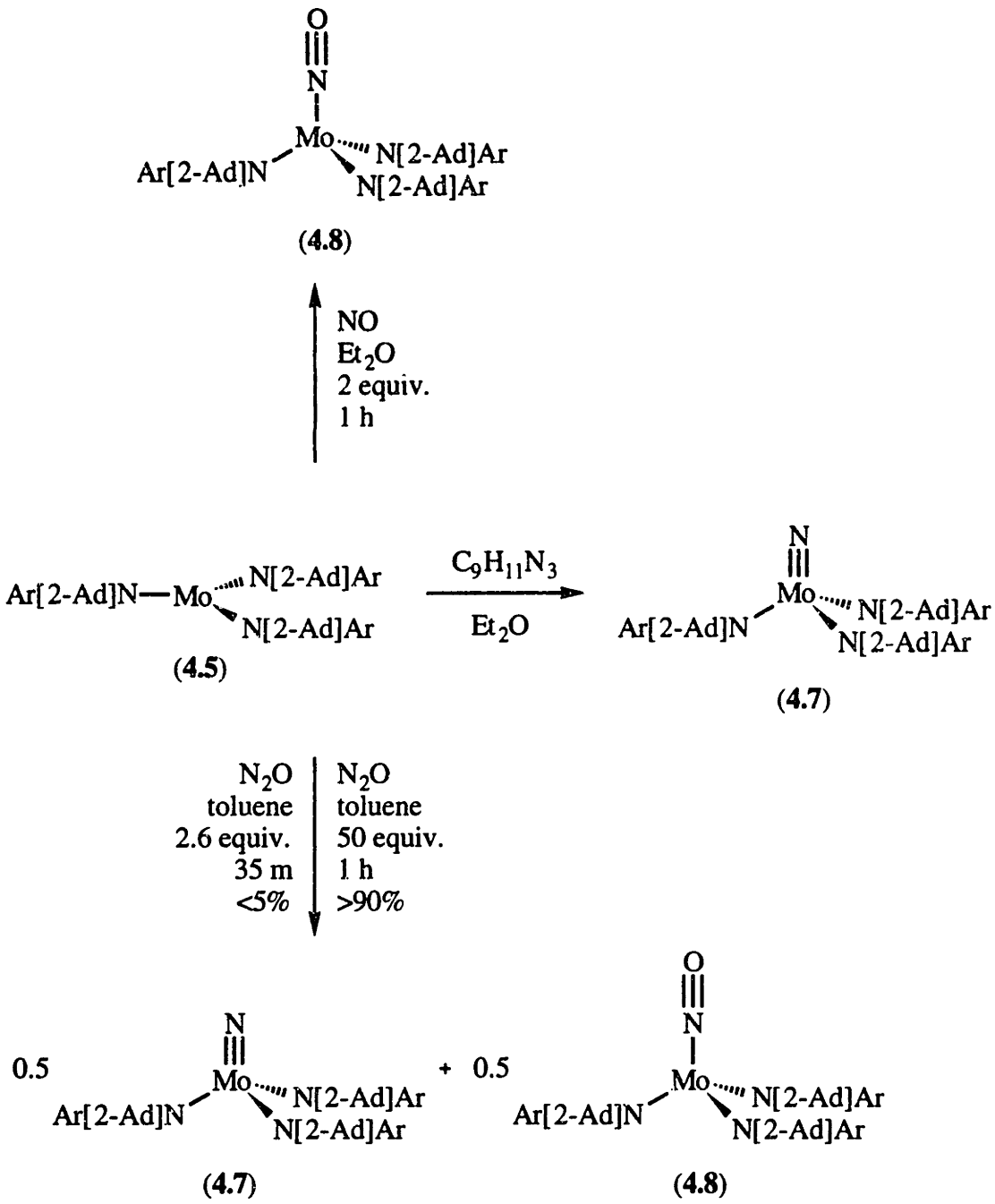

Scheme 4.3: Reactions of Mo(N[2-Ad]Ar)$_3$

References begin on page 240

(ii) Nitric Oxide, Synthesis of (ON)Mo(N[2-Ad]Ar)$_3$ (4.8)

Complex **4.5** also reacts with an excess of nitric oxide, cleanly generating the nitrosyl complex (ON)Mo(N[2-Ad]Ar)$_3$ (**4.8**) after about 20 minutes (Scheme 4.4). The complex is isolated in approximately 70% yield by recrystallization from THF, and the ^{1}H NMR resonances of this complex are again grossly similar to those observed in complexes **4.4** and **4.6**.

(iii) Nitrous Oxide

When tris anilide complex **4.5** is treated with one to two equivalents of nitrous oxide, added via syringe to a Schlenk flask containing **4.5** as is typical for the transformation,[16] no reaction is observed except for the generation of small amounts of free aniline **4.1**. Adding 2.6 equivalents of nitrous oxide to complex **4.5** using rigorous air-exclusion gas transfer techniques shows less than 5% conversion to the diamagnetic nitride and nitrosyl complexes **4.7** and **4.8** after 35 minutes (Scheme 4.3), as shown by ^{1}H NMR spectroscopy. When the reaction is repeated with approximately 50 equivalents of nitrous oxide (1 atm), and allowed to react for 60 minutes before removing the solvent, ^{1}H NMR spectroscopy shows approximately 90% conversion to **4.7** and **4.8**, with a detectable quantity (ca. 5%) of **4.5** (Scheme 4.3).

(iv) Comparison of Molybdenum Complexes

It is now possible to compare the reactivity of three different molybdenum complexes with different steric environments: Mo(N[R]Ar)$_3$ (**2.1**), Mo(N[1-Ad]Ar)$_3$ (**4.9**) and Mo(N[2-Ad]Ar)$_3$ (**4.5**). Mo(N[1-Ad]Ar)$_3$ is prepared analogously to complex **4.5** using the lithium anilide LiN[1-Ad]Ar.[32,54] Complex **2.1** reacts with either dinitrogen[14] or mesityl azide[16] to give NMo(N[R]Ar)$_3$ (**3.1**); nitric oxide to give

References begin on page 240

$(ON)Mo(N[R]Ar)_3$;[16] and nitrous oxide to give a 1:1 ratio of nitride and nitrosyl complexes.[16]

As discussed previously, $Mo(N[1\text{-}Ad]Ar)_3$ does not react with dinitrogen at reduced temperature to give a deep purple μ-dinitrogen complex. This is believed to be due to the deeper steric pocket which prohibits a two-atom bridge between two molybdenum centers.[32] $Mo(N[1\text{-}Ad]Ar)_3$ does react with mesityl azide, however, initially forming a purple color which fades to tan brown over a few minutes. Analysis of the product by ^1H NMR spectroscopy shows diamagnetic material corresponding to $NMo(N[1\text{-}Ad]Ar)_3$ with similar aryl resonances to nitride **3.1**. $Mo(N[1\text{-}Ad]Ar)_3$ also reacts with nitric oxide, rapidly changing color from orange red to very pale yellow. Proton NMR spectroscopy shows diamagnetic resonances consistent with $(ON)Mo(N[1\text{-}Ad]Ar)_3$. Finally, $Mo(N[1\text{-}Ad]Ar)_3$ reacts rapidly with 0.5 equivalents of nitrous oxide, and ^1H NMR shows the formation of a 1:1 mixture of the corresponding nitride and nitrosyl complexes. Under no conditions (solvent, temperature, number of equivalents of N_2O) could this ratio be altered.

The reaction chemistry of $Mo(N[2\text{-}Ad]Ar)_3$ (**4.5**) with mesityl azide and nitric oxide, and its lack of reaction with dinitrogen at reduced temperatures is analogous to the 1-adamantyl derivative **4.9**. The increased steric bulk is evident in the substantially slower reaction observed with nitrous oxide. Further details of this reaction are presented in Section 4.5.

Section 4.5: Competition Experiments between $Mo(N[R]Ar)_3$ (2.1) and $Mo(N[2\text{-}Ad]Ar)_3$ (4.5)

(i) Background

In the original report concerning the cleavage of the N-N bond in nitrous oxide,[16] there are no data to either support or refute the postulate that the reaction requires two molybdenum centers. Since that time, the *dinitrogen* cleavage reaction has been intensely

References begin on page 240

studied, and it is known that two molybdenum centers are required.[14,31,55] It is not yet possible to measure the kinetics of the nitrous oxide reaction due to the extremely fast rate. Even with the 1-adamantyl substituent, the reaction is extremely rapid and always generates equimolar amounts of nitride and nitrosyl complexes **4.8** and **4.9**. When the 2-adamantyl derivative **4.5** reacts with nitrous oxide, it also does so to form equimolar quantities of nitride and nitrosyl **4.10** and **4.11**. All this taken together suggests that the N-N cleavage in the nitrous oxide reaction also requires two molybdenum centers. However, as the new data shows that tris anilide **4.5** does *not* react with nitrous oxide on the usual timescale of the reaction, it should be possible to detect the presence of free nitric oxide during the reaction of $Mo(N[R]Ar)_3$ with N_2O, thereby determining whether any of the N-N bonds in N_2O are cleaved by a single $Mo(N[R]Ar)_3$ center.

(ii) Nitric Oxide

First, a competition study between **4.5** and **2.1** for NO must be carried out in order to see if it is possible for **4.5** to compete for free NO in solution. As it turns out, the 2-adamantyl derivative does compete to the extent of about 20% for free NO (Scheme 4.4). Equimolar amounts of both Mo(III) starting materials are loaded into a reaction bomb, and a deficiency of NO is injected through a septum. Analysis of the reaction mixture by ^1H NMR spectroscopy after 20 minutes shows a 3:1 ratio of $(ON)Mo(N[R]Ar)_3$ and nitrosyl **4.8**, along with significant amounts of both starting tris anilide complexes.

References begin on page 240

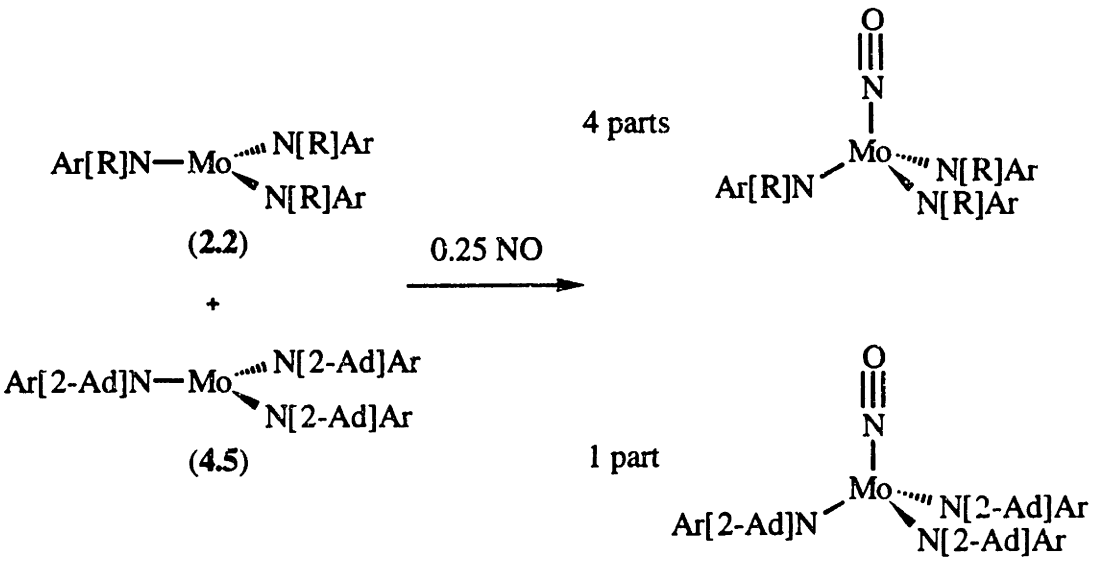

Scheme 4.4: Competition of molybdenum *tris*-anilides for NO

(ii) Nitrous Oxide

Next, equimolar quantities of **4.5** and **2.1** are treated with a deficiency of N_2O. After stirring for 35 minutes, the reaction mixture is analyzed by ^1H NMR spectroscopy. The only observed diamagnetic complexes are the nitride and nitrosyl complexes with the -N[R]Ar ligand (Scheme 4.5). This result strongly suggests that there is no free nitric oxide present in solution during the course of the nitrous oxide reaction, which points to a bimolecular cleavage pathway like that observed in the dinitrogen cleavage reaction. The fact that no diamagnetic complexes with the N[2-Ad]Ar ligand are observed indicates that there is no mixed-bimetallic N_2O cleavage; the only productive cleavage pathway is when two $Mo(N[R]Ar)_3$ molecules react together with one nitrous oxide molecule. These results also shed some light on the increased steric requirements of the 2-adamantyl group relative to the 1-adamantyl. Use of N[2-Ad]Ar not only shuts down intermolecular chemistry along a two-atom bridge (N_2), but significantly slows intermolecular reactions along a three-atom bridge (N_2O).

References begin on page 240

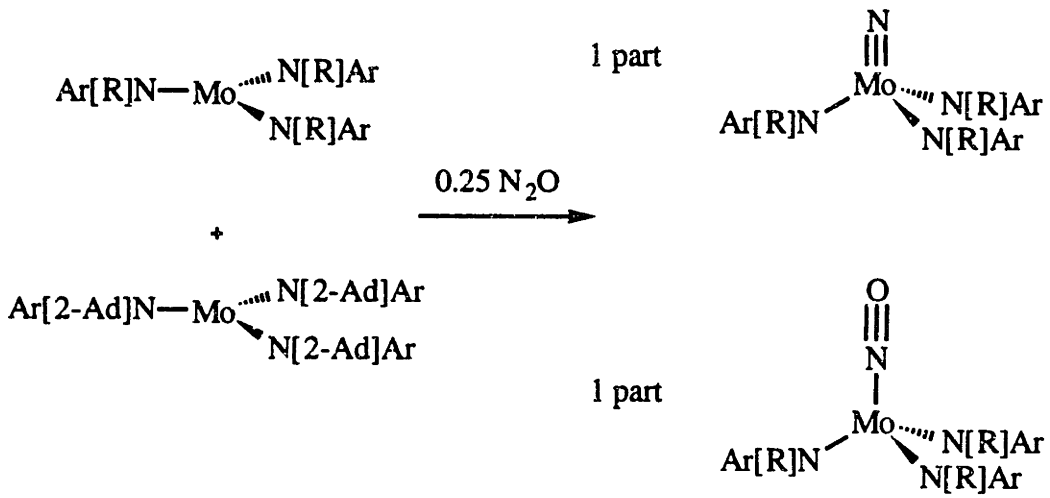

Scheme 4.5: Competition of molybdenum *tris*-anilides for N_2O

Section 4.7: Conclusion

Use of the 2-adamantyl substituent on an anilide ligand allows for the synthesis and characterization of both chromium (as expected) and molybdenum (as hoped) -(III) and -(VI) complexes. There appear to be no inherent problems of β-hydrogens with the reactive Mo(III) center. The fact that complex **4.5** reacts fairly rapidly with nitric oxide but does not react similarly with nitrous oxide allows for the determination of free NO in the N-N bond cleavage reaction of nitrous oxide mediated by $Mo(N[R]Ar)_3$. No free NO is observed, strongly suggesting an intramolecular reaction similar to that observed in the cleavage of dinitrogen. The significantly increased steric environment around a metal center with the 2-adamantyl ligand may be useful in other systems where more steric protection is required.

References begin on page 240

Section 4.8: Experimental

4.8.1 General Considerations

General experimental details are as described in Chapters I, II and III. Solvents were dried and deoxygenated according to previously published procedures.[17] Diethyl ether was dried according to a procedure by Grubbs.[56] P_4 was purified by recrystallization from toluene. $MoCl_3(THF)_3$[57,58] and $Mo(N[1\text{-}Ad]Ar)_3$[32] were prepared via standard procedures. Other chemicals were purified via standard procedures or used as received.[59] Magnetic susceptibilities were measured by NMR spectroscopy.[50] NMR spectra were recorded on Varian XL-300, Varian Unity-300 or Varian VXR-500 spectrometers. Chemical shifts are reported with respect to internal solvent. CHN analyses were performed by Oneida Research Services (Whitesboro, NY) or Microlytics (South Deerfield, MA). Melting points were obtained in sealed glass capillaries and are uncorrected.

4.8.2 Synthesis of Complexes

(i) HN[2-Ad]Ar (4.1).[46] 3,5-dimethylaniline (33.4 mL, 268 mmol, 2.01 eq.), formic acid (10.4 mL of a 95-98% solution, ca. 2 eq.) and 2-adamantanone (20.06 g, 133.5 mmol) were heated at 95-100 °C for 24 hours. Concentrated HCl (70 mL) was then added and the solution was heated at 95 °C for one hour. A copious amount of white solid appeared. The reaction mixture was diluted with water (100 mL), and the white solid was collected on a frit. The filtrate contained the hydrochloride of 3,5-dimethylaniline. The filter cake was washed with water (100 mL) and 3,5-dimethylaniline was recovered from the filtrate by adding concentrated NaOH solution (ca. 5 M) until the pH was ~14, at which point a yellow oil appeared. The aqueous layer was washed with ether (2 x 150 mL) and the solvent was removed *in vacuo* to yield a yellow oil (22 mL, 176 mmol). The filter cake

References begin on page 240

was then washed with ether (2 x 100 mL), removing unreacted 2-adamantanone, which was recovered by removing the ether *in vacuo* (9.82 g, 73.5 mmol). The filter cake was slurried in water (200 mL) and ether (200 mL), and NaOH (12 g) was added to neutralize the hydrochloride. The organic layer was separated and the aqueous layer was washed with ether (2 x 200 mL). The combined organics were washed with saturated aqueous sodium chloride (200 mL) and saturated aqueous sodium bicarbonate (200 mL). The combined aqueous layers were then extracted with ether (200 mL). The combined organics were evaporated, resulting in a white solid (14.9 g, 58.3 mmol, 43.7%). The solid was recrystallized from pentane at -35 °C in five crops (13.67 g, 53.54 mmol, 40%). M.p. 57-58 °C. ^{1}H NMR (500 MHz, C_6D_6): δ = 6.412 (s, 1H, para); 6.252 (s, 2H, ortho); 3.636 (s, 1H, N*H*); 3.502, (s, 1H, β-*H*); 2.222 (s, 6H, Ar*Me*); 1.948 (s, 2H); 1.614-1.802 (m, 10H); 1.4 (d, 2H). ^{13}C NMR (76 MHz, $CDCl_3$): δ = 147.406 (s, ipso); 138.733 (q, $^2J_{CH}$ = 5Hz, meta); 118.634 (d, *J* = 156 Hz, aryl); 110.818 (d, *J* = 153 Hz, aryl); 56.592 (d, *J* = 134 Hz, adamantyl-α); 37.683 (t, *J* = 127 Hz); 37.365 (t, *J* = 127 Hz); 31.652 (d, *J* = 135 Hz); 31.541 (t, *J* = 128 Hz); 27.431 (d, *J* = 135 Hz); 27.296 (d, *J* = 135 Hz); 21.432 (q, *J* = 126 Hz, Ar*Me*). MS (70 ev): *m/z*(%): 255(100)[M^+]. Anal. Calcd. for $C_{18}H_{25}N$: C, 84.65; H, 9.87; N, 5.48. Found: C, 84.94; H, 10.03; N, 5.52.

(ii) LiN[2-Ad]Ar (4.2). HN[2-Ad]Ar (**4.1**, 10.30 g, 40.33 mmol) was dissolved in pentane (50 mL) and cooled to -35 °C. *n*-Butyllithium (28 mL of a 1.6 M solution, 44.8 mmol, 1.1 eq.) was added via syringe over about a 5 minute period, causing the precipitation of a fine white powder. The solid was collected on a frit and dried *in vacuo* to constant weight (10.19 g, 38.99 mmol, 97%). ^{1}H NMR (500 MHz, C_4D_8O): δ = 5.590 (s, 2H, ortho); 5.349 (s, 1H, para); 3.306 (s, 1H, β-*H*); 2.150 (m, 2H); 1.962 (s, 6H, Ar*Me*); 1.87 (s, 2H); 1.83 (m, 4H); 1.716 (s, 3H); 1.38 (d, 2H); 1.28 (m, 1H). ^{13}C NMR (126 MHz, C_4D_8O): δ = 161.868 (s, aryl ipso); 137.093 (s, meta); 110.629 (br d, *J* = 149.73 Hz, ortho); 107.743 (d, *J* = 143.85 Hz, para); 62.323 (d, *J* = 126.83, β-*C*);

References begin on page 240

39.841 (t, J = 124.09); 39.294 (t, J = 125.46); 34.018 (t, J = 125.46); 33.971 (d, J = 130.96); 29.718 (d, J = 130.49); 22.595 (q, J = 123.93, Ar*Me*).

(iii) Cr(N[2-Ad]Ar)$_3$ (4.3). LiN[2-Ad]Ar (**4.2**, 1.8083 g, 6.9196 mmol, 2.73 eq) was dissolved in ether (60 mL) and frozen solid. $CrCl_3$ (0.4018 g, 2.537 mmol) was added as a solid and the reaction was stirred for 3.5 hours. The solution changed from colorless to dark brown as the solids reacted and dissolved. LiCl and excess $CrCl_3$ were removed by filtration through celite. The filter cake was washed with ether (10 x 25 mL) until the washings were essentially colorless, and the solvent was removed from the filtrate *in vacuo*. The dark solid obtained was slurried in ether (15 mL) and stored at -35 °C overnight. Two crops were obtained (0.7230 g, 1.0095 mmol, 43%). Two additional crops were obtained from pentane (0.6664 g, 0.8175 mmol, 36%). Low yields of analytically pure material were obtained by recrystallization from ether. M.p. 268-269 °C. ^{1}H NMR (300 MHz, C_6D_6): δ = 7.67 (~6H); $\Delta\nu_{1/2}$ = ~300; 3.883 (~12H); $\Delta\nu_{1/2}$ = 370; 2.241 (~6H); 3.427 (6H, ArMe); $\Delta\nu_{1/2}$ = 700. MS (70 eV): *m/z*(%): 814(0.27)[M^+]. μ_{eff} (300 MHz, C_6D_6): 3.982 μ_B. Anal. Calcd. for $C_{54}H_{72}CrN_3$: C, 79.56; H, 8.90; N, 5.15. Found: C, 79.74; H, 9.04; N, 5.15.

(iv) (ON)Cr(N[2-Ad]Ar)$_3$ (4.4). To a dark brown stirring solution of Cr(N[2-Ad]Ar)$_3$ (**4.3**, 0.3371 g, 0.4135 mmol) in ether (40 mL) was added NO (15 mL, 0.614 mmol, 1.5 eq) via syringe. The solution changed to red orange over a 10 minute period. The ether was removed *in vacuo* and the solid was redissolved in a minimum of ether and cooled to -35 °C to yield dark red faceted crystals in three crops (0.2796 g, 0.3308 mmol, 80%). M.p. 200-205 °C (dec). ^{1}H NMR (300 MHz, $CDCl_3$): δ = 6.715 (s, 3H, para); 5.666 (br s, 6H, orthos); 4.651 (s, 3H, β-*H*); 2.238 (br s, 6H); 2.092 (s, 18H, Ar*Me*); 1.842 (br s, 15H); 1.75 (m, 15H); 1.32 (m, 6H). ^{13}C NMR (76 MHz, $CDCl_3$): δ = 153.762 (s, ipso); 136.837 (q, $^2J_{CH}$ = 6 Hz, meta); 127.370 (d, J = 154 Hz); 126.458 (d,

References begin on page 240

J = 157 Hz); 75.984 (d, *J* = 118 Hz, adamantyl-α); 38.151 (t, *J* = 130);; 37.897 (t, *J* = 130); 34.596 (d, *J* = 133 Hz); 31.097 (t, *J* = 126 Hz); 27.732 (d, *J* = 130 Hz); 27.621 (d, *J* = 130 Hz); 21.385 (q, *J* = 126 Hz, Ar*Me*). IR (ether, 2 cm^{-1}): ν_{NO} = 1668 cm^{-1}. MS (70 eV): *m/z*(%): 844(0.22)[*M*+]. HRMS (EI, 70 eV): calcd mass: 844.51123. Found mass: 844.511(2) Anal. Calcd for $C_{54}H_{72}CrN_4O$: C, 76.74; H, 8.59; N, 6.63. Found: C, 75.55; H, 9.12; N, 6.11.

(v) Mo(N[2-Ad]Ar)$_3$ (4.5). LiN[2-Ad]Ar (**4.2**, 3.8001 g, 14.541 mmol, 2.02 eq) was slurried in ether (100 mL) and frozen solid. The frozen solution was allowed to thaw, and when magnetic stirring was just possible, $MoCl_3(THF)_3$ (3.0200 g, 7.2145 mmol) was added. The solution was stirred vigorously for 4.5 hours, during which time the solution turned dark brown. The reaction mixture was filtered through celite, and the filter cake was washed with ether (2 x 20 mL) until the washings were colorless. The filtrate was evaporated *in vacuo*, redissolved in ether (35 mL) and allowed to stand at room temperature overnight. A dark precipitate was removed by filtration, and the filtrate was reduced in volume and stored at room temperature until crystallization initiated. The saturated solution was then stored overnight at -35 °C. The solid powdery material was collected on a frit and washed with cold pentane (3 x 5 mL) yielding dark orange material. A second crop was obtained by a similar crystallization from pentane (15 mL) (2.279 g, 2.653 mmol, 64%). M.p. 211-212 °C. ^{1}H NMR (300 MHz, C_6D_6): $\delta(\Delta\nu_{1/2})$ = 12.818(71) (6H); 9.288(148) (6H); 5.299(~300); 3.534(109); 1.962(~300); -2.995(124) (18H, Ar*Me*); -47.64(193) (3H). MS (70 eV): *m/z*(%): 861.1(6.6)[*M*+]. μ_{eff} (300 MHz, C_6D_6): 3.875 μ_B. Anal. Calcd for $C_{54}H_{72}MoN3$: C, 75.49; H, 8.45; N, 4.89. Found: C, 74.96; H, 8.63; N, 4.70.

(vi) PMo(N[2-Ad])Ar)$_3$ (4.6). Mo(N[2-Ad]Ar)$_3$ (**4.5**, 0.5212 g, 0.6067 mmol) was dissolved in toluene (10 mL) and P_4 (0.0861 g, 0.695 mmol, 4.58 eq [P]) was added.

References begin on page 240

The reaction mixture was stirred for one hour, at which point the solvent was removed *in vacuo*. The solids obtained were dissolved in ether (20 mL) and filtered, removing a dark brown-orange solid (ca. 90 mg). The filtrate was evaporated to dryness and dissolved in methylene chloride (5 mL). Acetonitrile (10 mL) was added, causing precipitation of a brown solid, which was collected on a frit. This process was repeated with the filtrate, resulting in a second crop of material (0.2896 g, 0.3254 mmol, 54%). M.p. 223-224 °C (dec). ^{1}H NMR (500 MHz, C_6D_6): δ = 6.654 (s, 3H, para), 5.987 (s, 6H, ortho); 4.700 (s, 3H, β-*H*); 3.129 (s, 6H); 2.086 (s, 18H, Ar*Me*); 1.937 (m, 12H); 1.800 (br m, 6H); 1.651 (s, 12H); 1.413 (d, 6H). ^{13}C NMR (126 MHz, $CDCl_3$): 149.942 (s, ipso); 137.058 (q, $^2J_{CH}$ = 5.8 Hz, meta); 128.327 (d, *J* = 152.94 Hz, ortho); 127.150 (d, *J* = 147.89 Hz, para); 79.395 (d, *J* = 138.28 Hz, adamantyl-α); 38.675 (t, *J* = 128.44); 38.205 (t, *J* = 127.06); 35.319 (d, *J* = 130.50 Hz); 30.827 (t, *J* = 126.38 Hz); 28.108 (d, *J* = 132.33); 27.825 (d, *J* = 132.79 Hz); 21.570 (q, *J* = 126.07 Hz, Ar*Me*). ^{31}P NMR (203 MHz, $CDCl_3$): δ($\Delta\nu_{1/2}$) = 1215.46(86). MS (70 eV): *m/z*(%): 891.8(0.72)[*M*+]. HRMS (EI, 70 eV): calcd mass: 891.451793. Found mass: 892.451(2) Anal. Calcd for $C_{54}H_{72}MoN_3P$: C, 72.87; H, 8.15; N, 4.72. Found: C, 73.64; H, 7.92; N, 4.34.

(vii) NMo(N[2-Ad]Ar)$_3$ (4.7): Mo(N[2-Ad]Ar)$_3$ (**4.5**, 0.4747 g, 0.5525 mmol) was dissolved in ether (10 mL) and chilled to -35 °C. Mesityl azide (90 mL, .6186 mmol, 1.1 eq) was dissolved in Et_2O (15 mL) and chilled to -35 °C. The Molybdenum solution was added to the azide solution over a 15 minute period. The solution turned purple and then changed to brown over a five minute period. After one hour of stirring, the solvent was removed *in vacuo*. Two crops of tan-brown powder were obtained from a concentrated ether solution at -35 °C (0.1648 g, 0.1887 mmol, 34 %). M.p. 235-40 (dec). ^{1}H NMR (300 MHz, $CDCl_3$): δ = 6.730 (s, 3H, para); 6.708 (s, 6H, ortho); 3.898 (s, 3H, β-*H*); 2.490 (s, 6H); 2.082 (s, 18H, Ar*Me*); 2.000 (d, 6H), 1.84 (d, 12 H); 1.72 (m, 6H), 1.36 (d, 6H) 1.273 (6H). ^{1}H NMR (300 MHz, C_6D_6): δ = 6.886 (s, 3H, para);

References begin on page 240

6.031 (s, 6H, ortho); 4.29 (s, 3H, β-*H*); 2.96 (s); 2.35 (m); 2.097 (s, 18H, Ar*Me*); 1.851 (s); 1.682 (s); 1.52 (m). ^{13}C NMR (75 MHz, $CDCl_3$): δ = 151.951 (s, ipso); 137.731; 127.268; 127.125; 72.733; 38.414; 38.215; 32.327; 30.921; 28.540; 27.677; 21.632. IR (benzene, 2 cm^{-1}): 1600, 1585 cm^{-1}.

(viii) (ON)Mo(N[2-Ad]Ar)$_3$ (4.8): Mo(N[2-Ad]Ar)$_3$ (**4.5**, 0.6658 g, 0.7750 mmol) was dissolved in ether (10 mL) and NO (21 mL, 0.8594 mmol, 1.1 eq) was added via syringe. The reaction mixture was stirred for 20 minutes and the solution turned much lighter brown orange color. The solvent was removed *in vacuo* and the remaining solid was dissolved in ca. 10 mL THF with stirring. Two crops of powdery solid were collected (0.4800 g, 0.5399 mmol, 70%). M.p.: 280-285 (dec). ^1H NMR (300 MHz, $CDCl_3$): δ = 6.770 (s, 3H, para); 5.779 (s, 6H, ortho); 4.190 (s, 3H, β-*H*); 2.162 (s, 6H); 2.100 (s, 18H, Ar*Me*); 1.902-1.697 (m, 30 H); 1.40 (d, 6H). ^1H NMR (300 MHz, C_6D_6): δ = 6.884 (s, 3H, para); 6.092 (s, 6H, ortho); 4.579 (s, 3H, β-*H*); 2.638 (s, 6H), 2.10 (m, 9H); 2.080 (s, 18H, Ar*Me*); 1.866 (s, 12H); 1.7-1.5 (m, 15H). ^{13}C NMR (75 MHz, $CDCl_3$): δ = 148.943 (s, ipso); 137.929 (q, $^2J_{CH}$ = 7.72 Hz, ortho); 128.119 (d, *J* = 151.5 Hz, para); 127.515 (d, *J* = 157.5 Hz, meta); 75.536 (d, *J* ~ 145Hz, adamantyl-α); 38.361 and 38.194 (t, *J* = 128.3 Hz); 33.835 (d, *J* = 132.8 Hz); 31.019 (d, *J* = 130.6 Hz); 28.260 (d, *J* = 139.0 Hz); 27.897 (d, *J* = 134.1 Hz), 21.714 (q, *J* = 125.9 Hz, Ar*Me*). IR (benzene, 2cm^{-1}): 1604, 1582 cm^{-1}. Anal. calcd for $C_{54}H_{72}MoN_4O$: C,72.95; H, 8.16; N, 6.30. Found: C, 72.63; H, 8.43; N, 5.80.

References begin on page 240

4.8.3 Other Reactions

(i) Reaction of 4.5 with N_2. Several hundred milligrams of Mo(N[2-Ad]Ar)$_3$ were dissolved in ether (ca 10 mL) and stored at -35 °C overnight; there was no observed color change. ^{1}H NMR spectroscopy showed only starting tris-anilide **4.5**.

(ii) Reaction of 4.5 with N_2O. a) 2.6 equiv: Mo(N[2-Ad]Ar)$_3$ (**4.5**, 0.0177 g, 0.0206 mmol) was dissolved in toluene (5 mL) and removed from the glove box in a reaction bomb. The solution was degassed with 2 freeze-pump-thaw cycles, and nitrous oxide was added (3.1 mL, 320 torr, 2.6 eq). The reaction was stirred for 35 minutes, at which point the solvent was removed *in vacuo*. A ^{1}H NMR spectrum showed less than 5% conversion to the nitrido (**4.7**) and nitrosyl (**4.8**) complexes, with greater than 95% starting tris-anilide. **b) 50 equiv:** Mo(N[2-Ad]Ar)$_3$ (**4.5**, 0.0174 g, 0.0203 mmol) was dissolved in toluene (5 mL) and removed from the glove box in a reaction bomb. The solution was degassed, and nitrous oxide was added (~25 mL, 1 atm, ~1 mmol, ~50 eq). The reaction was stirred for 60 minutes, at which point the solvent was removed *in vacuo*. ^{1}H NMR spectroscopy showed greater than 90% conversion to **4.7** and **4.8** as well as about 5% starting tris-anilide.

(iii) Competition of 4.5 with 2.1 for NO. Mo(N[R]Ar)$_3$ (**2.1**, 0.0280 g, 0.0326 mmol) and Mo(N[2-Ad]Ar)$_3$ (**4.5**, 0.0231 g, 0.0359 mmol) were dissolved in toluene (5 mL) and removed from the glove box in a reaction bomb. The solution was evacuated, and nitric oxide was added to the head space through a septum (0.45 mL, 0.018 mmol). The gas was admitted to the bomb by opening the stopcock, and the reaction mixture was stirred for 20 minutes, at which point the solvent was removed *in vacuo*. ^{1}H NMR spectroscopy showed (ON)Mo(N[R]Ar)$_3$ and (ON)Mo(N[2-Ad]Ar)$_3$ **4.7** in a 4:1 molar ratio.

References begin on page 240

(iv) Competition of 4.5 with 2.1 for N_2O. $Mo(N[R]Ar)_3$ (**2.1**, 0.0252 g, 0.0392 mmol) and $Mo(N[2\text{-}Ad]Ar)_3$ (**4.5**, 0.0323 g, 0.0376 mmol) were dissolved in toluene (5 mL) and removed from the glove box in a reaction bomb. The solution was degassed with 3 freeze-pump-thaw cycles, and nitrous oxide was added (3.1 mL, 120 torr, 0.020 mmol, 0.51 eq based on $Mo(N[R]Ar)_3$). The reaction was stirred for 35 minutes, at which point the solvent was removed *in vacuo*. ^1H NMR spectroscopy showed $NMo(N[R]Ar)_3$ and $(ON)Mo(N[R]Ar)_3$ as the only diamagnetic products.

4.8.4 X-ray Structural Determination

(i) $Mo(N[2\text{-}Ad]Ar)_3$ (4.5). A dark orange needle of approximate dimensions 0.57 x 0.37 x 0.19 mm was obtained from a chilled ether solution. The crystal was mounted on a glass fiber. Data collection was carried out on a Siemens Platform goniometer with a CCD detector at 183 K using Mo Kα radiation (λ = 0.71073 Å). The total data collected were 20644 reflections ($-13 \le h \le 13$, $-21 \le k \le 11$, $-24 \le l \le 25$), of which 7395 were unique (R_{int} = 0.0300). Corrections applied: semi-empirical from psi-scans. The structure was solved by direct methods (SHELXTL V5.0, G. M. Sheldrick and Siemens Industrual Automation, Inc., 1995) in conjunction with standard difference Fourier techniques. Least-squares refinement based upon F^2 converged with residuals of R_1 = 0.0443, wR_2 = 0.1164, and GOF = 1.242 based upon $I > 2\sigma(I)$. All non-hydrogen atoms were refined anisotropically, and hydrogen atoms were placed in calculated ($d_{C\text{-}H}$ = 0.96 Å) positions. The largest residual peak and hole electron density was 0.476 and -0.259 e·Å^{-3}. Crystal data: monoclinic, a = 11.761(3) Å, b = 19.737(5) Å, c = 22.761(5) Å, V = 5170(2) Å^3, α = 90°, β = 101.89(2)°, γ = 90°, space group $P2_1/n$, Z = 4, μ = 0.294 mm^{-1}, M_r = 923.13 for $C_{58}H_{72}MoN_3O$, ρ(calcd) = 1.186 g/cm^3, and F(000) = 1540. See Tables 4.1 and 4.2 for metrical parameters, Table 4.3 for positional parameters and U(eq), and Figure 4.1 for an ORTEP diagram.

References begin on page 240

(ii) PMo(N[2-Ad]Ar)$_3$ (4.6). A yellow parallelepiped of approximate dimensions 0.31 x 0.25 x 0.22 mm was obtained from a chilled ether solution. The crystal was mounted on a glass fiber. Data collection was carried out on a Siemens Platform goniometer with a CCD detector at 183 K using Mo Kα radiation (λ = 0.71073 Å). The total data collected were 18823 reflections ($-42 \le h \le 41$, $-42 \le k \le 41$, $-42 \le l \le 42$), of which 2424 were unique (R_{int} = 0.0382). Corrections applied: semi-empirical from psi-scans. The structure was solved by direct methods (SHELXTL V5.0, G. M. Sheldrick and Siemens Industrual Automation, Inc., 1995) in conjunction with standard difference Fourier techniques. Least-squares refinement based upon F^2 converged with residuals of R_1 = 0.0868, wR_2 = 0.2662, and GOF = 1.257 based upon $I > 2\sigma(I)$. All non-hydrogen atoms were refined anisotropically, and hydrogen atoms were placed in calculated ($d_{C\text{-}H}$ = 0.96 Å) positions. The residual peak and hole electron density was 1.512 and -0.492 e·Å^{-3}. Crystal data are Rhombohedral, a = b = c =38.3067(6) Å, V = 5033.71(14) Å^3, α = β = γ = 18.6720(10)°, space group $R\bar{3}c$, Z = 4, μ = 0.329 mm^{-1}, M_r = 890.10 for $C_{58}H_{72}MoN_3P$, ρ(calcd) = 0.881 g/cm^3, and F(000) = 1896. See Tables 4.4 and 4.5 for metrical parameters, Table 4.6 for positional parameters and U(eq), and Figure 4.2 for an ORTEP diagram.

References begin on page 240

References

1) Alyea, E. C.; Basi, J. S.; Bradley, D. C.; Chisholm, M. H. *J. Chem. Soc., Chem. Commun.* **1968**, 495.
2) Bradley, D. C.; Hursthouse, M. B.; Newing, C. W. *J. Chem. Soc., Chem. Commun.* **1971**, 411-412.
3) Bradley, D. C.; Newing, C. W. *J. Chem. Soc., Chem. Commun.* **1970**, 219-220.
4) Bradley, D. C.; Hursthouse, M. B.; Newing, C. W.; Welch, A. J. *J. Chem. Soc., Chem. Commun.* **1972**, 567-568.
5) Bradley, D. C.; Copperthwaite, R. G. *Inorg. Synth.* **1978**, *18*, 112.
6) Bürger, H.; Wannagat, U. *Monatsh. Chem.* **1963**, *94*, 1007-1012.
7) Bürger, H.; Wannagat, U. *Monatsh. Chem.* **1964**, *95*, 1099-1102.
8) Bürger, H.; Stammreich, H.; Sans, T. T. *Monatsh. Chem.* **1966**, *97*, 1276.
9) Andersen, R. A.; Faegri, K.; Green, J. C.; Haaland, A.; Lappert, M. F.; Leung, W.-P.; Rypdal, K. *Inorg. Chem.* **1988**, *27*, 1782-6.
10) Berno, P.; Moore, M.; Minhas, R.; Gambarotta, S. *Can. J. Chem.* **1996**, *74*, 1930-1935.
11) Stokes, S. L.; Davis, W. M.; Odom, A. L.; Cummins, C. C. *Organometallics* **1996**, *15*, 4521-4530.
12) Peters, J. C.; Johnson, A. R.; Odom, A. L.; Wanandi, P. W.; Davis, W. M.; Cummins, C. C. *J. Am. Chem. Soc.* **1996**, *118*, 10175.
13) Odom, A. L.; Cummins, C. C. *Organometallics* **1996**, *15*, 898-900.
14) Laplaza, C. E.; Cummins, C. C. *Science* **1995**, *268*, 861-863.
15) Laplaza, C. E.; Davis, W. M.; Cummins, C. C. *Angew. Chem. Int. Ed. Engl.* **1995**, *34*, 2042-2044.
16) Laplaza, C. E.; Odom, A. L.; Davis, W. M.; Cummins, C. C.; Protasiewicz, J. D. *J. Am. Chem. Soc.* **1995**, *117*, 4999.
17) Johnson, A. R.; Davis, W. M.; Cummins, C. C. *Organometallics* **1996**, *15*, 3825-3835.
18) Fickes, M. G.; Davis, W. M.; Cummins, C. C. *J. Am. Chem. Soc.* **1995**, *117*, 6384-6385.
19) Barnhart, D. M.; Clark, D. L.; Grumbine, S. K.; Watkin, J. G. *Inorg Chem* **1995**, *34*, 1695-1699.
20) Driver, M. S.; Hartwig, J. F. *J. Am. Chem. Soc.* **1995**, *117*, 4708-4709.
21) Guan, J. G.; Shen, Q.; Jin, S. C.; Lin, Y. H. *Polyhedron* **1994**, *13*, 1695-1699.
22) Hoffman, D. M.; Rangarajan, S. P. *Acta Crystallogr C-Cryst Str* **1996**, *52*, 1616-1618.
23) Minhas, R. K.; Ma, Y. L.; Song, J. I.; Gambarotta, S. *Inorg Chem* **1996**, *35*, 1866-1873.
24) Gambarotta, S. *J. Organometal. Chem.* **1995**, *500*, 117-126.
25) Bryndza, H. E.; Tam, W. *Chem. Rev.* **1988**, *88*, 1163-1188.
26) Driver, M. S.; Hartwig, J. F. *J. Am. Chem. Soc.* **1996**, *118*, 4206-4207.
27) Hartwig, J. F. *J. Am. Chem. Soc.* **1996**, *118*, 7010-7011.
28) Hartwig, J. F.; Richards, S.; Barañano, D.; Paul, F. *J. Am. Chem. Soc.* **1996**, *118*, 3626-3633.
29) Song, J.-I.; Berno, P.; Gambarotta, S. *J. Am. Chem. Soc.* **1994**, *116*, 6927-6928.
30) Lappert, M. F.; Power, P. P.; Sanger, A. R.; Srivastava, R. C. *Metal and Metalloid Amides*; Ellis Horwood: Chichester, 1980.
31) Laplaza, C. E.; Johnson, M. J. A.; Peters, J. C.; Odom, A. L.; Kim, E.; Cummins, C. C.; George, G. N.; Pickering, I. J. *J Amer Chem Soc* **1996**, *118*, 8623-8638.

References begin on page 240

32) Johnson, A. R.; Peters, J. C.; Sutherland, R. D.; Cummins, C. C., Unpublished Results.
33) Ruppa, K. B. P.; Desmangles, N.; Gambarotta, S.; Yap, G.; Rheingold, A. L. *Inorg. Chem.* **1997**, *36*, 1194-1197.
34) Johnson, A. R.; Cummins, C. C. *Inorg. Synth.* **1997**, *In Press.*
35) Fickes, M. G.; Johnson, A. R.; Peters, J. C.; Cummins, C. C. *Manuscripts in Preparation.*
36) The steric shielding sometimes shuts substitution chemistry, forcing electron transfer, as described in Chapter III.
37) Johnson, M. J. A.; Odom, A. L.; Cummins, C. C. *Chem. Com.* **1997**, *in press.*
38) Johnson, M. J. A.; Lee, P. M.; Odom, A. L.; Davis, W. M.; Cummins, C. C. *Angew. Chem. Int. Ed. Engl.* **1997**, *36*, 87.
39) Also See chapter III of this thesis.
40) Chisholm, M. H.; Haitko, D. A.; Murillo, C. A. *Inorg. Synth.* **1982**, *21*, 51.
41) Chisholm, M. H.; Cotton, F. A.; Frenz, B. A.; Reichert, W. W.; Shive, L. W.; Stults, B. R. *J. Am. Chem. Soc.* **1976**, *98*, 4469.
42) Chisholm, M. H.; Reichert, W. *J. Am. Chem. Soc.* **1974**, *96*, 1249.
43) Chien, J. C. W.; Kruse, W. *Inorg. Chem.* **1970**, *9*, 2615.
44) Chisholm, M. H.; Extine, M.; Reichert, W. *Adv. Chem. Ser.* **1976**, *150*, 273.
45) Issleib, K.; Wenschuh, E. *Chem. Ber.* **1964**, *97*, 715.
46) Lavrova, L. N.; Klimova, N. V.; Shmar'yan, M. I.; Ul'yanova, O. V.; Vikhlyaev, Y. I.; Skoldinov, A. P. *Zh. Org. Khim.* **1974**, *10*, 761-5.
47) Leuckart, R. *Chem. Ber.* **1885**, *18*, 2341.
48) Odom, A. L.; Cummins, C. C. *J. Am. Chem. Soc.* **1995**, *117*, 6613-6614.
49) Odom, A. L., **1997**, Personal Communication.
50) Sur, S. K. *J. Magnetic Resonance* **1989**, *82*, 169-73.
51) Johnson, M. J. A.; Cummins, C. C., Unpublished results.
52) Johnson, A. R.; Davis, W. M.; Cummins, C. C.; Serron, S.; Nolan, S. P.; Musaev, D. G.; Morokuma, K. *J. Am. Chem. Soc.* **1997**, *submitted.*
53) Also see chapter II of this thesis.
54) Aldrich, P. E.; Hermann, E. C.; Meier, W. E.; Paulshock, M.; Prichard, W. W.; Snyder, J. A.; Watts, J. C. *J. Med. Chem.* **1971**, *14*, 535.
55) Laplaza, C. E.; Johnson, A. R.; Cummins, C. C. *J Am. Chem. Soc* **1996**, *118*, 709-710.
56) Pangborn, A. B.; Giardello, M. A.; Grubbs, R. H.; Rosen, R. K.; Timmers, F. J. *Organometallics* **1996**, *15*, 1518-1520.
57) Dilworth, J. R.; Zubieta, J. A. *J. Chem. Soc., Dalton Trans* **1983**, 397.
58) Dilworth, J. R.; Zubieta, J. *Inorg. Synth.* **1986**, 193.
59) Perrin, D. D.; Armarego, L. F. *Purification of Laboratory Chemicals*; Pergamon Press: New York, 1988.

References begin on page 240

Appendix I: Instructions for Extended Hückel Calculations And Orbital Visualization Using the Computer Programs EH and CACAO

References begin on page 281

Section 1: Introduction

CACAO[1,2] (Computer Aided Composition of Atomic Orbitals) is a collection of FORTRAN programs intended for the calculation and subsequent visualization of molecular orbitals at the extended Hückel level of theory. The original programs (CDNT, ICON and FMO) originate from the work of Hoffmann; the computational algorithms have not been substantially changed.[3-5] New features include the automatic recognition and assignment of molecular symmetry, assignment of Mulliken symbols to each MO, fragment molecular orbital (FMO)[6] analysis routines enabling the construction of Walsh diagrams, and a substantially improved user interface. The program can generate localized pictures of MOs similar to those seen in textbooks,[7] but is also capable of presenting a delocalized and more realistic picture. Generally, the extended Hückel method gives a good approximation of the shapes of molecular orbitals, but the absolute energies of the orbitals are best obtained by higher levels of theory. However, it is possible to gain significant insight to chemical reactivity of a molecule by investigating the frontier orbital set.[8]

This document is meant as a clear and general introduction to CACAO as the manual included with the program is not very easy to understand for a beginning user. Advanced features not found in this document are found in the manual. What follows in this section is a brief review of basic quantum mechanics in order to present a simple introduction to the extended Hückel method. A full discussion is clearly beyond the scope of this document, and more advanced understanding is readily available in one of many suitable texts.[9-11]

One of the most common ways to derive molecular orbitals is the linear combination of atomic orbitals (LCAO) approximation. The procedure is as follows for the creation of an extended π system in a conjugated carbon chain. Each π MO is written as a sum of the appropriate normalized atomic orbitals (in this case, p_z) of the various atoms in the

References begin on page 281

molecule. This is summarized mathematically by the following equations, where ψ_k is the k'th molecular orbital, ϕ_i is the i'th atomic orbital, and c_{ij} is a constant:

$$\psi_k = \Sigma c_{ik}\phi_i \qquad \text{the composition of } MO_k$$

$$\int \phi_i\phi_i \, d\tau = 1 \qquad \text{the normalization of each } p_z \text{ orbital}$$

The energy of the k'th molecular orbital, ψ_k, is found by solving the wave equation

$$(H - E)\psi_k = 0$$

where H is the Hamiltonian. The LCAO expression for ψ_k is introduced, giving

$$\Sigma c_{ik}(H - E)\phi_i = 0$$

This expression is expanded and manipulated to give a series of linear equations, one for each ψ_k. The first such equation (for ψ_1) is

$$c_{11}\int\phi_1(H - E)\phi_1 d\tau + c_{21}\int\phi_1(H - E)\phi_2 d\tau + \ldots + c_{i1}\int\phi_1(H - E)\phi_i d\tau = 0$$

To simplify notation, the following definitions are introduced:

$$H_{ii} = \int \phi_i H \phi_i \, d\tau$$

$$H_{ij} = \int \phi_i H \phi_j \, d\tau$$

$$S_{ij} = \int \phi_i\phi_j \, d\tau$$

H_{ii} gives the energy of the atomic orbital ϕ_i (the Coulomb integral), H_{ij} gives the energy of interaction between a pair of atomic orbitals ϕ_i and ϕ_j (the Resonance integral), and S_{ij} is the overlap integral between ϕ_i and ϕ_j. The equation is now written as:

$$c_{11}(H_{11} - ES_{11}) + c_{21}(H_{12} - ES_{12}) + \ldots + c_{i1}(H_{1i} - ES_{1i}) = 0$$

Similar equations are written for ψ_2 through ψ_k, and the secular determinant for this series of equations is:

$$\begin{vmatrix} H_{11} - ES_{11} & H_{12} - ES_{12} & \ldots & H_{1i} - ES_{1i} \\ H_{21} - ES_{21} & H_{22} - ES_{22} & \ldots & H_{2i} - ES_{2i} \\ \vdots \quad \vdots & \vdots \quad \vdots & \vdots & \vdots \quad \vdots \\ H_{i1} - ES_{i1} & H_{i2} - ES_{i2} & \ldots & H_{ii} - ES_{ii} \end{vmatrix} = 0$$

References begin on page 281

Solving this secular determinant gives values for c_{ij}. Since the atomic orbitals are normalized, each $S_{ii} = 1$. However, solving this series of equations without further simplification is difficult. This expression is substantially simplified by using the Hückel approximations, which are: $S_{ij} = 0$; and $H_{ij} = 0$ unless the i'th and j'th orbitals are on adjacent atoms. These simplifications make some sense, as most chemical bonds can be thought of in a localized fashion. The further simplifications of setting all remaining $H_{ii} = 0$ and $H_{ij} = \beta$ is often made. This means that the energy of interaction of any orbital with a like orbital is set to an arbitrary zero point, and that between any i and j atom is of the same energy. Again, for an extended π MO, this makes sense. This results in a simpler secular determinant, which is more easily solved:

$$\begin{vmatrix} -E & \beta & 0 & \dots & 0 \\ \beta & -E & \beta & \dots & 0 \\ 0 & \beta & -E & \dots & 0 \\ \vdots & \vdots & \vdots & \vdots & \vdots \\ 0 & 0 & \dots & \beta & -E \end{vmatrix} = 0$$

For more complicated molecules (naphthalene for example), symmetry considerations are employed to reduce a large matrix to several smaller irreducible matrices.

The above matrix is derived for a linear chain of carbon p_z orbitals in a conjugated system, and obviously is substantially different for one which would be derived for a transition metal complex. For example, each different kind of ligand or metal s, p, d and hybrid orbital has a different H_{ii}, and every possible interaction between each type of orbital would have a different H_{ij} term. Solving a determinant for even a relatively simple coordination complex is much more difficult than a simple extended π system, as the matrices involved are quite large, but the basic principles and simplifications remain the same as in this specific case.

References begin on page 281

Section 2: Program Architecture

There are two basic programs included in the CACAO package: EHC (Extended Hückel Calculation) which is the mathematical workhorse, and CACAO, which is the user controlled orbital visualization program. Also included in the package is a plotting program (PRINTGL), which is a third party shareware program. Two DOS batch files (pl.bat and plotf.bat) are used to allow CACAO to communicate with the plotting program.

EHC initially calculates Cartesian coordinates from the input internal coordinates. Alternatively Cartesian coordinates can be input directly. From the coordinates, MO calculation ensues, and the program can generate a wide variety of numerical output (wavefunction coefficients, energy levels, Mulliken population analysis, etc.). The program uses a modified version of the Wolfsberg-Helmholz formula,[12] with a double-ζ expansion of d orbitals. The parameters which the program uses are stored in the data file param.dat (this file can be modified if desired, see the manual for more details), with definitions are as follows:

SYM, NE, NS, ζs, H_{ss}, NP, ζp, H_{pp}, ND, H_{dd}, ζd_1, C_1, ζd_2, C_2

(where SYM = atomic symbol, NE = number of valence electrons in the neutral atom, NS, NP, ND = quantum numbers for s, p and d orbitals, ζs, ζp = exponents for s and p orbitals, ζd_1, ζd_2 = exponents for the double expansion of d orbitals, C_1, C_2 = coefficients for double expansion, H_{ss}, H_{pp}, H_{dd} = valence orbital ionization energy for s, p, d orbitals)

Sample parameters for an s, p and d block element are:

H, 1, 1, 1.300, -13.60

C, 4, 2, 1.625, -21.40, 2, 1.625, -11.40

MO, 6, 5, 1.960, -8.34, 5, 1.900, -5.24 , 4, 4.540, -10.50, .5899, 1.900 .5899

It is not yet possible to use f block elements or orbitals with EHC, though a later version of the program should have this capability.[1] The program identifies the correct molecular point group and each MO is assigned the correct Mulliken label. It is possible to carry out

References begin on page 281

MO analysis at a variety of steps in order to generate the necessary information for the construction of Walsh diagrams. It is also possible to perform fragment analysis,[6] allowing the subsequent construction of an interaction diagram between two molecular fragments. EHC always generates two output files for each input file (file.in): file.cor (the Cartesian coordinates derived for the molecule) and file.bin (binary data for MO construction). A third file, file.out, is a message file, which contains the desired numerical output, or error messages. The output files are not required for use of CACAO and they should periodically be deleted from the hard drive as they can be large. The maximum number of atoms per molecule is 125; the maximum number of orbitals per molecule is 500; the maximum number of steps in a Walsh diagram is 20; the maximum number of free variables is 10. These facts should be kept in mind during the generation of input files. More detailed information can be found in the CACAO manual.

CACAO takes the information present in file.bin and file.cor and generates either a Walsh or interaction diagram, depending on the type of input file, and pictures of the molecular orbitals. It is also allows viewing of the numerical output that is output to the file.out file, but this information is recalculated during the interactive session from the file.bin file (which is why the file.out files can be deleted). At the start of an interactive session, CACAO presents a list of available data sets. Once a data set is selected, the generation of diagrams and orbitals begins. The program is user friendly and menu driven. The user is asked questions that allow two or more choices which can usually be answered with Y(es), N(o) or a numerical input. Striking return chooses the default option, which is identified by DEF. Be careful to read the menus as inputting a negative number often makes the program choose an alternative pathway. The types of options which are selected include such things as maximum and minimum energies for a window, view orientation of a molecule, which MO to draw, and the resolution of the MO grid. The instruction manual for CACAO contains descriptions of more advanced features.

References begin on page 281

PRINTGL is a shareware program which enables better interaction between the DOS/Windows environment and a printer. There is a lengthy manual for this program, but in general, no options need to be changed. The major options are set through the interface programs. . .

pl.bat and plotf.bat, which are two DOS batch files that allow communication between CACAO and PRINTGL. When a diagram is printed from CACAO, the program activates pl.bat, which determines several options and then activates plotf.bat, which sends the options through a command line to PRINTGL. When viewing a diagram or orbital in CACAO, typing P plots the graphics on the printer. Typing S gives a sub-menu, allowing either plotting to the printer, or saving to a Postscript file. This latter option is useful for the generation of high-quality output on a laser printer.

Section 3: DOS Navigation

For those familiar with UNIX, using DOS will be a nightmare. Many of the commands for DOS and UNIX are similar enough that if you have been using UNIX for a while, you will be unable to use DOS. However, there are only a few commands in DOS that are required for successful use of the CACAO package. Remember, file names and directory names are limited by 8 characters, and files can have at most a 3 character extension (????????.???).

Directory hierarchy:	To move up a level, type cd .. To move down a level, type cd .\<directory name> . is defined as the current level, while .. is the next higher
Directories:	md .\<directory name> creates a new sub-directory rd .\<directory name> removes a directory.
File listings:	dir gives a file listing in the current directory dir /w gives a file listing "widened" out

list continues . . .

References begin on page 281

Wild cards:	* is the general wild card, dir *.in will find all files with the extension .in dir *.in/w "widens" the directory ? is a one letter wild card, dir fil?.in will find file.in, fill.in etc.
File creation:	For the purposes of CACAO, the edit command creates files
File editing:	After typing edit, the edit program is run. This program is very easy to use, is menu driven and utilizes the mouse. Anyone capable of using a Mac will be able to use the editor.
File removal:	del <file name>.<extension> will remove the selected file del *.out will delete all output files del file.* will delete file.in, file.out etc. del *.* will delete **ALL** files in the current directory
File renaming:	rename file.in input.in will rename the file "file.in" to the new name "input.in"
File moving:	move c:\moan\file.in c:\moan\adam will move the file "file.in" from the moan directory to the adam subdirectory of the moan directory.

Section 4: Program Installation

If the program is already installed, this process will not need to be repeated! To install the program, move to the DOS prompt, (c:\>) and create a subdirectory called moan (Molecular Orbital ANalysis) (c:\> md .\moan). Move to this subdirectory (c:\> cd .\moan) and copy the file cacao40.exe from the floppy to this subdirectory. This file is a self extracting file. To use it, type (c:\moan\>cacao40.exe -d). This will create a variety of files including cacao.exe, eh.exe, param.dat, manual.doc, as well as a "files" subdirectory of moan, which will include a variety of sample input files. Two batch files are created in this process, pl.bat and plotf.bat; however, it should be noted that the files automatically created by cacao40.exe WILL NOT WORK. The correct forms of the .bat files are included at the end of this manual. Manual.doc is a word for Windows file. This file may be deleted. The CACAO manual has been translated to a Macintosh format on the lab computer. More detailed instructions for installation are found in the manual.

References begin on page 281

PRINTGL also needs to be installed, if it is not already. To the c:\moan\ subdirectory, copy rsunzip.exe and printgld.zip. Then, type c:\moan\>rsunzip printgld.zip. Following installation, printgld.zip and cacao40.exe may be deleted from the hard drive, as they are no longer needed.

Section 5: Use of Program

It is highly recommended that each user create a sub-directory for files. The number of files in the moan directory expands exponentially with use of the program. It is very easy to create files, and therefore it becomes very difficult to find desired files when needed, especially given the eight character limit on file names! Within each sub-directory, further sub-directories may be created, so that all Walsh diagram files are kept separate from all interaction diagram files or each molecule has its own sub-directory, for example. Therefore, at the moan prompt type:

c:\moan\> md .\<your name>

Then, type c:\moan\> cd .\<your name>

to move into your subdirectory. The next portion of the instruction manual describes the creation of input files in detail. This is a simplified discussion from what appears in the manual.doc file, but clearly describes the input file creation for basic features of the program. More advanced features are described in the manual.

Section 6: Creation of Input Files

Introduction. There are three types of input file. The first is derived from X-ray crystal coordinates, the second is derived by using internal coordinates, and the third generates a Walsh diagram. This third type requires the use of internal coordinates. Three sample input files, xray.in, inter.in and walsh.in will be created in this section, with detailed line-by-line instructions for their modification. Remember, the numbers of spaces in the input file is very important. Therefore, the tilde (~) is used in this document to show

References begin on page 281

the correct numbers of spaces in each line. In general, to avoid problems, start with a working input file and modify it rather than creating a new one from scratch.

Crystal Data

This type of input file is useful when only a quick and dirty MO visualization of a specific molecule is required, without the possibility for Walsh diagrams or easy changing of the model. To generate the Cartesian coordinates, follow the following procedure. Port the X-ray data to Chem 3-D.[13] Remove all extraneous atoms (i.e. convert N[R]Ar to NH_2). Do this by deleting all carbons and hydrogens in the molecule except the ipso carbon and the quaternary carbon of the *tert*-butyl. Select these two atoms and change them to H's. Select one N-H bond and change its bond length to a suitable one (ca. 1 Å) using the ⌘= key combination (from the Build menu). Repeat for all N-H's. Next, it is a very good idea to center and orient the molecule for ease of viewing later on in CACAO. Select the central metal atom, and center it (from the View menu). Shift-click on a second atom (a nitrogen) and move it to the z-axis. Finally, shift-click on a third atom and move it to the x-z plane. Finally, from the Windows pull down menu, highlight the model, bringing up a sub menu. Select the Cartesian coordinates option which will bring up a window with atoms and x,y,z coordinates. Select this text and print it (from the file menu) or remember it. What follows is a description of an X-ray input file in detail.

line 1: title line
Mo(S)(NH2)3 from x-ray coordinates

Be as specific as possible. DOS only allows an 8 letter title for file names, and it becomes difficult to remember what names like "walsh1a.in vs. mowalshb.in" are. The title line is readily accessible from CACAO during an interactive session.

line 2: general parameter directive
~11~~0DIST~-1~~0~~0

Be careful to use the required number of spaces. Each integer is given three spaces to occupy, and each space not used by either a number or a negative sign must be present.

References begin on page 281

The first number is the total number of Real atoms (not counting dummy atoms which are only used with internal coordinates or for Walsh diagram input files, as discussed later). $Mo(S)(NH_2)_3$ has 11 atoms. The second number is the molecular charge. This will usually be 0. HELPFUL TIP: the calculated molecular charge, which is the last piece of information printed by the FMO part of EHC in the file.out file, should be equal to the value input in this line. If it is not, the calculation is most likely wrong, and the geometry of the molecule should be rechecked. DIST causes the EH program to generate output consisting of coordinates and interatomic separations. This field may be left blank if desired; add four spaces. The first number after the DIST card is the POPUL card. This field may be blank (three spaces), which will cause the MO occupation to be automatic, where electrons go into the lowest orbitals in order as usual. The unpairing of electrons (if it occurs) is done if the energy difference between two frontier orbitals is <0.1 eV. POPUL = 0 causes the HOMO to be doubly occupied even if there is an empty MO (LUMO) with the same energy. If POPUL is negative, its absolute value is taken as the imposed number of unpaired electrons. If POPUL is positive (not recommended), the electron population of each MO must be specified independently. In general, POPUL should be 0 or -n. The next two integers are used only in the generation of Walsh diagrams, and should be zero in this case.

line 3: Keywords
~EL~WF~RO~NC

These keywords control the output for the MO calculations. Choose one or more of the foliowing two letter words in any order. If this line is not present, output is limited to EL, total energy, reduced overlap and net charges.

DI = distances (ignored if DIST card is present in line 2)
WF = wave functions
OV = overlap matrix
OP = overlap population matrix
RO = reduced overlap matrix
CM = charge matrix
RC = reduced charge matrix
EL = energy levels

References begin on page 281

NC = net charges
HM = Hückel matrix
DM = density matrix
OD = overlap deletion matrix (requires additional parameter line, see the manual)
MP = Molecular orbital reduced overlap population matrix (also requires additional parameter line)

line 4: Cartesian coordinates
CELL 1.,1.,1.,90.,90.,90.

CELL alerts EHC to expect Cartesian coordinates. The next 6 numbers are A, B, C, α, β, γ, and should be set as above (1,1,1,90,90,90).

lines 5.1-5.n: coordinates
~S~~.000000,~~.000000,~~2.1680

Input the atoms one through n (where n is the number of atoms defined in line 2) keeping the following points in mind. Elements must be two digits and in all caps. If the element is only one digit, precede it with a space (i.e., ~S = sulfur, MO = molybdenum, CL = chlorine, ~C = carbon). The three numbers are x, y, and z. To avoid FORTRAN problems, keep the number of digits after the decimal point to 4 or 5, and include a comma after each number. Although it is not necessary to use commas, there must then be exactly six digits after the decimal point and the correct number of spaces between numbers. Be safe; use commas.

line 6: FMO directive
FMO

This card alerts the eh program to carry out a fragment MO analysis. If this card is absent and any other lines are present, the program will exit with an error message. If this card *and* other lines are absent, the program will attempt to generate Walsh diagram with zero variables and zero steps (from line 2). This will result in the generation of a Walsh diagram with the input molecule twice (step 1 and 2). It is not possible to view an interaction diagram this way since no FMO analysis is done, but it is possible to view the molecular orbitals. To generate an interaction diagram, this card must be present.

References begin on page 281

line 7: FMO keywords
~OP~RO~CM~TO~NC

These keywords are like those in line three. Choose one or more to select the output of the FMO calculations. If these keywords are not present, the output is limited to the overlap population and reduced overlap matrices for fragments.

DI = distances
WF = wavefunctions
OV = overlap matrix (between atomic orbitals)
TO = transformed overlap (between FMO's)
OP = overlap population between FMO's
CM = charge matrix
EL = energy levels
RO = reduced overlap matrix for fragments
RC = reduced charge matrix

line 8: Fragment definition
~~2~~1~10

The first integer is the number of fragments. This should always be two. Other numbers will be accepted, but then it is not possible to view MOs. The second integer is the number of atoms in the first fragment. In this example, the terminal sulfur is one fragment, so the first number is 1, and the $Mo(NH_2)_3$ is the second fragment, so the second number is 10. The two integers should add up to the total number of atoms in line two. It is highly recommended that the atoms of fragment one precede the atoms of fragment two during their original definition in lines 5.1-5.n. If a non-standard numbering scheme for the fragments is required, consult the manual.

line 9a-9b. Information about the fragments
~~0~EL~WF~CM

The first integer is the charge of fragment a/b. The sum of these numbers should add to the total charge given in line two. The two-letter words following the charge control the output, and the keywords available are the same as those given in line three. It is important to ***not*** hit return (enter) following the final keyword in line 9b. EHC ends with an error message if there is a blank line at the end. If return is accidentally pressed, or if a new line appears magically at the end of your input file, select the blank text with the mouse and

References begin on page 281

delete it using shift-delete in the editor. If all has gone well, a working input file for a truly exciting molecule has just been created (This author takes no responsibility for boring molecules). A sample, working input file is reproduced here:

XRAY.IN

```
Mo(S)(NH2)3~from~x-ray~coordinates
~11~~0DIST~-1~~0~~0
~EL~WF~RO~NC
CELL~~1.,1.,1.,90.,90.,90.
~S~~.000000,~~.000000,~~2.1680
MO~~.000000,~~.000000,~~.00000
~N~~1.612000,~~-1.023000,~~-.4610000
~N~~~-1.69400,~~~.7960000,~~~.531
~N~~~.000000,~~1.76200,~~~.89500
~H~~~1.52700,~~~2.007000,~~~.74700
~H~~~2.57900,~~~.7590000,~~~.23400
~H~~~-1.67400,~~~1.60900,~~~-1.159000
~H~~~-2.633000,~~~-0.48200,~~~.25500
~H~~~-.1280000,~~1.62300,~~~-1.90600
~H~~~.10400,~~2.73900,~~~.5950
FMO
~OP~RO~CM~TO~NC
~~2~~1~10
~~0~EL~WF~CM
~~0~EL~WF~CM
```

Internal Coordinates[14]

It is usually easier to generate an input file using internal coordinates, and it is essential that this is done in order to construct a Walsh diagram. Also, EHC sometimes has a difficult time seeing symmetry which is present in a molecule when the molecule is input with Cartesian coordinates. By using internal coordinates, the symmetric parts of the molecule can be defined to be mathematically identical, allowing EHC to see the full symmetry. As an example, when $Mo(NH_2)$ is modeled in D_{3h} using mathematically derived Cartesian coordinates (accurate to 6 decimal places), EHC does not see the molecule in D_{3h}, but instead, C_s. By using internal coordinates, it is very easy to create the input file, and EHC picks the correct point group. Although a bit mentally challenging at first, the internal coordinate system becomes logical after a few misfires, and for modeling

References begin on page 281

complexes in idealized symmetries, the input file can be created from a simple line drawing in a few minutes. Most of the file lines are similar to those discussed previously for the X-ray input file.

line 1: title line as before
(H2N)3MoNMo(SH)3~from~x-ray~structure~using~internal~coordinates

line 2: line 2:general parameter directive as before
~18~~0DIST~0~~0~~0

line 3: Keywords
~~EL~WF~RO~NC

line 4: internal coordinates, first atom at the origin
0.,0.,0.,MO

This first atom sits on the origin by definition. The atom may be a dummy atom, if that makes it easier to define the molecule (for example, a bimetallic molecule with no central atom). If that is the case, or if at any point a dummy atom is required, (as will be true for the generation of Walsh diagrams) use the symbol DU. If the origin atom is a dummy atom, its number by default is -1, the next real atom created should be atom number 1.

line 5: Atom 2
~1,2,~N~1.771,~0,0

The format of these lines is as follows. The new atom being created has six variables which need to be defined. These are (in order): the pointing atom (atom n-1, the atom it is coming from), the atom #, the symbol, a distance (from atom n-1), an angle α (defined as the angle between the three atoms n-2, n-1, and n) and a torsion angle τ (the dihedral between the planes defined by n-3/n-2/n-1 and n-2/n-1/n). Note that atom n-1 is not necessarily the atom preceding atom n in the list (lines 5.1-5.n). Similarly, atom n-2 is the atom which points to atom n-1, and is not necessarily the atom directly preceding atom n-1. Since this is only the second atom, atoms n-2 and n-3 are undefined. Therefore, two reference vectors are required. In CACAO, these two vectors are defined as the -z axis and the +x axis respectively. Therefore atom two is 1.771 Å from atom 1, with an angle of 0 ° from the -z axis, and an angle of 0 ° away from the +x axis.

References begin on page 281

line 6: Atom 3
~1,3,~N~1.977,~105.93,~120

This line places a nitrogen (atom 3) 1.977 Å from atom one (Mo). Atom n-2 and n-3 are still not defined, so the α angle of 105.93 refers to the -z axis, and the τ angle of 120 refers to the +x axis.

line 7: Atom 4
3,4,~H~0.96,~133.8,~26.2~

This line places a hydrogen 0.96 Å from atom 3 (N). The atom n-2 exists (Mo), but atom n-3 does not, so the reference vector is taken to be the -z axis (the first reference vector needed to define an atom is always taken to be the -z axis, a second vector, if required, is the +x axis). The Mo-N-H angle is defined as 133.8 ° by the first angle descriptor, and the Mo-N-H plane is bent away from the -z axis by 26.2 °.

It will probably be helpful at this point to look at Figure AI.1, which gives a more explicit depiction of the angles and lengths involved. The input lines and the corresponding resultant distances and angles are shown. A_1 is at the origin and A_2 is 1.25 Å away along the -z axis. A_3 is 1.47 Å from A_2, bent 90° from -z (placing it momentarily on the +x axis) and then bent an additional -90° from +x, placing it on the +y axis. A τ angle of +90° from + x would have placed A_3 on the -y axis. The τ angle is a simple rotation angle from +x (or sometimes -z, as above) until the n-4 atom is defined. A_4 and A_5 are 0.85 Å from A_3, with an A_2-A_3-$A_{4/5}$ angle of 120°. The τ angle in this case *does* refer to a dihedral angle. In order to determine the correct sign for this angle, hold a book, with its spine down along the A_2-A_3 vector. τ will be positive if the right side of the book opens when moving to A_4, while τ will be negative if the left side of the book opens when moving to A_5. Generally, (and especially with C_n or D_n-symmetric molecules) the *absolute* sign of τ is not important, as long as all related atoms are given identical signs of τ. Investigation of models derived from internal coordinates will allow familiarity with the coordinate system and reference vectors.

References begin on page 281

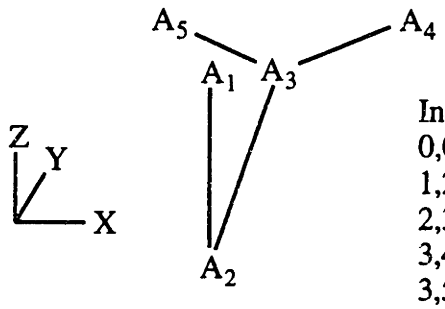

Input lines:
0,0,0,A_1
1,2,A_2 1.25,0.0, 0.0
2,3,A_3 1.47,90,-90
3,4,A_4 0.85,120,60
3,5,A_5 0.85,120,-60

resultant distances:	resultant angles:
r A_1-A_2 = 1.25 Å	θ A_1-A_2-A_3 = 90°
r A_2-A_3 = 1.47 Å	θ A_2-A_3-A_4 = 120°
r A_3 A_4 = 0.85 Å	θ A_1-A_2-A_3-A_4 = 60°
r A_3-A_5 = 0.85 Å	θ A_1-A_2-A_3-A_5 = - 60°

Figure AI.1: Description of Internal Coordinates in CACAO.

Lines 8-12: FMO directive, FMO keywords, fragment definition and information

```
FMO
~OP~RO~CM~TO~NC
~~2~11~~7
~~0~EL~WF~CM
~~0~EL~WF~CM
```

After inputting all the atoms from one to the total number assigned in line two, the rest of the input file is identical to that discussed previously for the X-ray input file (except, of course, the number of atoms in fragments one and two). The whole input file is reproduced here:

INTER.IN

```
(H2N)3MoNMo(SH)3~from~x-ray~structure~using~internal~coordinates
~18~~0DIST~0~~0~~0
~~EL~WF~RO~NC
0.,0.,0.,MO
~1,2,~N~1.771,~0,0
~1,3,~N~1.977,~105.93,~0
~1,4,~N~1.977,~105.93,~120
~1,5,~N~1.977,~105.93,~240
3,6,~H~0.96,~133.8,~26.2~
```


References begin on page 281

```
3,7,~H~0.96,~111.7,~212
4,8,~H~0.96,~133.8,~26.2
4,9,~H~0.96,~111.7,~212
5,10,~H~0.96,~133.8,~26.2
5,11,~H~0.96,~111.7,~212
~2,12,MO~1.882,~180,~0
12,13,~S~2.308,~93.71,~78.87
12,14,~S~2.308,~93.71,~198.87
12,15,~S~2.308,~93.71,~318.87
13,16,~H~0.96,~115.5,~159.9
14,17,~H~0.96,~115.5,~159.9
15,18,~H~0.96,~115.5,~159.9
FMO
~OP~RO~CM~TO~NC
~~2~11~~7
~~0~EL~WF~CM
~~0~EL~WF~CM
```

Walsh Diagrams

The final type of input file is one which generates data for a Walsh diagram. The use of internal coordinates is required, and for the most part, the input file remains the same as discussed previously. However, several changes are made. First, sets of atoms are assigned to groups, and these groups are rotated and translated relative to internally derived vectors defined with dummy atoms. Second, the general parameter directive line is changed to reflect the number of variables and steps in the diagram. Third, the values which the variables take is inserted as a new line between the general parameter directive and the MO keywords. Fourth, one or more of the internal coordinates is flagged to become a variable parameter. Keep in mind the fact that molecular symmetry MUST remain constant during the course of the molecular event. This may require slight distortions in either bond lengths (ca. 0.001 Å) or angles (ca. 0.1°) in the initial and final steps.

line 1: title line as usual

```
Mo(NH2)3~rotation~of~one~amide
```

line 2: general parameter directive

```
~10~~0DIST~~0~~1~10
```


References begin on page 281

This line lets the EHC program know that there are 10 atoms, the net charge is 0, the DIST card is on, and that the POPUL card is set to zero. The final two values are the number of variables (1) and the number of steps (10) in the Walsh diagram. If more than one internal coordinate is to take the same value (i.e., two bonds lengthening at the same rate), then the number of variables is still one; however, more than one coordinate will take the different values.

line 3: step values for the variable
0.1,20,40,60,80,100,120,140,160,179.9

These are the values that the variable parameter will take.

line 4: keywords as before
~EL~CM~NC~RO

line 5a-n: Internal coordinates as before
0.,0.,0.,MO
~1,2,~N~1.96,90.,90,1
~1,3,~N~1.96,90.,-30.,2
~1,4,~N~1.96,90.,-150,3
~2,5,~H~1.10,~120,0,1
~2,6,~H~1.10,~120,180,1
~3,7,~H~1.10,~120,0,2
~3,8,~H~1.10,~120,180,2
~4,9,~H~1.10,~120,0,3
~4,10,~H~1.10,~120,180,3
~1,-1,DU~3,90,90,1

In general, the coordinates are the same as before. However, each atom which potentially will be moved during the distortion is assigned to a group. In this example, atom one (Mo) is a member of group zero (the default), atom two (N) is a member of group one, and atom -1 (DU) is also a member of group one. Any atom not specifically assigned to a group is considered a member of group zero. Each group is a rigid object which can be moved or rotated while keeping relative bond lengths and angles constant. All other parameters are the same as discussed previously.

References begin on page 281

line 6: group rotation parameter
GR1~~2~-1~~1000.,0.

In this example, group one (GR1) is rotated about the axis defined by atom 2 and atom -1 by a variable parameter. Note that the dummy atom should be a member of the same group. The 1000 card alerts EHC that the coordinate to be varied is the rotation angle, and the final zero is a non-changing (in this example) translational value. To look at a Walsh diagram for rotating all three amides at the same time, two additional dummy atoms need to be defined;

1,-2,DU~3,90,-30,2 (this defines dummy atom -2)
~1,-3,DU~3,90,-150,3 (this defines dummy atom -3)

and add two lines to the end of the input file:

GR2~~3~-2~~1000.,0. (rotate group 2 about the 3/-2 vector)
GR3~~4~-3~~1000.,0. (rotate group 3 about the 4/-3 vector)

The number of variables in the general parameter directive does not need to be changed, as all three variable parameters take the same value at each step. If, instead of a group rotation, a group translation is desired, the input file could look something like this:

```
Mo(NH2)3~translation~of~one~amide
~10~~0DIST~~0~~1~10
1.96,1.97,1.98,1.99,2.00,2.02,2.04,2.06,2.08,2.10
~EL~CM~NC~RO
0.,0.,0.,MO
~1,2,~N~1000,90.,90,1
~1,3,~N~1.96,90.,-30.,2
~1,4,~N~1.96,90.,-150,3
~2,5,~H~1.10,~120,0,1
~2,6,~H~1.10,~120,180,1
~3,7,~H~1.10,~120,0,2
~3,8,~H~1.10,~120,180,2
~4,9,~H~1.10,~120,0,3
~4,10,~H~1.10,~120,180,3
```

This input file would move nitrogen 2 from 1.96 to 2.10 Å over 10 steps. Since H5 and H6 are defined from N2, the hydrogens will move with it. Alternatively, you could use the group translation parameter like before (after defining an appropriate dummy atom of

References begin on page 281

course). The "1000" variable card in the definition of N2 would need to be changed back to 1.96 like the other nitrogen atoms.

```
~1,-1,DU~3,90,-150,1
GR1~~1~-1~~0,1000.
```

This group translation parameter tells EHC to move group one along the 1/-1 vector by the variable amount. If two variables are desired, for example, if one amide is rotated *and* lengthened, the input file would look something like this (note, lines three and four are the values taken for variables one and two respectively):

```
Mo(NH2)3~translation~and~rotation~of~one~amide
~10~~0DIST~~0~~2~10
1.96,1.97,1.98,1.99,2.00,2.02,2.04,2.06,2.08,2.10
0.1,20,40,60,80,100,120,140,160,179.9
~EL~CM~NC~RO
0.,0.,0.,MO
~1,2,~N~1.96,90.,90,1
~1,3,~N~1.96,90.,-30.,2
~1,4,~N~1.96,90.,-150,3
~2,5,~H~1.10,~120,0,1
~2,6,~H~1.10,~120,180,1
~3,7,~H~1.10,~120,0,2
~3,8,~H~1.10,~120,180,2
~4,9,~H~1.10,~120,0,3
~4,10,~H~1.10,~120,180,3
GR1~~1~-1~2000,1000
```

This input file moves group one along the vector 1/-1 by the first variable, while rotating group one about the 1/-1 vector by the second variable. It should be clear that accurate definition of dummy atoms is critical for the desired molecular event to occur. The Walsh diagram input file used in the interactive session which follows is reproduced here:

WALSH.IN

```
Mo(NH2)3~rotation~of~one~amide
~10~~0DIST~~0~~1~10
0.1,20,40,60,80,100,120,140,160,179.9
~EL~CM~NC~RO
0.,0.,0.,MO
~1,2,~N~1.96,90.,90,1
~1,3,~N~1.96,90.,-30.,2
```


References begin on page 281

```
~1,4,~N~1.96,90.,-150,3
~2,5,~H~1.10,~120,0,1
~2,6,~H~1.10,~120,180,1
~3,7,~H~1.10,~120,0,2
~3,8,~H~1.10,~120,180,2
~4,9,~H~1.10,~120,0,3
~4,10,~H~1.10,~120,180,3
~1,-1,DU~3,90,90,1
GR1~~2~~1~~1000.,0.
```

There are additional commands and options for the input files which are not discussed in this document. For example, it is possible to do an FMO calculation during multiple steps of a Walsh diagram. For detailed instructions on these more advanced features, consult the manual.

Section 7: Explicit instructions for running EHC and CACAO

After the creation of the input file, all of the hard work is done. Now comes the fun part. The general procedure for running the program is as follows. At the c:\moan\subdir\> prompt, where the input files are located, type;

c:\moan\subdir\> eh . file

The command "eh" runs the EHC program. The "." tells EHC that the input files are in the current directory (c:\moan\subdir\). The "file" is the filename of the input file, without the "in" extension. This command, if no errors are encountered in the input file, will activate the eh program which generates file.bin, file.cor and file.out files. From time to time, it is a good idea to delete the file.out files, as they are not needed by CACAO, and only serve to provide information about the calculations to the user. What follows is a transcribed interactive session, giving an idea of the types of messages that will be seen on the screen while using EHC and CACAO. `What appears on the screen will appear in this font.` This includes any user-typed characters. **Any commentary about the session (which would not actually appear on the screen) will be in this font.** At any point where a default is taken, there will be no character typed after a menu, as the default character is the

References begin on page 281

return key. In anticipation of problems with the input file, this session starts with several error messages which occur when faulty input files are used. This session assumes that there are three input files (created earlier in this document), with the titles inter.in, xray.in, walsh.in, in the adam subdirectory of moan. It would be most beneficial at this point to follow along with the interactive session using CACAO with the three sample input files described above, in order to begin gaining familiarity with the program.

Interactive Session

Possible Error messages

```
C:\MOAN\ADAM>eh . inter

C:\MOAN\ADAM>ECHO OFF

---------- DOSVER

MS-DOS Version 6.22

        1 file(s) copied

C:\MOAN\ADAM>EHC >inter.out

C:\MOAN\ADAM>ECHO OFF
        1 file(s) copied
File not found - C:\MOAN\TEMPWF
        0 file(s) copied
 ****************************************************************
   Q = Exit
   C = Run CACAO
   K = Edit the current input file (inter.in)
   O = Edit the current output file (inter.OUT)
choose an option[Q,C,K,O]?o
```

Notice that the program eh can run the editor from within. Alternatively, select option "q" to exit, and then type C:\moan\adam> edit inter.out. The following are the contents of inter.out. Notice that the file contains the line which contains the error.

```
ERROR IN CARD. (Check Format).
≥ 18 0DIST 0  0  0
≥Stop - Program terminated.
```

This first file has an incorrect number of spaces in the first line. A second common error is forgetting to put a space before a one letter element. The contents of inter.out if this occurs is:

```
 ELEMENT N  MUST BE DEFINED BY THE USER
≥Stop - Program terminated.
```


References begin on page 281

Element N is undefined, as eh is looking for element ~N. Another common error is forgetting a comma. If no comma is placed where one should be, the contents of inter.out are:

```
ERROR IN CARD. (Check Format).
≥4,9, H 0.96 111.7, 212
≥Stop - Program terminated.
```

Sometimes, the inter.out file has no contents. If this is the case, there should be an error message generated by eh on the screen. An example of this type of session is:

```
C:\MOAN\ADAM>eh . xray

C:\MOAN\ADAM>ECHO OFF

---------- DOSVER

MS-DOS Version 6.22

        1 file(s) copied

C:\MOAN\ADAM>EHC >xray.out

run-time error F6103: READ(\moan\INPUT)
- invalid REAL

C:\MOAN\ADAM>ECHO OFF
        1 file(s) copied
File not found - C:\MOAN\TEMPWF
        0 file(s) copied
 ****************************************************************
   Q = Exit
   C = Run CACAO
   K = Edit the current input file (xray.in)
   O = Edit the current output file (xray.OUT)
choose an option[Q,C,K,O]?
```

The output file is blank, your only clue is the "invalid real" error message. This error message occurs because FORTRAN expected an integer with a certain number of characters, and one was missing. There will be a line in the input file without a comma or without the correct number of spaces. What follows is a long interactive session, in which all three files (xray, inter and walsh) are calculated, and subsequently viewed. This will demonstrate most of the options available in CACAO,. Normally most of the defaults would be taken, and not all options would be explored.

X-ray session

```
C:\MOAN\ADAM>eh . xray

C:\MOAN\ADAM>ECHO OFF

---------- DOSVER

MS-DOS Version 6.22

        1 file(s) copied

C:\MOAN\ADAM>EHC >xray.out

C:\MOAN\ADAM>ECHO OFF
        1 file(s) copied
```


References begin on page 281

```
       1 file(s) copied
 ****************************************************************
   Q = Exit
   C = Run CACAO
   K = Edit the current input file (xray.in)
   O = Edit the current output file (xray.OUT)
choose an option[Q,C,K,O]? C
```

Note that in the event of a successful eh run, three files will be copied. Typing c runs CACAO:

```
        ****************************************************************
        *            CARLO MEALLI and DAVIDE M. PROSERPIO              *
        *            C.A.C.A.O.  (Version 4.0, April 1994)             *
        *       (Computer Aided Composition of Atomic Orbitals)        *
        * Ref.: JOURNAL of the CHEMICAL EDUCATION (1990,67,399)        *
        ****************************************************************


      1)       INTER       2)       WALSH       3)       XRAY

The above files contain suitable CACAO datasets.
Select one of them by number (=N).
(CR=Escape this menu, L=List Files again, -N=Show Title of Nth Set)  -1
```

Your 4 options here are N, CR (return), L, -N. Typing -1 gives the title line from inter.in, a helpful feature as the number of suitable datasets grows:

```
------------------------------ TITLE FOR    INTER--------------------

(H2N)3MoNMo(SH)3 from x-ray structure using internal coordinates
----------------------------------------------------------------------


The above files contain suitable CACAO datasets.
Select one of them by number (=N).
(CR=Escape this menu, L=List Files again, -N=Show Title of Nth Set)  -2
------------------------------ TITLE FOR    WALSH--------------------

Mo(NH2)3 rotation of one amide
----------------------------------------------------------------------


The above files contain suitable CACAO datasets.
Select one of them by number (=N).
(CR=Escape this menu, L=List Files again, -N=Show Title of Nth Set)  -3
------------------------------ TITLE FOR     XRAY--------------------

Mo(S)(NH2)3 from x-ray coordinates
----------------------------------------------------------------------


The above files contain suitable CACAO datasets.
Select one of them by number (=N).
(CR=Escape this menu, L=List Files again, -N=Show Title of Nth Set)  L
```

Now, typing L gives the list again.

```
      1)       INTER       2)       WALSH       3)       XRAY

The above files contain suitable CACAO datasets.
Select one of them by number (=N).
(CR=Escape this menu, L=List Files again, -N=Show Title of Nth Set)  3
```


References begin on page 281

```
   Interaction Diagram / MO drawings ? (Any char. / CR=return)  j
```

Option three was used to select the X-ray data file. Then, typing any character causes the program to begin the interaction diagram generation:

```
  DATASET = XRAY
```

Strike Return to use the following default settings:

```
Energy Interval =    -25.0     3.0 eV
Minimum FMO contribution = 2.0%
Draw all MOs within the given range (i.e., no selection by symmetry or number)
Use the highest resolution between quasi-degenerate levels

Otherwise, start entering MINIMUN ENERGY (M=menu)   -16
                         MAXIMUM ENERGY -8
Minimum FMO Contribution (DEF=2.0%)
Magnify resolution between quasi-degenerate levels? [Def=Y]
do you wish to select orbitals? (DEF=N)
```

The diagram generated by these settings is shown in Figure AI.2 It is printed by typing P from the menu reproduced below. Alternatively, it can be written to a file by typing S, and then F. The menu bar shown below will also be below the diagram on the screen.

```
+0=Exit/1=New diagr./2=MO draw.s/3=Mullik/P,S=Prn/-N=get Nth Diag ( 1: 1)3
```

Typing "3" selects a Mulliken analysis of the molecule (first will be orbital 16, followed by fragment 13 of orbital 16):

```
Numerical results for:     XRAY
Enter treshold for orbital contribution to the various MOs (DEF=1.0%)
enter MO number (max.= 31) [CR = EXIT] 16
MO  16[ 16a  ] E(eV) =  -13.217 FILLED - Total Levels=  31
 S  1 px    31%(+)        FMO  13 (FRG 1)         5%(+)
 S  1 py     2%(-)        FMO  16 (FRG 1)        51%(+)
 N  3 py     3%(+)        FMO  17 (FRG 1)         3%(+)
 N  3 pz    30%(-)        FMO  18 (FRG 1)         5%(+)
 N  4 py     5%(-)        FMO  29 (  2 in FRG 2)  2%(-)
 N  4 pz    11%(+)        FMO  30 (  3 in FRG 2) 31%(+)
 N  5 px    16%(-)
one MO # OR one or two FMO(s) [negative] OR Atom # and At.Orb. type (eg: 1,px)
[CR/E/Z = EXIT/Energies/Mulliken Analysis]  -13
FMO 13[ 15a  ] E(eV) =   -9.638 EMPTY  - Total Levels=  27
MO  1 px     3%(+)/MO  1 xz    82%(+)/MO  1 yz     2%(-)/ N  2 pz     4%(-)/
 N  3 py     2%(-)/ N  3 pz     2%(+)/
Electrons in FMO  13 =   .215 ** Ov.Pop. with other FMOs:
<* | 29>=  1 <* | 30>= 15
     >> FMO  13 contributes to the following MOs:
 12 [32%(+)]  13 [ 9%(-)]  14 [48%(+)]  16 [ 5%(+)]  18 [ 3%(+)]
 21 [ 2%(-)]

one MO # OR one or two FMO(s) [negative] OR Atom # and At.Orb. type (eg: 1,px)
[CR/E/Z = EXIT/Energies/Mulliken Analysis]
```

Return goes back to the interaction diagram and menu. Selecting two goes to the MO drawings:

References begin on page 281

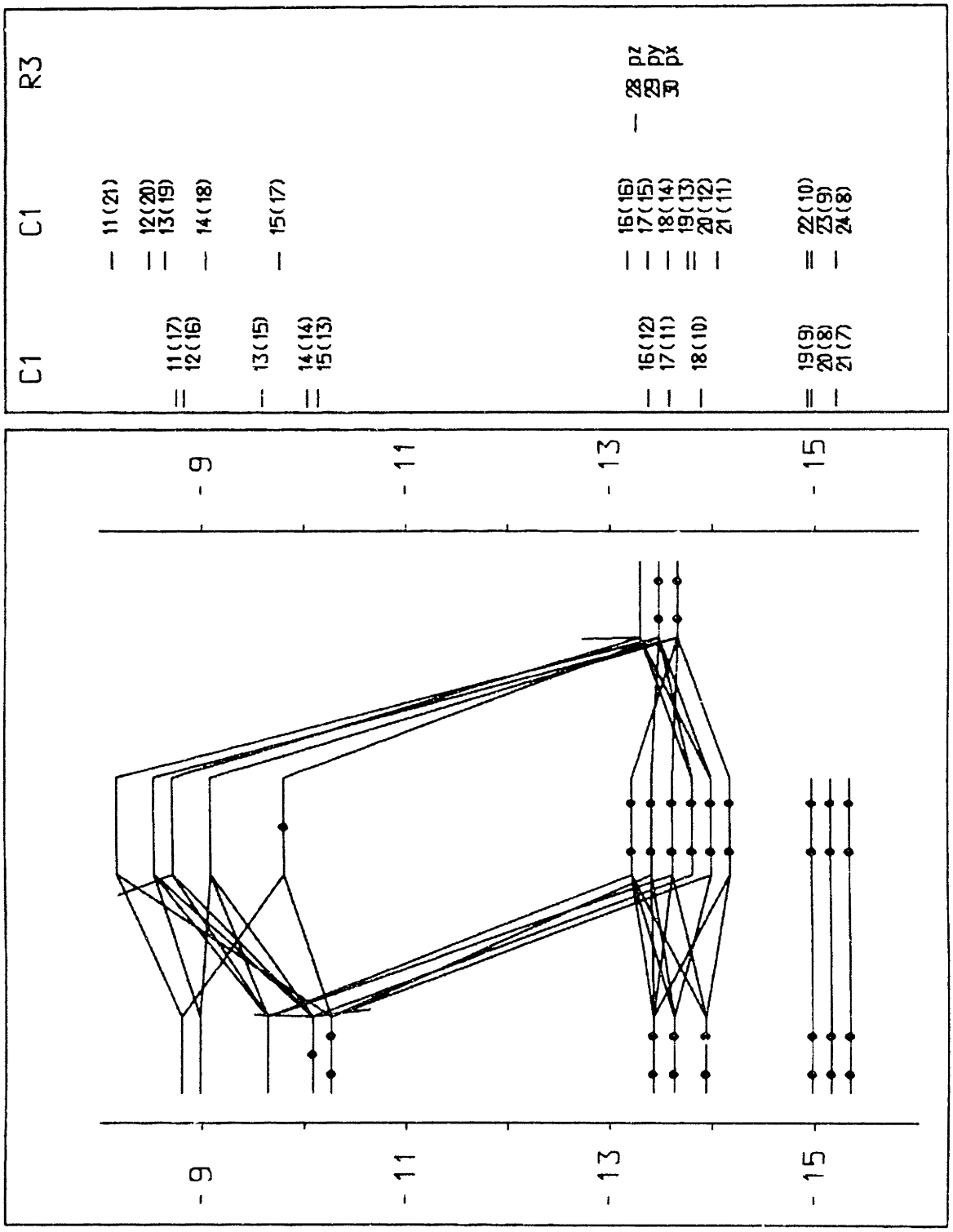

Figure AI.2: Interaction Diagram for X-Ray Input File

References begin on page 281

```
***the interaction diagram will be above this menu now***
+0=Exit/1=New diagr./2=MO draw.s/3=Mullik/P,S=Prn/-N=get Nth Diag ( 1: 1)2

   DATASET =      XRAY

Atoms shown as Symbols, Numbers or Balls? [Codes=1/2/3]
If Code is NEGATIVE, only the STRUCTURE is drawn (no MO) [DEF=3, M=Menu)]  1
```

Like the menu says, 1 uses atomic symbols, 2 uses the atom number and 3 uses a ball to represent the atom. Typing the negative integer only draws the molecule, no orbitals will be drawn. This is useful to quickly inspect the model:

```
Options: Perspective and other Details? (DEF=N) y
```

In general, keep the defaults (DEF) here. The options are:

```
perspective value? (DEF=  15.00)
draw stero pictures? (DEF=N)

1=atoms&bonds /2=bonds only /3=atoms only /4=no structure - (DEF=1)
tolerance on bond distances [D<R1+R2+TOL] (DEF= .40)

View direction              [down X (=1, Y= hor.) (=-1, Z= hor.)]
                            [down Y (=2, Z= hor.) (=-2, X= hor.)]
                            [down Z (=3, X= hor.) (=-3, Y= hor.)]
Multiple views (max 1 MO)   [down: X&Y (=4); X&Z (=5); Y&Z (=6); Z&X&Y (=7)]
[M=menu, DEF = 3]  -2
Rotation angle about  Y? (DEF=    .00)
Rotation angle about  X? (DEF=    .00)  20
Rotation angle about  Z? (DEF=    .00)
```

In general, if the molecule is centered with one amide nitrogen along the x-axis, this will result in a good view:

```
plot FMOs? [DEF=N]  y
MO energies, occ., symmetries for: $Mo(S)(NH2)3 from x-ray coordina ST. 1
Pointgroup:  C1  Total Energy =  -574.7108
  1[ 31a  ]  33.152( .0)     2[ 30a  ]  27.269( .0)     3[ 29a  ]  23.220( .0)
  4[ 28a  ]  21.942( .0)     5[ 27a  ]   6.019( .0)     6[ 26a  ]   5.423( .0)
  7[ 25a  ]   5.088( .0)     8[ 24a  ]   2.371( .0)     9[ 23a  ]   2.309( .0)
 10[ 22a  ]   2.087( .0)    11[ 21a  ]  -8.172( .0)    12[ 20a  ]  -8.535( .0)
 13[ 19a  ]  -8.687( .0)    14[ 18a  ]  -9.086( .0)    15[ 17a  ]  -9.806(1.0)
 16[ 16a  ] -13.217(2.0)    17[ 15a  ] -13.415(2.0)    18[ 14a  ] -13.615(2.0)
 19[ 13a  ] -13.812(2.0)    20[ 12a  ] -13.872(2.0)    21[ 11a  ] -14.100(2.0)
 22[ 10a  ] -14.975(2.0)    23[  9a  ] -15.014(2.0)    24[  8a  ] -15.248(2.0)
 25[  7a  ] -16.577(2.0)    26[  6a  ] -16.663(2.0)    27[  5a  ] -16.697(2.0)
 28[  4a  ] -20.754(2.0)    29[  3a  ] -28.064(2.0)    30[  2a  ] -28.104(2.0)
 31[  1a  ] -28.326(2.0)
        enter MO number to analize in terms of FMOs. Otherwise:
CR=only FMO drawings / Alph.char.=show levels again / Z = MO composition
```

Hitting return here allows visualization of the fragment MO's:

```
enter up to a max. of 12 FMO # that you wish to visualize
CR=end --- Alph. char.=show FMO levels
first fragment. pointgroup:  C1
  1[ 27a  ]  26.443( .0)     2[ 26a  ]  23.062( .0)     3[ 25a  ]  22.402( .0)
  4[ 24a  ]   5.789( .0)     5[ 23a  ]   5.219( .0)     6[ 22a  ]   4.763( .0)
  7[ 21a  ]   2.369( .0)     8[ 20a  ]   2.334( .0)     9[ 19a  ]   2.102( .0)
 10[ 18a  ]  -5.034( .0)    11[ 17a  ]  -8.797( .0)    12[ 16a  ]  -8.870( .0)
 13[ 15a  ]  -9.638( .0)    14[ 14a  ] -10.079(1.0)    15[ 13a  ] -10.181(2.0)
 16[ 12a  ] -13.422(2.0)    17[ 11a  ] -13.625(2.0)    18[ 10a  ] -13.935(2.0)
 19[  9a  ] -14.974(2.0)    20[  8a  ] -15.012(2.0)    21[  7a  ] -15.251(2.0)
 22[  6a  ] -16.575(2.0)    23[  5a  ] -16.662(2.0)    24[  4a  ] -16.697(2.0)
```


References begin on page 281

```
 25[  3a  ] -28.063(2.0)    26[  2a  ] -28.103(2.0)    27[  1a  ] -28.322(2.0)
Show: 1st frag. again /2nd frag. /Select FMOs (1/2/CR)
        Enter FMO number(s) [CR=end / Alph.Char.=show FMO levels] 15
        Enter FMO number(s) [CR=end / Alph.Char.=show FMO levels]

The following defaults are set for:
     Wavefunction Surface Value (WSV= .060)
     Plot Margin ( .00)
     Atomic Orbital Contraction Coefficient ( 1.50)
     Minimum Wavefunction Coefficient ( .0001)
     Two-dimensional Plot? (No)

redefine any of the above? (DEF=N, M=menu)  y
```

again, usually take the default here:

```
Value of Wavefunction (WSV) at the plotted MO Surface? (DEF=  .060)
Plot Margin (use PM>0.0 if some contours are not closed) [DEF=   .000]
AO Contraction Coefficient [=x in the expression exp(-xr)]
(enter 1.0 for No Contraction) [DEF= 1.5]
Mininum Wavefunction coeff. (Cij) to be considered [DEF=0.0001]
Two-Dimensional plot (no MO contraction)? [DEF=N]

Enter two Keys for Grid Finess and Mode

FINESS=Index between 1 (highest resol., slow) and 9 (lowest resol., fast)
MODE= one of the Key Characters listed below:

N (or blank)= Normal (molecule rotated, faster)
M= same as N with double grid points
P= Observation point rotated (slower)
S= same as P with double grid points
X= MO envelopes only
[Defaults: CR= 5,N --- Any Alph.Char.= 5,X]
Select atomic orbital contributions to MOs?
[DEF=Y / Z = examine MO compositions)  z
```

The MO compositions of the orbital can be examined by typing z:

```
Numerical results for:     XRAY
Enter treshold for orbital contribution to the various MOs (DEF=1.0%)
enter MO number (max.= 31) [CR = EXIT] 15
Mo(S)(NH2)3 from x-ray coordina                          Pointgroup:  C1
MO  15[ 17a  ] E(eV) =   -9.806 FILLED - Total Levels=  31
 S  1 py     4%(-)        FMO  11 (FRG 1)        12%(+)
MO  2 x2y2  51%(-)        FMO  15 (FRG 1)        82%(+)
MO  2 yz    37%(+)        FMO  29 (  2 in FRG 2)  4%(-)
one MO # OR one or two FMO(s) [negative] OR Atom # and At.Orb. type (eg: 1,px)
[CR/E/Z = EXIT/Energies/Mulliken Analysis]
 Select atomic orbital contributions to MOs?
[DEF=Y / Z = examine MO compositions)
```

Atoms can be excluded from the MO calculation or display:

```
Atom  S 1- Enter CODE (0/1/2 for Incl./Excl/Show only), RANGE (opt.)= Highest
atom number of the given type to which the CODE applies (A=all)  a

Atom MO 2- Enter CODE (0/1/2 for Incl./Excl/Show only), RANGE (opt.)= Highest
atom number of the given type to which the CODE applies (A=all) a

Atom  N 3- Enter CODE (0/1/2 for Incl./Excl/Show only), RANGE (opt.)= Highest
atom number of the given type to which the CODE applies (A=all) a

Atom  H 6- Enter CODE (0/1/2 for Incl./Excl/Show only), RANGE (opt.)= Highest
```


References begin on page 281

```
atom number of the given type to which the CODE applies (A=all) a


Scale for the hard copy of the drawing:
Scale=1cm./Amg. \Drawings rescaled to fit one page \User Scale [1\2\3, DEF=2]
P=Proceed  / R=Repeat  Questions / S=Symmetry Redef. / M=Main Menu (DEF=P)]

        *CACAO*CACAO*CACAO*CACAO*CACAO*CACAO*CACAO*CACAO*CACAO*CACAO*
        C                                                          C
        A                                                          A
        C     CALCULATION IN PROGRESS! Wait and See  1 Plot(s)     C
        A                                                          A
        O                                                          O
        *CACAO*CACAO*CACAO*CACAO*CACAO*CACAO*CACAO*CACAO*CACAO*CACAO*
```

The FMO diagram obtained is shown in figure A1.3 The normal menu is below the diagram. Typing 2 allows the drawing of a new MO:

```
+0=Exit/1=New diagr./2=MO draw.s/3=Mullik/P,S=Prn/-N=get Nth Diag ( 1: 1)2


   DATASET =     XRAY

Atoms shown as Symbols, Numbers or Balls? [Codes=1/2/3]
If Code is NEGATIVE, only the STRUCTURE is drawn (no MO) [DEF=3, M=Menu)]  1

Options: Perspective and other Details? (DEF=N)

View direction              [down X (=1, Y= hor.) (=-1, Z= hor.)]
                            [down Y (=2, Z= hor.) (=-2, X= hor.)]
                            [down Z (=3, X= hor.) (=-3, Y= hor.)]
Multiple views (max 1 MO)   [down: X&Y (=4); X&Z (=5); Y&Z (=6); Z&X&Y (=7)]
[M=menu, DEF = 3] -2
Rotation angle about  Y? (DEF=     .00)
Rotation angle about  X? (DEF=     .00)  20
Rotation angle about  Z? (DEF=     .00)
plot FMOs? [DEF=N]  The following defaults are set for:
     Wavefunction Surface Value (WSV= .060)
     Plot Margin ( .00)
     Atomic Orbital Contraction Coefficient ( 1.50)
     Minimum Wavefunction Coefficient ( .0001)
     Two-dimensional Plot? (No)

redefine any of the above? (DEF=N, M=menu) N

MO energies, occup., symmetries for: $Mo(S)(NH2)3 from x-ray coordina ST. 1
pointgroup: C1  total energy =  -574.7108
  1[ 31a  ]  33.152( .0)     2[ 30a  ]  27.269( .0)     3[ 29a  ]  23.220( .0)
  4[ 28a  ]  21.942( .0)     5[ 27a  ]   6.019( .0)     6[ 26a  ]   5.423( .0)
  7[ 25a  ]   5.088( .0)     8[ 24a  ]   2.371( .0)     9[ 23a  ]   2.309( .0)
 10[ 22a  ]   2.087( .0)    11[ 21a  ]  -8.172( .0)    12[ 20a  ]  -8.535( .0)
 13[ 19a  ]  -8.687( .0)    14[ 18a  ]  -9.086( .0)    15[ 17a  ]  -9.806(1.0)
 16[ 16a  ] -13.217(2.0)    17[ 15a  ] -13.415(2.0)    18[ 14a  ] -13.615(2.0)
 19[ 13a  ] -13.812(2.0)    20[ 12a  ] -13.872(2.0)    21[ 11a  ] -14.100(2.0)
 22[ 10a  ] -14.975(2.0)    23[  9a  ] -15.014(2.0)    24[  8a  ] -15.248(2.0)
 25[  7a  ] -16.577(2.0)    26[  6a  ] -16.663(2.0)    27[  5a  ] -16.697(2.0)
 28[  4a  ] -20.754(2.0)    29[  3a  ] -28.064(2.0)    30[  2a  ] -28.104(2.0)
 31[  1a  ] -28.326(2.0)
```


References begin on page 281

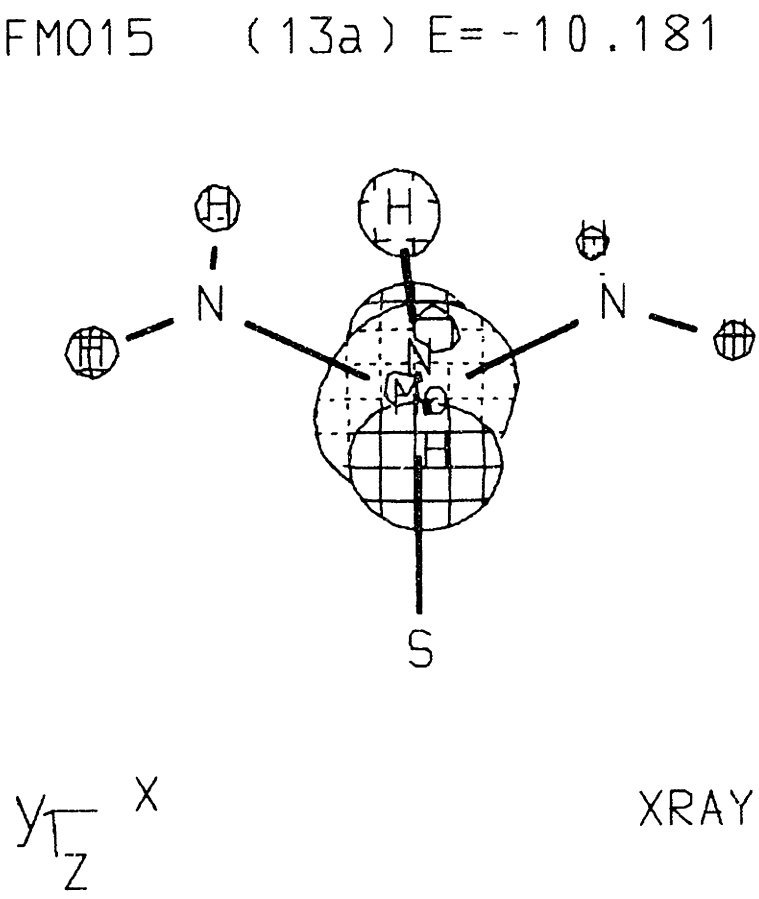

Figure AI.3: FMO Diagram for X-Ray Input File

References begin on page 281

```
Enter MO number for plot  1 (if <0 the MO phase is inverted).
[E=show levels again /CR=end input /Z=examine MO composition /M=menu]  2
Enter MO number for plot  2 (if <0 the MO phase is inverted).
[E=show levels again /CR=end input /Z=examine MO composition /M=menu]
```

Typing "2" indicated that MO #2 is selected (orbitals are numbered from high to low energy, orbital #2 is empty). Up to 6 MO's can be visualized at one time without loss of too much resolution:

```
Enter two Keys for Grid Finess and Mode

FINESS=Index between 1 (highest resol., slow) and 9 (lowest resol., fast)
MODE= one of the Key Characters listed below:

N (or blank)= Normal (molecule rotated, faster)
M= same as N with double grid points
P= Observation point rotated (slower)
S= same as P with double grid points
X= MO envelopes only
[Defaults: CR= 5,N --- Any Alph.Char.= 5,X]
Select atomic orbital contributions to MOs?
[DEF=Y / Z = examine MO compositions) N
Scale for the hard copy of the drawing:
Scale=1cm./Amg. \Drawings rescaled to fit one page \User Scale [1\2\3, DEF=2]
P=Proceed  / R=Repeat  Questions / S=Symmetry Redef. / M=Main Menu (DEF=P)]
```

The MO obtained is shown in Figure AI.4. The normal menu will be below. To quit the session, simply type 0 and return. The next session uses the input file inter.in. As the two sessions have identical options, fewer comments will be given. To run CACAO, type "eh ." with no file name:

Internal Coordinates Session

```
C:\MOAN\ADAM>EH .

C:\MOAN\ADAM>ECHO OFF

---------- DOSVER

MS-DOS Version 6.22

        ************************************************************
        *            CARLO MEALLI and DAVIDE M. PROSERPIO          *
        *            C.A.C.A.O.  (Version 4.0, April 1994)         *
        *       (Computer Aided Composition of Atomic Orbitals)    *
        * Ref.: JOURNAL of the CHEMICAL EDUCATION (1990,67,399)    *
        ************************************************************


     1)       INTER       2)       WALSH       3)       XRAY

The above files contain suitable CACAO datasets.
Select one of them by number (=N).
(CR=Escape this menu, L=List Files again, -N=Show Title of Nth Set)  1
    Interaction Diagram / MO drawings ? (Any char. / CR=return)  J
```


References begin on page 281

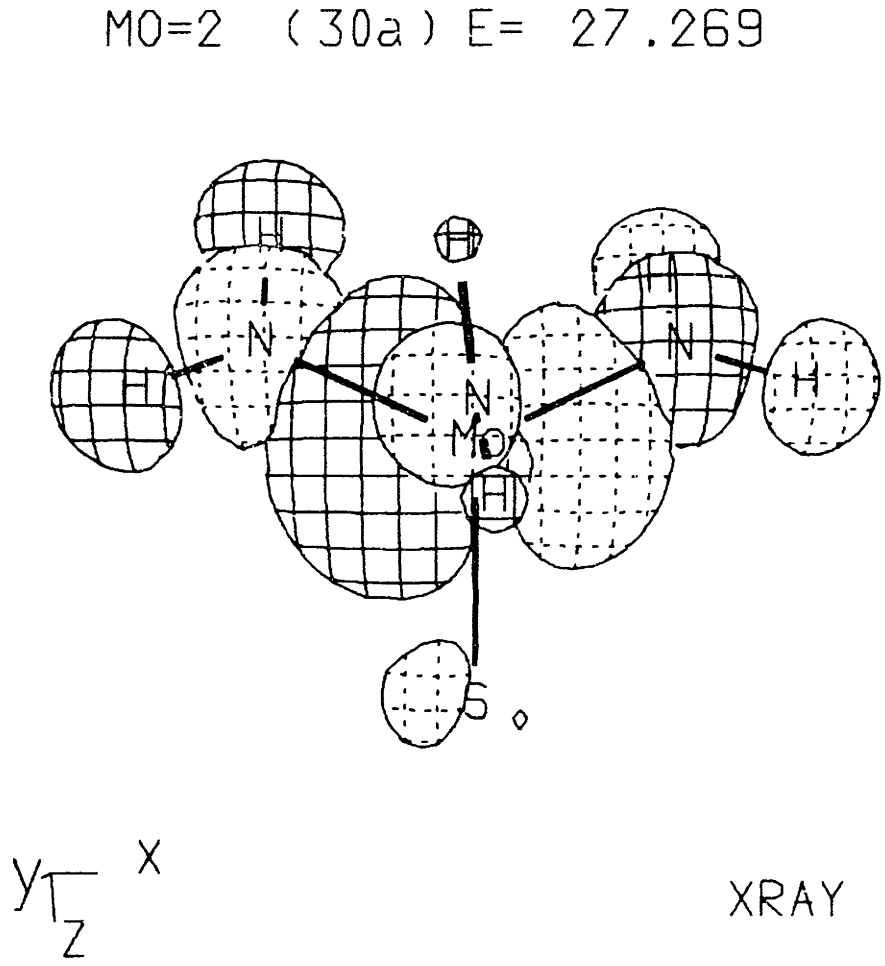

Figure AI.4: MO Diagram for X-Ray Input File

References begin on page 281

```
   DATASET = INTER

Strike Return to use the following default settings:

Energy Interval =    -25.0     3.0 eV
Minimum FMO contribution = 2.0%
Draw all MOs within the given range (i.e., no selection by symmetry or number)
Use the highest resolution between quasi-degenerate levels

Otherwise, start entering MINIMUN ENERGY (M=menu)
```

The interaction diagram thus obtained is shown in Figure AI.5.

```
+0=Exit/1=New diagr./2=MO draw.s/3=Mullik/P,S=Prn/-N=get Nth Diag ( 1: 1)2
   DATASET =    INTER

Atoms shown as Symbols, Numbers or Balls? [Codes=1/2/3]
If Code is NEGATIVE, only the STRUCTURE is drawn (no MO) [DEF=3, M=Menu)] 1

Options: Perspective and other Details? (DEF=N)

View direction              [down X (=1, Y= hor.) (=-1, Z= hor.)]
                            [down Y (=2, Z= hor.) (=-2, X= hor.)]
                            [down Z (=3, X= hor.) (=-3, Y= hor.)]
Multiple views (max 1 MO)   [down: X&Y (=4); X&Z (=5); Y&Z (=6); Z&X&Y (=7)]
[M=menu, DEF = 3]    -2
Rotation angle about  Y? (DEF=    .00)
Rotation angle about  X? (DEF=    .00)  20
Rotation angle about  Z? (DEF=    .00)
plot FMOs? [DEF=N]

The following defaults are set for:
     Wavefunction Surface Value (WSV= .060)
     Plot Margin ( .00)
     Atomic Orbital Contraction Coefficient ( 1.50)
     Minimum Wavefunction Coefficient ( .0001)
     Two-dimensional Plot? (No)

redefine any of the above? (DEF=N, M=menu)
MO energies, occup., symmetries for: $(H2N)3MoNMo(SH)3 from x-ray str ST. 1
pointgroup:C3   total energy = -1003.7394
  1[ 19a  ]  54.932( .0)     2[ 18e  ]  54.888( .0)     3[ 18e  ]  54.888( .0)
  4[ 18a  ]  43.288( .0)     5[ 17e  ]  30.827( .0)     6[ 17e  ]  30.827( .0)
  7[ 17a  ]  27.679( .0)     8[ 16a  ]  17.295( .0)     9[ 16e  ]  15.950( .0)
 10[ 16e  ]  15.950( .0)    11[ 15e  ]   7.681( .0)    12[ 15e  ]   7.681( .0)
 13[ 15a  ]   6.781( .0)    14[ 14e  ]   5.826( .0)    15[ 14e  ]   5.826( .0)
 16[ 14a  ]   5.407( .0)    17[ 13a  ]   4.174( .0)    18[ 13e  ]  -8.030( .0)
 19[ 13e  ]  -8.030( .0)    20[ 12a  ]  -8.300( .0)    21[ 11a  ]  -8.501( .0)
 22[ 12e  ]  -8.721( .0)    23[ 12e  ]  -8.721( .0)    24[ 11e  ]  -9.152( .0)
 25[ 11e  ]  -9.152( .0)    26[ 10e  ]  -9.940(1.0)    27[ 10e  ]  -9.940(2.0)
 28[ 10a  ] -13.193(2.0)    29[  9a  ] -13.428(2.0)    30[  9e  ] -13.484(2.0)
 31[  9e  ] -13.484(2.0)    32[  8e  ] -13.686(2.0)    33[  8e  ] -13.686(2.0)
 34[  7e  ] -13.754(2.0)    35[  7e  ] -13.754(2.0)    36[  8a  ] -13.790(2.0)
 37[  6e  ] -14.095(2.0)    38[  6e  ] -14.095(2.0)    39[  7a  ] -14.384(2.0)
 40[  5e  ] -14.970(2.0)    41[  5e  ] -14.970(2.0)    42[  6a  ] -15.223(2.0)
 43[  4e  ] -15.619(2.0)    44[  4e  ] -15.619(2.0)    45[  5a  ] -15.971(2.0)
 46[  4a  ] -16.712(2.0)    47[  3e  ] -16.715(2.0)    48[  3e  ] -16.715(2.0)
 49[  2e  ] -22.400(2.0)    50[  2e  ] -22.400(2.0)    51[  3a  ] -22.612(2.0)
 52[  2a  ] -27.105(2.0)    53[  1e  ] -28.290(2.0)    54[  1e  ] -28.290(2.0)
 55[  1a  ] -28.512(2.0)
```


References begin on page 281

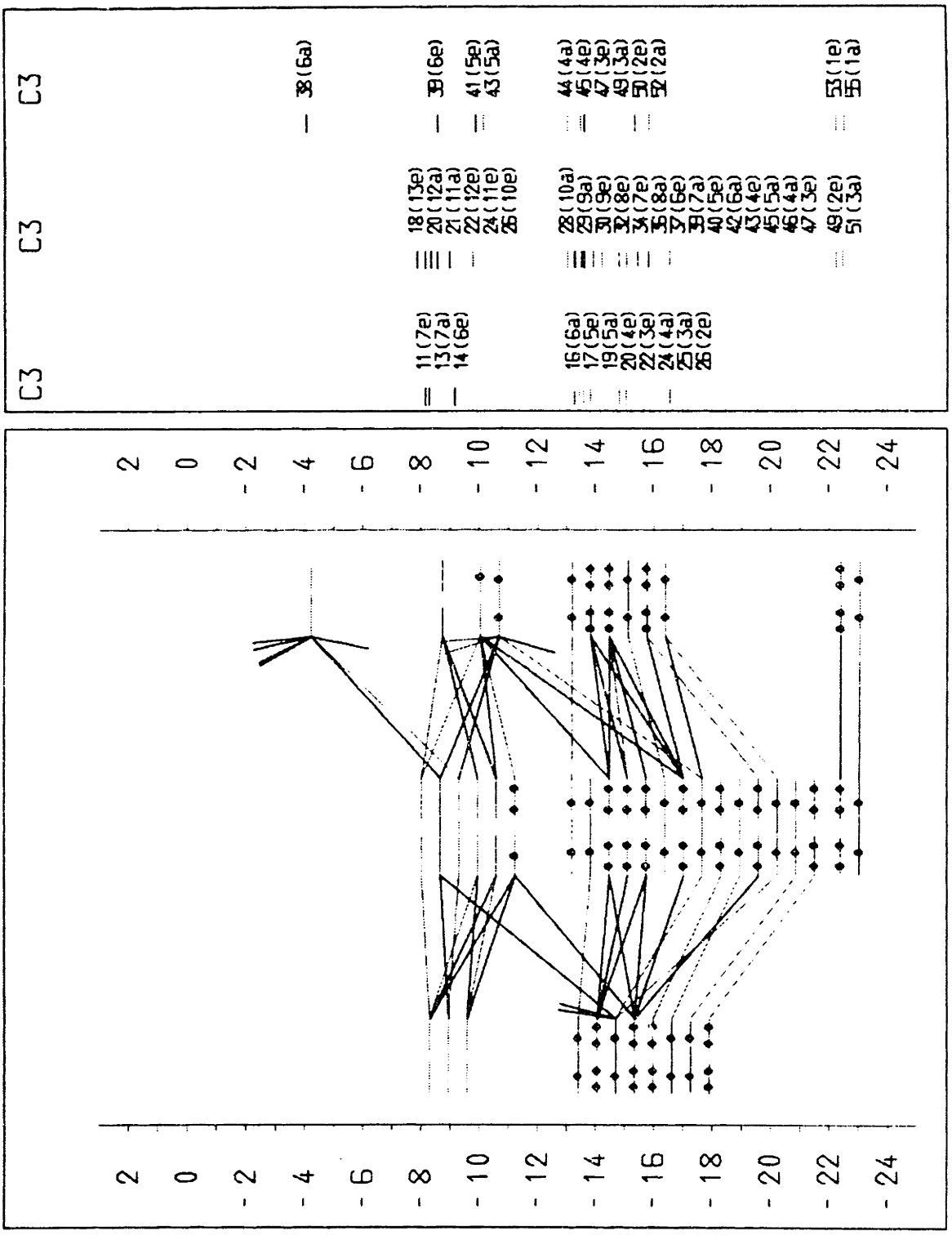

Figure AI.5: Interaction Diagram for Internal Coordinates Input File

References begin on page 281

```
Enter MO number for plot  1 (if <0 the MO phase is inverted).
[E=show levels again /CR=end input /Z=examine MO composition /M=menu]  26
Enter MO number for plot  2 (if <0 the MO phase is inverted).
[E=show levels again /CR=end input /Z=examine MO composition /M=menu]

Enter two Keys for Grid Finess and Mode

FINESS=Index between 1 (highest resol., slow) and 9 (lowest resol., fast)
MODE= one of the Key Characters listed below:

N (or blank)= Normal (molecule rotated, faster)
M= same as N with double grid points
P= Observation point rotated (slower)
S= same as P with double grid points
X= MO envelopes only
[Defaults: CR= 5,N --- Any Alph.Char.= 5,X]
Select atomic orbital contributions to MOs?
[DEF=Y / Z = examine MO compositions)  n

Scale for the hard copy of the drawing:
Scale=1cm./Amg. \Drawings rescaled to fit one page \User Scale [1\2\3, DEF=2]
P=Proceed  / R=Repeat  Questions / S=Symmetry Redef. / M=Main Menu (DEF=P)]
```

The MO diagram obtained is shown in Figure A1.6. Finally, the last session shows the generation of a Walsh diagram:

Walsh diagram Session

```
C:\MOAN\ADAM>eh .

C:\MOAN\ADAM>ECHO OFF

---------- DOSVER

MS-DOS Version 6.22


        ************************************************************
        *            CARLO MEALLI and DAVIDE M. PROSERPIO          *
        *            C.A.C.A.O.  (Version 4.0, April 1994)         *
        *       (Computer Aided Composition of Atomic Orbitals)    *
        * Ref.: JOURNAL of the CHEMICAL EDUCATION (1990,67,399)    *
        ************************************************************


     1)      INTER       2)      WALSH       3)       XRAY

The above files contain suitable CACAO datasets.
Select one of them by number (=N).
(CR=Escape this menu, L=List Files again, -N=Show Title of Nth Set)  2
         Walsh Diagram / MO drawings ? (Any char. / CR=return) k
```


References begin on page 281

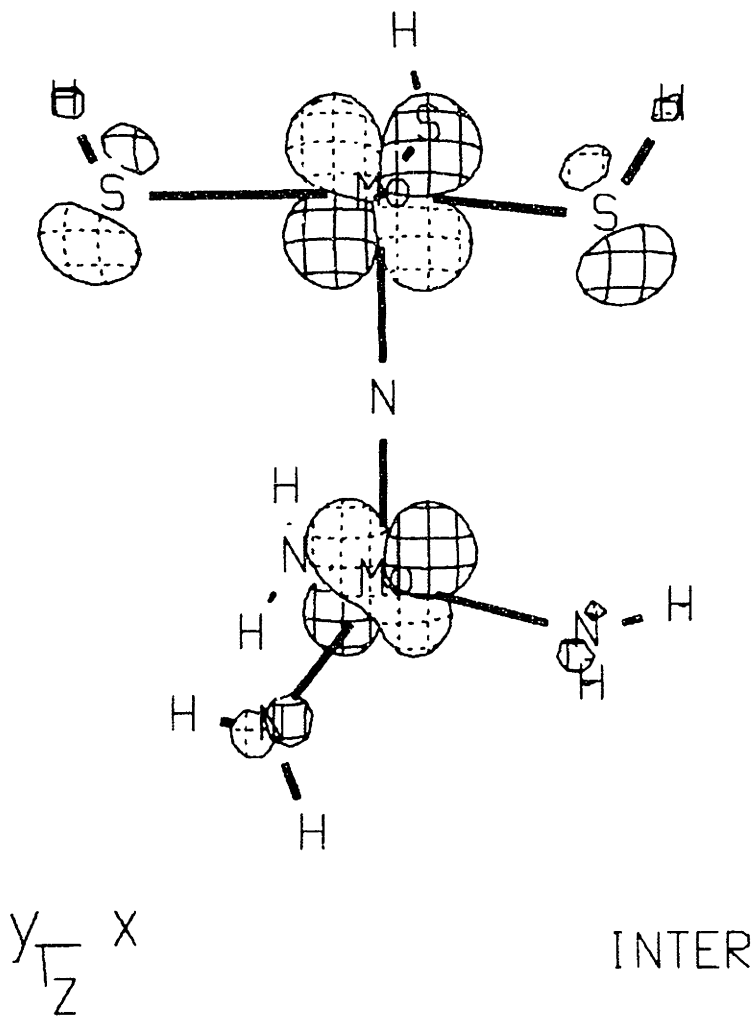

Figure AI.6: MO Diagram for Internal Coordinates Input File

References begin on page 281

```
   DATASET = WALSH

Strike Return to use the following default settings:

Energy interval =    -25.0     3.0 eV.
Total energy plotted with the scale of the MO levels
Steps in the original order
Draw all MOs within the given range (i.e., no selection by symmetry or number)

Otherwise, start entering MINIMUN ENERGY (M=menu)
```

To zoom in on the energy, reverse the order of the steps or change the defaults, eneter a minimum energy here, otherwise hitting return goes to the Walsh diagram, which is shown in Figure AI.7.

```
+0=Exit/1=New diagr./2=MO draw.s/3=Mullik/P,S=Prn/-N=get Nth Diag ( 1: 1)2

  DATASET =    WALSH

Atoms shown as Symbols, Numbers or Balls? [Codes=1/2/3]
If Code is NEGATIVE, only the STRUCTURE is drawn (no MO) [DEF=3, M=Menu)]

Options: Perspective and other Details? (DEF=N)

View direction              [down X (=1, Y= hor.) (=-1, Z= hor.)]
                            [down Y (=2, Z= hor.) (=-2, X= hor.)]
                            [down Z (=3, X= hor.) (=-3, Y= hor.)]
Multiple views (max 1 MO)   [down: X&Y (=4); X&Z (=5); Y&Z (=6); Z&X&Y (=7)]
[M=menu, DEF = 3] -2
Rotation angle about  Y? (DEF=     .00)
Rotation angle about  X? (DEF=     .00)  20
Rotation angle about  Z? (DEF=     .00)

There are 10 computed steps in the file.
Enter the number of a single step to visualize some of its MOs.
Otherwise, the evolution of one MO over the steps can be monitored
CR to select the steps one by one
A= Include all Steps  a
```

Typing return here allows for the selection of some of the steps:

```
The following defaults are set for:
     Wavefunction Surface Value (WSV= .060)
     Plot Margin ( .00)
     Atomic Orbital Contraction Coefficient ( 1.50)
     Minimum Wavefunction Coefficient ( .0001)
     Two-dimensional Plot? (No)

redefine any of the above? (DEF=N, M=menu)

MO energies, occup., symmetries for: $Mo(NH2)3 rotation of one amide  ST. 1
pointgroup:C2   total energy =  -470.1742
  1[ 13b  ]  22.585( .0)     2[ 14a  ]  22.585( .0)     3[ 13a  ]  15.979( .0)
  4[ 12b  ]   2.254( .0)     5[ 12a  ]   2.254( .0)     6[ 11a  ]   1.327( .0)
  7[ 11b  ]   -.004( .0)     8[ 10a  ]   -.114( .0)     9[ 10b  ]   -.114( .0)
 10[  9b  ]  -4.560( .0)    11[  9a  ]  -8.480( .0)    12[  8b  ]  -8.480( .0)
 13[  8a  ] -10.208( .0)    14[  7b  ] -10.232(1.0)    15[  7a  ] -10.232(2.0)
 16[  6b  ] -13.354(2.0)    17[  6a  ] -13.776(2.0)    18[  5b  ] -13.776(2.0)
 19[  5a  ] -14.905(2.0)    20[  4b  ] -14.905(2.0)    21[  4a  ] -15.187(2.0)
 22[  3b  ] -16.626(2.0)    23[  2b  ] -16.655(2.0)    24[  3a  ] -16.655(2.0)
 25[  2a  ] -27.902(2.0)    26[  1b  ] -27.902(2.0)    27[  1a  ] -28.098(2.0)
```


References begin on page 281

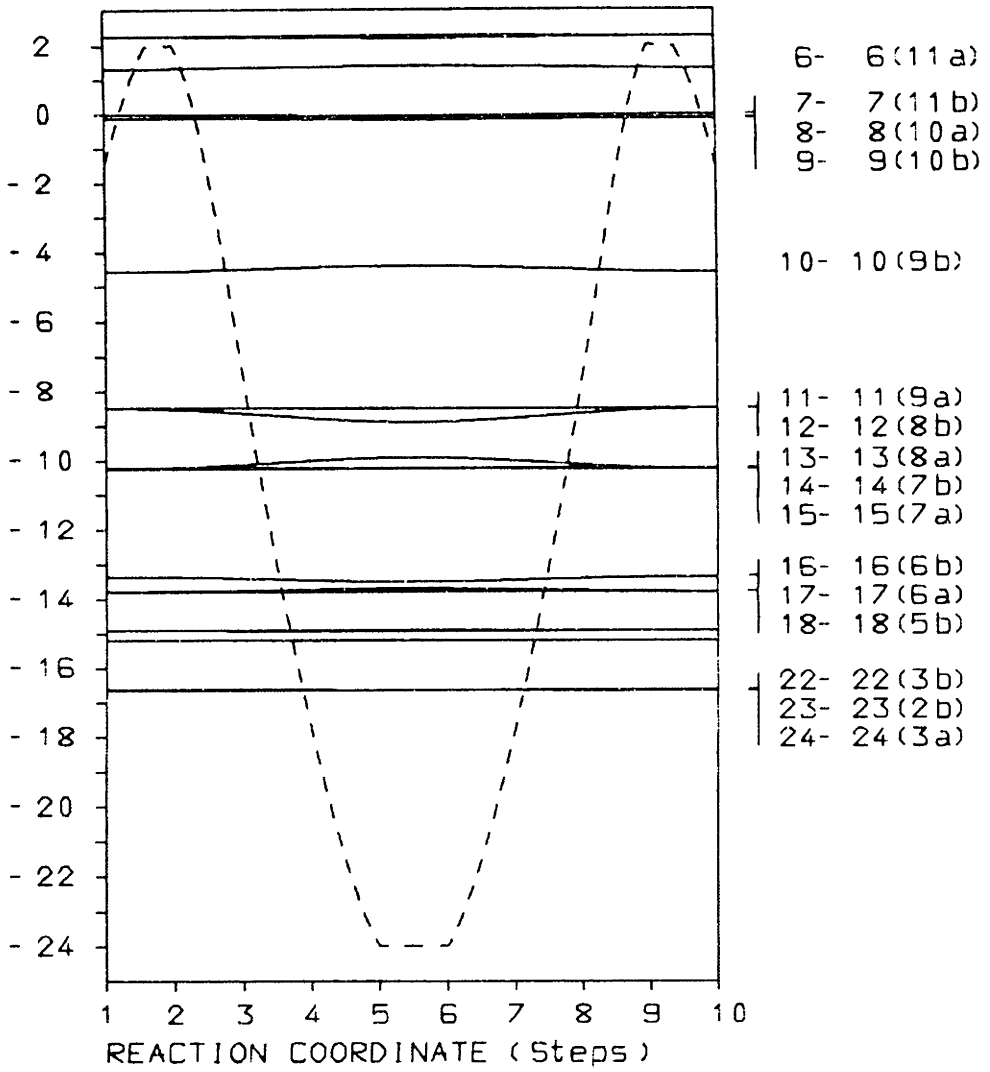

Figure AI.7: Walsh Diagram

References begin on page 281

```
     enter the number of a single MO to be drawn at 10 different steps
[Z=examine MO compositions - M=menu]  14

Enter two Keys for Grid Finess and Mode

FINESS=Index between 1 (highest resol., slow) and 9 (lowest resol., fast)
MODE= one of the Key Characters listed below:

N (or blank)= Normal (molecule rotated, faster)
M= same as N with double grid points
P= Observation point rotated (slower)
S= same as P with double grid points
X= MO envelopes only
[Defaults: CR= 5,N --- Any Alph.Char.= 5,X]
Select atomic orbital contributions to MOs?
[DEF=Y / Z = examine MO compositions) n

Scale for the hard copy of the drawing:
Scale=1cm./Amg. \Drawings rescaled to fit one page \User Scale [1\2\3, DEF=2]
P=Proceed  / R=Repeat  Questions / S=Symmetry Redef. / M=Main Menu (DEF=P)]
```

Several of the 10 orbitals observed are shown in Figure AI.8. This ends the interactive session. There are other features to be explored with this program, but the important and most useful ones have been covered. The best way to become familiar with the program is by making some models and looking at some orbitals. Thanks for reading!

References

1) Mealli, C.; Proserpio, D. M. *J. Chem. Educ.* **1990**, *67*, 399-402.
2) Mealli, C.; Proserpio, D. M. *CACAO (Computer Aided Composition of Atomic Orbitals);* 4.0 ed.Florence (Italy), 1994.
3) Hoffmann, R. *J. Chem. Phys.* **1963**, *39*, 1397.
4) Hoffmann, R.; Lipscomp, W. N. *J. Chem. Phys.* **1962**, *36*, 2179.
5) Hoffmann, R.; Lipscomb, W. N. *J. Chem. Phys.* **1962**, *36*, 3489.
6) Fujimoto, H.; Hoffmann, R. *J. Chem. Phys.* **1964**, *78*,
7) Albright, T. A.; Burdett, J. K.; Whangbo, M. H. *Orbital Interactions in Chemistry*; Wiley: New York, 1975.
8) See, for example, Chapter II of this thesis.
9) Carey, F. A.; Sundberg, R. J. *Advanced Organic Chemistry;* 3rd ed.; Plenum Press: New York, 1990.
10) Cotton, F. A. *Chemical Applications of Group Theory;* third ed.; John Wiley and Sons: New York, 1990.
11) Karplus, M.; Porter, R. N. *Atoms and Molecules*; Benjamin/Cummings Publishing Company: Reading, MA, 1970.
12) Mealli, C.; Proserpio, D. M.; Fachinetti, G.; Funaioli, T.; Fochi, G.; Zanazzi, P. F. *Inorg. Chem.* **1989**, *28*, 1122-1127.
13) *Chem3D*; Cambridge Scientific Computing: Cambridge, MA, 1993.
14) The molecule described in this section was originally prepared by Aaron Odom.

References begin on page 281

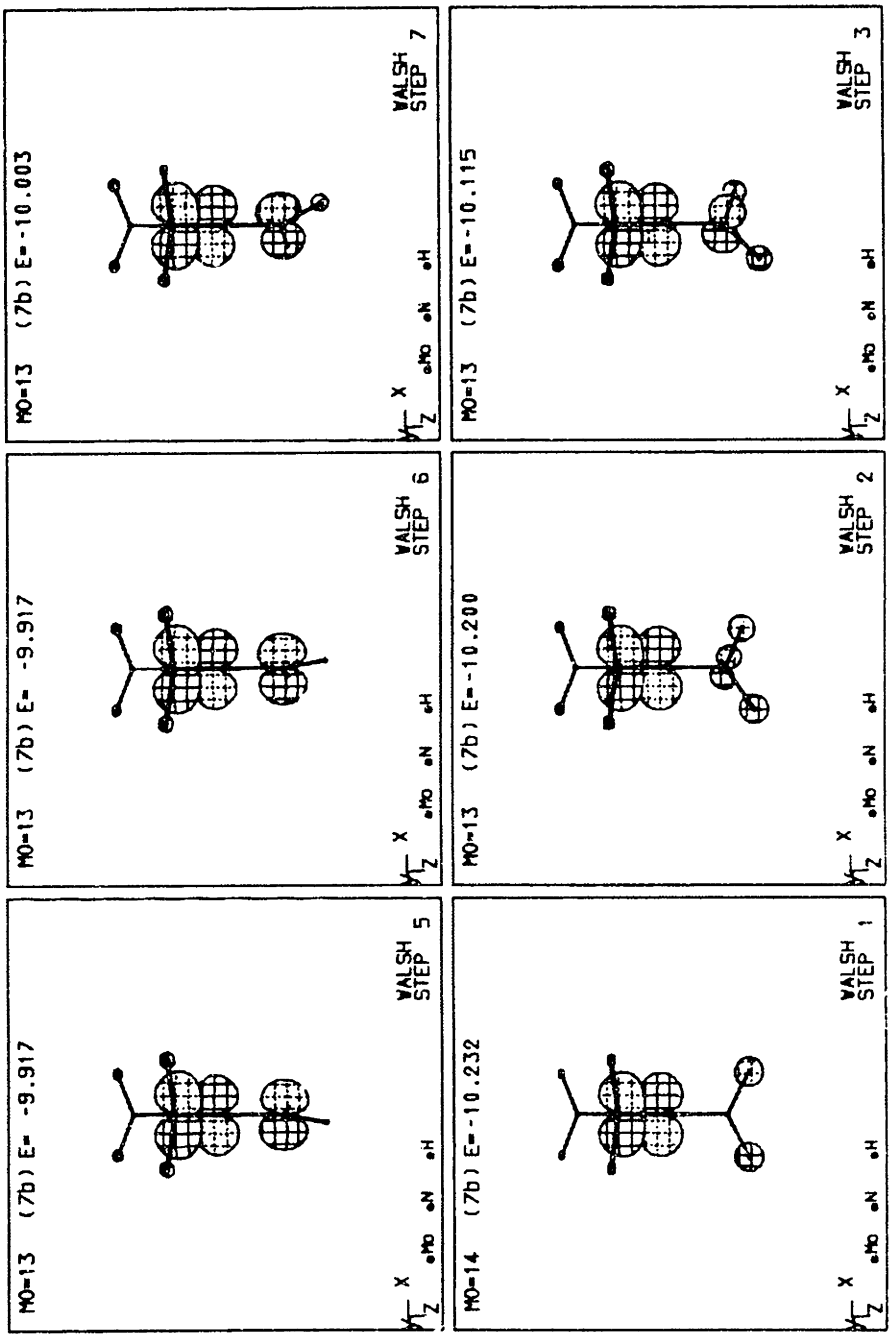

Figure AI.8: Some MOs Corresponding to Walsh Diagram

References begin on page 281

Section 8: DOS Batch Files

The DOS batch files included with CACAO for interfacing with printgl, are defective. Corrected batch files are included in this addendum.
pl.bat

```
@ECHO off
REM pl.bat
IF ""=="%1" GOTO HELP
:BEGIN
IF "MOAN"=="%1" GOTO DIAGRAM
IF "moan"=="%1" GOTO DIAGRAM
IF "CACAO"=="%1" GOTO CACAO
IF "cacao"=="%1" GOTO CACAO
IF "OUT"=="%1" GOTO PRINTOUT
IF "out"=="%1" GOTO PRINTOUT
IF "ALL"=="%1" GOTO PRINTALL
IF "all"=="%1" GOTO PRINTALL
IF  "%2"=="" GOTO PS2
GOTO PS1
:PS2
CALL PLOTF %1 253
GOTO END
:PS1
CALL PLOTF %1  %2
GOTO END
:CACAO
IF "P"=="%2" GOTO PSCAC
IF "p"=="%2" GOTO PSCAC
IF "F"=="%2" GOTO PSCAC
IF "f"=="%2" GOTO PSCAC
FOR %%F IN (\moan\CACAO*.hgl) DO CALL PLOTF %%F
GOTO END
:PSCAC
ECHO     POSCRIPT
FOR %%F IN (\moan\CACAO*.HGL) DO COPY %%F \moan\cacao*.tem
FOR %%F IN (\moan\CACAO*.HGL) DO CALL PLOTF  %%F  %2  R
FOR %%F IN (\moan\CACAO*.HGL) DO COPY %%F \moan\cacao*.ps
FOR %%F IN (\moan\CACAO*.TEM) DO COPY %%F \moan\cacao*.hgl
FOR %%F IN (\moan\CACAO*.TEM) DO ERASE %%F
GOTO END
:DIAGRAM
IF "PS"=="%2" GOTO PSDIA
IF "ps"=="%2" GOTO PSDIA
IF "F"=="%2" GOTO PSDIA
IF "f"=="%2" GOTO PSDIA
FOR %%F IN (\moan\MOAN*.hgl) DO CALL PLOTF %%F
GOTO END
:PSDIA
ECHO     POSCRIPT
FOR %%F IN (\moan\moan*.HGL) DO COPY %%F \moan\moan*.tem
FOR %%F IN (\moan\moan*.HGL) DO CALL PLOTF %%F  %2  R
FOR %%F IN (\moan\moan*.HGL) DO COPY %%F \moan\moan*.ps
FOR %%F IN (\moan\moan*.TEM) DO COPY %%F \moan\moan*.hgl
```


References begin on page 281

```
FOR %%F IN (\moan\moan*.TEM) DO ERASE %%F
GOTO END
:PRINTOUT
IF NOT EXIST \moan\CACAO.OUT GOTO NOPRINTOUT
PRINT \MOAN\CACAO.OUT
GOTO END
:NOPRINTOUT
ECHO ******** The file \moan\CACAO.OUT does not exist. ******
ECHO.
GOTO END
:PRINTALL
IF "P"=="%2" GOTO PSTUTTO
IF "p"=="%2" GOTO PSTUTTO
IF "F"=="%2" GOTO PSTUTTO
IF "f"=="%2" GOTO PSTUTTO
FOR %%F IN (\moan\CACAO*.hgl) DO CALL PLOTF   %%F    253   R
FOR %%F IN (\moan\moan*.hgl)  DO CALL PLOTF   %%F    253   R
GOTO PRINTOUT
:PSTUTTO
ECHO   POSCRIPT ALL
FOR %%F IN (\moan\CACAO*.HGL) DO COPY %%F \moan\cacao*.tem
FOR %%F IN (\moan\CACAO*.HGL) DO CALL PLOTF   %%F  %2  R
FOR %%F IN (\moan\CACAO*.HGL) DO COPY %%F \moan\cacao*.ps
FOR %%F IN (\moan\CACAO*.TEM) DO COPY %%F \moan\cacao*.hgl
FOR %%F IN (\moan\CACAO*.TEM) DO ERASE %%F
FOR %%F IN (\moan\moan*.HGL) DO COPY %%F \moan\moan*.tem
FOR %%F IN (\moan\moan*.HGL) DO CALL PLOTF %%F  %2  R
FOR %%F IN (\moan\moan*.HGL) DO COPY %%F \moan\moan*.ps
FOR %%F IN (\moan\moan*.TEM) DO COPY %%F \moan\moan*.hgl
FOR %%F IN (\moan\moan*.TEM) DO ERASE %%F
GOTO PRINTOUT
:HELP
ECHO    ------------------------------------------------------------
ECHO    Two parameters are required:
ECHO    1) any of the keywords below.
ECHO    2) the output device:
ECHO      (blank=normal printer, P=Postscr. Printer, F=Postscr. File)
ECHO                 *******
ECHO              ---- Keywords ------
ECHO    ALL  = PRINT ALL DRAWINGS AND NUMERIC OUTPUT
ECHO    OUT  = PRINT ONLY NUMERIC OUTPUT
ECHO    MOAN = PRINT ONLY THE EXISTING WALSH or INTERACTION
DIAGRAMS
ECHO    CACAO = PRINT ALL THE EXISTING CACAO DRAWINGS
ECHO    FILENAME = PRINT THE SPECIFIED FILE (ex. CACAO1 or MOAN2)
:END
```

plotf.bat

```
@echo off
REM plotf.bat
IF "P"=="%2" GOTO POSTSCRIPT
IF "p"=="%2" GOTO POSTSCRIPT
```


References begin on page 281

```
IF "F"=="%2" GOTO POSTSCRIPT
IF "f"=="%2" GOTO POSTSCRIPT
IF "R"=="%3" GOTO ALL
IF NOT EXIST \moan\%1.hgl GOTO NOFILE3
REM definition of the printer: /FA=deskjet, /FL=laserjet (or see Printgl manual)
PRINTGLD \moan\%1.hgl /d1/fa~/mf.9/ao0,0/o1/cok
GOTO END
:NOFILE3
ECHO ERROR: FILE \moan\%1.hgl DOESN'T EXIST
ECHO.
GOTO END
:ALL
IF NOT EXIST %1 GOTO NOFILE2
REM definition of the printer: /FA=deskjet, /FL=laserjet (or see Printgl manual)
PRINTGLD %1
GOTO END
:NOFILE2
ECHO ERROR: FILE %1 DOESN'T EXIST
ECHO.
GOTO END
:POSTSCRIPT
IF "R"=="%3" GOTO TUTTI
IF NOT EXIST \mo. ..%1.hgl GOTO NOFILE1
IF "P"=="%2" GOTO STAMPANTE1
IF "p"=="%2" GOTO STAMPANTE1
PRINTGLD \moan\%1.hgl /d%1.out/fs~/mf.9/ao0,0/o1
GOTO END
:STAMPANTE1
echo printer
PRINTGLD \moan\%1.hgl /d1/fa~/mf.9/ao0,0/o1/cok
GOTO END
:NOFILE1
ECHO ERROR: FILE \moan\%1.hgl DOESN'T EXIST
ECHO
GOTO END
:TUTTI
IF NOT EXIST %1 GOTO NOFILA
IF "P"=="%2" GOTO STAMPANTE
IF "p"=="%2" GOTO STAMPANTE
COPY %1 \moan\pippo
ERASE %1
\printgl\PRINTGLD pippo /FS /AO0,0 /M1. /O1 /LF7.60,10.87 /XSFU
/CKBMGRYCKB /WB /D%1
erase pippo
GOTO END
:STAMPANTE
echo printer
\printgl\PRINTGLD %1 /FS /AO0,0 /M1. /O1 /LF7.60,10.87 /XSFU /WB
/CKBMGRYCKB
GOTO END
:NOFILA
ECHO ERROR: FILE %1 DOESN'T EXIST
```


References begin on page 281

Appendix II: Raw Kinetics and SQUID Data

Table AII.1: Kinetics Data for the Decomposition of $OMo(N[R]Ar)_3$ (**2.2**) and $SMo(N[R]Ar)_3$ (**2.3**)

$OMo(N[R]Ar)_3$		$SMo(N[R]Ar)_3$	
Temp (K)	k_r	Temp (K)	k_r
335.95	6.1609E-06	339.05	1.4168E-04
335.95	5.6257E-06	339.05	1.3314E-04
335.95	5.7852E-06	339.05	1.2008E-04
345.65	1.9740E-05	343.35	2.2059E-04
345.65	1.6940E-05	343.35	2.0670E-04
345.65	1.9140E-05	343.35	2.3876E-04
355.55	5.8206E-05	343.35	2.3535E-04
355.55	8.7019E-05	348.45	3.7078E-04
355.55	5.2684E-05	348.45	3.7232E-04
355.65	5.9564E-05	348.45	4.1490E-04
355.65	1.0378E-04	355.95	6.3955E-04
355.65	5.6855E-05	355.95	8.9039E-04
355.65	3.6671E-05	355.95	9.3965E-04
365.95	2.4271E-04	355.65	9.7348E-04
365.95	2.1857E-04	355.65	1.0252E-03
365.95	2.0438E-04	365.95	2.0054E-03
365.55	1.8627E-04	365.95	1.8592E-03
365.55	2.9581E-04	365.95	2.1676E-03
365.55	2.1955E-04	375.35	4.0235E-03
376.95	5.8877E-04	375.35	3.3400E-03
376.95	7.6760E-04	375.35	2.9621E-03
376.95	7.2767E-04	375.35	3.1737E-03
376.95	7.1334E-04	375.35	3.9610E-03
376.95	5.7497E-04		

Avg. Temp (K)	Avg. k_r	Avg. Temp (K)	Avg. k_r
335.95	5.8573E-06	339.05	1.3163E-04
345.65	1.8607E-05	343.35	2.2535E-04
355.61	6.4968E-05	348.45	3.8600E-04
365.75	2.2788E-04	355.83	8.9365E-04
376.95	6.7447E-04	365.95	2.0107E-03
		375.35	3.4921E-03

Table AII.2: SQUID magnetic data for $Ti(N[R]Ar)_2(CH[SiMe_3]_2)$ (**1.31**), $OMo(N[R]Ar)_3$ (**2.2**) and $SMo(N[R]Ar)_3$ (**2.3**).

$Ti(N[R]Ar)_2(CH[SiMe_3]_2)$		$OMo(N[R]Ar)_3$		$SMo(N[R]Ar)_3$	
TEMP	χ	Temp (K)	χ	Temp (K)	χ
5	0.066184	4.98	0.0686493	5	0.06453372
6	0.05561155	5.98	0.05773247	6.01	0.05488402
6.98	0.04805512	6.98	0.04978452	7	0.04781123
7.97	0.0422427	7.98	0.04365139	8	0.04227974
8.97	0.03762058	8.98	0.03888876	9	0.03787366
9.98	0.03394181	9.98	0.03515432	9.99	0.03433599
11.99	0.02837201	11.99	0.02935758	12	0.02884894
14.01	0.0243435	14	0.02519323	14.02	0.02483154
16.02	0.02134613	16.03	0.02203479	16.06	0.02175907
18.04	0.0190043	18.07	0.01957496	18.06	0.01940691
20.07	0.01712206	20.07	0.01764783	20.09	0.01748563
23.11	0.01492298	23.04	0.01537109	23.02	0.01526794
26.07	0.0132717	26.11	0.01361461	26.07	0.01352583
29.07	0.01193588	29.06	0.01223305	29.08	0.01213744
32.04	0.01085753	32.03	0.01109478	32	0.01102007
35.05	0.00993187	35.02	0.010141	35.02	0.01007461
38.05	0.00914342	38.02	0.0093188	38.03	0.00926914
40.99	0.00849277	41.01	0.00866558	41.01	0.00860049
43.97	0.00791941	43.98	0.00804827	43.99	0.00799598
46.97	0.00747123	46.97	0.00751557	46.97	0.00745449
49.98	0.00704121	50	0.00706056	50	0.00700193
54.97	0.00668055	54.92	0.00638847	54.9	0.00633276
59.93	0.0060896	59.93	0.00581377	59.96	0.00575461
65.04	0.00562152	65.04	0.00535165	65.05	0.00529138
70.12	0.00521741	70.05	0.00497305	70.06	0.00490864
74.87	0.00487496	75.08	0.00464538	75.09	0.00458151
80.07	0.0045887	80.05	0.00436075	80.08	0.00429513
85.09	0.00432858	85.1	0.00409049	85.1	0.00402653
90.1	0.00409697	90.09	0.00385338	90.07	0.0037849
95.11	0.00388959	95.09	0.0036405	95.1	0.0035779
100.13	0.00370093	100.1	0.00345346	100.11	0.00338466
110.16	0.00337123	110.08	0.00312241	110.1	0.00304511
120.18	0.00309919	120.06	0.00284765	120.07	0.00277406
130.2	0.00286883	130.08	0.00261828	130.1	0.00254025
140.21	0.00267196	138.82	0.00239409	138.87	0.00228719
150.21	0.00251461	150.11	0.0022791	150.48	0.00217463
160.2	0.00235819	158.84	0.00208268	158.83	0.00197972
170.22	0.00222884	170.54	0.00200227	170.55	0.00189011
180.2	0.00211514	180.21	0.00186178	180.2	0.00174437

Table AII.2 continued.

$Ti(N[R]Ar)_2(CH[SiMe_3]_2)$		$OMo(N[R]Ar)_3$		$SMo(N[R]Ar)_3$	
TEMP	χ	Temp (K)	χ	Temp (K)	χ
190.17	0.00200775	190.2	0.00174122	190.2	0.00162794
200.16	0.00191417	200.19	0.00163503	200.19	0.00154276
220.18	0.00174415	220.15	0.00148278	220.12	0.0013776
240.16	0.00160104	240.15	0.0013481	240.15	0.0012439
260.16	0.00148385	260.16	0.00122684	260.16	0.00113578
280.14	0.00138235	280.17	0.00113018	280.16	0.00103859
300.21	0.00129042	300.16	0.00104195	300.15	0.00094552

Table AII.3: SQUID magnetic data for $SeMo(N[R]Ar)_3$ (**2.4**), $TeMo(N[R]Ar)_3$ (**2.5**) and $IMo(N[R]Ar)_3$ (**3.4**).

$SeMo(N[R]Ar)_3$		$TeMo(N[R]Ar)_3$		$IMo(N[R]Ar)_3$		
Temp (K)	χ	Temp (K)	χ	Temp (K)	χ	μ_{eff}
5	0.0596293	5	0.0403891	4.99	-0.0002156	---
6.01	0.05218658	6	0.03815989	10	0.00026802	0.14133433
6.99	0.04627807	6.99	0.03546776	14.99	0.00049131	0.23428345
7.98	0.04145898	7.99	0.03285237	20.02	0.00062841	0.30620676
8.98	0.03749608	8.97	0.03052822	25.04	0.00071699	0.36579255
9.98	0.03425019	9.96	0.0283816	30.1	0.00077915	0.41807689
11.98	0.02917384	11.99	0.02471836	35.04	0.00083296	0.46639725
13.98	0.02541295	14	0.02181599	39.98	0.00087269	0.50993446
16.02	0.02248196	16.04	0.01948849	44.97	0.00090232	0.54992534
18.05	0.02018477	18.06	0.01758465	49.95	0.00092407	0.58652109
20.07	0.01834212	20.05	0.01604217	55	0.00094255	0.62157978
23.1	0.01615508	23	0.01415591	60.06	0.00096508	0.65726099
26.08	0.01447584	26.09	0.0126564	65.09	0.00098777	0.69222633
29.06	0.01311579	29.07	0.01144273	70.01	0.00100373	0.72368923
32.05	0.01198864	32.04	0.01045616	75.23	0.00101733	0.75524794
35	0.01102002	35.01	0.009604	80.04	0.00102897	0.78346121
38.06	0.01024498	38.01	0.00887043	85.04	0.00103831	0.81121972
41	0.00958503	41	0.00825871	90.05	0.00104784	0.83859418
43.99	0.00900278	43.97	0.00769384	95.06	0.00105486	0.86448732
46.97	0.00845847	46.96	0.00721178	100.09	0.0010615	0.88985356
49.98	0.00798793	49.95	0.00677314	105.11	0.00106775	0.91457614
55.01	0.00738103	54.9	0.00615173	110.13	0.00107501	0.93933946
60.02	0.00680663	59.96	0.00561248	115.13	0.0010808	0.96300846
65.02	0.00633148	65.05	0.00517752	120.16	0.00108673	0.98651344
70.11	0.00594466	70.07	0.00482394	125.15	0.00109035	1.00846728
75.05	0.00557821	75.09	0.00451092	130.14	0.00109582	1.03094931
80.06	0.00528405	80.09	0.0042319	135.14	0.00109916	1.05216583
85.1	0.00502119	85.11	0.0039813	140.14	0.00110232	1.07299254
90.1	0.00478244	90.11	0.00375555	145.12	0.00110479	1.0931168

Table AII.3 continued.

$SeMo(N[R]Ar)_3$		$TeMo(N[R]Ar)_3$		$IMo(N[R]Ar)_3$		
Temp (K)	χ	Temp (K)	χ	Temp (K)	χ	μ_{eff}
95.11	0.00456963	95.11	0.00355292	150.14	0.00110722	1.11308263
100.13	0.00437821	100.12	0.00336088	155.12	0.00111036	1.13299505
110.16	0.00404207	110.1	0.00304074	160.13	0.00111642	1.15428681
120.19	0.00376661	120.04	0.00279399	165.13	0.00112105	1.1745968
130.19	0.00353197	130.12	0.00256479	170.15	0.00112279	1.19324055
140.2	0.0033338	138.87	0.0023411	175.13	0.00112415	1.21130812
150.21	0.00315813	150.42	0.0022426	180.13	0.0011267	1.22987184
160.19	0.00300923	158.83	0.00204403	185.11	0.00112958	1.24834737
170.22	0.00290047	170.52	0.00196426	190.11	0.00113217	1.26654856
180.19	0.00278299	180.19	0.00182422	195.1	0.00113256	1.283284
190.24	0.00267804	190.2	0.00158377	200.09	0.00113259	1.29960595
200.16	0.00257815	200.2	0.00150402	205.13	0.00113844	1.31926828
220.17	0.00240568	220.17	0.00136884	210.13	0.00113942	1.33582299
240.17	0.00226664	240.15	0.00126003	215.13	0.00114055	1.35229203
260.15	0.00214422	260.17	0.00118232	220.13	0.00115099	1.37416141
280.16	0.00204721	280.17	0.0011391	225.11	0.00115366	1.39122847
300.1	0.00195737	300.15	0.00109784	230.13	0.00114836	1.40342211
				235.07	0.00114117	1.41396013
				240.06	0.00114509	1.43133763
				245.06	0.00114649	1.44705241
				250.02	0.00114788	1.46251064
				255.02	0.00115419	1.48111644
				259.98	0.00115112	1.49345775
				264.96	0.00115787	1.51210816
				269.98	0.00115869	1.52690267
				274.97	0.00116941	1.54806144
				279.9	0.00116274	1.55742054
				286.38	0.00115302	1.56874813
				289.96	0.00115871	1.5824112
				294.98	0.0011631	1.59907147
				301.36	0.00116034	1.61435295
				305.05	0.00116777	1.62939415
				310.08	0.0011656	1.64125111
				316.33	0.0011563	1.65108057
				320.05	0.00116198	1.66483235
				326.49	0.00115852	1.67899413
				329.54	0.00114709	1.67848022
				335.95	0.0011194	1.67414141
				340.05	0.00112407	1.6878392
				346.45	0.00111874	1.69960245
				350.17	0.00112104	1.7104616

Table AII.4: Variable Temperature Evans Method Magnetic Susceptibility Data for $IMo(N[R]Ar)_3$ (**3.4**).

Temp (K)	μ_{eff} (μ_B)
293	1.57381285
283	1.51559062
273	1.45252019
263	1.38938218
253	1.33257828
243	1.26932861
233	1.21855119
213	1.13498373
203	1.09634133
208	1.10976094
213	1.12901781
218	1.14709862
223	1.16852846
228	1.1933511
238	1.24375054
248	1.28881979
258	1.34947556
268	1.40894955
278	1.47213675
288	1.53488143
298	1.60420795
303	1.63533002
308	1.67884817
313	1.72796297
318	1.77681313

Acknowledgments

As this is the section of the thesis that will most frequently be read (perhaps the *only* section to be read), it is the hardest section to write. There are so many people who deserve recognition here that I could not possibly begin to mention them all, and for any omissions, I apologize outright. During the last four years I have experienced both the happiest and the darkest moments of my life, and there have been times that I did not feel I had the strength to carry on, either emotionally or physically. For helping me through these tough times I wish to specifically thank my parents, Lee and Ann, my brother Karl, my extended family, and most importantly, my wife Wendy, to whom this thesis is dedicated. For giving me a solid foundation in the field of chemistry, I wish to thank the faculty at Oberlin College, especially Marty Ackermann and Norm Craig. Marty's genuine love of inorganic chemistry rubbed off on me, at least a little bit, and his treasured mentoring role continues to this day. I would also like to thank my former mentors, Ken Shea, Regina Wang and Rolf Wagner, for allowing me to learn from and with you. For getting the Cummins lab off the ground and being wonderful friends and co-workers, the other members of the "first five" deserve special recognition: Aaron Odom (not Greg Fu), Marc Johnson (screwdriver), Mike Fickes (grain bag) Sheree Stokes (Lybia), and yes, I include Jonas Peters (flatbread) as an honorary member of this group. The five of you have helped me in innumerable ways, not only in the loaning (giving) of starting materials, but also by sharing your unique viewpoints on chemistry and life in general. I will truly miss you and your company. Much of the chemistry described in this thesis is based on work carried out by our first UROPs Catalina Laplaza and Paulus Wanandi; I hope they continue to do well. The newest members of the group, Jane Brock and Dan Mindiola probably don't understand any of the rest of us very well; we have all spent far too much time together. I wish the two of you well in the continuation of your studies. I also want to specifically thank: Fred, for finding that first apartment, reminding me of OC days, and helping me out in the lab way back when; Doug, for teaching me everything I know about EPR; Aaron and Bill, for putting up with my X-ray questions; Marc, for your Ti-support (and lately Mo-support) and much needed editing help (!); Mike, for many helpful suggestions and needed discussions; and the Schrock and Fu labs, for indirectly (and sometimes directly) giving me chemicals, information, and interesting reading material. To anyone else whom I fail to mention specifically, I apologize, but it has been a long two weeks. Finally, it goes without saying that my research advisor, Kit Cummins, deserves a lot of credit for the contents of this thesis. Kit has a love of and skill in chemistry that is truly astonishing. I will certainly always remember the conversations we have had, and hope to someday approach your level of chemical knowledge. Most of my understanding of and excitement about group theory comes from close interactions with you in the classroom and the lab. But, if I have learned anything at all from you, it is the importance of "telling a story," and preferably an interesting one. I hope that I have done so in the preceding pages, and I intend to carry that thought with me as I continue on in chemistry.